University of Southampton

Faculty of Natural and Environmental Sciences

Ocean and Earth Science

Cenozoic CO_2: Chance History or Inevitable Outcome?

by

Ross Whiteford

ORCiD iD: 0000-0002-2178-3476

Thesis for Doctor of Philosophy

March 2019

Abstract

Earth's climate has undergone dramatic change, but as far as we know this change has never been severe enough to make the planet uninhabitable, despite what might be considered as close calls. External climate drivers (those which are caused by factors unrelated to climate) are known to be operating on long timescales, but it is not yet clear what the impact of these drivers has been due to the complex behaviour of the Earth system. To address this, I have developed GECCO (Geological Evolving Carbon Cycle + Ocean model), a new carbon cycle box model specifically designed to represent the carbon cycle and climate interactions on multimillion year timescales.

To equip GECCO with the tools necessary for modelling of the long term carbon cycle and climate systems, a picture of the carbon cycle has been built up from previous work and then supplemented with novel features where certain aspects had not previously been considered. Key components of the carbon cycle that are novel to GECCO, or are an improvement on previous efforts, include the representations of plate tectonics, ice dynamics, the terrestrial carbonate reservoir and ocean carbonate chemistry. In Chapter 2 each component of GECCO is described in detail, including a discussion of the simplifications and limitations of each part of GECCO in its current state, and potential future improvements to GECCO.

Once developed, GECCO was applied to simulate changes in oceanic calcium and magnesium ion concentration, and how these might have affected the carbon cycle and climate over the Cenozoic. Available fluid inclusion data indicates that calcium concentration has approximately halved over the Cenozoic, and magnesium concentration has approximately doubled. Driving GECCO with this forcing initially showed steady state atmospheric CO_2 fell by $\sim$250ppm, regardless of the timescale over which the change in ion concentrations occurred. Further ensembles runs were performed to estimate the sensitivity of this result to four key climate feedbacks. Results from these ensembles show that both transient and steady state atmospheric CO_2 and CCD response to calcium and magnesium forcing is highly sensitive to feedback

strength. In terms of the power of forcings, magnesium is shown to be approximately the same strength as calcium as a driver of atmospheric CO_2 change, and the effects of calcium and magnesium are found to be synergistic rather than simply additive.

GECCO was also used to explore the potential for changes in some aspects of plate tectonics to drive changes in climate. An ensemble of runs was performed during which the temporal lag between plate subduction and volcanic outgassing (the 'outgassing lag') was varied. Another ensemble was conducted during which the variability around that lag (the 'outgassing spread') was varied. Finally, the robustness of these results was tested by performing a multitude of runs to estimate the importance of four key feedbacks in regulating climate response to changing outgassing lag. Changes in outgassing lag drive important changes to atmospheric CO_2 by altering carbon storage capacity of the subterranean reservoir. The magnitude of carbon cycle and climate response to this tectonic driver is extremely dependent on climate feedback strength. Varying the outgassing spread had a more muted effect, primarily acting to alter the timescale over which atmospheric CO_2 variability occurs.

In summary, two external drivers of climate were analysed for their potential to drive carbon cycle change. Ensembles of runs show both drivers are able to cause large transient changes in atmospheric CO_2, however neither driver was able to drive climate instability using a sensible range of forcing strengths unless feedbacks are altered from their estimated Precenozoic strength. Feedback strength is shown to be extremely important in determining long term climate evolution, and the response to changes in feedback strength is found to be similar regardless of the nature of the climate driver. Furthermore, the interplay between different climate feedbacks is found to explain most of the observed behaviours, suggesting that the relative strength of climate feedbacks is the dominant control on Earth's long term climate. In some situations, external drivers are able to drive transient or steady state climate responses, but the magnitude of both transient and steady state change is highly dependent on feedback strength.

Contents

List of Figures

List of Tables

UNIVERSITY OF Southampton

Research Thesis: Declaration of Authorship

Print name:	

Title of thesis:	

I declare that this thesis and the work presented in it is my own and has been generated by me as the result of my own original research.

I confirm that:

1. This work was done wholly or mainly while in candidature for a research degree at this University;
2. Where any part of this thesis has previously been submitted for a degree or any other qualification at this University or any other institution, this has been clearly stated;
3. Where I have consulted the published work of others, this is always clearly attributed;
4. Where I have quoted from the work of others, the source is always given. With the exception of such quotations, this thesis is entirely my own work;
5. I have acknowledged all main sources of help;
6. Where the thesis is based on work done by myself jointly with others, I have made clear exactly what was done by others and what I have contributed myself;
7. Either none of this work has been published before submission, or parts of this work have been published as: [please list references below]:

_____

_____

_____

_____

Signature:		Date:	

Acknowledgements

There are so many people I would like to thank. My supervisors, Toby Tyrrell and Gavin Foster, provided invaluable guidance and suggestions throughout the PhD, as well as insightful advice on the presentation of ideas in many manuscripts and abstracts. Thank you also to GSNOCS, who provided the funding for this project.

I would like my partner Michael, for countless discussions about all manner of topics from the carbon cycle to computing - not to mention keeping me sane through the working and reworking of every part of this thesis. To Becca, my Uni soulmate, who has read and offered constructive comments on almost every page I've written and every figure I've drawn in the last 8 years, thank you so much. Thanks also to my family, who have sat and watched many presentations, looked at many posters, and patiently listened to my excitement over the most esoteric discoveries. Finally, a special thank you to Helen, Olly and Martin the sound man, and their podcast, Answer Me This!, which was a near constant source of companionship. Since being introduced to your podcast near the beginning of my PhD, I've been an avid fan, and some episodes still send me back to pivotal moments in the last few years.

What could be cuter,
Than to feed a computer,
With wrong information,
But naïve expectation,
To obtain with precision,
A Napoleonic decision?

Originally by Major Alexander P. de Seversky.

Reprinted by John C. Davis in Statistics and Data Analysis in Geology.

Chapter 1 - Introduction

1.1. Broad Outline

The primary question prompting this thesis is that of Earth's ongoing climate stability. Current understanding indicates that Earth has been stable enough to remain habitable for approximately 4 billion years (*Schopf* and *Packer*, 1987; *Mojzsis et al.*, 1996; *Brasier et al.*, 2002). Habitability is often defined based on the presence of liquid water at the planet surface (*Spiegel et al.*, 2008). This definition can be problematic, however, because planets with temperatures very different to that of Earth would be expected to behave in a fundamentally different way - for example during snowball Earth events where exchange between the ocean and atmosphere is severely or entirely restricted. One way of resolving this issue is to focus on the trend in variables known to affect the climate state (*Berner* and *Caldeira*, 1997). For instance, if the projected trend in atmospheric CO_2 concentration is a progressive decline, then it may be inferred that the planet would eventually become uninhabitable due to perpetual cooling. This interpretation relies on the assumption that feedbacks do not exist outside of the modellable range which would prevent runaway climate behaviour. This version of habitability, based on the climate stability, is the definition used in this thesis.

Earth has remained habitable despite large changes in the external and internal climate forcings. External forcings are defined as those which are unrelated to climate, for example changes in the solar forcing or plate tectonics. Such long term stability suggests the presence of constraining feedbacks that prevent runaway warming or cooling, however long term climate stability could also be the result of chance. Superficially, while it seems exceedingly unlikely that Earth has remained stable simply by chance, this impression is subject to observer self selection bias. It may be exceedingly rare for a planet to remain stable for such a length of time, nevertheless due to the tremendously large number of planets in the Universe it is feasible to suggest stability would happen somewhere. If such stability is necessary for intelligent life to arise, then it follows that intelligent life will necessarily be found on one of these rare quiescent planets. Planets with stabilising feedbacks may be identifiable by finding those which have remained habitable longer than expected, statistically speaking, based on chance. Within the last few years, many exoplanets have been discovered (*Kopparapu et al.*, 2013), and a small fraction of these are thought to be in the habitable zone (*Traub*, 2012). Despite this, the number of known exoplanets and the uncertainties surrounding their climatic stability mean the available dataset, in its current state, is not yet large enough to

provide statistically significant results regarding planetary stability. Planets with stabilising feedbacks would also be expected to have a more constrained temperature evolution, however it would require millions of years of observation to understand the level of stability of any given planet. This may be achievable for Earth through the use of proxy datasets, but is not yet feasible for any other planet. Earth is currently the only known planet with life, so any question of habitability is hindered by only having a single sample. At this stage, to further inform our current understanding of planetary stability it is necessary to use modelling approaches, which require a detailed understanding of the mechanisms controlling Earth's long term climate. The climate and carbon cycle are inextricably linked, predominantly through the effect of CO_2 in the atmosphere on the radiative budget of Earth, but also as a result of ocean carbon species and their role in determining ocean acidity. A detailed understanding of the carbon cycle is therefore critical to understanding the long term stability of Earth and potentially other planets.

1.2. The Carbon Cycle

Carbon is one of the most important elements on Earth. Not only does it form the basis of life, but it is also constitutes and integral part of Earth's climate. Radiation from the Sun that reaches Earth occupies a wide swathe of the electromagnetic spectrum with a peak in the visible band. Earth's atmosphere is only transparent to visible light and radio waves, and is translucent for UV and infrared light, so a large fraction of incoming radiation is blocked. Radiation that penetrates Earth's atmosphere will be either be reflected by clouds and surface albedo, or will be absorbed by the Earth itself, and then reradiated. The spectrum of radiation leaving Earth is different to that of the original radiation. Earth's temperature is much lower than that of the Sun's, so the peak emission wavelength is in the infrared band. Infrared radiation is absorbed by compounds in the Earth's atmosphere, including water vapour, carbon dioxide, methane, nitrous oxide and more, then re-emitted in all directions. Energy will continue to be reabsorbed and re-emitted until it leaves the Earth, and radiative balance will be achieved when the amount of radiation emitted balances the amount of incoming radiation. CO_2 is able to influence the radiative balance of the Earth by changing the atmospheric opacity to infrared radiation. Increasing atmospheric CO_2 concentration therefore acts to slow down the emission of energy and reduce the outgoing radiative flux. This concept is known as the greenhouse effect. While there are potent greenhouse gasses other than CO_2, their effect is mitigated for one of several reasons (*Rodhe*, 1990):

- The gas is found in very low concentrations (e.g. methane)
- The gas concentration is a function of climate itself (e.g. water vapour)
- The absorption spectrum of the gas is already saturated
- The gas has a short atmospheric lifetime

Nonetheless it is important to remember that, while greenhouse gasses other than CO_2 are important in maintaining background climate temperature, and may be dominant during transient events, CO_2 is the most salient greenhouse gas, both today and over the Cenozoic (*Anagnostou et al.*, 2016).

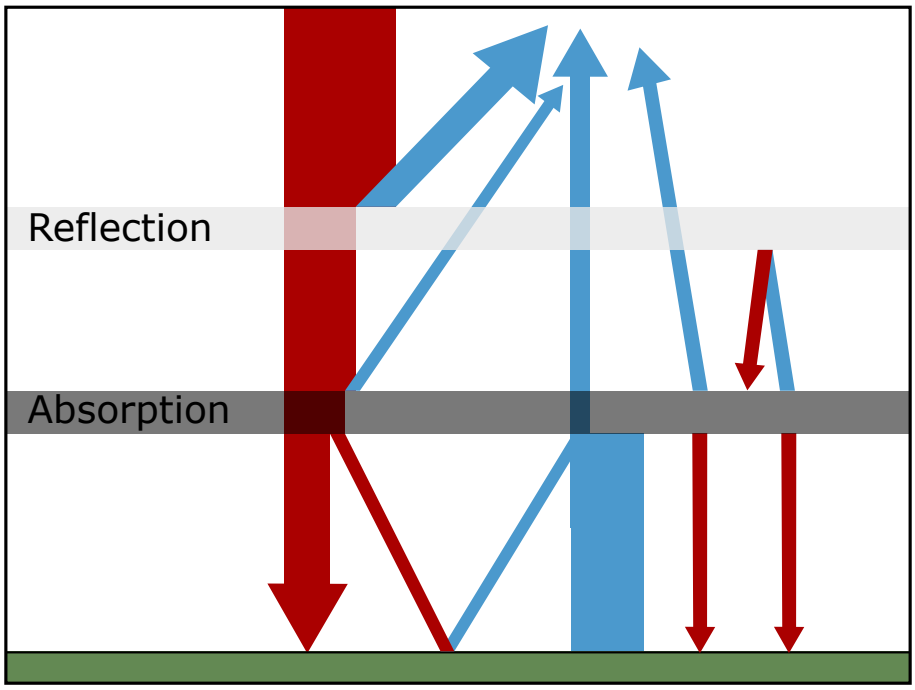

Figure 1.1: ***Incoming solar radiation (red) is partially reflected back to space, partially absorbed in the atmosphere and partially absorbed by the Earth. Energy that makes it to Earth is reradiated, however the wavelength of this radiation is decreased by this process, and the atmosphere is more opaque to this wavelength of radiation, meaning a greater proportion is absorbed in the atmosphere. From the atmosphere, the radiation is re-emitted in a random direction, meaning that the greenhouse layer slows the escaping radiation. Energy balance is achieved when the sum of escaping energy (blue arrows) is equal to the incoming energy.***

Carbon is not only present in the atmosphere, but also in the oceanic and lithological reservoirs. In fact, the total mass of carbon in the atmosphere is minute in comparison to the mass of carbon in the ocean, which is in turn minute in comparison to the amount in rocks (*Kump et al.*, 2009). The movement of carbon between reservoirs is known as the carbon cycle, and is often split into short term and long term cycles (though truly there is a continuum of

processes operating across a spectrum of timescales). The smaller carbon reservoirs tend to have fast dynamics, whereas larger reservoirs have slow dynamics.

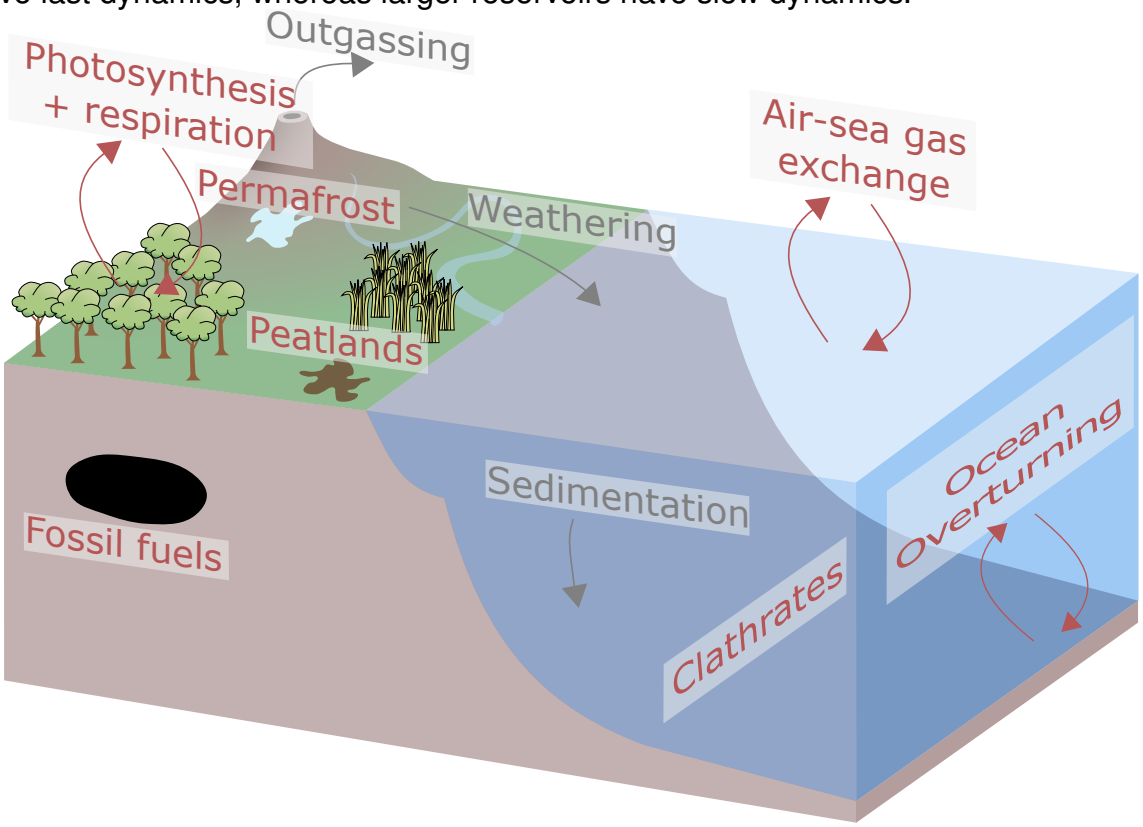

Figure 1.2: ***A schematic showing the main short term (red) and long term (grey) carbon cycle fluxes and reservoirs. Submillenial processes and reservoirs are shown in red. The largest annual CO_2 fluxes are caused by photosynthesis and respiration, however these fluxes are closely balanced so have little interannual impact on the carbon cycle. Additional fluxes come from the interaction of the ocean and atmosphere, and other surficial carbon stores.***
Long term carbon fluxes are shown in grey. The primary source of CO_2 to the atmosphere is volcanic outgassing, CO_2 is transported to the ocean through weathering and becomes sediment primarily through the action of ocean plankton, which is then exported through subduction zones. To close the carbon cycle on timescales of millions of years, the flux of subducted carbon must be balanced by efflux from the mantle or other subterranean sources.

The short term carbon cycle primarily deals with fluxes affecting the concentration of carbon in the ocean and atmosphere, operating on timescales of years to millennia (shown in red in Figure 1.2). On these timescales the flow of carbon is controlled by the terrestrial biosphere, ocean mixing, and oxidation of surficial carbon reservoirs. The effects of these short term drivers have been observed in time series datasets, such as the Keeling curve (*Keeling et al.*, 1995). This curve displays the yearly changes in atmospheric CO_2 driven by seasonal variation in the terrestrial biosphere. Glacial-interglacial cycles are also a clear example of dramatic climate change driven fluctuations in the short term carbon cycle (*Archer et al.*, 2000; *Sigman* and *Boyle*, 2000; *Sigman et al.*, 2010), however the atmospheric CO_2 change

across these cycles ($\sim$100ppm (*Petit et al.*, 1999)) is small in comparison to atmospheric CO_2 variation in deeper time (*Foster et al.*, 2017). Though surficial reservoirs are comparatively small in terms of carbon storage/release potential, they demonstrably have the potential to drive large climate change, which may be magnified during times of high climate sensitivity, or may push the climate over irreversible tipping points (*Armstrong McKay* and *Lenton*, 2018), further enhancing their power to drive important change. Another example of the interaction between the short term carbon cycle and climate is the oxidation of fossil fuels, which is particularly important in the present day, as human activity rapidly increases the concentration of CO_2 in the atmosphere. The results of this rapid increase are already being observed, however the true extent of this climate experiment remains to be seen. By looking into the past we may be able to study events that are similar to anthropogenic forcing, in an attempt to understand the likely impact, and we can look to intervals where atmospheric CO_2 was much higher than the present day, to understand how the climate behaves during those intervals (*Hollis et al.*, 2019). The legacy of large scale carbon release to the atmosphere has already been shown to last at least hundreds of thousands of years (*Tyrrell et al.*, 2007), however the ramifications of CO_2 release might last for millions of years, feeding into long term carbon cycle behaviour.

On timescales of millions of years, the primary source of carbon into the atmosphere is volcanic CO_2, fed by some combination of mantle CO_2, country rock assimilation, and slab decarbonation (*Kump et al.*, 2009). The primary sink of atmospheric CO_2 is consumption by silicate weathering (*Kump et al.*, 2009). Crucially, we have reason to believe that the amount of chemical weathering that occurs is influenced by climate. The link between the CO_2 concentration and CO_2 sink offers the opportunity for climate stabilisation, but the precise relationship between these factors is difficult to quantify due to the complexity of the carbon cycle.

There are 3 pathways by which carbon moves from the atmosphere into the ocean: directly by air-sea gas exchange, indirectly by carbonate weathering and indirectly by silicate weathering. Of these, only the silicate weathering pathway (hereafter silicate pathway) is a net sink of carbon from the atmosphere on the timescale of hundreds of thousands to millions of years. Carbonate weathering, though a temporary sink of atmospheric CO_2, is thought to be 'carbon neutral' (to not affect atmospheric CO_2 concentration) on geological timescales, because the carbonate weathering reaction is undone when calcification occurs.

The Silicate Pathway

$$CaSiO_3 + H_2O + \mathbf{2CO_2} \rightarrow 2HCO_3^- + Ca^{2+} + SiO_2 \quad (1.1)$$

(*Berner et al.*, 1983)

Weathering of silicate (simplified here to the mineral wollastonite) occurs by reaction of one mole of calcium-magnesium silicate with two moles of atmospheric CO_2 and water, forming two bicarbonate ions, one calcium ion and silica (Equation 1.1). The products of this reaction are transported to the ocean by the action of rivers (red in Figure 1.3).

The Carbonate Pathway

$$CaCO_3 + H_2O + \mathbf{CO_2} \rightarrow 2HCO_3^- + Ca^{2+} \quad (1.2)$$

(*Berner et al.*, 1983)

Weathering of carbonate occurs by reaction of one mole of carbonate with one mole of atmospheric CO_2 and water, forming two bicarbonate ions, and one calcium ion. The products of this reaction are transported to the ocean by the action of rivers (blue in Figure 1.3).

Air-Sea Gas Exchange

CO_2 diffuses directly across the ocean surface. The magnitude and direction of air-sea gas exchange is determined by the partial pressure of CO_2 in the atmosphere compared to that of the surface ocean (Henry's Law). The Preindustrial ocean was a CO_2 source (approximately 5×10^{13} mol/yr (*Sabine* and *Feely*, 2007; *Reay* and *Grace*, 2007)), but the present day ocean is a CO_2 sink (*Sabine* and *Feely*, 2007). This is a direct result of anthropogenic release of CO_2 into the atmosphere, which has overwhelmed the relatively small Preindustrial ocean CO_2 source (*Sabine* and *Feely*, 2007), reversing the flux direction. Such a situation may also have occurred in the past, for example, during the numerous hyperthermal events that occurred during the Cenozoic.

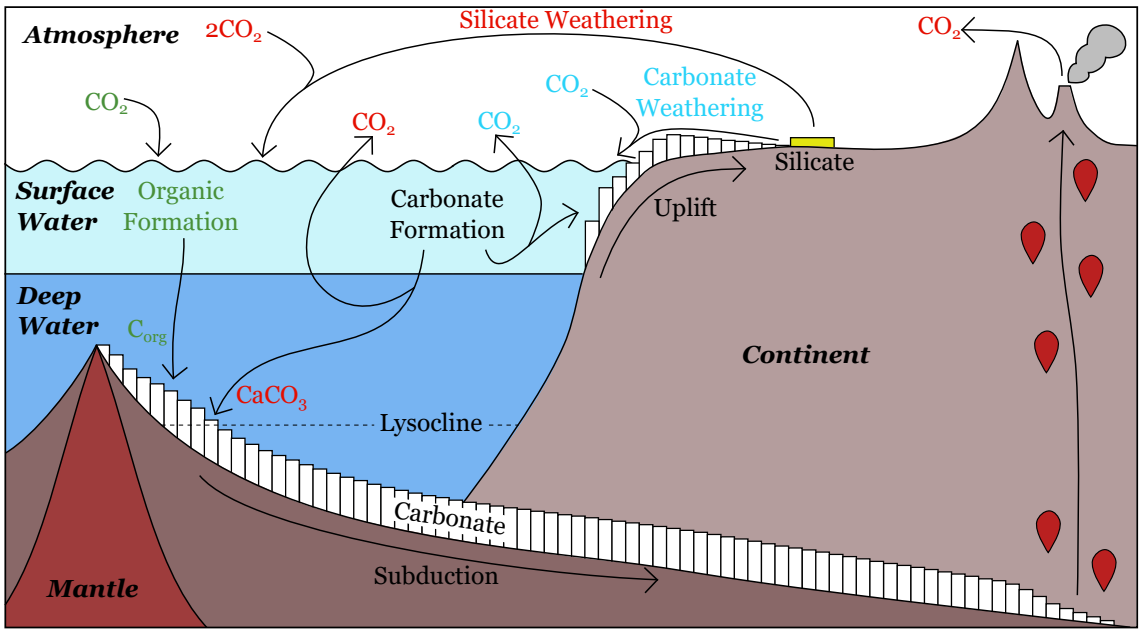

Figure 1.3: ***The carbon fluxes by weathering of silicates (red) and carbonates (blue) are shown for a steady state system. Carbonate weathering is 'carbon neutral', as CO_2 removed from the atmosphere by weathering is rereleased during calcium carbonate formation. Silicate weathering removes one mole of CO_2 for each mole of silicate weathered, and this carbon is eventually returned to the atmosphere after processing through the subduction zones. As with silicate weathering, organic carbon formation consumes CO_2 and buries this in sediments to be recycled, either through subduction zones (as pictured) or by uplift and weathering (not shown).***

1.2.1 Ocean Carbonate Chemistry

Ocean carbonate chemistry details how carbon behaves in the ocean. Crucially, the partitioning of different forms of carbon changes the flux between the ocean and atmosphere, and the flux between ocean and sediments. In this way the state of carbonate chemistry in the ocean mediates the transition of atmospheric CO_2 to carbonate sediment. An introduction to the most salient parts of the ocean carbonate chemistry system is provided here, and additional details beyond the scope of this introductory material can be found in Appendix B.

Carbon is present in many forms in the ocean. These can be broadly classified into two types, organic and inorganic. Inorganic carbon is present in four forms: CO_2 (carbon dioxide), HCO_3^- (bicarbonate ion), CO_3^{2-} (carbonate ion) and H_2CO_3 (carbonic acid) (*Zeebe* and *Wolf-Gladrow*, 2001). CO_2 in seawater forms carbonic acid, which rapidly dissociates into bicarbonate ions, then dissociates again into carbonate ions. Carbonic acid is highly unstable, and its concentration at any one time is negligible, so the system is generally portrayed without this intermediary component (*Zeebe* and *Wolf-Gladrow*, 2001) (Figure 1.4). The ability for carbon to transform between these three main species means they exist in dynamic equilibrium. The position of that equilibrium state is dependent on temperature, pressure, salinity

and ocean composition (*Zeebe* and *Wolf-Gladrow*, 2001).

Locally, inorganic carbon species approach their equilibrium state on timescales on the order of minutes, much shorter than the timescale of interest here, so the carbonate chemistry system may be treated as steady state. Ocean dynamics operate on longer timescales, allowing distant regions to exist at their own steady state. At steady state, the stoichiometric ratio of carbonate system products to reactants is expressed using so called 'equilibrium constants'. Despite being called constants, these values are affected by temperature, pressure, salinity and ocean composition, so here they are instead referred to as Carbonate Chemistry K values (CCK's). The temperature, pressure and salinity dependence of CCK's has been extensively studied and focus has recently shifted to the relationship of CCK's with ocean composition (*Tyrrell* and *Zeebe*, 2004; *Hain et al.*, 2015; *Zeebe* and *Tyrrell*, 2019).

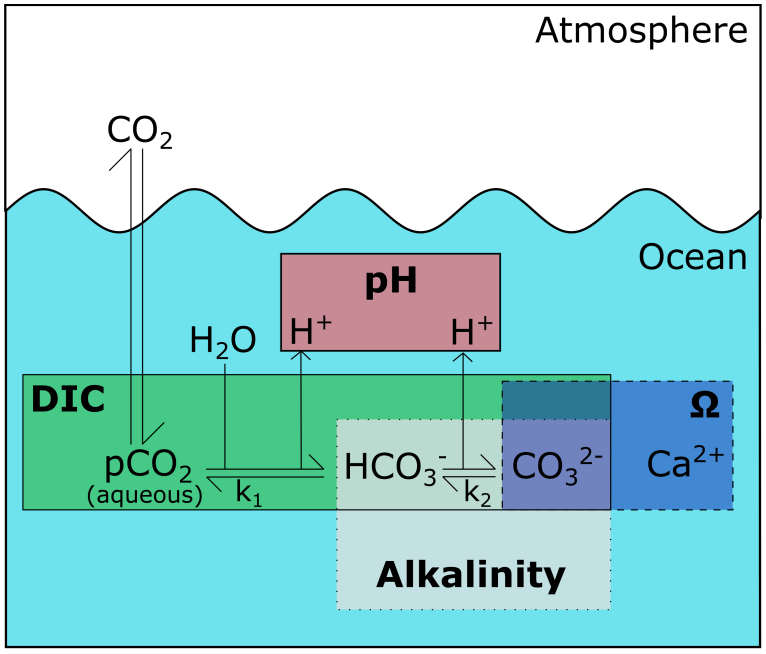

Figure 1.4: ***The ocean carbonate system is shown with key parameters highlighted by coloured boxes, corresponding with Equation 1.3 through Equation 1.6 shown below.***

From the three inorganic carbon species (CO_2, HCO_3^- and CO_3^{2-}), a number of parameters may be defined, including:

$$DIC = [CO_{2(aq)}] + [HCO_3^-] + [CO_3^{2-}] \tag{1.3}$$

$$Alkalinity \approx [HCO_3^-] + 2[CO_3^{2-}] \tag{1.4}$$

$$pH_F = -log([H^+]_F) \tag{1.5}$$

$$\psi_C = \frac{[Ca][CO_3^{2-}]}{k_{sp}} \tag{1.6}$$

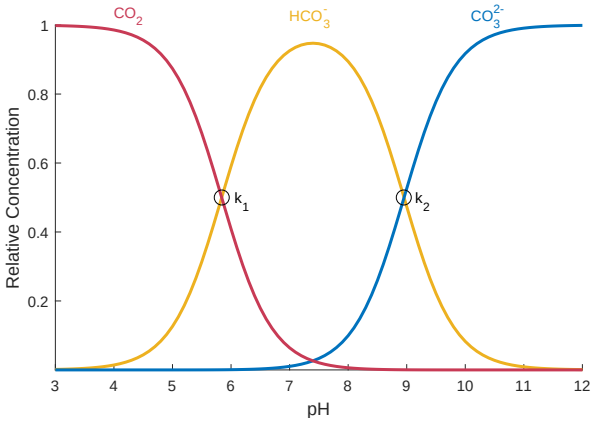

Figure 1.5: ***A Bjerrum diagram shows how the partitioning of carbonate species is related to pH at a constant DIC. Equivalence points (CCK's) are found at the crossing points of species.***

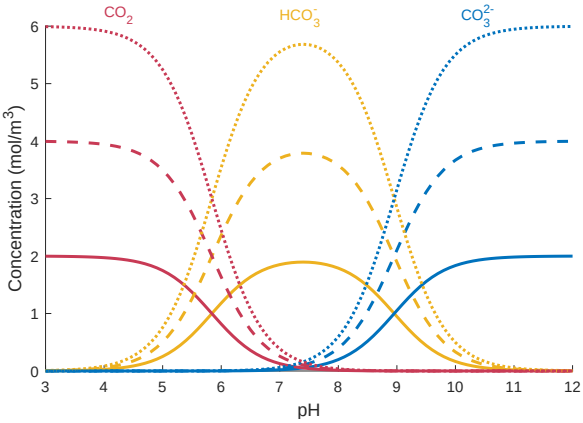

Figure 1.6: ***Concentrations of each ion are transformed from a relative concentration (as in Figure 1.5) to a series of example absolute concentrations. This shows how two carbonate system parameters can be used to calculate the concentration of any individual ion.***

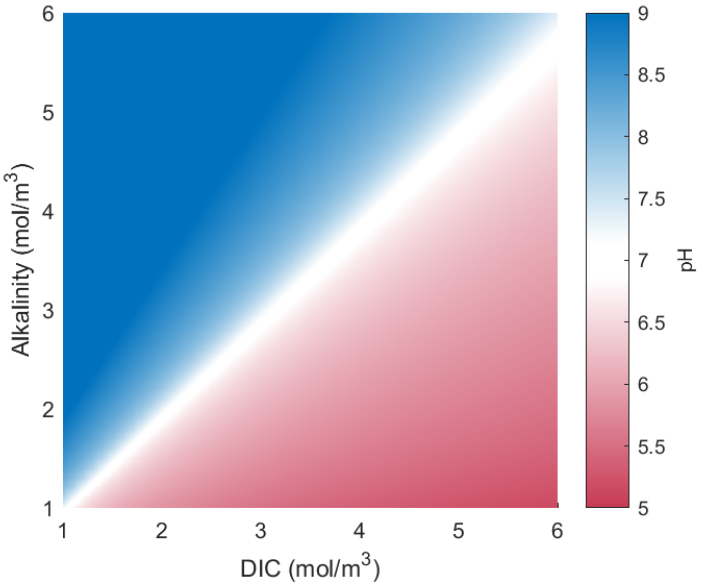

Figure 1.7: ***A visualisation of the carbonate system more appropriate for use with models shows pH in DIC and alkalinity space. A high DIC:alkalinity ratio is associated with low pH, and low DIC:alkalinity ratio with high pH. By observation of Equation 1.3 and Equation 1.4, high DIC relative to alkalinity must mean a high concentration of CO_2, which equates to a low pH (Figure 1.5). Conversely, high alkalinity relative to DIC must mean a high concentration of CO_3^{2-} and a low concentration of CO_2, which equates to a high pH (Figure 1.5).***

As has already been alluded to, carbonate system parameters are not independent. It is often said that the carbonate system has two degrees of freedom, but a more instructive view is that there are two levels of variability. In normal situations, when the conditions are close to standard surface ocean water, the most important factors are the concentrations of the carbonate species. Given any two parameters, and assuming more minor factors are close to standard conditions, it is possible to calculate the value of all others. For modelling purposes, the two chosen parameters are typically DIC and alkalinity concentrations (Figure 1.7) because both of these are conservative properties. It should be noted that Equation 1.4 shows a simplified form of alkalinity (carbonate alkalinity), which is roughly equal to total alkalinity (which consists of the contributions of many compounds). All calculations shown here use a full definition of alkalinity using the method developed by *Follows et al.* (2006) and generally assuming that contributing compounds have constant concentrations through time (with the exception of carbonate alkalinity, which is variable). Technically speaking, however, the calculation of other carbonate system parameters from the two which are specified uses CCK's, which are affected by temperature, pressure, salinity and ocean composition, adding at least four further degrees of freedom to the system. This can be viewed as two levels of importance - carbonate system parameters are of the utmost importance, and auxiliary parameters, though still required, are secondary to those carbonate system values (detailed further in Appendix B). Derivation of CCK's is based on estimation from empirical data (*Ben-Yaakov* and *Goldhaber*, 1973), sometimes combined with dynamical understanding of the carbonate chemistry system (*Hain et al.*, 2015). In essence, the calculation of CCK's is done using stoichiometric concentrations of ions, meaning changes in the activity of ions is parameterised into the CCK value. For example, an increase in calcium ion concentration

decreases the activity of the carbonate ion without affecting its concentration. This makes the carbonate ion less able to participate in reactions, which is reflected by a change in the CCK value associated with all reactions involving carbonate ions.

In summary, aqueous inorganic carbon exists in three primary forms (CO_2, HCO_3^- and CO_3^{2-}) which are linked in a dynamic equilibrium. The relative concentrations of these three forms are determined by temperature, pressure, salinity and ocean composition, and the absolute concentrations are important in determining the fluxes of carbon into and out of the ocean, as detailed below.

1.2.2 Biological Interaction

In the modern ocean, carbon export from the surface ocean to the deep ocean and sediments is biologically mediated (*Riebesell et al.*, 2009). Plankton in the ocean use Dissolved Inorganic Carbon (DIC) to form their organic tissues (Particulate Organic Carbon - POC) and, if they are calcifying plankton, they use dissolved inorganic carbon and Ca^{2+} to form their calcareous shells (Particulate Inorganic Carbon - PIC) (see Equations 1.7–1.9). When plankton perish, their POC and PIC begin to sink through the water column.

$$CO_3^{2-} + Ca^{2+} \rightarrow CaCO_3 \tag{1.7}$$

$$HCO_3^- + Ca^{2+} \rightarrow CaCO_3 + H^+ \tag{1.8}$$

$$CO_2 + Ca^{2+} + H_2O \rightarrow CaCO_3 + 2H^+ \tag{1.9}$$

Organic Carbon Fate

POC exported by plankton is subject to intense scavenging in the water column (*Charette* and *Moran*, 1999; *Buesseler et al.*, 2006) and the vast majority of POC is remineralised in the surface ocean, with further POC remineralisation occurring in the deep ocean (*Jahnke*, 1996; *Dunne et al.*, 2007) and in sediments. Only a very small fraction of the POC production flux is permanently buried (*Jahnke*, 1996), and burial predominantly occurs in shallow settings (*Dunne et al.*, 2007) due to the high sedimentation rate (which prevents organic oxidation occurring before permanent burial). Anoxic and suboxic environments, such as oxygen minimum zones, are also important regions of POC burial (*Suess*, 1980; *Pedersen* and *Calvert*, 1990; *Hartnett et al.*, 1998).

Inorganic Carbon Fate

The burial of inorganic carbon is controlled by how saturated deep ocean water is with respect to calcium carbonate. This is determined by the product of the concentrations of calcium and carbonate ions, relative to the solubility product (the expected product of the concentrations based on thermodynamic understanding) - as described in Equation 1.6. When water is holding more calcium carbonate that would be expected, it is said to be supersaturated, whereas when water is holding less calcium carbonate than would be expected, it is said to be undersaturated. Average surface ocean water is supersaturated with respect to calcite, whereas deeper ocean water ($\gtrsim$4km in the present day) is undersaturated with respect to calcite (see the carbonate chemistry overview in Appendix B). The decrease in calcite saturation at depth is driven by the changes in pressure and temperature (*Zeebe* and *Wolf-Gladrow*, 2001). Pressure is the primary driver, while temperature plays a more minor role. Vertical gradients in oceanic ion composition may also have an impact, because ocean ion composition (especially calcium and magnesium ion concentration) has an impact on CCK's (see Appendix B and *Hain et al.* (2015)), though in terms of affecting the vertical gradient in carbonate systematics this impact is likely to be negligible due to the long residence time of calcium and magnesium, which allows them to be homogenised throughout the ocean.

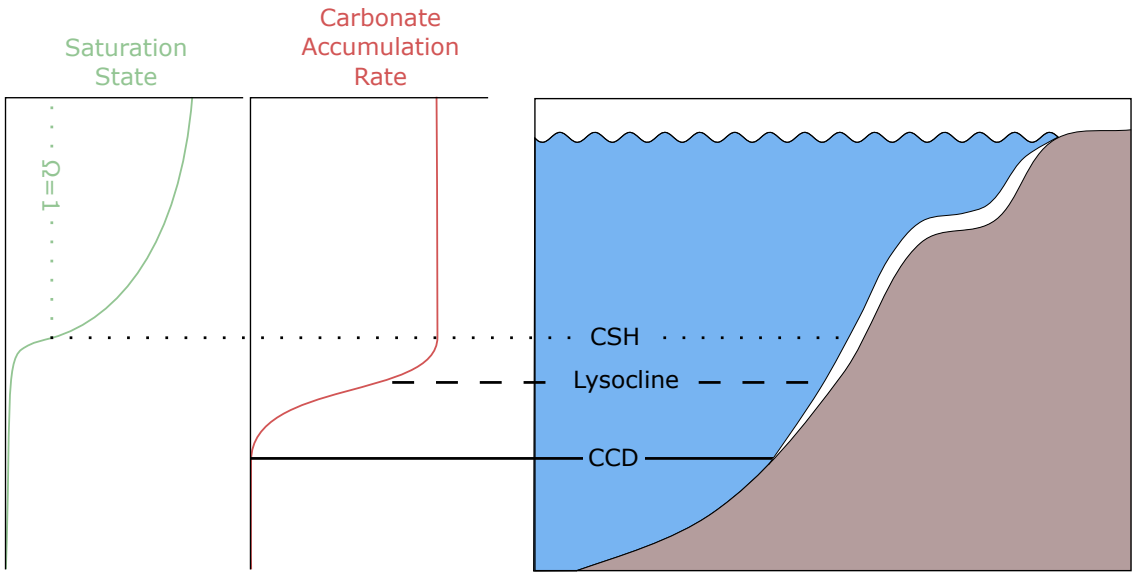

Figure 1.8: ***Several horizons can be defined relating to the behaviour of oceanic and sedimentary carbonate.Ocean saturation state decreases with depth (green) and at the boundary between carbonate supersaturation and undersaturation lies the Carbonate Saturation Horizon (CSH - dotted black line). Sedimentary carbonate is still preserved below the CSH however, as the dynamics of dissolution are slow, meaning another horizon can be defined at the depth below which no carbonate accumulation occurs - this is the Carbonate Compensation Depth (CCD - solid black line). Between the CCD and CSH lies another, more loosely defined, horizon, which identifies the sudden decrease in sedimentary carbonate preservation, this is called the lysocline (dashed black line).***

It is possible to define a boundary between water that is supersaturated with respect to calcite and water that is undersaturated with respect to calcite, termed the Carbonate/Calcite Saturation Horizon (CSH). PIC below the CSH should theoretically undergo dissolution, however this is a kinetically slow process, meaning some PIC may be buried below the CSH (*Ridgwell* and *Zeebe*, 2005). For this reason, additional horizons have been defined: the lysocline identifies the inflection point between sedimentary carbonate accumulation and dissolution (the exact position can be somewhat subjective), and the Carbonate/Calcite Compensation Depth (CCD) delineates the boundary between net carbonate accumulation and net carbonate dissolution - below this horizon no carbonate is preserved. A summary of these horizons and their bathymetric relationship is shown in Figure 1.8.

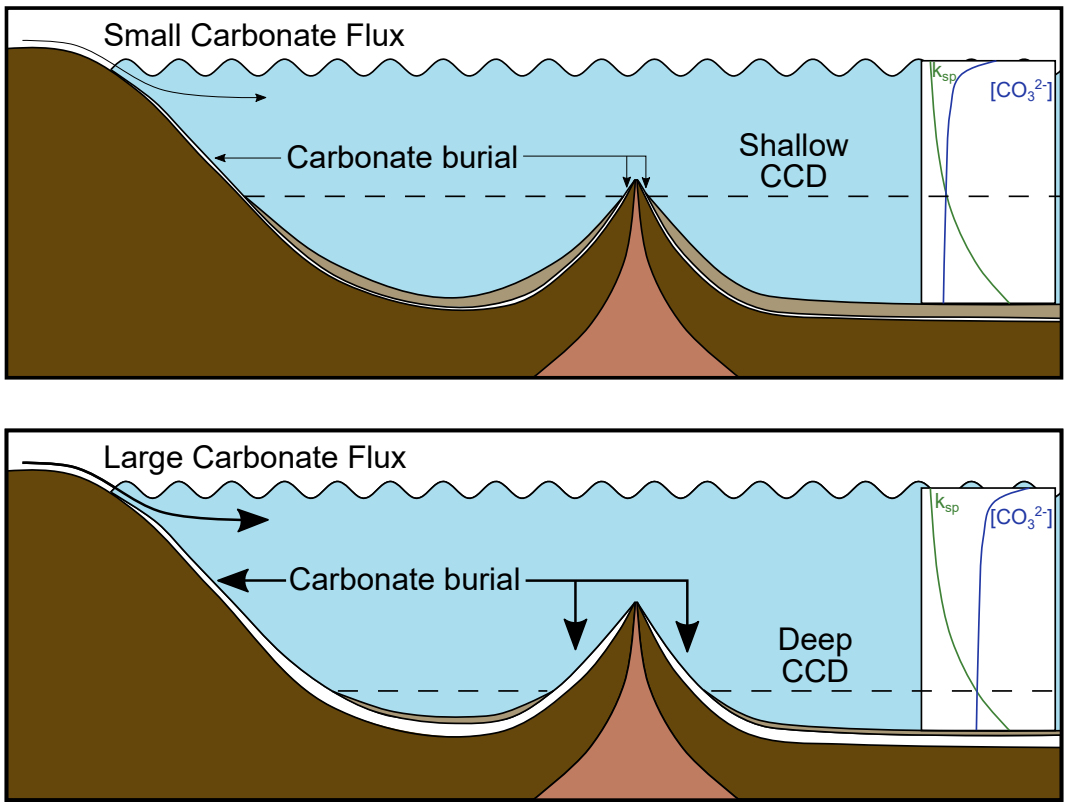

Figure 1.9: ***The impact of the CCD is twofold. First the depth of CCD directly controls the fraction of PIC export which is buried. Shoaling and deepening of the CCD is therefore able to act as a stabilising feedback, whereby increases in the input of carbonate ion will deepen the CCD until the sink is equal to the source. Secondly, the CCD also controls the hypsometric distribution of carbonate deposition. A shallow CCD will only permit carbonate accumulation on the tallest of bathymetric highs, which may exist in different tectonic regimes to the deeper portions of ocean crust.***

1.2.3 Sedimentary Carbon

Sedimentary carbonate is deposited at bathymetric depths above the CCD. Broadly speaking these environments can be split into neritic and pelagic (for different water depths), or shelf and deep sea (for different sediment depth ranges). The ratio of neritic to pelagic productivity is not well known, nor is the ratio of shelf to deep sea carbonate burial. For most applications these factors are of minor importance, however when considering the long term carbon cycle then the fate of shelf carbonates becomes a salient factor. Despite this lack of knowledge, there exists a ratio of shelf to deep sea carbonate burial, which may have changed through time. Some sedimentary carbon will remain static for long period of time, for example when sat in a passive basin, whereas other sedimentary carbon may undergo significant uplift or subsidence. Plate tectonics is a complex three dimensional process, so this description is a simplified global average perspective.

Some carbonaceous sediments are uplifted towards the terrestrial environment. Organic

carbon that is uplifted goes on to become terrestrial organic rich shale or kerogen deposits, whereas uplifted inorganic carbon goes on to become a carbonate, or carbonate rich, lithology (such as limestone).

The shelf and obducting regions are the only plausible major sources of terrestrial carbonate, which has an estimated inventory of $\sim 5 \times 10^{21}$ moles (*Berner* and *Caldeira*, 1997; *Liu* and *Zhao*, 2000; *Zeebe* and *Ridgwell*, 2011). At steady state, the source of terrestrial carbonate must be equal to the sink, both of which are poorly constrained. *Gaillardet et al.* (1999) estimate a carbonate weathering flux of 1.2×10^{12} mol/yr but *Liu et al.* (2011) suggest it is perhaps three times as much, meaning sedimentary uplift must be a significant carbon flux. The uplift of carbonate may occur sporadically, changing due to tectonic forcing, but the average uplifting flux must have been nearly balanced with the terrestrial carbonate sink over very long timescales ($>$100Myr), because Earth's surface is not devoid of carbonate, nor is it completely covered by carbonate sediment.

Carbon deposited as deep sea sediment is more likely to be moved deeper into the ocean by plate tectonics, moving away from a Mid-Ocean Ridge (MOR) axis. As explained in Section 1.2.2, water becomes increasingly corrosive to carbonate with increasing depth. Sedimentary carbonate is therefore temporarily exposed to corrosive water as tectonics moves the sediment deeper into the water column, but may be protected by highly saturated pore water and the development of a clay cap, which isolates the carbonate from corrosive water (*Ridgwell* and *Zeebe*, 2005) (as seen in Figure 1.9).

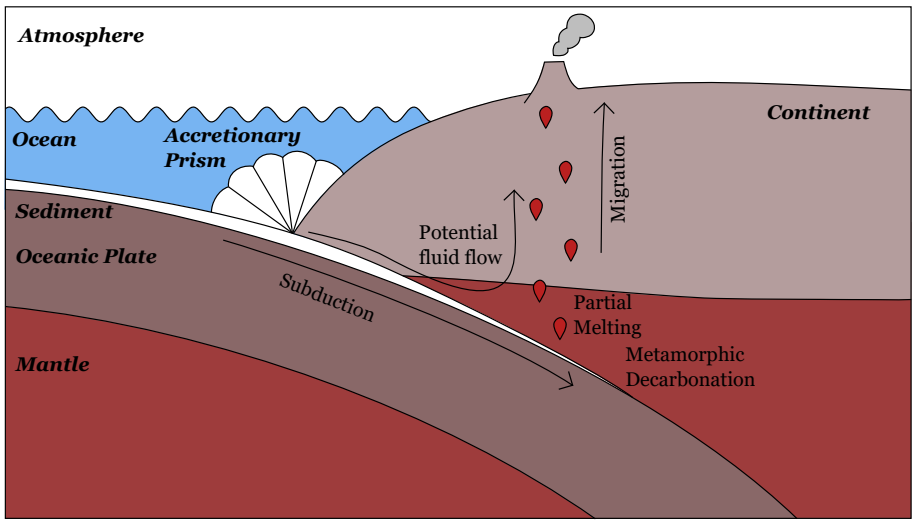

Figure 1.10: ***A highly simplified schematic of a subduction zone shows the motion of sedimentary carbon in the region of subducting plate boundaries. Carbonate sediment may be scraped into an accretionary prism, or obducted (not shown), however a large amount is taken down with the subducting slab (*Kelemen *and* Manning*, 2015). The increased pressure and temperature experienced by the sedimentary package results in metamorphic decarbonation and partial melting, and carbon from incoming sediment is carried towards the surface (tear shaped symbols).***

Subsiding sedimentary carbonate is transported progressively deeper until it reaches a subduction zone. Generally, sediments move with the subsiding slab, and are taken under the overlying plate, at which point the sediments experience a considerable increase in pressure and temperature. The slab has an extremely high thermal inertia, which allows it to survive deep into the mantle (*Richards* and *Engebretson*, 1992; *Grand*, 2002), but the upper edge of the slab, where sediments are located, experience much greater heating. The introduction of carbonaceous material and fluids to the supraslab environment can result in partial melting and metamorphic decarbonation (Figure 1.10). Partial melting is thought to occur at $\sim$100km depth (*Pearce* and *Peate*, 1995; *Peacock* and *Wang*, 1999; *Kessel et al.*, 2005), whereas the depth of metamorphic decarbonation is dependent on the regional temperature profile (*Kerrick* and *Connelly*, 2001). Generally speaking decarbonation occurs when the temperature reaches on the order of 600°C (*Menzies et al.*, 2018). Assuming an average geothermal gradient of 30°C/km, and perfect thermal transmission to the carbon bearing rocks, then this would occur at roughly 20km depth, though subduction zones naturally have atypical thermal profiles.

Some sediment may be scraped off of the subsiding slab to form an accretionary prism, but the accommodation space here is limited, so eventually a steady state will be formed where carbon moving into the subduction zone is equal to carbonate removal. Most removal

happens as carbonate sticks to the subsiding slab, but complex plate flexure and plate morphological features can result in obduction (the uplift of previously submarine lithologies into the terrestrial realm) in specific regions (*Dewey*, 1976). Such processes are highly spatially dependent, and are themselves the subject of complex 3D models (*Davies* and *Stevenson*, 1992; *Syracuse et al.*, 2010; *Hayes et al.*, 2012), so it is difficult to develop simple rules which can accurately predict the behaviour of carbon in these environments. Nonetheless the behaviour of carbon in such environments is naturally important in determining the size of the terrestrial carbonate reservoir on long timescales.

1.2.4 Volcanic Outgassing

The long term carbon cycle is generally viewed as though the source of atmospheric carbon is volcanic, and the sink is sedimentary. This traditional view of the carbon cycle is, however, not appropriate on multimillion year timescales, because the carbon sink (subduction) feeds into the atmospheric carbon source (volcanism) (*Kelemen* and *Manning*, 2015; *Mason et al.*, 2017). The source of carbon for volcanic outgassing is not well established. There are three possible sources: mantle CO_2, country rock assimilation, and slab decarbonation. The proportion of each of these sources is unclear, with studies suggesting that anywhere between 50% and 99% of carbon processed through subduction zones is released back to the atmosphere (*Dasgupta* and *Hirschmann*, 2010; *Kelemen* and *Manning*, 2015; *Mason et al.*, 2017). The speed with which this carbon migrates from the slab to the surface is also difficult to estimate. *Stern* (2002) and *Paterson* and *Tobisch* (1992) estimated that melt ascension rates were on the order of 1-3m/yr, but carbon may feasibly travel much faster due to interactions with fluid (*Stern*, 2002). The speed of fluid migration is difficult to predict and likely to be highly spatially variable, as it would be expected to depend on the nature of the material through which the fluid must pass. Carbon which reaches the surface is released as CO_2, allowing the link between subducted carbon and outgassed carbon to close the carbon cycle on million year timescales (Figure 1.3).

1.2.5 Additional Carbon Reservoirs

In addition to the carbon cycle as described above, there are reservoirs which are not persistently involved with the flow of carbon, but sporadically provide a carbon source/sink. These include the terrestrial biosphere, fossil fuel deposits, permafrost, methane clathrates and peatlands. These reservoirs are thought to have been close to steady state during the Preindustrial, but on occasion, carbon reservoirs such as these may be perturbed, and contribute a rapid and potentially large flux into the atmosphere. Reservoirs are frequently associated with a specific isotopic composition, so it is sometimes possible to identify the source of carbon cycle perturbations by combining knowledge of the mass of carbon released and the isotopic perturbation observed. This has been done extensively for some palaeo events, such as the Paleocene Eocene Thermal Maximum (PETM) (*Cui et al.*, 2011; *McInerney* and *Wing*, 2011; *Gutjahr et al.*, 2017; *Panchuk et al.*, 2008; *Penman* and *Zachos*, 2018), and highlights the capability of such reservoirs to drive climate change. While it is important to acknowledge the potential of these reservoirs to drive carbon cycle change, especially during specific short term events, they are not considered further here.

1.2.6 Carbon Cycle Synthesis

The carbon cycle is intimately linked with Earth's climate, predominantly through the impact of atmospheric CO_2 but also by the state of ocean carbonate chemistry. These are some of the smallest and most dynamic carbon cycle reservoirs, and yet, so far as we know, Earth has not at any time in the last $\sim$4Byr become uninhabitable. The paths carbon takes from the atmosphere are numerous, and complex, but at broad scales the system can be heavily simplified, making the problem tangible. Despite this potential for simplification, there are still large gaps in current understanding of the long term carbon cycle. A major part of addressing these gaps in knowledge is acknowledging their existence, and outlining the potential routes for improvement. Even more so, the act of quantifying what is known about the carbon cycle can improve our ability to infer the behaviour of more poorly constrained carbon cycle components. Having said that, there is value in simply collating up to date knowledge of the carbon cycle. As with many aspects of geoscience, those works were limited by the data and knowledge available at the time, and unfortunately the sector of Cenozoic timescale carbon cycle modelling has since languished.

1.3. Key Questions

There remain many unanswered questions about the carbon cycle and its link to long term climate evolution. Some of the principal open questions are listed below, followed by a broad description of the approaches necessary to derive potential answers.

- What is the reason for Earth's ongoing climatic stability and habitability?
- How resistant is Earth's climate to carbon cycle perturbations?
- Have plausible Cenozoic forcings had the strength to potentially destabilise the climate?
- What has been the primary driving factor of Cenozoic CO_2?
- How strong is the link between the climate of the deep past and the climate of the present day?
- Could previously unexplored climatic drivers and feedbacks have shaped the Cenozoic?
- Can modelling shed light on the potential for external drivers to cause large climatic shifts?

1.4. Approach To Key Questions

Most of the key questions in Section 1.3 focus on understanding climate drivers, climate feedbacks or the interactions between them. Chance drivers and stabilising feedbacks coexist such that the strength of feedbacks is able to modulate the impact of chance drivers. To evaluate the stability of a planet without long term observations of its climate, it is necessary to understand the mechanics of its climate system, then develop a model to simulate the response of that planet to a variety of forcings. Presently, Earth is unique in that it is the only known planet with a climate understood to have remained habitable for an extended period of time. In contrast, our nearest neighbour planets are both uninhabitable, with Venus experiencing the effect of a runaway greenhouse and Mars, though understood to have been habitable in the past (*Knauth et al.*, 2005; *Vago* and *Westall*, 2017) has since had its atmosphere stripped away by the solar wind. While the ongoing habitability of Earth is undoubtedly beneficial for us, it limits the questions it is possible to ask about the reasons for that

stability because it is always necessary to consider the potential for coincidence and chance to play an important role in the evolution of our planet. Use of a model to understand system dynamics circumvents that limitation, and enables the answering of 'what if' questions. What if the Earth had been dealt a different hand? What if the Sun burned hotter? What if the meteorite at the K-Pg boundary had been twice the size? What if plate tectonics had rearranged the continents into a different orientation? Questions like these are profoundly difficult to answer without a detailed understanding of the Earth system, and a mathematical representation of that understanding able to calculate the numerous and complex interactions of different aspects of our climate. The ability to simulate a planet in this way opens the door to answering some of the questions listed in Section 1.3, without necessarily reaching the unsatisfactory conclusion that the climate stability of Earth could have been simply down to chance. Furthermore, this approach allows the disentangling of the impact of each potential driver and feedback. Not only is it possible to investigate whether stability might be an expected outcome (or exceedingly rare), it is also possible to understand the mechanism of said stability and it's potential susceptibility to disruption.

While there are known feedbacks that offer paths to climate stability, there are also known carbon cycle and climate drivers which could have challenged this stability. For example, changes to factors such as palaeogeography, terrestrial weatherability, and ocean carbon export are expected to influence the carbon cycle, however while CO_2 has changed significantly over the last 4 billion years, the changes have not been so dramatic as to drive climate inhospitability. For this, there are three potential explanations:

1. **Carbon cycle drivers are not strong enough to drive climate instability, even when feedbacks are weak or nonexistent.**
   This is not consistent with extinction level events that occurred during the past, when internal or external drivers did challenge Earth's stability, and by extension Earth's habitability.

2. **Climate drivers are strong enough to drive climate instability, but by chance this strength of driver has not been experienced in Earth history.**
   The first step in verifying this hypothesis is to quantify the strength of carbon cycle drivers using a combination of data and modelling.

3. **Earth has strong climate regulating feedbacks, which are only challenged in exceptional circumstances.**

   Again, the first step in testing this hypothesis is estimating the power of carbon cycle drivers using a combination of data and modelling, then varying the strength of climate feedbacks to observe the impact on climate evolution. Complementary to this is the estimation of feedback strength, both in the present day and how the strength of feedbacks may have changed in the past.

1.5. Modelling

1.5.1 Concept

The word model describes a wide range of concepts. In this work, the word model will be used to indicate numerical, mechanistic, forward models (unless otherwise specified). Models may also be statistical (using correlations between variables in contrast to mechanistic links), or even conceptual. In essence the word model is used to describe one object which seeks to represent another through a series of rules, where the rules may be qualitative or quantitative, causative or correlative.

There are many considerations when designing and building a model. One of the first is to determine the spatial and temporal requirements, such that the model will be a suitable representation of the system in question. This is a somewhat strange concept, because it might be expected that in order to achieve a valid result, every relevant factor should be considered. This is rarely the case, however, and almost all calculations must rely on a series of assumptions and axioms which render some parts of the calculation negligible. When creating a model, those assumptions and limits must be clearly established beforehand to ensure that the architecture of the model is appropriate for the nature of the question being asked. The needs of the model must be balanced with the computer resources available so it is always necessary to economise in several ways when building a model.

- The model should simulate as much time as possible within as short a time as possible while retaining the important dynamics (i.e. it should be computationally efficient)
- The number of hours of programming required to achieve a scientifically robust result should be minimised
- Our knowledge of a system is never perfect, which imposes a limit on which aspects of that system can be represented in a meaningful way

Of key concern here, given the spatiotemporal scale of interest, is model efficiency. We can naïvely quantify the efficiency of a model by using the ratio of simulated time to elapsed time (Figure 1.11), which will be referred to here as the model-real ratio (MRR). The MRR is dependent on a huge number of factors, and of key importance are the processor on which the calculations are performed and the language in which the program is written. In their default run environment, weather and complex climate models generally have an MRR greater than, but close to, 1. In order to perform lengthy palaeoclimate simulations the model MMR's must be much greater than 1. For instance, to simulate 4By (approximately the length of Earth history) within 24 hours, a model would have to have an MRR of 1.46×10^{12} - or equivalently would have to produce $\sim$40,000 years of results per second. Models of this MRR are not infeasible, however must be highly simplified. There is a compromise between model complexity and model MRR. Improved processing power can alleviate this compromise somewhat, but this is unlikely to allow a significant increase in MRR in the near future. Modern personal computers are able to perform on the order of 5 billion floating point operations (flops) per core, approximately twice the speed of the best available supercomputer during the 1980's, so there has been massive improvement in the past 30 years. Much of the improvement in computational ability has come from the usage of alternative techniques, such as parallel or quantum computing. Parallel computing is already extensively used in a extremely computationally expensive modules, however box models geared towards palaeoclimate applications generally have less to gain by employing these methods (because there is less repetition of the same type of calculation), and so are not routinely configured in this way. Quantum computing is currently very new technology, and while in future it may be used to perform more detailed simulations which incorporate estimates of the uncertainty in results, as it currently stands quantum computing is too experimental to be of practical use. Even with all modern computational techniques applied, we are still a long way from being able to apply models detailed as General Circulation Models (GCM's) to simulate the Cenozoic in a continuous way.

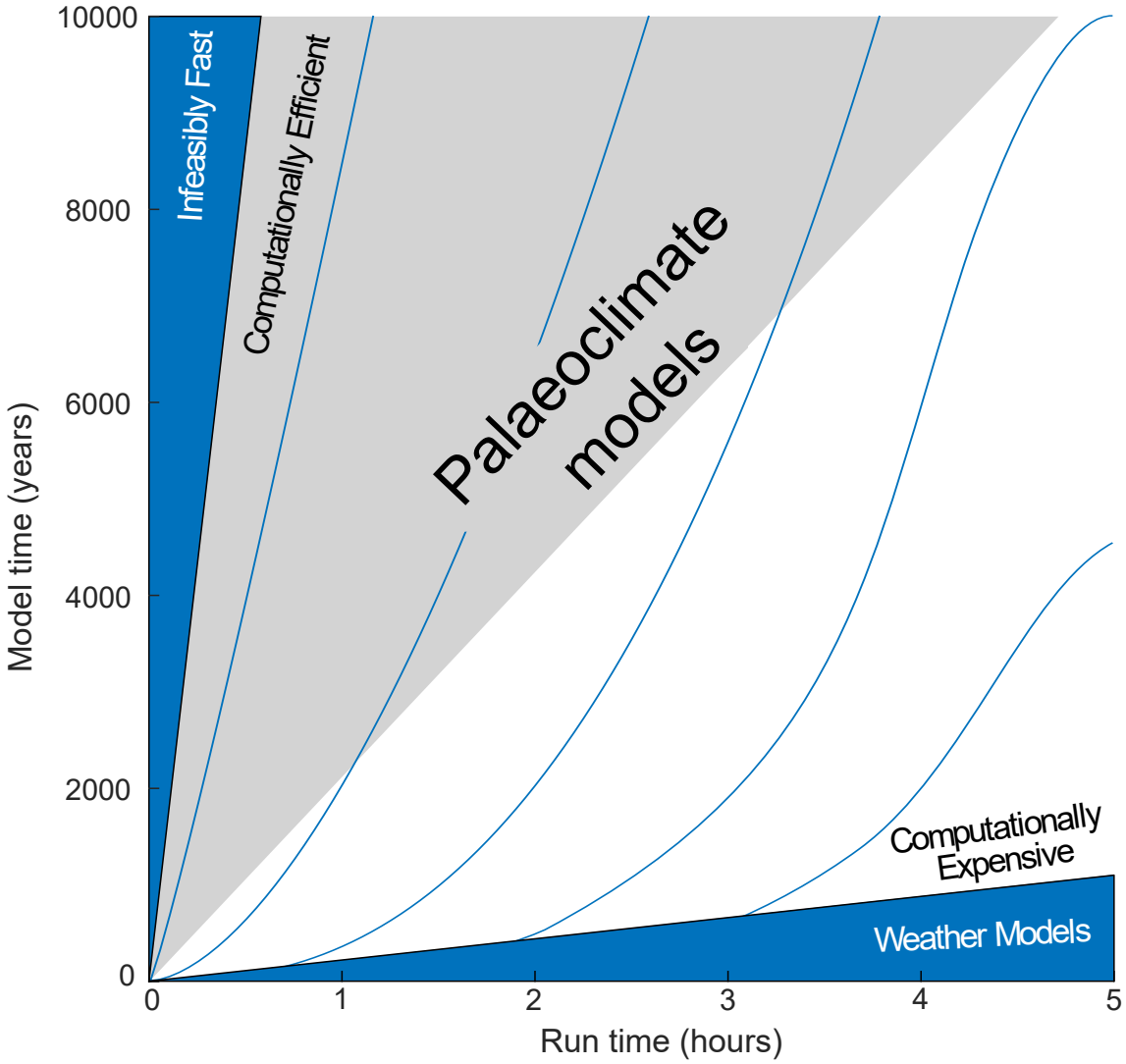

Figure 1.11: ***Schematic of model efficiency is shown with a series of curved lines intended to represent potential efficiency curves for individual models. Models often have high start up costs, leading to initially shallow gradients which flatten to a linear relationship as modelled interval becomes larger. At some point the model scaling will asymptotically approach horizontal, as computer resources are exhausted and longer intervals can not be modelled. Weather models cluster on the bottom of this graph, while palaeoclimate models tend to be located along the left hand side.***

Broadly speaking, numerical mechanistic models consist of three parts (Figure 1.12) - a series of values which represent quantities to be modelled (sometimes known as state variables), a series of rules which govern how these values evolve through time and space, and an indeterminate number of values and rules which are used to inform these calculations. To simulate the system, a starting value (or initial condition) is chosen for each of the quantities to be modelled, then the rules which determine how each of the initial conditions evolves through time are applied iteratively to produce a time series for each initial condition. Ancillary parameters that are used may be constants, or may determine the behaviour of the values being modelled at the edge of the region which is being modelled (boundary condi-

tions). Boundary conditions may be of several types, typically either the value is known and set as a constant through time, or the gradient of the value is known and evolves through time according to the specified gradient. In this way, modelling of this type is no more than a codification of the observations and behaviours of a system, which allows projection forward in time for as long as the encoded behaviour remains true.

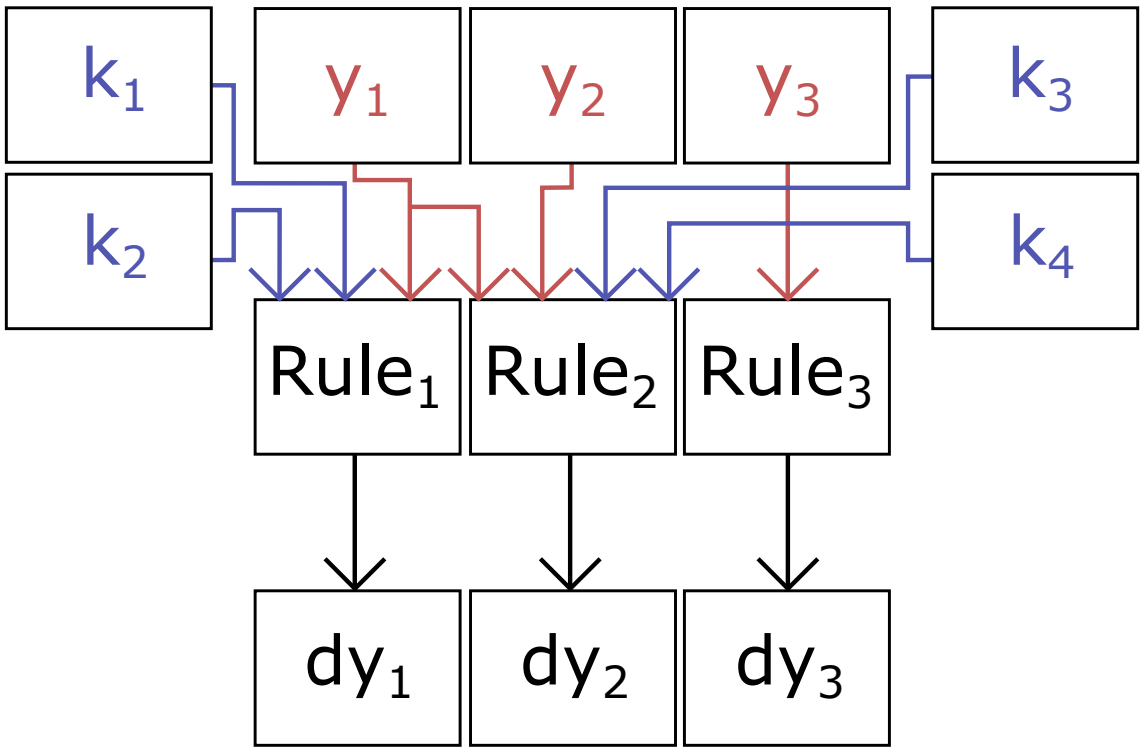

Figure 1.12: ***State variables (y_n in red) and ancillary parameters (k_n in blue) are used to inform the differential equations (Rule$_n$) which calculate a gradient (dy_n) for each state variable.***

There are two major challenges when designing geoscientific models such as the one described in Chapter 2. The first is establishing the initial conditions, boundary conditions and other ancillary parameters that are required. For this, models are reliant on existing observations of the Earth system. The second is establishing the rules which govern precisely how each component of the Earth system behaves as well as its interactions with other components. While much of the physics that governs these behaviours is known, the scale of the Earth system is immense and it is not feasible to simulate the Earth at the molecular scale. Instead, more generalised rules must be designed or discovered, which reduce the complexity of the system at the cost of decreased accuracy. The generalised rules may not represent all the dynamics which underlie the process in question, but should still reflect the behaviour of the system. Often, the generalised rules involve some form of parameterisation, which involves using ersatz parameters which may not have any physical meaning but

allow us to portray the system in a simplified way while retaining the appropriate behaviour.

Having now established what a numerical, forward model is and how to go about creating one, it is useful to introduce some potential behaviours and the associated terminology to describe model output. One of the main themes of thesis is the analysis of planetary stability through time. Planets with highly unstable climates would be expected to be barren, because the temperature would be expected to veer into and out of the habitable zone, or to experience a runaway progression putting the planet into an uninhabitable state. As such, it is necessary to be able to describe results from model output in terms of their propensity to promote or impede long term climate stability. In many cases, model results are compared either to a control run (which undergoes no forcing) or to a steady state assumption (meaning they are compared to a value that is not changing with time). If the results of a model run, or several model runs, tend to coalesce close to each other, the control run, or the initial condition, then they may be said to converge. Intuitively then, model runs in which the results split away from one another, the control run or the initial condition are said to diverge. Naturally convergence is typically indicative of climate stability and, by extension, habitability (assuming the initial condition is a habitable state). Rarely, parameters may be observed to neither converge nor diverge but instead run parallel to the reference condition. This would typically indicate that the variable in question is entirely a dependent property of the system. Finally, results from model output frequently show a variety of these behaviours depending on the timescale of the simulation. For example, a perturbation will typically cause the model results to initially diverge from the control run, but they may then begin to converge if simulated for a sufficient timescale. A behaviour that typifies this concept is the formation of oscillations. While the model output does not necessarily follow the control run, there is a pattern to the behaviour in that it repeats through time. Oscillations themselves may be either convergent (damped), divergent (growing) or stable. Figure 1.13 graphically depicts these different behaviours.

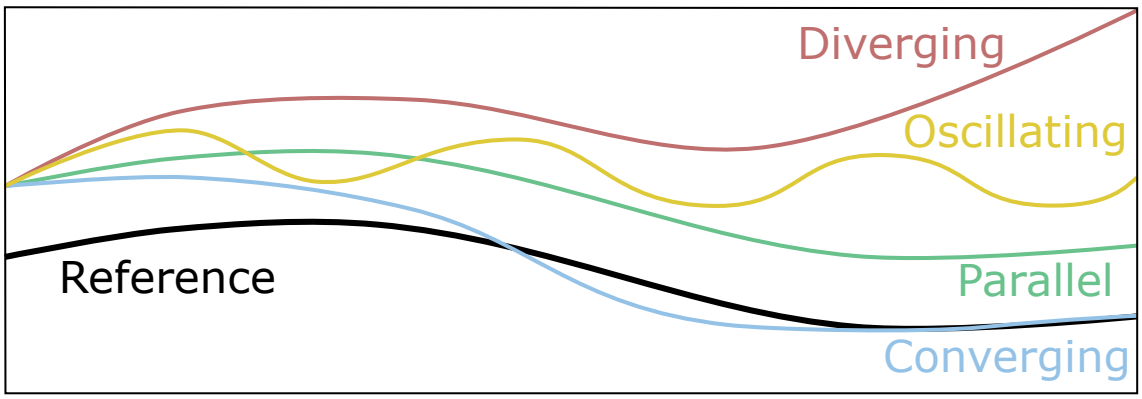

Figure 1.13: ***Making a change to model parameters may cause any of several behaviours. Here, some theoretical results from a reference run are shown in black alongside schematics of various system behaviour in red, blue, green and yellow. If the system is stabilised then it might be expected to follow a trajectory similar to the blue curve, which converges to the reference run, indicating that the evolution of the system is constrained. Alternatively, simulations may evolve along a line such as the red line, which completely diverges from the reference run, suggesting that the system is unstable.***

1.5.2 Outline of Extant Carbon Cycle Models

Existing models of the carbon cycle appropriate for palaeo work can be broadly split into two categories, those which are focussed on geological processes, and those which are focussed on shorter term carbon cycle drivers. Models focussing on geological processes, such as the BLAG (*Berner et al.*, 1983) and GEOCARB (*Berner*, 1991, 1994; *Berner* and *Kothavala*, 2001) models, are older and are centred around correlative parameterisations of carbon cycle fluxes. Extant models focussing on subgeological timescales include: CYCLOPS (*Keir*, 1988), LOSCAR (*Zeebe*, 2012), the JModels (*Chuck et al.*, 2005) and cGEnIE (*Ridgwell* and *Hargreaves*, 2007). Each of these models occupies its own niche (Figure 1.14) by incorporating different processes and representing some processes differently. A full description of each model, alongside the reasons why it was unsuitable for answering the questions underpinning this thesis, is presented in Appendix A. The GECCO model revitalises geological timescale modelling by introducing more realistic, mechanistic relationships between carbon reservoirs where possible, as well as adding new functionality specifically intended to represent long term carbon cycle processes. The most notable advantages of GECCO over preexisting models are:

- Incorporation of a geological cycle that links subduction of carbonaceous sediment to volcanic outgassing of CO_2
- A representation of carbonate uplift and weathering

- A representation of ice dynamics, which allows fluctuation in sea level to be represented
- Improvements to the carbonate chemistry and CSH calculation routines
- A closed carbon cycle on million year timescales
- Computational efficiency - GECCO is able to simulate $\sim$1Myr every 3 minutes (an MRR of 1.752×10^{11}) on a standard PC
- Bespoke user interface for model configuration

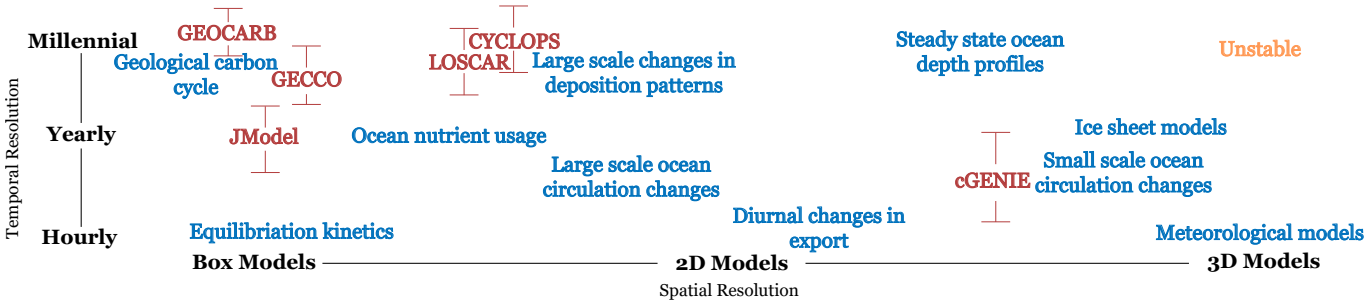

Figure 1.14: ***Models targetting different processes will occupy different spatiotemporal niches. Example processes of the correct spatiotemporal scale are shown in blue, alongside existing carbon cycle models used for palaeoclimate work in red. Most carbon cycle models are spatially simple, using a single globally averaged box or a series of boxes to represent different regions. There is a link between the spatial and temporal complexities, in that spatially complex processes often demand high temporal resolution, and processes which can be discretised into box model typically require low temporal resolution. Hence there is a cluster of carbon cycle models of low spatiotemporal complexity which are able to represent the pertinent climatic fluxes.***

The trend towards models of higher spatiotemporal resolution is a result of both an increase in the resolution of available data and in increase in available computer power. Simulating shorter intervals means the system can be simplified by ignoring very long term processes which would have a negligible impact on the results of the simulation. In contrast, when performing long timescale simulations it might be expected that short term fluxes would have to be included (though they may be parameterised). The carbon cycle has a fortuitous property, in that the reservoirs with the shortest response times also tend to be the smallest. Such reservoirs are able to drive rapid carbon cycle perturbations, however simply do not contain the mass of carbon required to drive a persistent long term carbon cycle trend in the absence of amplifying feedbacks. It is therefore possible to model long term carbon cycle drivers without incorporating much smaller and more responsive reservoirs. While there

are advantages to modelling on timescales of tens of thousands of years, especially for the representation of specific palaeo events, a holistic approach to investigation of carbon cycle behaviour would further improve understanding of the carbon cycle.

1.5.3 Role of GECCO

As discussed in Section 1.5.2, GECCO has several distinct advantages over previous existing models for understanding how the carbon cycle behaviour on multimillion year timescales. Generally speaking, GECCO is intended to be applied to a system which is mostly similar to Earth. This means that the system in question should be composed of connected atmospheric, hydrological and lithological reservoirs. While it is possible to alter or turn off many components of the model, care should be taken to ensure that the system mechanics are not so different from the Earth system that the model is not informative. Within the Earth system, GECCO is designed to have the flexibility to represent the planet as it was at any time during the past several billion years. In most cases, this is accomplished by simplification of carbon cycle fluxes. In this thesis, GECCO is set up to represent the Cenozoic carbon cycle, because this is the time during which most is known about the evolution of the climate. The carbon cycle has undergone several fundamental changes through Earth history, one such example of which is the evolution of pelagic calcifiers. Development of a substantial carbon flux to deep sea sediments resulted in a shift in carbonate burial away from the neritic environment and into the pelagic realm (*Ridgwell* and *Zeebe*, 2005). GECCO is able to represent changes such as this by allowing the specification of controlling factors on the fluxes of pelagic and neritic calcification.

1.6. The Cenozoic

1.6.1 Introduction

Understanding of the carbon cycle and knowledge of how to model it must be combined with palaeoclimate data, to tune the model to realistic values, test the behaviour of the model, and to give simulations a target. Palaeo carbon cycle and climate information is predominantly based on proxy datasets. A proxy is one value which can be used to represent another - in this context an example is a measurement of something which has been preserved in the geological record that gives information about atmospheric CO_2 concentration in the past. Ideally, each proxy measurement would unambiguously relate to a single climate parameter, but in reality proxies are often contaminated by noise, or represent some combination of two or more climate signals. Proxies are therefore subject to a level of compromise between the

amount of information encoded by a proxy and the ambiguity in the proxy driver. One solution to the problem is to use a multiproxy approach to deconvolve multiple climate signals (such as done in *Lear et al.* (2000)) but this can be technically difficult and is only possible with appropriate information for a series of proxies that can be combined to isolate individual climate signals. There are several isotope systems currently in use for palaeo work, but these are only able to reconstruct a few key climate variables, such as temperature, atmospheric CO_2 concentration, global ice volume and water dynamics. More proxies may be discovered in future which will expand the available palaeoclimate investigation arsenal, but there are many climate parameters for which there is currently no foreseeable method of reconstruction in the geological past. Below, a series of the most common proxy systems used for carbon cycle interpretation are presented.

1.6.2 CO_2

Central to this work is the palaeo CO_2 dataset. For palaeo work in the past $\sim$1Myr, it is possible to directly measure atmospheric CO_2 using gas bubbles trapped in polar ice (*Bereiter et al.*, 2014). In the deeper past, atmospheric CO_2 can not be directly measured, so it is necessary to use a proxy. There are four primary classes of palaeo CO_2 proxy - two marine methods: boron isotopes and δ^{13}C of marine organisms (specifically alkenones and phytane), and two terrestrial methods: analysis of fossil leaves and palaeosols (*Hollis et al.*, 2019). Some of these methods are subdivided into more specific categories, based on the particular kind of analysis that is run or the methodology applied to the proxy data. Two of the categories, boron isotopes and palaeosols, are based on a mechanistic understanding of the link between CO_2 and the proxy record (*Hollis et al.*, 2019). Leaf proxies are more variable, with earlier methods being qualitative, and newer methods using a more mechanistic understanding (*Beerling* and *Royer*, 2002; *McElwain*, 2004; *Franks* and *Beerling*, 2009). Finally there is the δ^{13}C of alkenones which have in the past sought a mechanistic understanding, but currently use correlative observations to predict palaeo atmospheric CO_2 (*Pagani*, 2002).

As shown in Figure 1.15, CO_2 proxies record concentrations of $\sim$600ppm in the earliest Cenozoic, which rise to peak values of $\sim$1000ppm during the Eocene, then fall to values of $\sim$300ppm in the Preindustrial. Overprinting this broad trend are a multitude of carbon cycle perturbations and shorter term trends. The long term trend is robust, as it is recorded by numerous proxy methodologies, however the magnitude of change may be magnified

or dampened depending on which records are thought to be the most accurate. CO_2 reconstructions during short intervals often disagree (both using the same and different proxy systems). Each method has associated assumptions and potential pitfalls that could result in this disagreement, so it can be difficult to ascertain the exact reason for the disagreement or establish which proxy, if any, is producing the most accurate reconstruction. There are ongoing efforts to improve the record of palaeo atmospheric CO_2, especially within the Cenozoic (*Beerling* and *Royer*, 2011; *Foster et al.*, 2017). Some of these efforts focus on compilation and analysis of existing data, whereas others focus on improving the understanding of the how the proxy functions, and further efforts look to validate each proxy against modern day or ice core CO_2 concentrations (*Seki et al.*, 2010; *Martinez-Boti et al.*, 2015). Each of these represents somewhat of a moving target, as new data is created, new understanding is forged, and improved methods and technology become available.

As it currently stands, boron has undergone comparatively extensive comparison to ice core records (*Seki et al.*, 2010; *Martinez-Boti et al.*, 2015), but this has not yet occurred with other CO_2 proxies (though this is imminent for the alkenone proxy (*Badger et al.*, 2018)). It is not always feasible to generate proxy data in such a way that it can be meaningfully compared to ice core records. For example, palaeosols are thought to exhibit greater sensitivity at higher CO_2 concentrations, and are believed to integrate CO_2 concentrations over the timescale of their formation (on the order of thousands of years (*Hollis et al.*, 2019)), meaning it's not necessarily feasible to compare directly to ice core records. In order to reconstruct glacial-interglacial cycles, the proxy in question needs to be able to reconstruct $\sim$100ppm of CO_2 variability on timescales of tens of thousands of years. Given the boron proxy has been validated against ice core records, it is also possible to perform interproxy comparisons (for example between boron and alkenones, such as in *Badger et al.* (2018)) to extend our validation ability. This can feasibly increase the effective CO_2 range of validation, as well as extending the ability to validate back further in time. This opens the ability to perform a kind of 'proxy validation relay', by exploring periods where there is overlap between records.

One of the main areas where proxy work could improve current understanding is in Paleocene, where proxies appear to be recording low CO_2 concentrations (Figure 1.15) during a time thought to be particularly warm (*Thomas et al.*, 2000). This disconnect between temperature and atmospheric CO_2 is not yet robust, as it must be made certain that the proxies for both CO_2 and temperature are accurately reflecting global conditions at the time, however

is particularly important for establishing the initial conditions of models designed to replicate Cenozoic carbon cycle trends, such as done in this thesis. Despite any shortcomings of the existing data, the long term trend is well constrained, so for the purposes of this work it forms an ideal dataset.

There are several existing hypotheses to explain the long term trend in atmospheric CO_2 concentration observed through the Cenozoic:

- Growth of the deep sea sediment carbon reservoir due to formation of the Atlantic basin (*Edmond* and *Huh*, 2003).
- An increase in silicate weatherability driven by orogeny in the Himalayas (*Raymo* and *Ruddiman*, 1992).
- Changes in plate tectonics resulting in variations in CO_2 outgassing fluxes (*Owen* and *Rea*, 1985).
- Changes to the oceanic carbonate system, which affect the destiny of carbon delivered to the ocean.
- Formation of LIP's which release carbon magmatically, but also change silicate weathering fluxes (*Jones et al.*, 2016).
- Individual events (such as the Paleocene Eocene Thermal Maximum and Eocene-Oligocene Transition) meaningfully altered the climate trajectory.

These hypotheses mostly revolve around potential changes to the source or sink of CO_2 from the atmosphere. While the direction of change in atmospheric CO_2 concentration driven by any one of the factors listed above might be predictable, quantifying the impact of one (or more) drivers in the context of a dynamic climate system requires complex mathematical calculations.

1.6.3 δ^{18}O and δ^{13}C

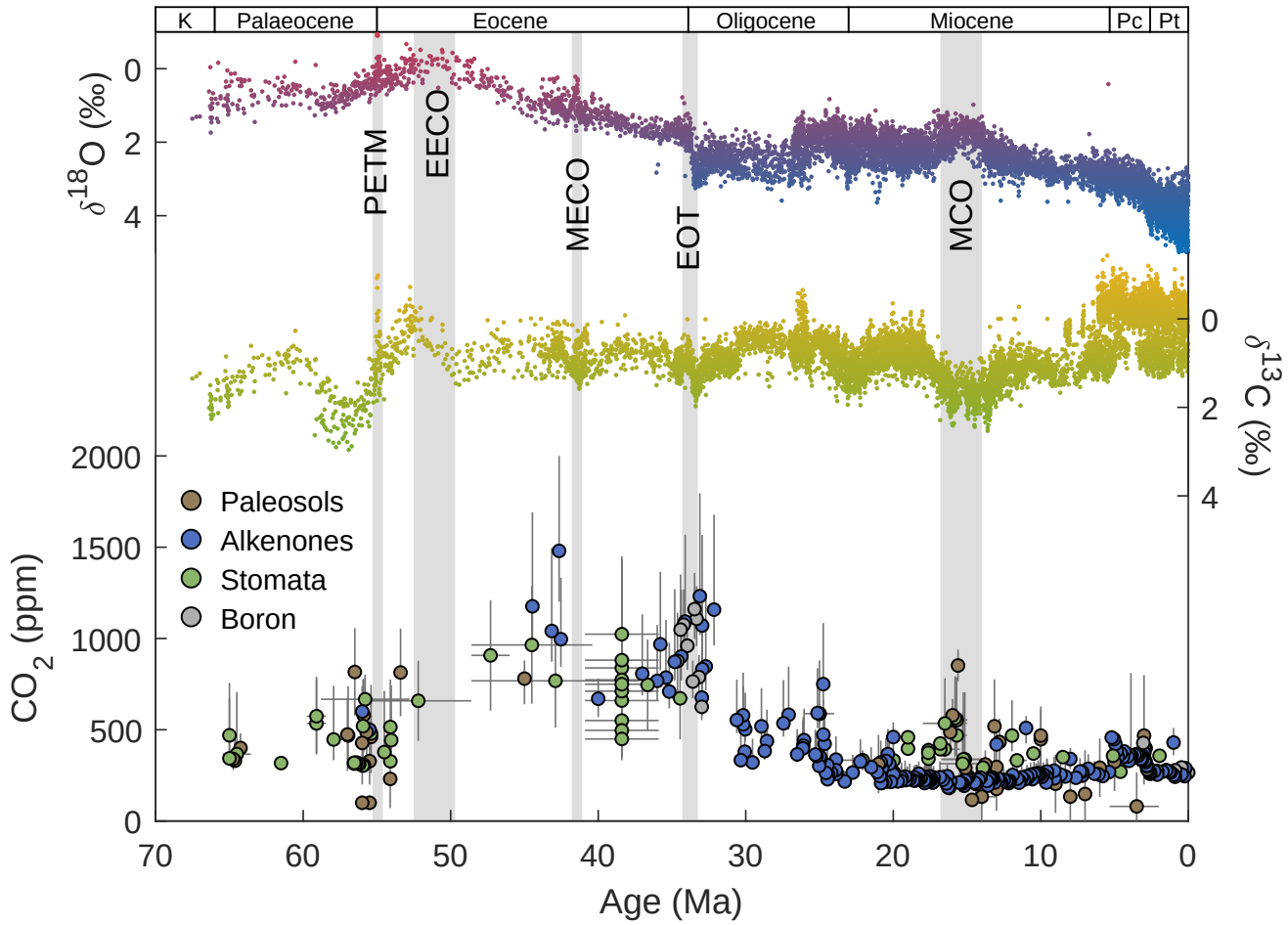

Figure 1.15: ***δ^{18}O, shown in red/blue (blue for colder/more ice, red for warmer/less ice) in the uppermost panel (*Zachos et al.*, 2001), has experienced a gradual increase over the Cenozoic, indicating some combination of ice growth and cooling. δ^{13}C, shown in green/yellow (perturbations towards yellow are typically inferred as carbon release to the atmosphere) in the central panel, has no long term trend (*Zachos et al.*, 2001). The final panel displays atmospheric CO_2 data from* Foster et al. *(2017), which shows a rise from the Paleocene into the Eocene, then a gradual fall to the Preindustrial value.***

By far the most densely populated palaeo datasets are those of oxygen (δ^{18}O) and carbon (δ^{13}C) isotopes (Figure 1.15). δ^{18}O is used as proxy for both temperature and sea level, where heavier δ^{18}O signatures correlate with greater ice volumes and lower temperatures. Benthic records show values of $\sim$0‰ during the warmest intervals in the Cenozoic and $\sim$5‰ during the coldest intervals (Figure 1.15). The largest rapid change in δ^{18}O occurs at the Eocene-Oligocene Transition, around 35Ma (Figure 1.15).

δ^{13}C is used as a proxy for carbon cycle behaviour. Negative perturbations in δ^{13}C (i.e. a lightening of the atmospheric carbon reservoir) are often used to infer a carbon release to the atmosphere. Large δ^{13}C perturbations are known throughout the Cenozoic, with the most notable examples occurring at the Paleocene-Eocene Thermal Maximum (PETM), Eocene-Oligocene Transition (EOT) and Miocene Climatic Optimum (MCO) (Figure 1.15). Events such as these are often expressed by both δ^{18}O and δ^{13}C records, indicating they are combined carbon cycle-climate events (*Kirtland Turner* and *Ridgwell*, 2016).

1.6.4 Carbonate Compensation Depth

Some of the earliest available CCD records are those of *van Andel* (1975), who presented a CCD record for each major basin. The broad scale picture of the records presented in *van Andel* (1975) is of a comparatively shallow CCD during the Eocene (at ~3km depth), which deepened significantly at the EOT, shoaled during the Miocene, then deepened again into the Preindustrial, where it reached ~4.5km depth (global average). Additional records (shown in Figure 1.16) have refined this picture, but have not changed the broad scale trend first shown by *van Andel* (1975).

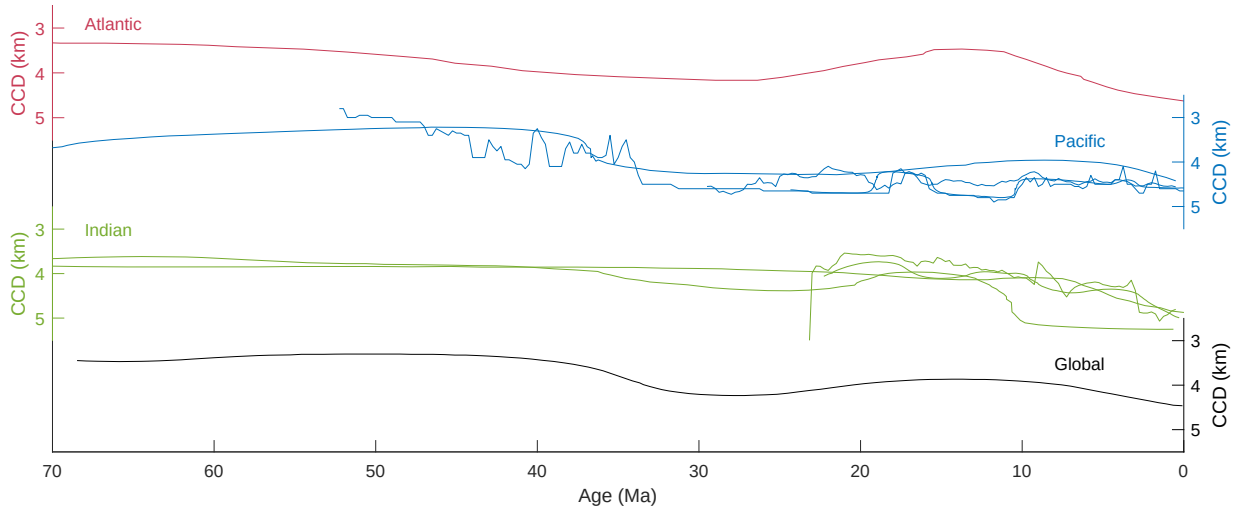

Figure 1.16: ***Estimates for the CCD across a variety of basins are compiled here from* van Andel *(1975),* Sclater *and* Abbott *(1977),* Delaney *and* Boyle *(1988),* Peterson *and* Backman *(1990),* Lyle *(2003),* Pälike et al. *(2012) and* Campbell et al. *(2018).***

Caution must be taken when interpreting sedimentary records to calculate a CCD. While it is immediately appealing to use physical core records to identify the CCD, this does not necessarily translate into deflections in the CSH or changes in carbon burial fraction. The interpretation of a CCD from carbonate fraction data is generally based on finding the deepest location where carbonate is preserved, however often there is not a clear transition from

carbonate rich sediment to carbonateless sediment. It is important to remember that many of these CCD records represent a single basin, and are not necessarily representative of the global CCD change. Additional complications include changes in productivity, the calculation of palaeodepth, and condensing of a three dimensional plane into a single value for an entire basin. Overall, these complications mean that existing records of the CCD over the Cenozoic should be interpretted qualitatively rather than quantitatively. Relative to the present day, the shallower CCD and higher CO_2 concentrations inferred for the Paleocene suggest a lower ocean pH. Care must be taken when interpretting the record in this way, however, as other factors that influence the CCD (such as major ion ocean composition) are known to have changed. This serves to highlight the need for an integrated approach to understand CCD behaviour.

1.6.5 pH

Boron isotopes in foraminiferal calcite are a proxy for ocean pH (*Rae et al.*, 2011). This proxy is typically used to calculate CO_2 by assumption of a second carbonate system parameter. The translation of δ^{11}B to palaeo pH requires several assumptions and ancillary data, especially so for the more distant past. Given the CO_2 derived from the boron proxy has been validated against ice core CO_2 records, there is good reason to believe that the proxy records the correct ocean pH even in deeper time. This is therefore a mostly independent method of extracting information about the behaviour of the carbonate system in the geological past. Alternatively palaeo pH may be calculated by quantifying the whole carbonate system by using two other parameters (such as done by *Tyrrell* and *Zeebe* (2004) and *Boudreau et al.* (2019)). Generally speaking, these methods of quantifying ocean pH find that there has been a rise on the order of 0.6 units over the Cenozoic, so there is the beginning of a consistent history of the carbonate system from 60Ma to present. This is extremely important as a target for model simulations, as it allows quantification of both degrees of freedom of the carbonate system.

1.6.6 Temperature

Temperature proxies can be drawn from multiple lines of evidence, including palaeontological and palaeopalynological data, as well as δ^{18}O (*Zachos et al.* 1994;*Zachos et al.* 2001) and other geochemical measurements (*Lear et al.*, 2000; *Conte et al.*, 2006; *Tierney* and *Tingley*, 2014). These suggest that temperature has fallen over the Cenozoic, roughly in line with the long term CO_2 trend. The temperature curve might be expected to exactly follow the same evolution as atmospheric CO_2, however additional factors such as changes in palaeogeography, planetary albedo and solar energy output also affect Earth's energy balance. The magnitude of temperature fall is difficult to quantify, as it is highly variable across the globe, and changes in temperature are not globally uniform. One way of obfuscating this is to focus on deep sea records, which integrate the global signal on thousand year timescales. Methods such as this suggest roughly 10°C of temperature fall from 66Ma to present (*Lear et al.*, 2000; *Hansen et al.*, 2013).

As with CO_2, there is currently an ongoing project specifically seeking to integrate existing data to produce a global temperature curve covering the Cenozoic and earlier. This will greatly improve the understanding of how temperature has evolved on long timescales, and its relationship to atmospheric CO_2.

1.7. Cenozoic Summary

The datasets most relevant to answering questions about carbon cycle behaviour during the Cenozoic are summarised above. Overall, the long term picture of the Cenozoic is predominantly one of falling atmospheric CO_2 concentration, deepening CCD and decreasing global temperature. Existing estimates of carbon cycle fluxes and reservoir sizes, both in the present day and in the past, have been compiled in Figure 1.17.

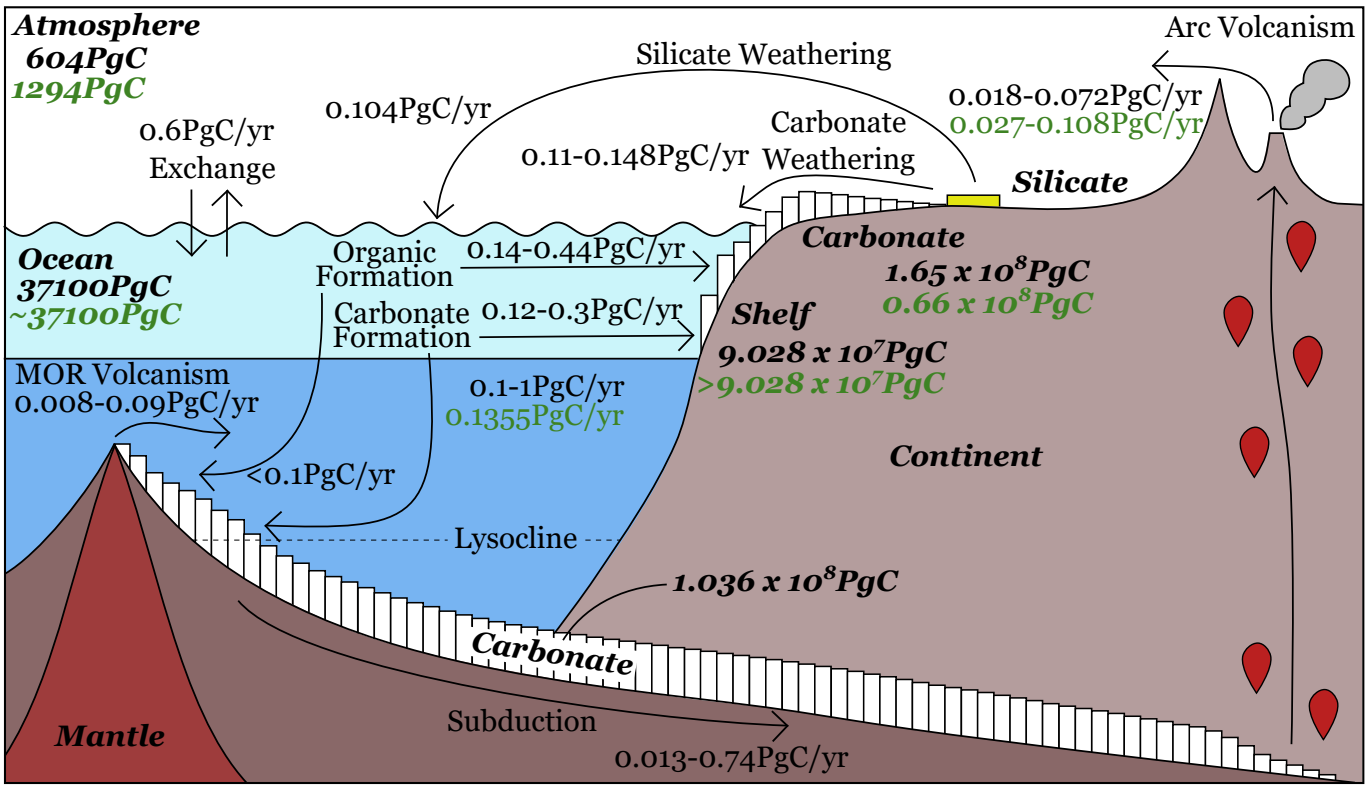

Figure 1.17: ***Estimated reservoir sizes (bold italic) and flux magnitudes (regular font) for the carbon cycle in the present day (black) and earliest Cenozoic where available (green). Where more than one estimate is available, the minimum and maximum values are presented. These estimates come from a wide array of literature resources, listed here in order of contribution:*** **Kelemen *and* Manning *(2015);* Dasgupta *and* Hirschmann *(2010);* Sabine et al. *(2004);* Foster et al. *(2017);* Opdyke *and* Wilkinson *(1988);* Ridgwell *and* Zeebe *(2005);* Hay et al. *(1988);* Rea *and* Ruff *(1996);* Gaillardet et al. *(1999);* Liu *and* Zhao *(2000);* Morse *and* Mackenzie *(1990);* Van Der Meer et al. *(2014).***

1.8. Thesis Aims

Given this combination of carbon cycle, modelling, and Cenozoic climate trends, the broad questions outlined in Section 1.3 can be refined to more specific hypotheses that inform the broader questions this thesis seeks to address. These questions focus on evaluating the potential impact of external (or 'chance') climate drivers.

1. How resistant is the climate to 'chance' forcings?

2. Can any potential carbon cycle drivers be deemed unimportant on Cenozoic timescales?

3. Could realistic external forcing lead to climates inimical to life?

1.9. Thesis Structure

This thesis aims to improve current understanding of the Cenozoic carbon cycle by focussing on the long term processes that control atmospheric CO_2. There have been several external drivers which are thought to have influenced the carbon cycle over the Cenozoic (see Section 1.6.2), however the magnitude of their impact is difficult to ascertain. By analysing individual drivers and the climatic response to them, this thesis will aim to establish how contingent the long term carbon cycle is on previous climate states. Chapter 1 introduced the concept of modelling, the behaviour of the carbon cycle, and the observations available to constrain the results of that behaviour during the Cenozoic. Chapter 2 details the development of the new carbon cycle model that is the primary methodology used in this thesis. Chapter 3 and Chapter 4 apply the newly developed model to understand the impact of changes in ocean composition and changes in tectonic parameters respectively. A synthesis of these results and the conclusions that can be drawn are presented in Chapter 5.

References

Anagnostou, E., John, E. H., Edgar, K. M., Foster, G. L., Ridgwell, A., Inglis, G. N., Pancost, R. D., Lunt, D. J., and Pearson, P. N., 2016, Changing atmospheric CO_2 concentration was the primary driver of early Cenozoic climate, *Nature*, **533**(7603), 380–384.

Archer, D., Winguth, A., Lea, D., and Mahowald, N., 2000, What caused the glacial/interglacial atmospheric pCO_2 cycles? *Reviews of Geophysics*, **38-2**(1999), 159–189.

Armstrong McKay, D. I., and Lenton, T. M., 2018, Reduced Carbon Cycle Resilience across the Palaeocene-Eocene Thermal Maximum, *Climate of the Past Discussions*, **14**, 1–19.

Badger, M., Chalk, T. B., Foster, G. L., Bown, P. R., Gibbs, S. J., Sexton, P., Schmidt, D. N., Pälike, H., Mackensen, A., and Pancost, R. D., 2018, Insensitivity of alkenone carbon isotopes to atmospheric CO_2 at low to moderate CO_2 levels, *Climate of the Past Discussions*, 1–30.

Beerling, D., and Royer, D., 2002, Reading a CO_2 signal from fossil stomata, *New Phytologist*, **153**, 387–397.

Beerling, D. J., and Royer, D. L., 2011, Convergent Cenozoic CO_2 history, *Nature Geoscience*, **4**(7), 418–420.

Ben-Yaakov, S., and Goldhaber, M. B., 1973, The influence of sea water composition on the apparent constants of the carbonate system, *Deep-Sea Research and Oceanographic Abstracts*, **20**(1), 87–99.

Bereiter, B., Eggleston, S., Schmitt, J., Nehrbass-Ahles, C., Stocker, T. F., Fischer, H., Kipfstuhl, S., and Chappellaz, J., 2014, Revision of the EPICA Dome C CO_2 record from 800 to 600 kyr before present, *Geophysical Research Letters*, **42**(2), 542–549.

Berner, R. A., 1991, A model for atmospheric CO_2 over Phanerozoic time, *American Journal of Science*, **291**(4), 339–376.

Berner, R. A., 1994, GEOCARB II: a revised model of atmospheric CO_2 over Phanerozoic time, *American Journal of Science*, **294**(1), 56–91.

Berner, R. A., and Caldeira, K., 1997, The need for mass balance and feedback in the geochemical carbon cycle, *Geology*, **25**, 955–956.

Berner, R. A., and Kothavala, Z., 2001, GEOCARB III: A revised model of atmospheric CO_2 over Phanerozoic time, *American Journal of Science*, **301**(2), 182–204.

Berner, R. A., Lasaga, A. C., and Garrels, R. M., 1983, Carbonate-silicate geochemical cycle and its effect on atmospheric carbon dioxide over the past 100 million years, *American*

Journal of Science, **283**(7), 641–683.

Boudreau, B. P., Middelburg, J. J., Sluijs, A., and Ploeg, R., 2019, Secular Variations in the Carbonate Chemistry of the Oceans over the Cenozoic, *Earth and Planetary Science Letters*, **512**, 194–206.

Brasier, M. D., Green, O. R., Jephcoat, A. P., Kleppe, A. K., Kranendonk, M. J. V., Lindsay, J. F., Steele, A., and Grassineau, N. V., 2002, Questioning the evidence for Earth's oldest fossils, *Nature*, **416**, 76–81.

Buesseler, K. O., Benitez-Nelson, C. R., Moran, S. B., Burd, A., Charette, M., Cochran, J. K., Coppola, L., Fisher, N. S., Fowler, S. W., Gardner, W. D., Guo, L. D., Gustafsson, Ö., Lamborg, C., Masque, P., Miquel, J. C., Passow, U., Santschi, P. H., Savoye, N., Stewart, G., and Trull, T., 2006, An assessment of particulate organic carbon to thorium-234 ratios in the ocean and their impact on the application of ^{234}Th as a POC flux proxy, *Marine Chemistry*, **100**(3-4), 213–233.

Campbell, S. M., Moucha, R., Derry, L. A., and Raymo, M. E., 2018, Effects of Dynamic Topography on the Cenozoic Carbonate Compensation Depth, *Geochemistry, Geophysics, Geosystems*, 1025–1034.

Charette, M. A., and Moran, S. B., 1999, Rates of particle scavenging and particulate organic carbon export estimated using ^{234}Th as a tracer in the subtropical and equatorial Atlantic Ocean, *Deep Sea Research Part II: Topical Studies in Oceanography*, **46**, 885–906.

Chuck, A., Tyrrell, T., Totterdell, I., and Holligan, P., 2005, The oceanic response to carbon emissions over the next century: investigation using three ocean carbon cycle models, *Tellus B*, **57**(B), 70–86.

Conte, M. H., Sicre, M.-A., Rühlemann, C., Weber, J. C., Sonja, S., Schulz-Bull, D., and Blanz, T., 2006, Global temperature calibration of the alkenone unsaturation index (U^K_{37}) in surface waters and comparison with surface sediments, *Geochemistry, Geophysics, Geosystems*, **7**(2), 1–22.

Cui, Y., Kump, L., Ridgwell, A. J., Charles, A. J., Junium, C. K., Diefendorf, A. F., Freeman, K. H., Urban, N. M., and Harding, I. C., 2011, Slow release of fossil carbon during the Palaeocene-Eocene Thermal Maximum, *Nature Geoscience*, **4**(7), 481–485.

Dasgupta, R., and Hirschmann, M. M., 2010, The deep carbon cycle and melting in Earth's interior, *Earth and Planetary Science Letters*, **298**(1-2), 1–13.

Davies, J. H., and Stevenson, D. J., 1992, Physical model of source region of subduction zone volcanics, *Journal of Geophysical Research: Solid Earth*, **97**(B2), 2037–2070.

Delaney, M. L., and Boyle, E. A., 1988, Tertiary paleoceanic chemical variability: Unintended

consequences of simple geochemical models, *Paleoceanography*, **3**(2), 137–156.

Dewey, J. F., 1976, Ophiolite obduction, *Tectonophysics*, **31**(1-2), 93–120.

Dunne, J. P., Sarmiento, J. L., and Gnanadesikan, A., 2007, A synthesis of global particle export from the surface ocean and cycling through the ocean interior and on the seafloor, *Global Biogeochemical Cycles*, **21**(4), 1–16.

Edmond, J. M., and Huh, Y., 2003, Non-steady state carbonate recycling and implications for the evolution of atmospheric PCO_2, *Earth and Planetary Science Letters*, **216**, 125–139.

Follows, M. J., Ito, T., and Dutkiewicz, S., 2006, On the solution of the carbonate chemistry system in ocean biogeochemistry models, *Ocean Modelling*, **12**(3-4), 290–301.

Foster, G. L., Royer, D. L., and Lunt, D. J., 2017, Future climate forcing potentially without precedent in the last 420 million years, *Nature Communications*, **8**, 1–8.

Franks, P. J., and Beerling, D. J., 2009, Maximum leaf conductance driven by CO_2 effects on stomatal size and density of geologic time, *Proceedings of the National Academy of Sciences*, **106**(25), 10343–10347.

Gaillardet, J., Dupré, B., Louvat, P., and Allegre, C., 1999, Global silicate weathering and CO_2 consumption rates deduced from the chemistry of large rivers, *Chemical Geology*, **159**, 3–30.

Grand, S. P., 2002, Mantle shear-wave tomography and the fate of subducted slabs, *Philosophical Transactions of the Royal Society A: Mathematical, Physical and Engineering Sciences*, **360**(1800), 2475–2491.

Gutjahr, M., Ridgwell, A., Sexton, P. F., Anagnostou, E., Pearson, P. N., Pälike, H., Norris, R. D., Thomas, E., and Foster, G. L., 2017, Very large release of mostly volcanic carbon during the Palaeocene-Eocene Thermal Maximum, *Nature*, **548**(7669), 573–577.

Hain, M. P., Sigman, D. M., Higgins, J. A., and Haug, G. H., 2015, The effects of secular calcium and magnesium concentration changes on the thermodynamics of seawater acid/base chemistry: Implications for Eocene and Cretaceous ocean carbon chemistry and buffering, *Global Biogeochemical Cycles*, 517–533.

Hansen, J., Sato, M., Russell, G., and Kharecha, P., 2013, Climate sensitivity, sea level and atmospheric carbon dioxide, *Philosophical Transactions of the Royal Society A*, **371**, 1–31.

Hartnett, H., Keil, R., Hedges, J., and Devol, A., 1998, Influence of oxygen exposure time on organic carbon preservation in continental margin sediments, *Nature*, **391**(February), 572–575.

Hay, W. W., Sloan, J. L., and Wold, C. N., 1988, Mass/Age Distribution and Composition

of Sediments on the Ocean Floor Drilling Project to estimate, *Journal of Geophysical Research*, **93**(B12), 14933–14940.

Hayes, G. P., Wald, D. J., and Johnson, R. L., 2012, Slab1.0: A three-dimensional model of global subduction zone geometries, *Journal of Geophysical Research: Solid Earth*, **117** (1), 1–15.

Hollis, C. J., Dunkley Jones, T., Anagnostou, E., Bijl, P. K., Cramwinckel, M. J., Cui, Y., Dickens, G. R., Edgar, K. M., Eley, Y., Evans, D., Foster, G. L., Frieling, J., Inglis, G. N., Kennedy, E. M., Kozdon, R., Lauretano, V., Lear, C. H., Littler, K., Meckler, N., Naafs, B. D. A., Pälike, H., Pancost, R. D., Pearson, P., Royer, D. L., Salzmann, U., Schubert, B., Seebeck, H., Sluijs, A., Speijer, R., Stassed, P., Tierney, J., Tripati, A., Wade, B., Westerhold, T., Witkowski, C., Zachos, J. C., Zhang, Y. G., Huber, M., and Lunt, D. J., 2019, The DeepMIP contribution to PMIP4: methodologies for selection, compilation and analysis of latest Paleocene and early Eocene climate proxy data, incorporating version 0.1 of the DeepMIP database, *Geoscientific Model Development Discussions*, 1–98.

Jahnke, R. A., 1996, The global ocean flux of particulate organic carbon: Areal distribution and magnitude, *Global Biogeochemical Cycles*, **10**(1), 71–88.

Jones, M. T., Jerram, D. A., Svensen, H. H., and Grove, C., 2016, The effects of large igneous provinces on the global carbon and sulphur cycles, *Palaeogeography, Palaeoclimatology, Palaeoecology*, **441**, 4–21.

Keeling, C., Whorf, T., Wahlen, M., and Plicht, J., 1995, Interannual extremes in the rate of rise of atmospheric carbon dioxide since 1980, *Nature*, **375**(6533), 666–670.

Keir, R. S., 1988, On the Late Pleistocene ocean geochemistry and circulation, *Paleoceanography*, **3**(4), 413.

Kelemen, P. B., and Manning, C. E., 2015, Reevaluating carbon fluxes in subduction zones, what goes down, mostly comes up, *Proceedings of the National Academy of Sciences*, **112**(30), E3997–E4006.

Kerrick, D. M., and Connelly, J. A., 2001, Metamorphic devolatilization of subducted marine sediments and the transport of volatiles into the Earth's mantle, *Nature*, **411**(6835), 293–296.

Kessel, R., Schmidt, M. W., Ulmer, P., and Pettke, T., 2005, Trace element signature of subduction-zone fluids, melts and supercritical liquids at 120-180 km depth, *Nature*, **437** (7059), 724–727.

Kirtland Turner, S., and Ridgwell, A., 2016, Development of a novel empirical framework for interpreting geological carbon isotope excursions, with implications for the rate of carbon

injection across the PETM, *Earth and Planetary Science Letters*, **435**, 1–13.

Knauth, L. P., Burt, D. M., and Wohletz, K. H., 2005, Impact origin of sediments at the Opportunity landing site on Mars, *Nature*, **438**(7071), 1123–1128.

Kopparapu, R. K., Ramirez, R., Kasting, J. F., Eymet, V., Robinson, T. D., Mahadevan, S., Terrien, R. C., Domagal-Goldman, S., Meadows, V., and Deshpande, R., 2013, Habitable zones around main-sequence stars: New estimates, *Astrophysical Journal*, **765**(2).

Kump, L., Kasting, J., and Crane, R., 2009, *The Earth System*, Pearson Prentice Hall, Upper Saddle River, New Jersey, 3rd edition.

Lear, C. H., Elderfield, H., and Wilson, P., 2000, Cenozoic Deep-Sea Temperatures and Global Ice Volumes from Mg/Ca in Benthic Foraminiferal Calcite, *Science*, **287**(5451), 269–272.

Liu, Z., and Zhao, J., 2000, Contribution of carbonate rock weathering to the atmospheric CO_2 sink, *Environmental Geology*, **39**(9), 1053–1058.

Liu, Z., Dreybrodt, W., and Liu, H., 2011, Atmospheric CO_2 sink: Silicate weathering or carbonate weathering? *Applied Geochemistry*, **26**, 292–294.

Lyle, M., 2003, Neogene carbonate burial in the Pacific Ocean, *Paleoceanography*, **18**(3), 1–19.

Martinez-Boti, M., Marine, G., Foster, G., Ziveri, P., Henehan, M., Rae, J., Mortyn, P., and Vance, D., 2015, Boron isotope evidence for oceanic carbon dioxide leakage during the last deglaciation, *Nature*, **518**(7538), 219–222.

Mason, E., Edmonds, M., and Turchyn, A. V., 2017, Remobilization of crustal carbon may dominate volcanic arc emissions, *Geochemistry*, **294**(July), 290–294.

McElwain, J. C., 2004, Climate-independent paleoaltimetry using stomatal density in fossil leaves as a proxy for CO_2 partial pressure, *Geology*, **32**(12), 1017–1020.

McInerney, F. A., and Wing, S. L., 2011, The Paleocene-Eocene Thermal Maximum: A Perturbation of Carbon Cycle, Climate, and Biosphere with Implications for the Future, *Annual Review of Earth and Planetary Sciences*, **39**(1), 489–516.

Menzies, C. D., Wright, S. L., Craw, D., James, R. H., Alt, J. C., Cox, S. C., Pitcairn, I. K., and Teagle, D. A., 2018, Carbon dioxide generation and drawdown during active orogenesis of siliciclastic rocks in the Southern Alps, New Zealand, *Earth and Planetary Science Letters*, **481**, 305–315.

Mojzsis, S. J., Arrhenius, G., McKeegan, K. D., Harrison, T. M., Nutman, A. P., and Friend, C. R., 1996, Evidence for life on Earth before 3,800 million years ago, *Nature*, **384**(6604), 55–59.

Morse, J. W., and Mackenzie, F. T., 1990, Sedimentary Carbonate in the Evolution of Earth's Surface Environment In *Developments in Sedimentology*,, 511–598.

Opdyke, B. N., and Wilkinson, B. H., 1988, Surface area control of shallow cratonic to deep marine carbonate accumulation, *Paleoceanography*, **3**(6), 685–703.

Owen, R. M., and Rea, D. K., 1985, Sea-floor hydrothermal activity links climate to tectonics: The Eocene carbon dioxide greenhouse, *Science*, **227**(4683), 166–169.

Pagani, M., 2002, The alkenone-CO_2 proxy and ancient carbon dioxide, *Philosophical Transactions of the Royal Society A*, **360**, 609–632.

Pälike, H., Lyle, M. W., Nishi, H., Raffi, I., Ridgwell, A., Gamage, K., Klaus, A., Acton, G., Anderson, L., Backman, J., Baldauf, J., Beltran, C., Bohaty, S. M., Bown, P., Busch, W., Channell, J. E. T., Chun, C. O. J., Delaney, M., Dewangan, P., Dunkley Jones, T., Edgar, K. M., Evans, H., Fitch, P., Foster, G. L., Gussone, N., Hasegawa, H., Hathorne, E. C., Hayashi, H., Herrle, J. O., Holbourn, A., Hovan, S., Hyeong, K., Iijima, K., Ito, T., Kamikuri, S.-i., Kimoto, K., Kuroda, J., Leon-Rodriguez, L., Malinverno, A., Moore Jr, T. C., Murphy, B. H., Murphy, D. P., Nakamura, H., Ogane, K., Ohneiser, C., Richter, C., Robinson, R., Rohling, E. J., Romero, O., Sawada, K., Scher, H., Schneider, L., Sluijs, A., Takata, H., Tian, J., Tsujimoto, A., Wade, B. S., Westerhold, T., Wilkens, R., Williams, T., Wilson, P. A., Yamamoto, Y., Yamamoto, S., Yamazaki, T., and Zeebe, R. E., 2012, A Cenozoic record of the equatorial Pacific carbonate compensation depth, *Nature*, **488**(7413), 609–614.

Panchuk, K., Ridgwell, A., and Kump, L. R., 2008, Sedimentary response to Paleocene-Eocene thermal maximum carbon release: A model-data comparison, *Geology*, **36**(4), 315–318.

Paterson, S. R., and Tobisch, O. T., 1992, Rates of processes in magmatic arcs: implications for the timing and nature of pluton emplacement and wall rock deformation, *Journal of Structural Geology*, **14**(3), 291–300.

Peacock, S. M., and Wang, K., 1999, Seismic consequences of warm versus cool subduction metamorphism: Examples from southwest and northeast Japan, *Science*, **286**(5441), 937–939.

Pearce, J., and Peate, D., 1995, Tectonic Implications of Volcanic Arc Magmas, *Annual Review of Earth and Planetary Sciences*, **23**, 251–285.

Pedersen, T., and Calvert, S., 1990, Anoxia vs. Productivity: What Controls the Formation of Organic-Carbon-Rich Sediments and Sedimentary Rocks? *AAPG Bulletin*, **4**(74), 454–466.

Penman, D. E., and Zachos, J. C., 2018, New constraints on massive carbon release

and recovery processes during the Paleocene-Eocene Thermal Maximum, *Environmental Research Letters*, **13**(10).

Peterson, L. C., and Backman, J., 1990, Late Cenozoic carbonate accumulation and the history of the carbonate compensation depth in the western equatorial Indian Ocean, *Proceedings of the Ocean Drilling Program, Scientific Results*, **115**, 467–489.

Petit, J., Jouzel, J., Raynaud, D., Barkov, N., Barnola, J.-M., Basile, I., Bender, M., Chappellaz, J., Davis, M., Delaygue, G., Delmotte, M., Kotlyakov, V., Legrand, M., Lipenkov, V., Lorius, C., Pepin, L., Ritz, C., Saltzman, E., and Stievenard, M., 1999, Climate and atmospheric history of the past 420,000 years from the Vostok ice core, Antarctica, *Nature*, **399**, 429–436.

Rae, J. W., Foster, G. L., Schmidt, D. N., and Elliott, T., 2011, Boron isotopes and B/Ca in benthic foraminifera: Proxies for the deep ocean carbonate system, *Earth and Planetary Science Letters*, **302**(3-4), 403–413.

Raymo, M. E., and Ruddiman, W. F., 1992, Tectonic forcing of late Cenozoic climate, *Nature*, **359**, 117–122.

Rea, D. K., and Ruff, L. J., 1996, Composition and mass flux of sediment entering the world's subduction zones: Implications for global sediment budgets, great earthquakes, and volcanism, *Earth and Planetary Science Letters*, **140**, 1–12.

Reay, D., and Grace, J., 2007, Carbon Dioxide: Importance, Sources and Sinks In *Greenhouse Gas Sinks*, CABI, Cambridge, MA.

Richards, M. A., and Engebretson, D. C., 1992, Large scale mantle convection and the history of subduction, *Nature*, **355**, 242–244.

Ridgwell, A., and Hargreaves, J. C., 2007, Regulation of atmospheric CO_2 by deep-sea sediments in an Earth system model, *Global Biogeochemical Cycles*, **21**(2), 1–14.

Ridgwell, A., and Zeebe, R., 2005, The role of the global carbonate cycle in the regulation and evolution of the Earth system, *Earth and Planetary Science Letters*, **234**(3-4), 299–315.

Riebesell, U., Kortzinger, A., and Oschlies, A., 2009, Sensitivities of marine carbon fluxes to ocean change, *Proceedings of the National Academy of Sciences*, **106**(49), 20602–20609.

Rodhe, H., 1990, A comparison of the contribution of various gases to the greenhouse effect, *Science*, **248**(1), 1217–1219.

Sabine, C., and Feely, R. A., 2007, The Oceanic Sink for Carbon Dioxide In *Greenhouse Gas Sinks*, CABI, Oxfordshire, UK.

Sabine, C. L., Heimann, M., Artaxo, P., Bakker, D. C. E., Chen, C.-T. A., Field, C. B., Gruber, N., Le Quéré, C., Prinn, R. G., Richey, J. E., Lankao, P. R., Sathaye, J. A., and Valentini, R., 2004, Current Status and Past Trends of the Global Carbon Cycle In *The Global Carbon Cycle: Integrating Humans, Climate, and the Natural World*,, number SCOPE 62 Island Press, Washington DC.

Schopf, J., and Packer, B., 1987, Early Archean (3.3-Billion to 3.5-Billion-Year-Old) Microfossils from Warrawoona Group, Australia, *Science*, **237**(4810), 70–73.

Sclater, J. G., and Abbott, D., 1977, Paleobathymetry and Sediments of the Indian Ocean, *Indian Ocean Geology and Biostratigraphy: Studies Following Deep-Sea Drilling Legs*, **9**, 25–59.

Seki, O., Foster, G. L., Schmidt, D. N., Mackensen, A., Kawamura, K., and Pancost, R. D., 2010, Alkenone and boron-based Pliocene pCO_2 records, *Earth and Planetary Science Letters*, **292**(1-2), 201–211.

Sigman, D. M., and Boyle, E. A., 2000, Glacial/interglacial variations in atmospheric carbon dioxide, *Nature*, **507**, 859–869.

Sigman, D. M., Hain, M. P., and Haug, G. H., 2010, The polar ocean and glacial cycles in atmospheric CO_2concentration, *Nature*, **466**(7302), 47–55.

Spiegel, D. S., Menou, K., and Scharf, C. A., 2008, Habitable Climates, *The Astrophysical Journal*, **681**, 1609–1623.

Stern, R. J., 2002, Subduction zones, *Reviews of Geophysics*, **40**(4), 1–13.

Suess, E., 1980, Particulate organic carbon flux in the oceans - Surface productivity and oxygen utilization, *Nature*, **288**(5788), 260–263.

Syracuse, E. M., Keken, P. E., Abers, G. A., Suetsugu, D., Bina, C., Inoue, T., Wiens, D., and Jellinek, M., 2010, The global range of subduction zone thermal models, *Physics of the Earth and Planetary Interiors*, **183**(1-2), 73–90.

Thomas, E., Zachos, J. C., and Bralower, T. J., 2000, Deep-sea environments on a warm earth: latest Paleocene-early Eocene, *Warm Climates in Earth History*, 132–160.

Tierney, J. E., and Tingley, M. P., 2014, A Bayesian, spatially-varying calibration model for the TEX86 proxy, *Geochimica et Cosmochimica Acta*, **127**, 83–106.

Traub, W. A., 2012, Terrestrial, habitable-zone exoplanet frequency from Kepler, *Astrophysical Journal*, **745**(1).

Tyrrell, T., and Zeebe, R. E., 2004, History of carbonate ion concentration over the last 100 million years, *Geochimica et Cosmochimica Acta*, **68**(17), 3521–3530.

Tyrrell, T., Shepherd, J. G., and Castle, S., 2007, The long-term legacy of fossil fuels, *Tellus,*

Series B: Chemical and Physical Meteorology, **59**(4), 664–672.

Vago, J. L., and Westall, F., 2017, Habitability on Early Mars and the Search for Biosignatures with the ExoMars Rover, *Astrobiology*, **17**(6-7), 471–510.

Andel, T. H., 1975, Distribution of Calcareous Sediments, *Earth and Planetary Science Letters*, **26**, 187–194.

Van Der Meer, D. G., Zeebe, R. E., Van hinsbergen, D. J. J., Sluijs, A., Spakman, W., and Torsvik, T. H., 2014, Plate tectonic controls on atmospheric CO_2 levels since the Triassic, *Proceedings of the National Academy of Sciences*, **111**(12), 4380–4385.

Zachos, J., Pagani, M., Sloan, L., Thomas, E., and Billups, K., 2001, Trends, rhythms, and aberrations in global climate 65 Ma to present. *Science (New York, N.Y.)*, **292**(April), 686–693.

Zachos, J. C., Stott, D., and Lohmann, K. C., 1994, Evolution of early Cenozoic marine temperatures at Equator, *Paleoceanography*, **9**(2), 353–387.

Zeebe, R., and Ridgwell, A., 2011, Past changes of ocean carbonate chemistry In *Ocean Acidification*, Oxford University Press, Oxford, UK.

Zeebe, R. E., 2012, LOSCAR: Long-term Ocean-atmosphere-Sediment CArbon cycle Reservoir model v2.0.4, *Geoscientific Model Development*, **5**(1), 149–166.

Zeebe, R. E., and Tyrrell, T., 2019, History of carbonate ion concentration over the last 100 million years II : Revised calculations and new data, *Geochimica et Cosmochimica Acta*, 1–20.

Zeebe, R. E., and Wolf-Gladrow, D., 2001, *CO_2 in Seawater: Equilibrium, Kinetics, Isotopes*, Elsevier Ltd., Amsterdam, 3rd edition.

Chapter 2 - The Geologically Evolving Carbon Cycle + Ocean Model - GECCO

What could be faster,
Than teaching a computer to master,
Equations, constrained or not?
Actually, quite a lot...

Abstract

On million year timescales carbon moves between the atmosphere, ocean, seafloor, terrestrial, mantle and subterreanean reservoirs. Much of the behaviour that underpins the connections between these reservoirs is mechanistically understood, meaning it is possible to codify such behaviour into a quantitative framework. In order to achieve this, each part of the carbon cycle as detailed in Chapter 1 is broken down into its constituent parts, then expressed as a series of equations. These equations are combined to produce a new, forward, mechanistic carbon cycle box model, designed specifically to integrate geological fluxes over millions of years. The Geologically Evolving Carbon Cycle + Ocean model (GECCO) is designed, developed, verified and validated. During this process, I found new insightful perspectives on the long term carbon cycle that suggest previously unappreciated or unknown behaviours could be important in determining long term climate evolution. Additionally, some of the initial uses of GECCO are explained. These include the creation of steady states as a basis for future work, and the experiments that have been done to ensure that the model is behaving both as intended and appropriately. Four key climate feedbacks are outlined in preparation for proceeding studies. In order to estimate the potential role of each feedback in the determination of long term climate trends, it must be possible to tune the strength of each feedback individually. Methodologies for performing said tuning of each feedback are described. Finally, potential future improvements to GECCO, and their expected impact on the function of the model, are discussed.

2.1. GECCO Model Development

The Geologically Evolving Carbon Cycle and Ocean model (GECCO model) is a box model intended to represent carbon cycle processes on multimillion year timescales. The default architecture is composed of 1 atmospheric box, 2 ocean boxes, 2001 sedimentary boxes (split evenly between oceanic and terrestrial) and a variable number of outgassing boxes. GECCO is designed to allow quantitative examination of the interplay between atmospheric CO_2, ocean carbonate chemistry, sedimentary carbon, volcanic outgassing and weathering fluxes.

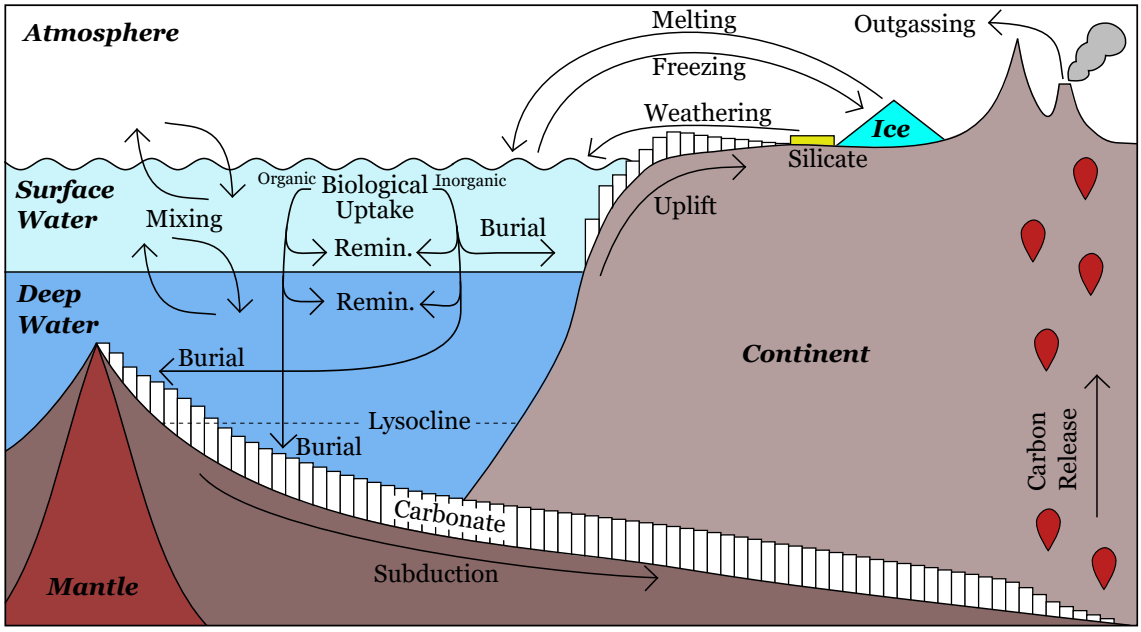

Figure 2.1: ***A schematic of the GECCO model showing the primary reservoirs of interest and the pathways of carbon between those reservoirs.***

As stated in Section 1.5.2, extant carbon cycle box models (described further in Appendix A), fall into one of two categories. They are either focussed on timescales so short as to make the geological carbon cycle irrelevant (cGENIE, LOSCAR, JModels), or focussed on long timescales and incorporate geological carbon cycle behaviour through simplistic laws (BLAG, GEOCARB). The motivation for GECCO is to revitalise the latter category of carbon cycle box models by introducing a more mechanistic approach to representing long term carbon cycle processes. By having a better representation of the geological aspect of the carbon cycle, it will be possible to test how this can potentially act as both a carbon cycle driver and feedback and how other drivers propagate through the carbon cycle on long timescales.

To facilitate investigation of the strength of climate constraint during the Cenozoic, GECCO incorporates multiple new components. One of the most important is the inclusion of the geological carbon cycle, which closes the carbon cycle on timescales greater than $\sim$1 million years. The link between subducting carbon and volcanic outgassing has important ramifications, both for Cenozoic carbon cycle evolution, and for long term planetary stability. GECCO links the formation of sediments (and their storage at a variety of depths) to a subduction routine, which, in turn, feeds into an algorithm to calculate volcanic outgassing. This allows GECCO to run indefinitely without specifying decoupled input and output fluxes of carbon.

GECCO also incorporates a state of the art carbonate chemistry solver that quantifies the full oceanic carbonate system. The solver is able to take into account the effect that changes in oceanic calcium and magnesium concentration have on the ocean carbonate speciation. The carbonate chemistry routine is connected to a bespoke CCD solver, which controls the burial of inorganic carbon and its distribution over the seafloor. The ocean carbonate system mediates the transition of atmospheric CO_2 to seafloor carbonate, and is therefore able to impact on volcanic outgassing flux.

Finally, GECCO includes an ice component, which simulates the growth and decay of ice sheets, and the associated impact on sea level. Changes in sea level are an important carbon cycle driver, as they not only change the extent of subaerial weatherable material, but also change how the sedimentary carbon is distributed across the seafloor. In the past, there have been large fluctuations in sea level as a result of changing global ice volume (*DeConto* and *David Pollard*, 2003) and potentially also changes in plate buoyancy as a result of plate tectonics (*Haq et al.*, 1988), but the long term impact of this carbon cycle driver has not been quantitatively explored due to the lack of available tool.

The GECCO model is built from a series of nearly independent components. In most cases each component is functionally independent, and passes only a single value to the next component (for example, the *Phosphate Component* (Section 2.1.4) calculates the surface ocean phosphate export, which is passed to the *Oceanic Carbon Component* (Section 2.1.5) to calculate surface ocean carbon export). This is beneficial because it allows modular development of the model, meaning each component can be developed and validated somewhat independently. Below, the structure and composition of each component of the model is described in detail, alongside relevant equations detailing the behaviour of the component and the efforts undertaken to verify and validate that component.

2.1.1 Programmatic Structure

The standard programming paradigm is a procedural approach - indicating that each instruction is run in the order that it is given. This approach works well with small or simple projects, but with a complex interconnected project such as GECCO it is beneficial to move to a more structured methodology. The paradigm chosen here is so called object oriented programming, which allows the custom definition of variable types and associated functions. Using the procedural approach, variables are typically declared containing a single value, an array of values, or a matrix of values (Figure 2.2).

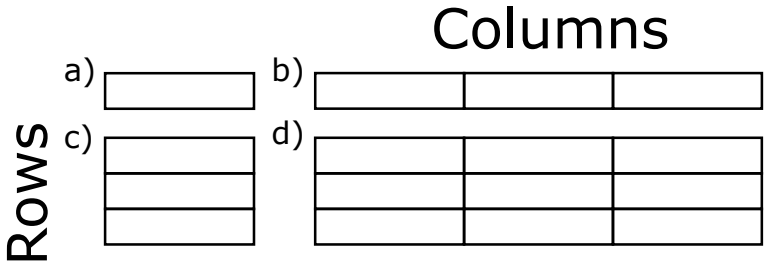

Figure 2.2: ***An example of typical data storage structures employed in script based programming, including a) a single value, b) a row vector - here 3 values, c) a column vector - here 3 values and d) a matrix - here 9 values.***

In contrast, the object oriented paradigm allows the definition of a data structure which can contain arbitrarily complex data. An illustrative example of the benefits of the object oriented methodology is representation of the time by a computer. Times are inherently formed by a combination of structured pieces of information, for example three values which detail the hour, minute and second. Without using an object oriented approach, there are many ways to represent these pieces of information (see Figure 2.3), for example three independent variables, or a single array of three variables, and it is not possible for the computer to predict which value constitutes which part of the date. Using an object oriented ap-

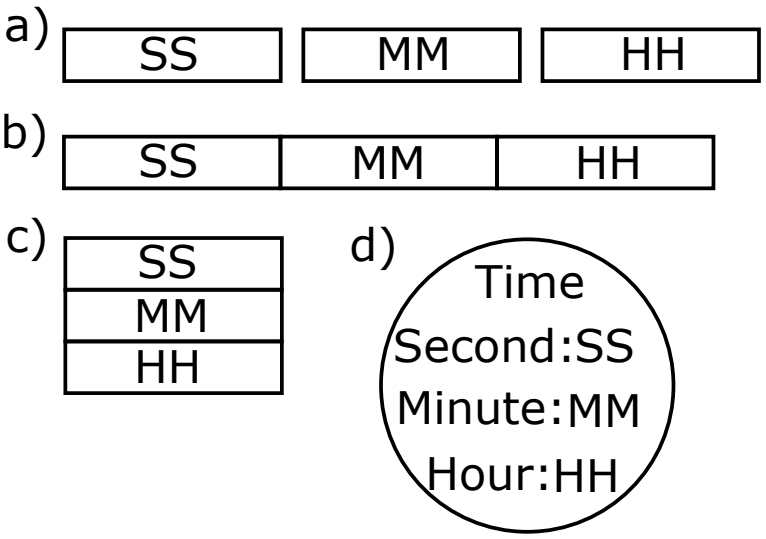

Figure 2.3: ***Various methods of storing date comprising of a day (DD), month (MM) and year (YYYY) using the matrix paradigm (a, b and c) and the object oriented paradigm (d).***

proach, a new data type would be

defined that must contain an hour field, a minute field and a second field (Figure 2.3). These fields may be empty, but are nonetheless declared. Immediately there are advantages to the object oriented approach in terms of providing a clear place to store each piece of information, reducing the possibility for errors in data entry. The computer also now has additional knowledge of exactly how the data will be structured, and so functions may be defined without concern about the order or name of the input arguments. For example, a function called 'Format' may be defined, that when provided with the hour, minute and second, returns 'hh:mm:ss' as a string type variable. If it is not known whether the input will be three individual values, or an array of three values (which may be in any order) then it is difficult to define an appropriate function. In contrast, if it is known where the hour, minute and second fields will be found, then it is only necessary to provide the entire time data structure, from which the program can isolate the appropriate values with ease. Furthermore, the functionality of the time object can be enhanced when storing more complex information, such as the timezone of the specified time. One might then define a function called 'UpdateTimezone', which, when the timezone is updated (e.g. from GMT to GMT+5) the hour contained in the variable is simultaneously updated (Figure 2.4). Functions such as these are defined and stored alongside the relevant data, which atomises their function and reduces the possibility of naming clashes.

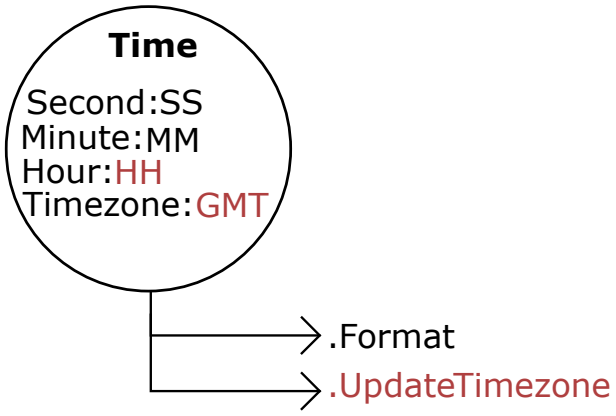

Figure 2.4: ***The time class defines the storage of data. Here there are four fields: seconds, minutes, hours and the timezone. Functions may be attached to the class, which operate on the data contained within. For example the 'UpdateTimezone' function (red) which can simultaneously control the hour and timezone fields (red) to keep them synchronised.***

The new data type that is defined is called a 'class'. This class acts somewhat like a blueprint, detailing the data and functions that it will store. Using the class to realise a variable is called instantiation, and creates what is called an object. Frequently, code is defined to run when an object is instantiated (a constructor), in order to, for example, initialise the fields of the object to their default values, parse any input arguments that are provided and load any data that is re-

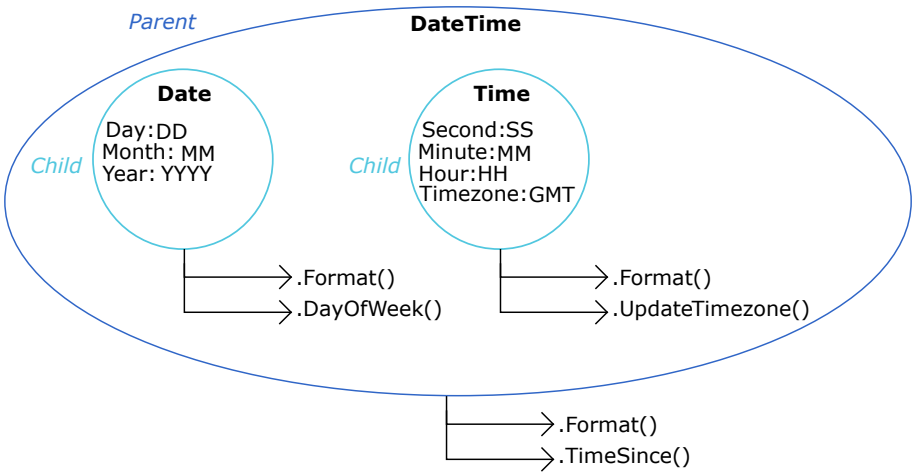

Figure 2.5: ***The DateTime object is compound of the Date object (which contains information such as the day, month and year, and is associated with functions which control the Date object), and a Time object (which contains information such as the second, minute and hour, and contains functions relevant to manipulation of the Time object).***

quired in ensuing calculations. The fields that are defined within a class can be of any type, including other classes. Returning to the example above, it is common to define a 'datetime' format, which is a hybrid format of a date and a time object (as shown in Figure 2.5).

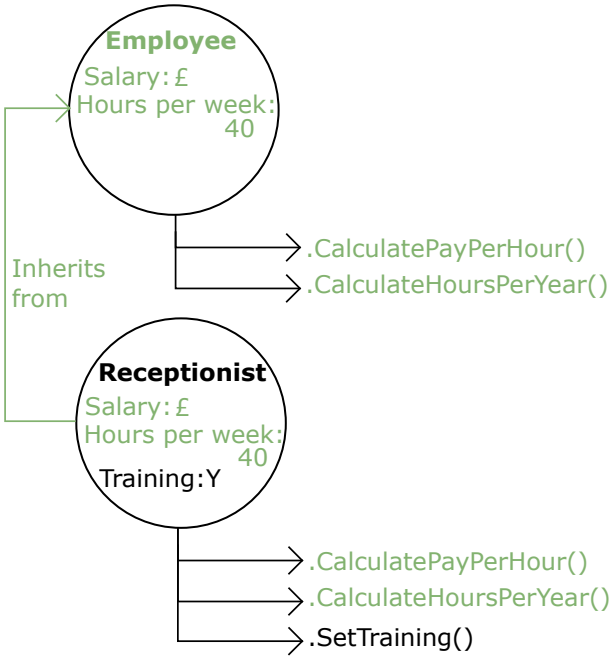

Figure 2.6: ***Two objects, an Employee and a Receptionist, are depicted. The Receptionist class inherits from the Employee class, meaning that it has the same properties and functions, and in addition any extra specified properties and functions that are applicable to the Receptionist class only.***

Objects that contain another object are called parents, and objects contained by another object are called children. Parents have access to their children, including their fields and functions, but children are typically limited in scope to themselves (and their children).

Classes are also able to inherit from one another. This indicates the building of a new subclass which contains all the properties of a superclass, with some additional information. The canonical example of this behaviour is the building of a class called 'employee' which might detail information like salary and benefits, common to all employees, which is extended by a new subclass called 'receptionist' that contains all the same properties as employee, as well as additional information only

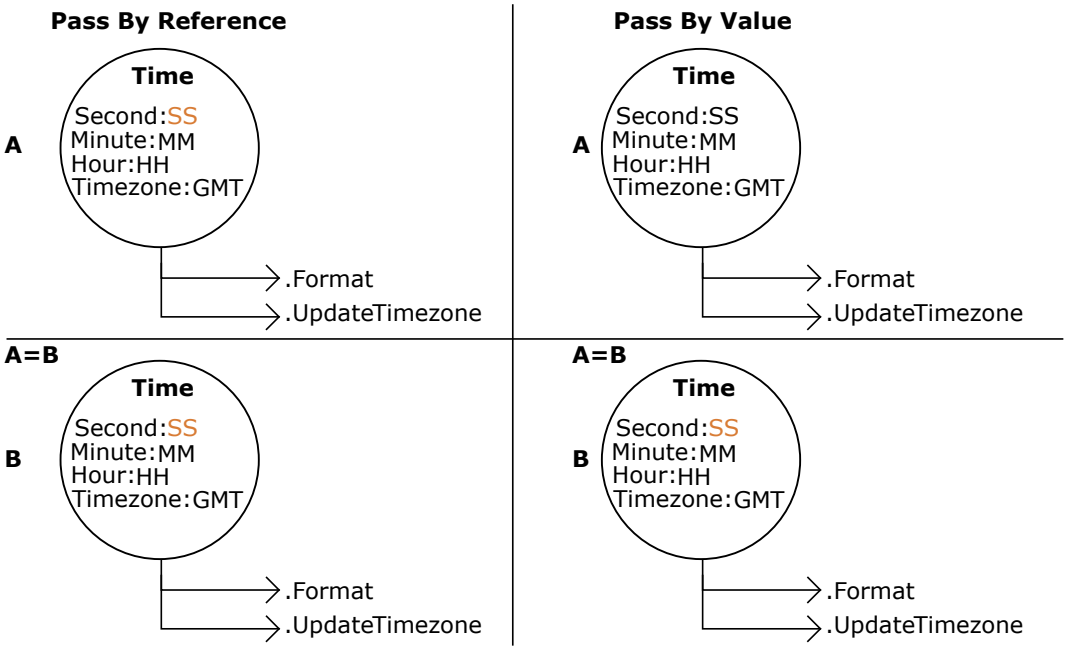

Figure 2.7: ***In the upper row, identical objects are instantiated as variable 'A'. The only difference between these objects is whether they are defined as pass by reference or pass by value. When a copy 'B' is set equal to A, the behaviour depends on whether the class is pass by reference or pass by value. When the class is pass by reference, variable B will simply contain a reference to A, and any changes to B are equivalent to changing A. When the class is a pass by value class, B is an independent copy of A, and any changes to B are not reflected by equivalent changes in A.***

relevant to members of the receptionist class (as shown in Figure 2.6). Subclasses may inherit from multiple superclasses, so long as there is no clash in the class definition. Finally, objects may be passed by one of two methods, pass by value or pass by reference (see Figure 2.7). Pass by value indicates that when something is set equal to the object, it will be identical in value, but a new and different copy of the object. Assigning to the new copy of the object will not affect the original object. Conversely, pass by reference indicates that when a new variable is set equal to the object, it is simply a reference to the existing object, and no new copy is made. Changes to the new variable change the origin object.

Having now developed the understanding of what a class is, and how it may be used, the structure of the GECCO model can be explained. GECCO is an object of the *GECCO* class, which is a pass by reference class containing a number of children corresponding to individual components of the model. *GECCO* may be a child of the *GUI* class, which builds a user interface, or may be used independently of the GUI through the Matlab interface or via the command line. The *GECCO* object contains an array of objects which define the conditions which inform each *Run*. In turn, each *Run* is composed of a series of *Chunks*,

which define time contiguous sections of a *Run*. This allows each *Run* to be broken into as many segments as required, where between each segment perturbations or changes to model values can be made. At the same depth as the array of *Chunks* is a *Region* object. Currently, GECCO can only perform simulations for a single *Region*, however this may be expanded in future to simultaneously perform calculation for a series of connected *Regions*. Each *Region* contains space for the output of model runs to be stored (in the *Outputs* object), and space for the values required to start the Run in the *Conditions* object, which is itself composed of objects that store the initial conditions (*Initials* object) and the constant values (*Constants*). This is only a schematic of the programmatic structure, as an example of how the object oriented paradigm may be used to store highly complex data in an organised and useful fashion. In fact the structure is significantly more complicated than shown and includes space for metadata, functions which can force model conditions and an object to represent each of the components of the model described below. This is extremely effective as a means of disentangling the complex web of connections between variables, and allowing the development of a modular model with atomic functions.

The accumulation of data in the *GECCO* object is passed to an external ODE solver function (as described in Section 2.1.13). This function is deliberately kept separate to the model code so that it can be easily swapped out for other solvers as required. The ODE solver function ingests the initial conditions, constants values and various other parameters to set up the model run, then begins to apply the rules to calculate the gradient in each state variable. Overall there are 16 state variables: algal concentration, phosphate concentration, atmospheric CO_2 concentration, DIC concentration, alkalinity, atmospheric temperature, ocean temperature, surficial silicate, silicate weathering fraction, carbonate weathering fraction, radiative forcing, ice mass, sea level, snow line height, sedimentary carbon and volcanic outgassing. Each of these may be one or more values (for instance, phosphate concentration is two values, one for the surface ocean and one for the deep). Several additional dependent variables are stored alongside these, such as pH, and the amount of subaerially exposed carbonate. The temporal evolution of each state variable is calculated by the solver, then returned to the *GECCO* object and, if requested, saved to disk. GECCO is able to perform multimillion year runs on a standard desktop PC, running at a speed a approximately 3 minutes to simulate million years. This level of efficiency is partially due to the low spatial resolution and partially because care has been taken to ensure the model is highly computationally efficient. Most time is spent in the carbonate chemistry routines, which are

extremely detailed and involve finding the roots of complicated non linear functions.

The GECCO model will evolve through time, both to add new functionality and to update the program as new knowledge becomes available. GECCO follows a semantic versioning scheme, and, as described in this chapter, is designated as version 1.0.0. The first integer is incremented for major changes, which render code incompatible with older versions, the second integer is reserved for more minor changes, and final value for bug fixes. This major version of GECCO is codenamed 'House' for easy reference, so can be referred to as House GECCO. The GECCO model is available online at: https://github.com/Sciross/GECCO

2.1.2 Mathematical Notation

The mathematical notation used in the this thesis is atypical. In the context of the link between mathematical formulae and programmatic struture, there are several benefits to the approach used here.

In typical notation, a given concept (such as temperature) might be given a specific letter (say T), which is then subscripted to indicate the context of the value (for example T_o for the temperature of the ocean). For this thesis, in most situations the ordering of these symbols is reversed (for instance o_T for ocean temperature), because this much more closely follows the programmatic structure of the GECCO model. The reason for this is outlined in Section 2.1.1 which describes the object oriented approach to programming. Many components in the model are represented by objects, which are organised hierarchically from largest to smallest. For example, it is logical to collate all the parameters relevant to the *Phosphate Component* (Section 2.1.4) in a single object - which is given the letter B (for Biology). This therefore leads to constructions such as B_x for biological export, and B_Ω for biological mortality. Each of these values is a value or set of values which describe the component that does the biological calculations - the *Phosphate Component*.

This notation is also highly modular. Parameters may be intuitively stacked together to represent a combination of ideas. For example, if B_x is taken to represent biological export, then B_{xP} can be used for biological export of phosphate, and B_{xC} for biological export of carbonate (given the letter C is used to represent carbonate in any equation in which it is found). This modularity is further enhanced by the used of 'decorators'. Here decorators are symbols put on top of parameters in order to clarify the structure or contents of a particular variable. This is particularly beneficial in this case because there are recurring sizes of ma-

trix that inform specific contexts of the calculations. For example, the ocean in GECCO is represented by two boxes, a surface and deep box. In order to vectorise calculations, this is represented as an 2×1 array i.e. with two rows and a single column. Values in this form are exclusively used to represent ocean values, so in order to distinguish between variables containing a single value an variables containing two vertically aligned values, the decorator $|$ is used. Taking D as the symbol for DIC, it is therefore possible to write $[D]$ which is a single value or $[\begin{smallmatrix}D\\|\end{smallmatrix}]$ which is two values, one on top of the other, representing surface ocean and deep ocean DIC respectively. Decorators can be stacked, such as $\underline{\ }$ (an n×1 array) and $\odot$ (boolean), which can be combined to: $\underline{\odot}$ meaning an n×1 array of booleans.

Organisation of the mathematical notation of this has a further benefit, which is that parameters related by their component are listed together in an alphabetised list of all values, meaning the collection of variables likely to be used within a single equation will be found adjacent to one another in a list of their definition or values.

2.1.3 Architecture Component

The architecture component defines the physical structure of the model, including parameters which control the volume of the atmosphere and oceans, and the shape of the seafloor. There are no equations directly associated with this portion of the model, as the values inform other components of the model. In the current version of GECCO, the architecture is hard coded into the model, meaning the number of atmosphere boxes (1), ocean boxes (2) and sediment boxes (2001) can not be changed.

Parameter	Environment	Symbol	Value	Units	Justification
Atmosphere Volume		a_V	1.8×10^{20}	mols	1.8×10^{20}:*Chuck et al.* (2005)
Riverine Volume		r_V	3.8857×10^{13}	m^3/yr	3.8857×10^{13}:*Peucker-Ehrenbrink* (2009)
Ocean Depths	(surface)	o_z	500	m	-
	(deep)		3200	m	-
Ocean Midpoints	(surface)		Dependent	m	-
	(deep)		Dependent	m	-
Ocean Area		o_A	3619×10^{12}	m^2	3.61×10^{14}:*Chuck et al.* (2005)
Ocean Mixing Coefficient		o_X	3	m/yr	3:*Tyrrell* (1999)
Hypsometry		H	Array		IOC, IHO, and BODC (2003)

Table 2.1: ***A collection of the parameters used in the*** **Architecture Component*.***

2.1.4 Phosphate Component

The phosphate component uses Michaelis-Menten dynamics (Equation 2.1) to compute the change in algal concentration through time (*Johnson* and *Goody*, 2011), under the assumption that phosphate is the only limit to productivity (*Tyrrell*, 1999). Riverine phosphate flux is calculated based on a combination of weathering components and an independent component (detailed further in Section 2.1.10). The riverine phosphate flux is split into neritic and pelagic components based on specified constants.

$$B_G = B_{G_\lambda} \left(\frac{[P]}{[P] + B_{\frac{1}{2}}} \right) B_\tau \tag{2.1}$$

Where:

$B =$ Biology

$G =$ Growth rate (/yr)

$G_\lambda =$ Maximum Growth rate (/yr)

$B_{\frac{1}{2}} =$ Half saturation constant

$[\ ] =$ Concentration (mol/m^3)

$P =$ Phosphate

$\tau =$ Timescale/slowing factor

When $[P] << B_{\frac{1}{2}} : B_G \approx 0$ When $[P] >> B_{\frac{1}{2}} : B_G \approx G_\lambda$ When $[P] = B_{\frac{1}{2}} : B_G = \frac{1}{2} G_\lambda$

Algal phosphate export to the deep ocean and sediments is controlled by algae mortality, and the fraction of phosphate remineralised in the surface and deep ocean. The neritic portion of phosphate export undergoes surface remineralisation then burial, while the pelagic portion of phosphate export undergoes both surface ocean and deep ocean remineralisation, then burial. The fraction of phosphate export remineralised at each ocean depth is controlled by constants. Once buried, phosphate is assumed to be permanently locked in sediments, meaning any remineralisation that happens within sediments is subsumed into the deep ocean remineralisation term. The phosphate module produces neritic and pelagic phosphate export fluxes.

$$\overset{/}{B}_{xP} = [B]\overset{/}{B}B_{\Omega}o_A o_s \tag{2.2}$$

Where:

$x =$ Export Flux (mol/yr) $\quad P =$ Phosphate

$\Omega =$ Mortality (/yr) $\quad o_A =$ Ocean Area (m^2)

$/ =$ Neritic/Pelagic Split $\quad o_s =$ Surface Ocean Box Thickness (m)

Algae are the most volatile component of the model (i.e. they have the shortest response time because they are able to grow exponentially), meaning the length of each model timestep is limited by this component of the model. Due to the fact that algal dynamics are not the primary focus of this model study, a slowing factor is used to slow down the response of algae to changes in phosphate concentration. Use of a slowing factor does not change the magnitude or direction of algal response to changes in phosphate concentration, but changes the timescale over which those dynamics occur, allowing the use of a larger timestep and improved model computational efficiency. This alteration does not affect the model results, because the timescale of interest is much longer than the dynamics of this individual component.

Parameter	Environment	Symbol	Value	Units	Justification
Maximum Growth Rate		B_{G_λ}	91.25	/yr	36.5-1496.5:*Goldman* (1979) 109.5-985.5:*Banse* (1982) 346.75:*Furnas* (1990) 91.25:*Chuck et al.* (2005) 36.5-91.25:*Edwards et al.* (2012)
Mortality		B_Ω	73	/yr	91.25-438:*Banse* (1992) 73:*Chuck et al.* (2005)
Half saturation constant		$B_{\frac{1}{2}}$	0.03×10^{-3}	mol/m^3	0.03×10^{-3}:*McAllister et al.* (1964) 0.05×10^{-3}:*Davies* and *Sleep* (1989) 0.03×10^{-3}:*Chuck et al.* (2005)
Proportionality to silicate		$B_{P:S}$	0.006	fraction	Calculated to match the riverine phosphate flux of *Chuck et al.* (2005)
Proportionality to carbonate		$B_{P:C}$	0.003	fraction	
Proportionality to nothing		$B_{P:N}$	0	fraction	
Phosphate remineralisation	(surface neritic)	$\not{P}_{\Gamma s}$	0.999	fraction	**Upper 100m** 0.75-0.9:*Barnes* and *Hughes* (1988) 0.86:*Schlesinger* (1997) 0.85:*Martin et al.* (1987) 0.9:*Berger et al.* (1987)
	(surface pelagic)		0.9010	fraction	**100-400m** 0.098:*Martin et al.* (1987) 0.09:*Schlesinger* (1997)
	(deep neritic)	$\not{P}_{\Gamma d}$	-	-	
	(deep pelagic)		0.0980	fraction	
Phosphate burial	(neritic)	$\not{P}_\Omega$	0.001	fraction	Neritic + Pelagic 0.002:*Jahnke* (1992)
	(pelagic)		0.001	fraction	0.002:*Schlesinger* (1997) 0.001-0.002:*Mackenzie et al.* (1993)
Productivity split	(neritic)	$\not{P}$	0.5	fraction	0.5:*Ridgwell* and *Zeebe* (2005)
	(pelagic)		0.5	fraction	

Table 2.2: ***A collection of the parameters used in the*** **Phosphate Component.**

2.1.5 Oceanic Carbon Component

The carbon component of GECCO takes the phosphate export fluxes calculated by the *Phosphate Component* (Section 2.1.4), and calculates the organic carbon export flux using the Redfield ratio. Inorganic export flux is calculated by combining the organic carbon flux with the percentage of primary producers that are calcifiers, and average calcifier production ratio (i.e. PIC:POC of the calcifier at the moment of death). This method makes the assumption that there is an average Redfield ratio that can be applied to all algae (*Martiny*

et al., 2013; *Teng et al.*, 2014), and that the calcifier fraction and production ratio can be treated as globally averaged constants. The burial of organic carbon is also controlled by constants, however in the current version of GECCO organic burial in neritic environments is prohibited. This is due to the fact that uplift of organic carbon would result in terrestrial exposure, and terrestrial organic deposits are not yet represented in the model. Organic carbon burial therefore happens in the deep sea only, and all organic carbon produced in the neritic realm must be remineralised. In reality, a large proportion of organic carbon burial occurs in the shelves (*Haas et al.*, 2002; *Dunne et al.*, 2007), so this omission is potentially problematic, and the burial of organic carbon is thought to be a significant component of the total oceanic carbon burial flux (*Chuck et al.*, 2005). Overall this means that the shelf carbon burial flux is likely to be underestimated by the model, and similarly, due to the lack of representation of terrestrial organic deposits, the riverine carbon flux is also underestimated. At steady state the riverine flux of organic carbon and the shelf burial flux of organic carbon must balance, so GECCO tacitly makes the assumption that the shallow and terrestrial organic carbon subcycle is at steady state. The *Carbon Component* of the model produces inorganic carbon export fluxes for both neritic and pelagic environments.

POC

$$\overset{/}{B}_{x\Theta} = \overset{/}{B}_{xP}\frac{\Theta}{P} \tag{2.3}$$

PIC

$$\overset{/}{B}_{x\Phi} = \overset{/}{B}_{x\Theta}\frac{\overset{/}{\Phi}}{\Theta}\overset{/}{B}_{F\Phi} \tag{2.4}$$

Where:

$\Theta =$ Particulate Organic Carbon

$\frac{\Theta}{P} =$ P:C Redfield Ratio

$\Phi =$ Particulate Inorganic Carbon

$\frac{\Phi}{\Theta} =$ PIC:POC Production Ratio

$B_{F\Phi} =$ Calcifier Fraction

Simply put, Equation 2.3 links the biological export of phosphate to the ratio of organic carbon to phosphate in algal matter at the moment of death. Combining these factors allows the calculation of the organic carbon export flux. Similarly, Equation 2.4 can be calculated by combining the organic carbon export flux with the average ratio of organic to inorganic carbon in dying algae. In order to calculate the average organic carbon to inorganic carbon ratio, the fraction of algae that are calcifiers, and the organic to inorganic carbon ratio of those calcifiers are multiplied (Equation 2.4). Most of these values are specified separately for the neritic and pelagic realms, but the average phosphate to organic carbon ratio (the Redfield ratio) is assumed to be the same in both environments.

Once the export fluxes of organic carbon and inorganic carbon in both the pelagic and neritic realms have been calculated, they can be split into the flux that is remineralised (in both the surface and deep ocean) (Equation 2.5 and Equation 2.8), and the flux which is buried in sediment (Equation 2.6 and Equation 2.9). Equation 2.7 and Equation 2.10 shows that the coefficients which control burial and remineralisation must sum to 1, meaning that the biological export is simply split into different parts, each of which is a flux to a different reservoir.

$$\overset{|/}{\Theta}_{\Gamma} = \overset{/}{B}_{x\Theta}\overset{|/}{\Gamma}_{\Theta} \quad (2.5)$$

$$\overset{|/}{\Theta}_{\Omega} = \overset{/}{B}_{x\Theta}\overset{|/}{\Omega}_{\Theta} \quad (2.6)$$

$$\Sigma(\Gamma_{\Theta} + \Omega_{\Theta}) = 1 \quad (2.7)$$

$$\overset{|/}{\Phi}_{\Gamma} = \overset{/}{B}_{x\Phi}\overset{|/}{\Gamma}_{\Phi} \quad (2.8)$$

$$\overset{|/}{\Phi}_{\Omega} = \overset{/}{B}_{x\Phi}\overset{|/}{\Omega}_{\Phi} \quad (2.9)$$

$$\Sigma(\Gamma_{\Phi} + \Omega_{\Phi}) = 1 \quad (2.10)$$

Where:

- $\Theta =$ POC
- $\Gamma =$ Remineralised
- $B =$ Biology
- $x =$ Export
- $\Phi =$ PIC
- $\Omega =$ Sink
- $| = 2 \times 1$ array
- $/ = 1 \times 2$ array
- $\Sigma =$ Sum

Parameter	Environment	Symbol	Value	Units	Justification
Redfield Ratio		$\frac{P}{\Theta}$	117	fraction	106:*Redfield* (1934) 117:*Anderson* and *Sarmiento* (1994) Summary:*Lenton* and *Watson* (2000)
Production Ratio	(neritic)		0.1	fraction	
	(pelagic)	$\frac{\diagup}{\frac{\Theta}{\Phi}}$	0.1	fraction	0.4-0.85:*Zondervan* and *Riebesell* (2002) 0.5-1.0:*Iglesias-Rodriguez et al.* (2008) 0.4-1.6:*Gerecht et al.* (2014)
Calcifier Fraction	(neritic)		0.035	fraction	
	(pelagic)		0.035	fraction	
POC Remineralistion	(surface neritic)		1	fraction	
	(surface pelagic)	$\overset{\diagup}{\Theta}_{\Gamma s}$	0.9125	fraction	0.97:*Chuck et al.* (2005)
	(deep neritic)		0	fraction	
	(deep pelagic)	$\overset{\diagup}{\Theta}_{\Gamma d}$	0.0874	fraction	0.025:*Chuck et al.* (2005)
POC Burial	(neritic)	$\overset{\diagup}{\Theta}_{\Omega}$	0	fraction	-
	(pelagic)		1×10^{-4}	fraction	5×10^{-3}:*Chuck et al.* (2005)
POC Maximum Burial Depth		Θ_{z_λ}	8000	m	-
Surface PIC Dissolution	(surface neritic)		0	fraction	0:*Chuck et al.* (2005)
	(surface pelagic)	$\overset{\diagup}{\Phi}_{\Gamma s}$	0	fraction	0:*Chuck et al.* (2005)
	(deep neritic)		0	fraction	-
	(deep pelagic)	$\overset{\diagup}{\Phi}_{\Gamma d}$	Dependent	fraction	
PIC Burial	(neritic)	$\overset{\diagup}{\Phi}_{\Omega}$	1	fraction	-
	(pelagic)		Dependent	fraction	

Table 2.3: ***A collection of the parameters used in the*** **Carbon Component.**

2.1.6 Carbonate Chemistry Component

Ocean pH is calculated using an iterative scheme (after *Follows et al.* (2006)), using equilibrium 'constants' (here called Carbonate Chemistry K values, or CCK's for short) calculated for the surface and deep ocean (incorporating the magnesium/calcium correction presented in *Hain et al.* (2015)), model calculated DIC and alkalinity concentrations, and a prior estimate of pH (taken from the previous model time step). The carbonate chemistry routine is very efficient and highly accurate, incorporating alkalinity contributions from many species

(see Appendix B). Unfortunately, when carbonate system conditions are dramatically different from the present day (particularly when both DIC and alkalinity are low) the routine produces a nonreal pH, meaning the model crashes. The range of pH values able to be calculated using this routine is roughly 7-9 units, which is sufficient for this study.

$$[\overset{|}{H^+}] = \frac{1}{2}\left(\left(\frac{[\overset{|}{D}]}{[\Pi]} - 1\right)\overset{|}{k_1} + \left(\left(1 - \frac{[\overset{|}{D}]}{[\Pi]}\right)^2 \overset{|}{k_1}^2 - 4\overset{|}{k_1}\overset{|}{k_2}\left(1 - 2\frac{[\overset{|}{D}]}{[\Pi]}\right)\right)^{\frac{1}{2}}\right) \tag{2.11}$$

Where:

$[H^+]$ = Hydrogen Ion Concentration

D = DIC

Π = Alkalinity

k_1 = Carbonate Chemistry K value 1

k_2 = Carbonate Chemistry K value 2

$|$ = Two Element Vertical Array

Shallow ocean PIC dissolution and burial are controlled by constants and are not dynamically related to the ocean carbonate system state, whereas deep ocean PIC dissolution is related to saturation state and controlled by the *Lysocline Component*.

$$[CO_2] = \frac{DIC}{1 + \frac{k_1}{[H^+]} + \frac{(k_1 k_2)}{[H^+]^2}} \tag{2.12}$$

$$[HCO_3^-] = \frac{DIC}{\frac{[H^+]}{k_1} + 1 + \frac{k_2}{[H^+]}} \tag{2.13}$$

$$[CO_3^{2-}] = \frac{DIC}{\frac{[H^+]^2}{(k_1 k_2)} + \frac{[H^+]}{k_2} + 1} \tag{2.14}$$

Once the hydrogen ion concentration is calculated (Equation 2.11), it can be used with the DIC concentration as shown in Equations 2.12–2.14 to calculate the absolute concentrations of aqueous carbon dioxide, bicarbonate ion and carbonate ion. The carbon dioxide concentration is used to calculate air-sea gas exchange based on the difference in partial pressures between the atmosphere and surface ocean, and the carbonate ion concentration is used to calculate the saturation state (as shown in Equation 2.15).

$$\psi_C = \frac{[Ca][CO_3^{2-}]}{k_{spC}} \tag{2.15}$$

Parameter	Environment	Symbol	Value	Units	Justification
Surface Salinity		β_s	35	-	Canonical
Deep Salinity		β_d	35	-	Canonical
Surface Pressure		p_s	Dependent	bar	-
Deep Pressure		p_d	Dependent	bar	-
Surface Boron		$[Bo]_s$	4.5×10^{-1}	mol/m^3	4.5×10^{-1}:*Lemarchand et al.* (2002) 4.5×10^{-1}:*Zeebe* and *Wolf-Gladrow* (2001)
Deep Boron		$[Bo]_d$	4.9×10^{-1}	mol/m^3	4.9×10^{-1}:*Zeebe* and *Wolf-Gladrow* (2001)
Surface Silica		$[Si]_s$	15×10^{-3}	mol/m^3	$15\times10^{-}$ 3:*Dickson* and *Goyet* (1994)
Deep Silica		$[Si]_s$	15×10^{-3}	mol/m^3	$15\times10^{-}$ 3:*Dickson* and *Goyet* (1994)
Surface Phosphate		$[P]_s$	Dependent	mol/m^3	-
Deep Phosphate		$[P]_d$	Dependent	mol/m^3	-
Surface Fluoride		$[Fl]_s$	7×10^{-2}	mol/m^3	7×10^{-2}:*Dickson* and *Goyet* (1994)
Deep Fluoride		$[Fl]_d$	7×10^{-2}	mol/m^3	7×10^{-2}:*Dickson* and *Goyet* (1994)
Surface Sulphate		$[Su]_s$	282.45	mol/m^3	282.45:*Dickson* and *Goyet* (1994)
Deep Sulphate		$[Su]_d$	282.45	mol/m^3	282.45:*Dickson* and *Goyet* (1994)
Surface Calcium		$[Ca]_s$	10.28	mol/m^3	10.28:*Broecker* and *Peng* (1982)
Deep Calcium		$[Ca]_d$	10.28	mol/m^3	10.28:*Broecker* and *Peng* (1982)
Surface Magnesium		$[Mg]_s$	53	mol/m^3	53:*Broecker* and *Peng* (1982)
Deep Magnesium		$[Mg]_d$	53	mol/m^3	53:*Broecker* and *Peng* (1982)

Table 2.4: ***A collection of the parameters used in the*** **Carbonate Chemistry Component.**

2.1.7 Lysocline Component

In order to calculated the fraction of carbon that is buried, and the hypsometric region in which carbon is buried, the model must calculate the CCD (a sedimentary property) from the CSH (a water column property). The CSH is calculated using the model predicted dynamic variables: DIC, alkalinity, temperature and CCK's - other parameters used include pressure and salinity, however these are typically constant throughout a model run. An iter-

ative scheme has been derived to efficiently calculate the CSH depth, using the CSH depth from the previous model timestep to guide the calculation. The CSH is then used as the CCD, i.e. there is 100% preservation of PIC above the CSH and 0% preservation of PIC below the CSH. In GECCO, the CSH, lysocline and CCD are at the same depth, but there is a terminological difference. The term lysocline is used programatically, to avoid the use of acronyms within GECCO model code, whereas within the term CCD is used to represent the concept of a burial horizon. Changes in carbon burial are what drive many of the observed model behaviours in Chapter 3 and Chapter 4, and the term CCD is used here to reflect the concept of a horizon that, by shoaling and deepening, is able to affect carbonate burial. The term CSH is used only when talking specifically about the water column saturation property. Further discussion of this distinction can be found in Section 1.2.2. Within GECCO, once sediment is formed it is able to move topographically but is not able to undergo further chemical alteration, such as dissolution. This means that, once buried, sediment is locked in, and future shoaling of the CCD can not cause dissolution.
At the CSH:

$$1 = \frac{[Ca^{2+}][CO_3^{2-}]}{k_{spC}} \quad (2.16)$$

$$k_{spC} = [Ca^{2+}][CO_3^{2-}] \quad (2.17)$$

$$0 = [Ca^{2+}][CO_3^{2-}] - k_{spC} \quad (2.18)$$

$$[CO_3^{2-}] = f(T, p, \beta, i) \quad (2.19)$$

$$k_{spC} = f(T, p, \beta, i) \quad (2.20)$$

$$T, p = f(z) \quad (2.21)$$

Where:

$[Ca^{2+}]$ = Calcium Ion Concentration

$[CO_3^{2-}]$ = Carbonate Ion Concentration

k_{spC} = Solubility Product for Calcite

z = Depth

T = Temperature

p = Pressure

β = Salinity

i = Ionic Composition

The calculated lysocline is used to establish the deep ocean PIC burial fraction and the deep ocean PIC remineralisation fraction. This is done by piecewise linear interpolation of the hypsometric data, which is used to calculate the fractional area of seafloor below sea level and above the lysocline. A linear relationship between supra-lysocline seafloor area and PIC burial fraction is assumed (i.e. if 100% of the seafloor is above the lysocline, then 100% of the extant pelagic PIC flux is buried). The lysocline also controls the distribution of the buried carbonate (Figure 1.9), meaning a shallow lysocline will result in PIC burial only at shallow depths (above the lysocline). This is encapsulated in Equation 2.23, which

splits the total sedimentary sink of PIC into an array which represents the sink into each topographic box which is both submarine and above the lysocline. For POC, a maximum depth at which burial occurs is specified, and then used to equally distribute the POC flux over the submarine area above the specified maximum depth (as shown in Equation 2.22).

$$\overline{\Theta}_{\Omega} = \Theta_{\Omega}\overset{\odot}{\overline{\Theta}}_{z} \qquad (2.22) \qquad\qquad \overline{\Phi}_{\Omega} = \Phi_{\Omega}\overset{\odot}{\overline{o}} \qquad (2.23)$$

Where:

$\Theta =$ PIC

$\Phi =$ POC

$\Omega =$ Sink

$o =$ Ocean

$z =$ Depth

$\odot =$ Boolean

$\_ =$ n $\times$ 1 array

2.1.8 Sediment Component

The *Sediment Component* controls the movement of sedimentary carbon, including uplift of carbon and subsidence of carbon towards eventual subduction. Sedimentary boxes are established that represent topography and bathymetry, from 10000m high to 10000m deep relative to present day sea level, at 10m resolution (that's 2001 sedimentary boxes). Carbon is deposited in these boxes in the ocean according to the chosen burial coefficients, CCD behaviour, and global sea level. Each box is associated with an uplifting fraction and a subsiding fraction, which specify the fraction of carbon in that box that moves topographically upwards or downwards each timestep, respectively. This is expressed in Equations 2.24–2.25, which describe how the uplifting or subsiding flux are calculated from the array of carbonate masses and the array of uplifting or subsiding fractions. In the default model configuration, the uplifting and subsiding zones are mutually exclusive, and the boundary between zones occurs at 500m below present day sea level (as shown in Figure 2.8).

$$\overset{\uparrow}{\overline{C}} = \overline{C}\overline{C}_{\uparrow} \qquad (2.24) \qquad\qquad \overset{\downarrow}{\overline{C}} = \overline{C}\overline{C}_{\downarrow} \qquad (2.25)$$

Where:

$\uparrow =$ Uplifting

$C =$ Carbonate

$\downarrow =$ Subsiding

$\_ =$ Array

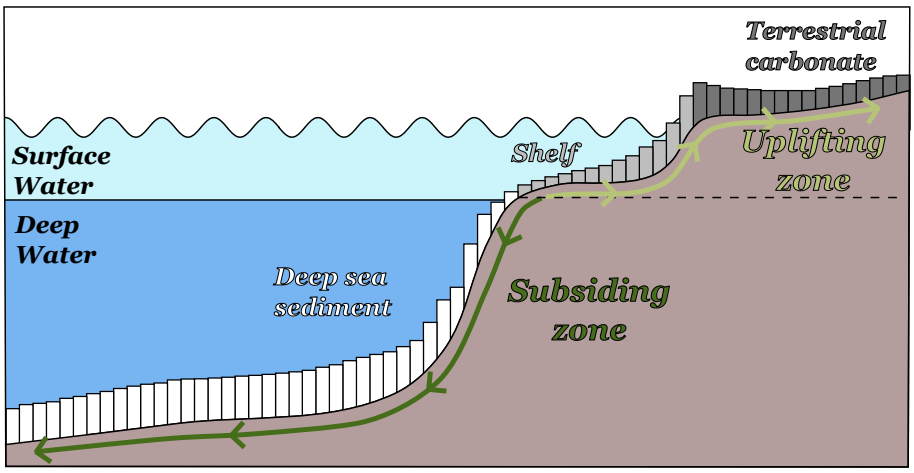

Figure 2.8: ***The locations of terrestrial carbon sediment (dark grey), shelf carbon sediment (light grey) and deep sea carbon sediment (white) are shown. The boundary between the uplifting zone (light green) and the subsiding zone (dark green) is also highlighted.***

Carbon deposited in the uplifting zone is destined to become terrestrial, and will continue uplifting until subaerially weathered. Sedimentary boxes above sea level are subaerially exposed to weathering processes. Currently only inorganic carbon should be deposited in the uplifting zone, as GECCO has no representation of terrestrial organic carbon. Assuming that uplifting organic carbon becomes inorganic carbon would introduce an artificial alkalinity source into the model, so instead the assumption is made that no organic carbon burial happens in the uplifting zone (this may be re-evaluated in future, as the percentage of organic carbon burial in shallow settings can be large (*Dunne et al.*, 2007)).

$$\bar{\Psi}_{\xi} = \frac{1}{\Psi_{\sigma}\sqrt{2\pi}} e^{-\frac{1}{2}(\frac{\bar{H}_z - \Psi_{\mu}}{\Psi_{\sigma}})^2} \tag{2.26}$$

$$\Psi_{\Omega} = \Sigma(\bar{\Psi}_{\xi}) \tag{2.27}$$

Where:

Ψ = Subduction

μ = Mean

σ = Standard Deviation

ξ = Distribution

H = Hypsometry

z = Depth

$\_$ = Array

Σ = Sum

Ω = Sink

Carbon deposited in the subsiding zone is destined to be subducted. The amount of carbon consumed by subduction in a given timestep is calculated using a Gaussian distribution whose mean, standard deviation and maximum are specified parameters (as shown in Equation 2.26). This allows carbon to be simultaneously removed from multiple depths (allowing representation of the global variability in subduction zone depth) in an easily tunable way.

This total subducted carbon flux (Equation 2.27) is passed to the *Outgassing Component* (Section 2.1.11).

Parameter	Environment	Symbol	Value	Units	Justification
Subduction Mean		Ψ_μ	8000	m	-
Subduction Spread		Ψ_ς	500	m	-
Subduction Risk		Ψ_ζ	0.001	fraction	-
Subsidence Rate		$\overline{C}_\downarrow$	Array	fraction	Tuned for average travel time of 10Myr
Uplift Rate		$\overline{C}_\uparrow$	Array	fraction	Tuned to produce sensible carbonate topographic profile
Core Depths		$\overline{\kappa}_z$	10000 8000 5000 3000 2000 1000 0 -1000 -2000 -3000 -5000 -8000 -10000	m	-

Table 2.5: ***A collection of the parameters used in the*** **Sediment Component.**

2.1.9 Energy Component

The energy component of GECCO is responsible for calculating planetary temperature. This is done using a simple energy balance equation (Equation 2.40), which balances incoming solar radiation against outgoing radiation from a grey-body planet. CO_2 is included by an additional radiative forcing term, the sensitivity to which must be specified. The magnitude of the response of temperature to forcing (i.e. climate sensitivity) must also specified.

In order to achieve this energy balance model, the sensitivity of global temperature to changes in the outward energy flux is estimated by differentiation of the Stefan-Boltzmann law, as shown in Equations 2.28–2.31. This shows that when the outward energy flux changes by 3.7W/m^2, the canonical value for a doubling of atmospheric CO_2 concentration (*IPCC*, 2001), the temperature will change by 1°C when the global temperature is in the range of 15°C and the other parameters are as shown in Equation 2.31 (and detailed in Table 2.6). Equations 2.28–2.31 therefore allow a linearisation of the non linear Stefan-Boltzmann law, which applies when the temperature is in the region of 15°C.

$$E_{\uparrow} = \epsilon \nu T_k^4 \tag{2.28}$$

$$\frac{dE_{\uparrow}}{dT_k} = 4\epsilon \nu T_k^3 \tag{2.29}$$

$$\frac{dT_k}{dE_{\uparrow}} = \frac{1}{4\epsilon \nu T_k^3} \tag{2.30}$$

$$dT_k = 3.7 \times \frac{1}{4 \times 0.61334 \times 5.67e^{-8} \times (15 + 273.15)^4} \approx 1 \tag{2.31}$$

Where :

$T_k =$ Temperature (°K) $\quad E_{\uparrow} =$ Energy Out (W)

$\equiv =$ Equilibrium $\quad \varkappa =$ Albedo (fraction)

$a =$ Atmosphere $\quad \epsilon =$ Emissivity (fraction)

$R_0 =$ Solar Constant (W/m^2) $\quad \nu =$ Stefan-Boltzmann Constant (W/m^2/K^4)

Having determined that the sensitivity of temperature to changes in radiative forcing is 1°C/3.7W/m^2 (Equations 2.28–2.31), it is then necessary to express the change in radiative forcing driven by a change in atmospheric CO_2 concentration. As stated above, the canonical value for this parameter is 3.7W/m^2 for each doubling of atmospheric CO_2 concentration (*IPCC*, 2001). Equation 2.32 then shows how the radiative forcing state variable evolves through time, using the number of doublings of atmospheric CO_2, and the sensitivity of radiative forcing to CO_2. The radiative forcing state variable therefore expresses how much additional radiative forcing equivalent is occurring due to the current atmospheric CO_2 concentration. This is expressed relative to the present day, meaning the parameters are tuned to achieve a global average atmospheric temperature of 15°C with 0W/m^2 of radiative forcing caused by the Preindustrial 300ppm atmospheric CO_2 concentration. A doubling of CO_2 concentration, for instance, then causes the specified change in radiative forcing equivalent (by default 3.7W/m^2).

$$\frac{dR}{dt} = \frac{dR}{dCO_2} \ln\Big(\frac{[CO_2] + \Delta[CO_2]}{[CO_2]}\Big) \frac{1}{\ln(2)} \tag{2.32}$$

Where :

$R =$ Radiative Forcing (W/m^2) $\qquad$ $[\ ] =$ Concentration

The radiative forcing equivalent is used in Equations 2.37–2.40 to calculate the equilibrium atmospheric temperature, using a scaling factor to account for the climate sensitivity. The energy balance equations (Equations 2.37–2.40) balance the incoming solar radiation (Equation 2.33) against outgoing radiation (Equation 2.35) to calculate the temperature.

$$E_{\downarrow} = R_0(1 - \varkappa)\bigcirc_{A\#} \tag{2.33}$$

$$E_{\uparrow} = \bigcirc_A(\epsilon\nu T^4 - \frac{dT}{dR}R) \tag{2.35}$$

$$\bigcirc_{A\#} \approx \pi\bigcirc_r^2 \tag{2.34}$$

$$\bigcirc_A \approx 4\pi\bigcirc_r^2 \tag{2.36}$$

Where:

$E_{\downarrow} =$ Energy In (W) $\qquad$ $\bigcirc_A =$ Earth Area (m^2)

$\frac{dT}{dR} =$ Climate Sensitivity (scalar) $\qquad$ $\bigcirc_{A\#} =$ Earth Cross Sectional Area (m^2)

$$\pi \bigcirc_r^2 R_0(1 - \varkappa) = 4\pi \bigcirc_r^2 (\epsilon\nu T^4 - \frac{dT}{dR}R) \tag{2.37}$$

$$R_0(1 - \varkappa) = 4\epsilon\nu T^4 - 4\frac{dT}{dR}R \tag{2.38}$$

$$\frac{R_0(1 - \varkappa) + 4\frac{dT}{dR}R}{4\epsilon\nu} = T^4 \tag{2.39}$$

$$\overset{\equiv}{T}_a = \sqrt[4]{\Big(\frac{R_0(1 - \varkappa) + 4\frac{dT}{dR}R}{4\epsilon\nu}\Big)} \tag{2.40}$$

$$\overset{|\equiv}{T}_o = \overset{\equiv}{T}_a - \overset{|}{\Delta}_{To} \tag{2.41}$$

Where:

$o =$ Ocean (2.42) $\qquad$ $\Delta =$ Difference

$| = 2 \times 1$ array (2.43)

The calculated temperature is an equilibrium atmospheric temperature, and is used to update the present atmospheric temperature over a specified relaxation timescale. GECCO assumes there is a constant steady state offset between the temperatures of the ocean and atmosphere (Equation 2.41). For instance, one might specify that the steady state surface

ocean temperature is 1°C cooler than the steady state atmospheric temperature, and the deep ocean temperature is 10°C less than the steady state temperature of the atmosphere. While the steady state magnitude of temperature change is presumed to be the same in all three reservoirs (the atmosphere, surface ocean and deep ocean), the timescale over which this change occurs is different. Therefore to calculate the change in ocean temperature with time, the equilibrium ocean temperature is calculated using specified offsets from the equilibrium atmospheric temperature (Equation 2.41), and the ocean temperature is made to approach the steady state value over a specified timescales (see Equation 2.45). Albedo and emissivity values do not (by default) directly respond to the atmospheric temperature.

$$\frac{dT_a}{dt} = (\overline{\overline{a}}_T - a_{T(t)})a_\tau \tag{2.44}$$

$$\frac{d\overset{|}{T}_o}{dt} = (\overset{|}{\overline{\overline{o}}}_T - \overset{|}{o}_{T(t)})\overset{|}{o}_\tau \tag{2.45}$$

Parameter	Environment	Symbol	Value	Units	Justification
Radiative Sensitivity		$\frac{dR}{dCO_2}$	3.7	$\frac{W/m^2}{doublingCO_2}$	3.7:*IPCC* (2001)
Climate Sensitivity		$\frac{dT}{dR}$	3.5	$\frac{°C}{doublingCO_2}$	1.5-4.5:*IPCC* (2001)
Solar Constant		S_0	1370	W/m^2	Canonical
Albedo		$\varkappa$	0.3	fraction	Canonical
Emissivity		ϵ	0.61334	fraction	Calculated for atmospheric temperature of 15°C at default conditions
Stefan-Boltzmann Constant		ν	5.67$\times$10^{-8}		Canonical
Atmosphere Equilibration Timescale		a_τ	50	years	-
Surface Ocean Equilibration Timescale		$\overset{\|}{o}_\tau$	100	years	10-100:*England* (1995)
Deep Ocean Equilibration Timescale			1000	years	500-5000:*England* (1995)
Surface Ocean Temperature Offset		$\overset{\|}{\Delta}_{To}$	-1	°C	-
Deep Ocean Temperature Offset			-12	°C	Canonically deep ocean water is about 3°C meaning -12

Table 2.6: ***A collection of the parameters used in the*** **Energy Component.**

2.1.10 Weathering Component

The *Weathering Component* relates atmospheric temperature to the weathering flux of both carbonate and silicate lithologies. The relationship between silicate weathering and temperature is thought to be exponential in nature. As shown in Figure 2.9, a fit can be performed to the data of *Li et al.* (2016), which allows the calculation of coefficients which control the relationship between silicate weathering and temperature. There is noticeable scatter in the data surrounding this fit line, especially when taking into account different lithologies which have different weatherabilities, but the form of the equation appears to be consistent with the data, which suggests that the dynamics of the system will be appropriate. The fit is performed to so called 'inactive' regions, meaning that this estimate of the strength of the silicate weatherability feedback does not include contributions from mafic lithologies, and may represent a low estimate of the true silicate weathering feedback strength. It should also be noted that the data from *Li et al.* (2016) is given in terms of MmolCO_2/km^2/yr, which must be transformed into appropriate units for use in GECCO. GECCO assumes that the fraction of the available reservoir that is weathered (termed the 'silicate/carbonate weathering fraction') is controlled by temperature (as shown in Equation 2.47). The size of the available reservoir is determined by multiplying the tracked state variable, which is intended to represent the mass of silicate in the surficial reservoir, with the fraction of this reservoir that is subaerially exposed (a specified constant value). The flux of weathered silicate material is therefore linearly dependent on the size of 'exposed' silicate material, and exponentially dependent on temperature. An additional factor is provided to tune the weatherability of silicates, relative to the present day, to account for potential orogeny and magmatism, which may not change the total size of the reservoir, but provide fresh material which is more easily weathered. The relationship between these factors is shown in Equation 2.49.

Unfortunately, the relationship between carbonate weathering fluxes and temperature is less well studied, as existing literature which looks at the factors controlling carbonate weathering has so far focussed on controls other than exclusively temperature (such as a biological dependence (*Calmels et al.*, 2014), or CO_2 dependence (*Romero-Mujalli et al.*, 2018)). In GECCO the form of the equation is presumed to be the same as silicate weathering (i.e. it is presumed that the fraction of available material which is weathered is determined by atmospheric temperature - see Equation 2.46). The coefficients which control carbonate weathering are also, by default, the same as those used to describe the silicate weathering-temperature relationship, though these are subject to change in future as more data become

available. Carbonate weathering is more complicated though, because GECCO represents both terrestrial and marine carbonate sediment in a series of topographic boxes, so an additional calculation is required to determine the currently subaerial areal extent. Essentially, this involves determining the topographic boxes which are currently above sea level, and are therefore undergoing active weathering. Once the subaerial extent has been established, the calculation for carbonate weathering flux proceeds in the same way as silicate weathering, a multiplicative combination of subaerial carbonate mass, exposed fraction, weatherability relative to present day and weathering fraction (see Equation 2.48).

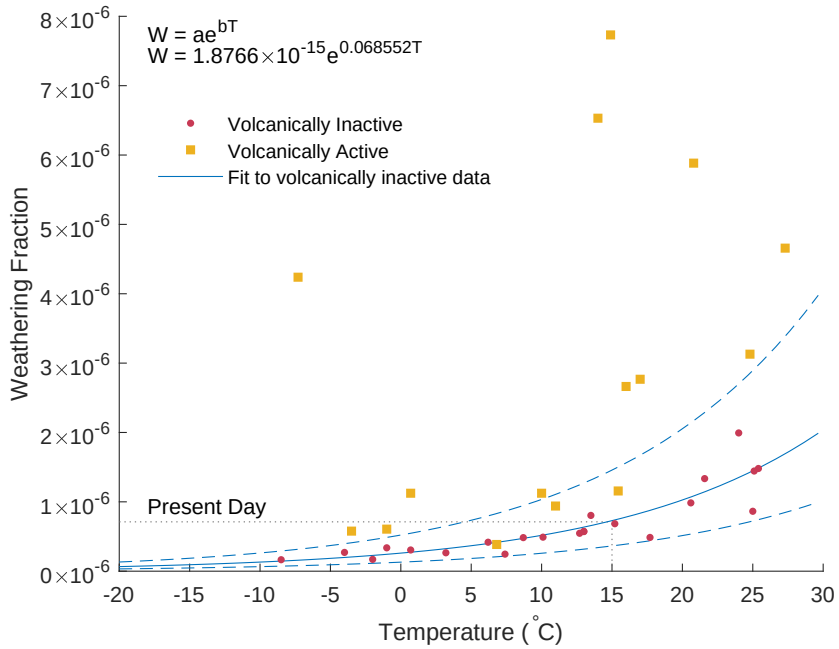

Figure 2.9: ***Replotted data from* Li et al. *(2016), who compile data from a number of sources, shows the relationship between silicate weathering and temperature. The original data was presented in terms of KCO_2 (units of 10^6 mol/km^2/yr) - this has been recast in terms of the fraction of the total silicate reservoir weathered per year by estimating the total silicate weathering flux per year, and the subaerially exposed silicate inventory. Data from volcanically inactive localities are shown in red circles and data from volcanically active localities are shown as yellow squares. The fit (blue) has been performed on data from inactive localities, so this represents a low estimate of the strength of coupling between silicate weathering and temperature. The dashed blue lines show the impact of a doubling/halving of weatherability. The values shown are for the number of moles of carbon produced, therefore the values should be halved to calculate the number of moles of silicate or carbonate that are weathered.***

$$C_{\varphi} = C_{k1}e^{C_{k2}T_c} + C_{k3} \quad (2.46) \qquad S_{\varphi} = S_{k1}e^{S_{k2}T_c} + S_{k3} \quad (2.47)$$

Where :

$\varphi =$ Weathering fraction (fraction/yr)

$K =$ Weathering Coefficient (unitless)

$C =$ Carbonate (mol)

$S =$ Silicate (mol)

$T =$ Temperature (°K)

$$\bar{C}_W = C\overset{\odot}{\bar{a}}C_{\chi}C_{\varphi}C_{\omega} \quad (2.48) \qquad S_W = SS_{\chi}S_{\varphi}S_{\omega} \quad (2.49)$$

Where :

$W =$ Weathering (mol/yr)

$\overset{\odot}{\bar{a}} =$ Boolean subaerial array

$\chi =$ Exposure (fraction)

$\omega =$ Weatherability (fraction)

$$\frac{d\bar{C}}{dt} = \frac{\overset{\uparrow}{d\bar{C}}}{dz} + \frac{\overset{\downarrow}{d\bar{C}}}{dz} + \bar{\Psi}_{\xi} - \bar{C}_W \quad (2.50) \qquad \frac{dS}{dt} = S_G - S_W + (S_W S_{\varrho}) \quad (2.51)$$

Where :

$C =$ Carbonate

$z =$ Depth

$\uparrow =$ Uplifting

$\downarrow =$ Subsiding

$\Psi =$ Subduction

$\xi =$ Distirbution

$S =$ Silicate

$t =$ Time

$W =$ Weathering

$G =$ Replenishment

$\varrho =$ Replacement

In early experiments with GECCO, the silicate areal extent was allowed to evolve through time - however, without a feedback that regulates the production and consumption of silicate the model was entirely a slave to the silicate production flux. If silicate production was high, then CO_2 drawdown continued until the atmospheric CO_2 reservoir was exhausted, whereas if silicate production was low, then CO_2 would rise far beyond reasonable bounds. To avoid this instability in the default model configuration, the silicate areal extent is locked. This is achieved by using two parameters to regulate silicate production, termed replen-

ishment and replacement. Replenishment specifies the production of new silicate (mol/yr), whereas replacement specifies what fraction of silicate weathering exposes new silicate material (fraction). For example, if replacement is set to 0.5, then half of all moles of silicate that are weathered unearth a new mole of silicate. Replenishment is an independent input flux of silicate into the model, whereas replacement links the sink of silicate to its source. By setting replacement to 1, and replenishment to 0mol/yr, the total silicate inventory is static through time. The potential impact of this decision is discussed in Section 2.2.1.

In GECCO, the flux of phosphate to the ocean is dependent on the weathering fluxes of carbonate and silicate lithologies (Equation 2.52). This is accomplished by taking a specified fraction of silicate weathering, a specified fraction of the total carbonate weathering flux, and an independent component.

$$P_r = P_{P:S_W} S_W + P_{P:C_W} \Sigma(\bar{C}_W) + P_W \tag{2.52}$$

Where :

P_r = Riverine Phosphate

C = Carbonate

S = Silicate

W = Weathering

$\_$ = Array

Σ = Sum

Parameter	Subparameter	Symbol	Value	Units	Justification
Silicate Replenishment		S_G	0	mol/yr	Described in text
Silicate Replacement		S_ϱ	1	fraction	Described in text
Silicate Weathering Coefficients		S_{kn}	Array		Described in text
Silicate Weatherability		S_ω	1		By definition
Carbonate Weathering Coefficients		C_{kn}	Array		Described in text
Carbonate Weatherability		C_ω	1		By definition
Carbonate Exposure		C_χ	0.05		Tuned to produce a sensible carbonate weathering flux

Table 2.7: ***A collection of the parameters used in the*** **Weathering Component.**

2.1.11 Outgassing Component

The outgassing component takes the flux of carbonate from the *Subduction Component* (Section 2.1.8) and allocates this to be outgassed in the future (Equation 2.53). The transformation from mass of carbon that has been subducted (a single value) to the mass of carbon outgassed in the future (an array of values) is controlled by a Gaussian distribution (Equation 2.56), with specified mean lag and standard deviation (see Figure 2.10). It is presumed that all carbonate that is subducted is eventually released volcanically based on the mass balance estimates performed in *Kelemen* and *Manning* (2015), although new isotopic data casts this into doubt (*Mason et al.*, 2017). Carbon that is not tectonically recycled (as described above), would eventually become part of the mantle reservoir.

$$O_\alpha = \Sigma(\bar{\Psi}_\Omega) \tag{2.53}$$

$$\bar{O}_\xi = \frac{1}{O_\sigma\sqrt{2\pi}} e^{-\frac{1}{2}(\frac{\bar{O}_t - O_\mu}{O_\sigma})^2} \tag{2.54}$$

(2.55)

Where :

$O =$ Outgassing

$\Psi =$ Subduction

$\alpha =$ Source

$\Omega =$ Sink

$\xi =$ Distribution

$t =$ Time

$\mu =$ Mean

$\sigma =$ Standard Deviation

$\_ =$ Array

$\Sigma =$ Sum

It is currently unclear how large the mantle reservoir of carbon is and whether the mantle provides a significant carbon flux to the surficial carbonate reservoir. In this absence of this information, GECCO assumes that the mantle carbon reservoir is at steady state, and that all carbon that is subducted reemerges through volcanic outgassing after a given timespan. This assumption may be relaxed in future if the mantle is found to be an important carbon cycle reservoir on the timescale of interest.

$$\frac{d\bar{O}}{dt} = O_\alpha \bar{O}_\xi \tag{2.56}$$

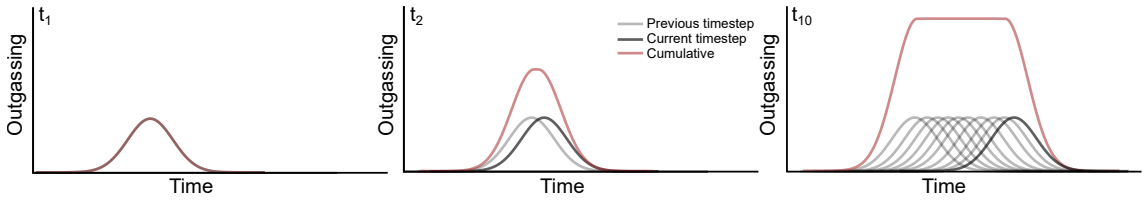

Figure 2.10: ***At t_1, the flux of subducted carbon is spread into a Gaussian distribution (black) and added to the outgassing array (red). This is repeated at t_2 and so on, leading to a volcanic outgassing flux that is the sum of many individual Gaussian distributions. This gives the model a 'memory' of past subduction that is expressed in future volcanic outgassing.***

Parameter	Subparameter	Symbol	Value	Units	Justification
Outgassing Mean Lag		O_μ	2.5×10^6	yr	Described in text
Outgassing Spread		O_σ	0.5×10^6	yr	-
Outgassing Temporal Resolution		O_Ξ	1000	yr	-

Table 2.8: ***A collection of the parameters used in the* Outgassing Component*.***

2.1.12 GECCO Summary

The GECCO model is the combination of each of the components described in Sections 2.1.3–2.1.11. The components describe how climate behaviour is translated into a mathematical representation. That mathematical representation provides a mechanism through which to calculate the temporal gradient in each of the state variables, many of which directly represent carbon reservoirs. In order to produce a time series of each of the state variables using the calculations portrayed in Sections 2.1.3–2.1.11 a differential equation solver is required (see Section 1.5.1).

2.1.13 Ordinary Differential Equation Solver

Differential equation solvers are a method of applying gradients in state variables to produce time series of these variables. The simplest method of achieving this is to simply use the gradient to project forward in time over the specified timestep size - this is known as the Euler scheme (as shown in Figure 2.11). This method has the benefit of being easy to implement and intuitive, but has numerical disadvantages in that it is prone to instability.

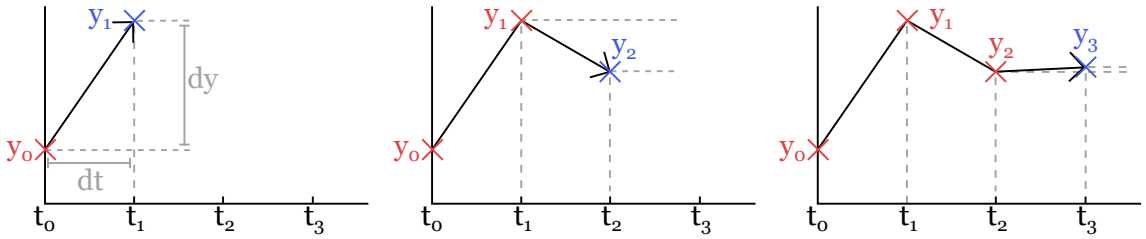

Figure 2.11: ***A simple differential equation solver is shown. This Euler solver uses specified equations to calculate the gradient at the initial condition, then extrapolates forward in time. This process is the repeated to generate a record through time.***

A refinement to the Euler scheme is to evaluate the gradient both at the initial condition and at the subsequent timestep. An estimate of the value of each state variable can be calculated by using the Euler scheme, then the differential equations can be used to provide an estimate of the gradient after the timestep. The average of these gradients can be taken as an estimate of the gradient between the initial condition and the subsequent timestep, then applied to calculate a more accurate value for the state variables. This is known as a predictor-corrector scheme, as it first predicts the value of the parameters, then applies a correction based on a new estimation of the gradients at the subsequent timestep. The operation of this scheme is shown in Figure 2.12.

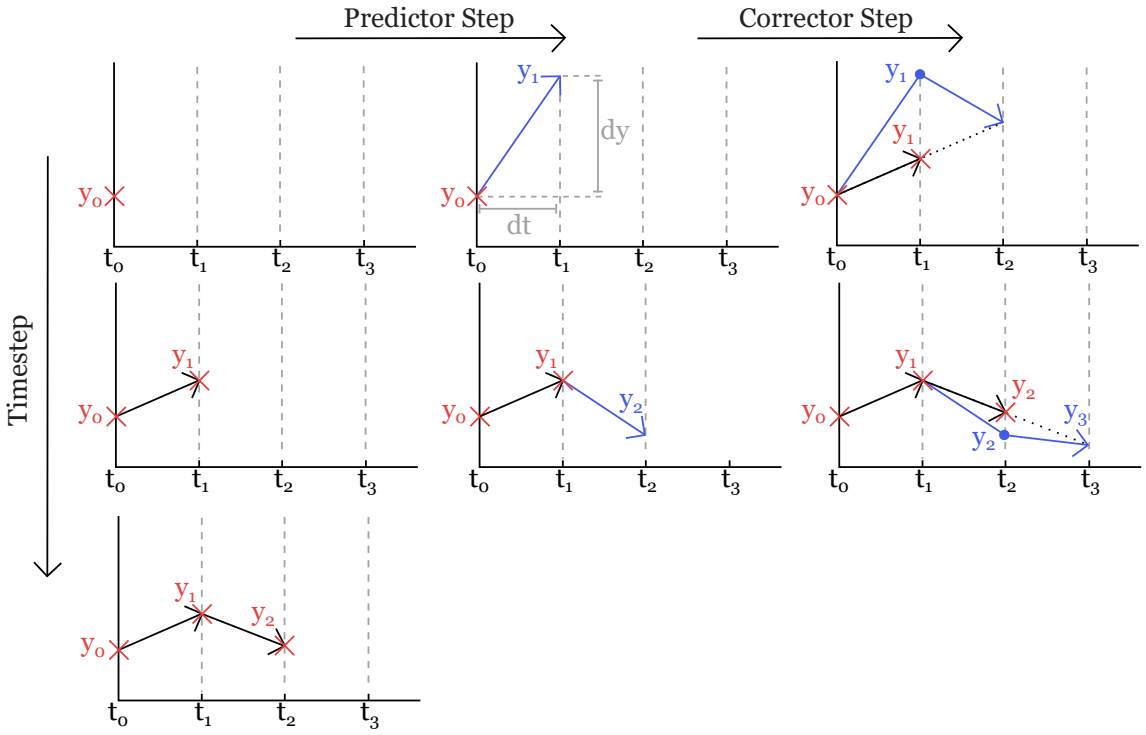

Figure 2.12: ***The default differential equation solver used in GECCO is explained. A slightly more complex differential equation solver than the Euler scheme shown in Figure 2.11 is the predictor-corrector scheme. The predictor step is equivalent to the Euler scheme as displayed in Figure 2.11. The corrector step then uses the result of the forward Euler step to calculate a new gradient. The mean of the two gradient values is taken, and this is used to extrapolate forward in time. This is known as Heun's scheme, or the trapezium rule.***

Matlab comes packaged with several ordinary differential equation solvers, all of which are more complex than the schemes shown here. There are two primary problems with existing Matlab ordinary differential equation solvers: they are variable time step solvers, and they are inefficient with respect to memory. Variable time step solvers are generally computationally efficient, and are especially useful when tackling stiff problems, however they make it difficult to implement the scheme designed to replicate the temporal evolution of volcanic outgassing in the model presented here. Memory inefficiency of Matlab solvers stems from the fact that every gradient that is calculated is stored in memory until the calculation is completed, at which point the results are summed and interpolated. This scheme is fast, but results in unnecessarily high memory usage, which is of particular concern here as the GECCO model can be required to run for millions of years and thus calculate billions of values.

To resolve the problems with available Matlab differential equations solvers, I have developed bespoke ordinary differential equation solver based on the predictor-corrector scheme described in Figure 2.12. This solver has a fixed time step size and is highly memory efficient. To combat the high memory usage of Matlab solvers, the solver that I have written does not store gradients, but instead applies those gradients on the fly to calculate the evolution in state variables, and only writes these to the output array at the requested resolution (e.g. if the model runs at 20 years resolution, and output is required every 100 years, then the model will only store the previous 5 results), performing interpolation as required. This scheme is slightly less computationally efficient, but drastically reduces the memory requirements when performing long model runs. Additionally, due to the fixed step size, the computational methodology for the *Outgassing Component* (Section 2.1.11) is drastically simplified.

2.2. Novel Carbon Cycle Behaviours in GECCO

Development of the GECCO model involved logically thinking through each component of the carbon cycle in order to codify it in a meaningful way. As mentioned in Section 2.1, previous models seeking to represent the carbon cycle on similar timescales (such as BLAG and GEOCARB) were constrained by the knowledge and resources of their time and therefore could not represent the dynamics of many aspects of the carbon cycle. This means that during GECCO development, several previously undocumented features of the carbon cycle were discovered, and these are detailed below.

2.2.1 Missing Silicate Feedback

In Section 2.1.10 it was established the early experiments with the GECCO model allowed the size of the silicate reservoir to vary through time, and that results from these experiments were universally unstable. It was therefore necessary to clamp the silicate inventory to a static value through time. This requirement points to a feedback that regulates the silicate areal exposure through time, though the mechanism for this feedback is unclear. Some evidence points to the fact that silicate supply rate could provide such a feedback (*West et al.*, 2005) (shown in Figure 2.13). GECCO assumes that the fractional area which undergoes weathering at a given time is dependent only on temperature. This allows the silicate weathering flux to depend on both the available areal extent and the temperature, however at the default conditions the fractional area of silicate that is weathered is very small (on the order of a millionth), so the weathering flux is not limited by the rate of supply. It should be noted that invoking supply limitation as a potential feedback on global silicate areal extent does not necessarily resolve the issue of balancing long term silicate production flux. It is possible to imagine that the silicate creation rate could be much greater than the present day (for example during the formation of a LIP, or simply due to globally increased magmatic activity) at some point in time, or on a planet with slightly different chemical composition or dynamics.

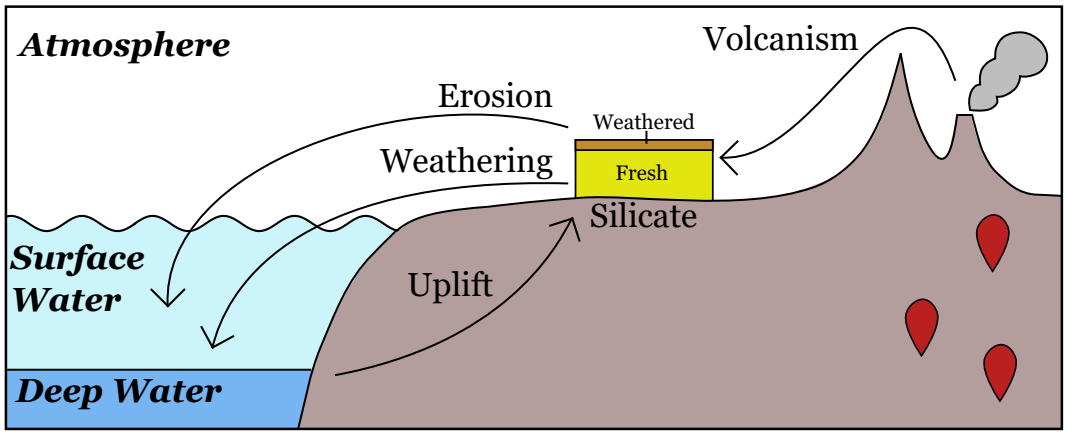

Figure 2.13: ***Silicate is produced through volcanism or uplifted from submarine environments. The sink of silicate is erosion and weathering. In this case, weathering refers to chemical alteration of the silicate lithology (as described in Section 1.2). Erosion refers to mechanical removal of the weathered lithology. In this way 'fresh' silicate may be weathered and form a block to further weathering until eroded.***

Given the premise of this thesis is the examination of long term planetary stability, eliminating what could potentially be a strong driver of long term atmospheric CO_2 has the potential to bias the results of model runs towards stability. The alternative, however, is to have a

model in which long term CO_2 always reaches ridiculous values when silicate production is meaningfully different from the present day. In fact, changes in the silicate reservoir size can also act as a strong destabilising feedback. If, after starting with a steady state climate, CO_2 concentration decreases as a result of changes in volcanic outgassing, causing temperature to decrease, this would typically be inferred to cause a decrease in the silicate weathering flux until it is rebalanced with volcanic outgassing of CO_2. If the decrease in silicate weathering flux is not met with an equivalent decrease in silicate source, however, then the size of the silicate inventory must change. Presuming that the change in silicate inventory will result in more silicate weathering, this will drawdown more CO_2, and potentially lead to a runaway feedback (Figure 2.14).

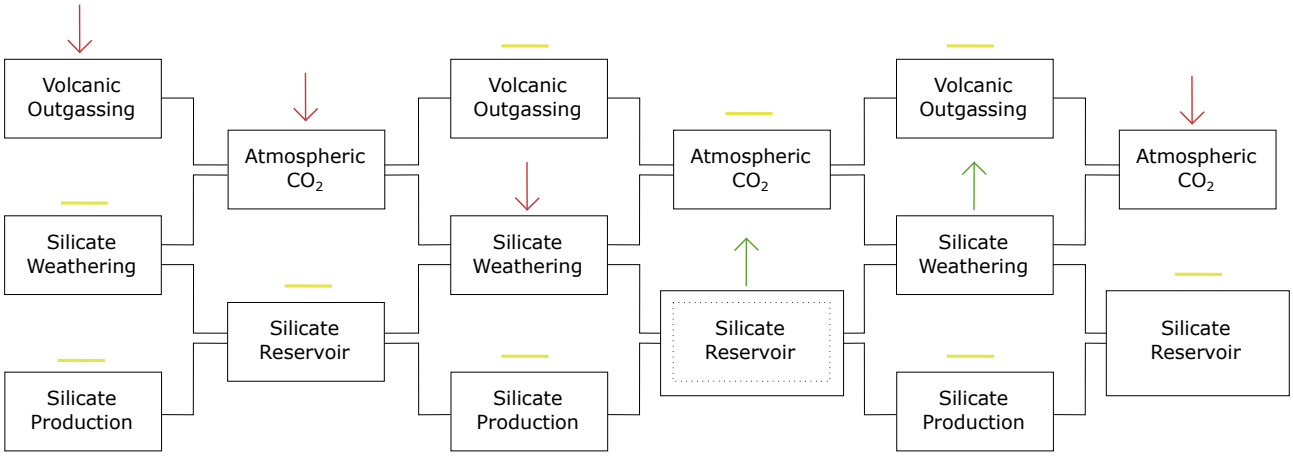

Figure 2.14: ***Three processes (volcanic outgassing, silicate weathering and silicate production) are connected to two reservoirs (atmospheric CO_2 and subaerially exposed silicate). With time moving left to right, an initial decrease in volcanic outgassing results in a decrease in atmospheric CO_2, which in turn drives a decrease in silicate weathering. Without a corresponding change in the source of silicate material, the silicate reservoir increases in size, leading to greater silicate weathering and further drawdown of atmospheric CO_2.***

The fact that Earth has remained stable for such a long time would seem to indicate that there must be a reason that the silicate production has not driven radical climate change, either due to a feedback or simply due to bulk planetary chemistry, but it is not possible to rule out the effect of chance in this instance. It is therefore necessary to proceed with the caveat that all model runs with GECCO (in its current state) may be contingent on the assumption that the surficial reservoir of silicate is so large that it is almost unaffected by changes in climate on the timescale of interest. It is not known that this is the case, and there have been suggestions to the contrary (*Kump*, 2018), though these are based on interpretation of palaeoclimate behaviour, so it is difficult to be certain that changes in the silicate reservoir were truly the cause of the observed change.

2.2.2 Uplifting and Subsiding Zones

Predicting the evolution of any individual sediment package is extremely complicated, as it may be uplifted, or subside, it may move independently of the underlying plate (for example through slumping) or may move with the underlying plate, which itself experiences a complex evolution due to the numerous influencing factors (such as regional mantle variations, global tectonic regime and local country rock fabric). For this reason it seems quite a difficult problem to tackle within a model, but it is eminently possible to simplify the observed behaviour by thinking only of the source and sink or sedimentary material. Given the source of sedimentary carbon to the seafloor is thought to be predominantly controlled by biology and processes occurring with the water column, this is not really a complication of the sediment behaviour, though any diagenetic effects or other sedimentary processes may affect the magnitude of this source. Putting this aside for a moment, in terms of the sink, there are only two potential avenues for sediment to take - either it must be subducted, or uplifted and then weathered. Sediment may transiently take neither of these avenues, for example by entering a passive basin, however on very long timescales the sediment is extremely likely to be either subducted or uplifted into the subaerial realm. Any internal dynamics which move sediment around may simply be parameterised in terms of their propensity to cause uplift or subsidence. Viewed through this lens, the system becomes much more tractable, and the components which deal with internal dynamics may be made as complex as need be without affecting the nature of the two possible pathways for sediment, and by extension seafloor carbon, to take.

Having established that the sedimentary system may be viewed as simply areas which are on average uplifting and areas which are on average subsiding (Figure 2.15), it is possible to perform some informative thought experiments to reveal something of the nature of the relationship this phenomenon has with the carbon cycle. Firstly, it is logical to make the assumption that sediment at shallow ocean depths is more likely to be uplifted into the terrestrial realm than sediment in the deep sea. Secondly, revisiting the description of the source of sedimentary carbon, this is predominantly driven by a combination of biology and ocean carbonate chemistry, as stated above. Carbonate chemistry is thought to be particularly important in the deep sea, as it controls the fraction of the PIC flux that is preserved. In the shallow ocean though, the controls on carbon burial flux are more nuanced. It has been suggested that the shallow ocean carbonate burial flux is related to ocean saturation state (presumably as a result of the inference of possible deleterious effect of ocean acidification (*Honisch et al.*, 2012)), though this is more empirical that mechanistic. In any case, there is a discrepancy between the controls of carbonate burial in the shallow and deep ocean. The combination of these two principals means that there is one set of processes that dominate the uplifting flux of carbonate, and another that dominate the subsiding flux.

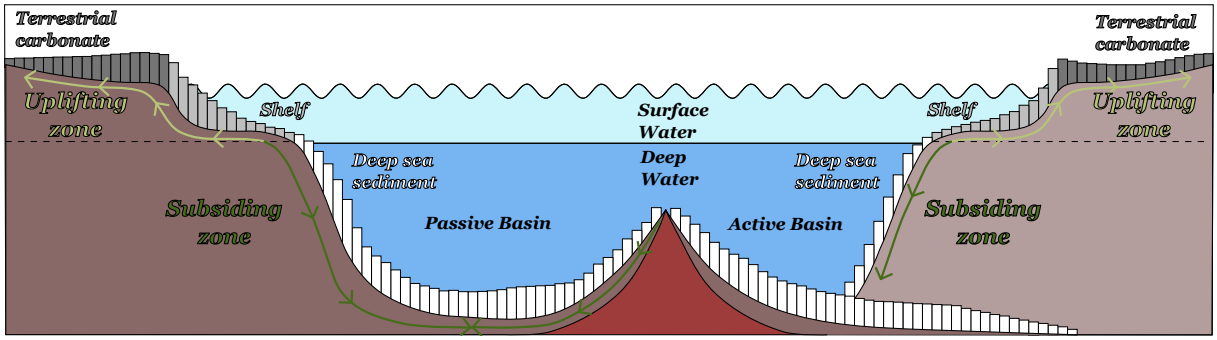

Figure 2.15: ***A schematic cross section of a passive and active basin with associated carbonate sediment is shown. Carbonate sediment that is subaerially exposed is shown in dark grey, shallow ocean carbonate sediment is shown in light grey, and deep sea carbonate sediment is shown in white. The tectonic zones (uplifting and subsiding) are shown in light and dark green respectively.***

In an absolute sense, the topographic range of the shallow ocean is partly dependent on sea level. A decrease in ice volume and associated rise in sea level will raise the topographic range at which shallow sea calcifiers exist. In contrast, the tectonic zones are not related to sea level, and would instead be expected to be driven primarily by global plate behaviour. It is therefore feasible for the burial zones and tectonic zones to change alignment, which could drive changes in the carbon cycle. For example, imagine if ice volume were to grow particularly large, causing sea level to fall by several hundred metres. This should radically

decrease the uplifting flux of carbon, leading to almost all carbon derived from weathering being buried in the subsiding environment and being processed through subduction zones rather than through the terrestrial carbonate reservoir. Similarly, when sea level is particularly high, then additional carbon can be buried in the uplifting zones. There is a level of asymmetry here, as there is only a small submarine area at which uplift can occur. A large enough fall in sea level could feasibly completely eliminate carbon burial in the uplifting zone, whereas only if sea level were to rise by several kilometres could carbon burial in the subsiding zone be stopped (see Figure 2.16).

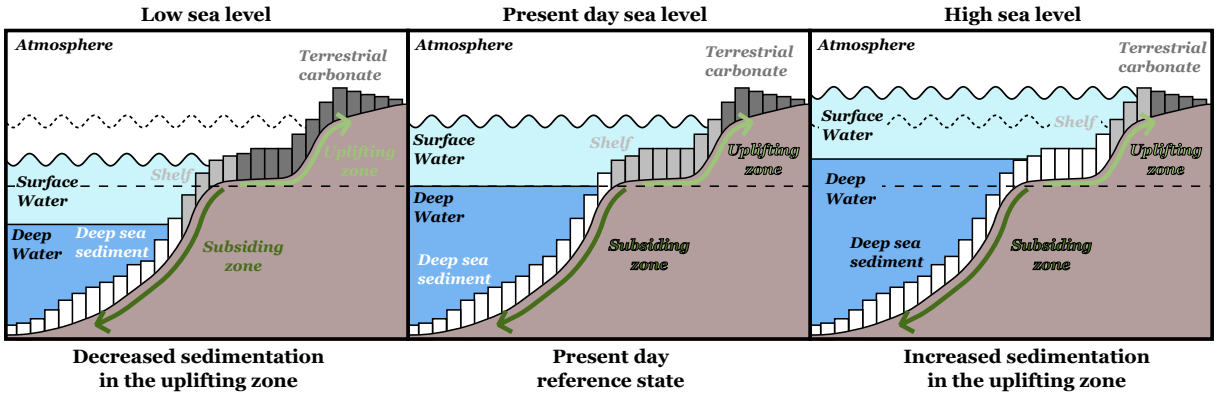

Figure 2.16: ***The different topographic ranges of sedimentary carbonate, relative to sea level, are coloured in dark grey (terrestrial), light grey (shelf) and white (deep sea). Tectonic zones are colours in light green (uplifting) and dark green (subsiding). A fall in sea level focusses oceanic carbon burial into the subsiding zone, while a rise in sea level shift some burial of carbonate into the uplifting zone.***

2.2.3 Long Term Shelf Behaviour

There is thought to be a large mass of carbon currently stored in shelf environments, both as organic carbon and inorganic carbonate. The magnitude of the source of carbon to shelf environments is very poorly quantified, and the long term sinks of carbon from shelves have not been established. As mentioned in Section 2.2.2, there are only two potential sinks of shelf carbon - migration into the deep sea or uplift into the terrestrial environment. The relative magnitude of these sinks is difficult to estimate, but at steady state it must be the case that the source of terrestrial carbonate is equal to the sink, meaning that the uplifting carbonate flux must be equal to the carbonate weathering flux. It could be envisaged that the system is never really at steady state, but that on average, on timescales of hundreds of millions of years, the source and sink of terrestrial carbonate must be roughly balanced, as the Earth is neither covered with, nor devoid of, sedimentary carbonate. Working out the true behaviour of shelf environments on long timescales is an important part of understanding the carbon cycle (*Armstrong McKay et al.*, 2016).

2.2.4 Carbon Cycle Subcycles

One way to view the geological carbon cycle is as two independent subcycles (Figure 2.17), one in which the carbon is uplifted and exposed as terrestrial carbonate, then reweathered (carbonate pathway), and one in which carbon is buried and subducted, then released to the atmosphere after processing in the supraslab or mantle environment (silicate pathway).

At steady state, the source and sink of terrestrial carbonate must be balanced. The only plausible source of terrestrial carbonate is uplift of marine sedimentary carbonate, and the primary terrestrial carbonate sink is weathering. This means that at steady state, the flux of uplifted carbonate must be equal to the flux of weathered carbonate. Given uplift of lithologies is more likely at shallower depths, it is possible to generalise that the shallow burial flux of PIC must be roughly equal to the carbonate weathering flux. Some carbon buried in shallow settings migrates to the deep sea via slumping, but this is effectively equivalent to changing the shallow-deep sea carbon burial fractionation, so provides a one way link from the carbonate to silicate subcycle without affecting the overarching concept.

At steady state, the silicate pathway must also be balanced. This is achieved by processing sedimentary carbon in subduction zones and the supraslab environment, and releasing the stored carbon as CO_2. The efficiency of subduction zone carbon recycling is not known, however at steady state the carbon flux from the mantle (whether through arc regions or MOR regions) must balance the subsiding carbonate flux. It is unclear whether this assumption of steady state is valid, as very little is know about the carbon concentration within the mantle (*Dasgupta* and *Hirschmann*, 2006). It is not currently known whether the mantle is at an approximate steady state with respect to its carbon content, or whether there is gradual ingassing or outgassing.

The residence time of carbon in the silicate pathway is likely to be much less than the residence time of carbon in the carbonate pathway due to the very large amount of carbon in the terrestrial reservoir (though again this is poorly constrained). Movement of carbon from the silicate pathway to the carbonate pathway can have important impacts on the carbon cycle, and therefore the climate, due to the difference in residence times (*Edmond* and *Huh*, 2003), however this is not a system that is represented in most current carbon cycle models. When decreasing the mass of carbon in a reservoir, the carbon must be redistributed into alternative reservoirs. Therefore, if the source of terrestrial carbonate were to be removed, the carbonate currently stored lithologically on land would be eroded without being replaced,

and would feed reservoirs in the silicate pathway, leading to changes in atmospheric CO_2 and climate.

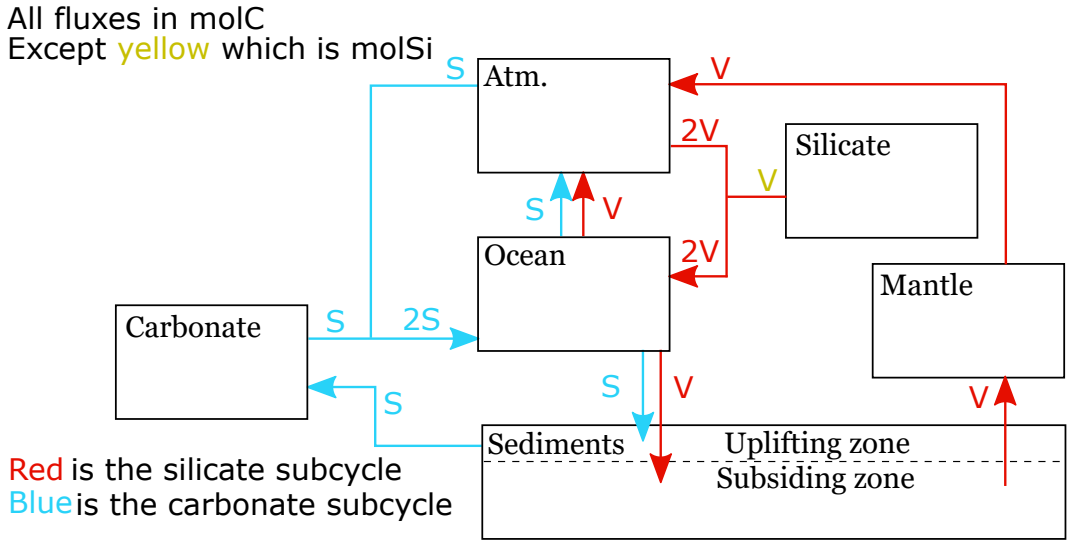

Figure 2.17: ***Steady state fluxes between the primary long term carbon cycle reservoirs are shown. Blue fluxes represent the carbonate pathway and red fluxes represent the silicate pathway. At steady state all fluxes are balanced. To achieve balance, the tectonically uplifting flux must balance the carbonate weathering flux, and the volcanic outgassing flux must balance the silicate weathering flux.***

2.2.5 Importance of Terrestrial Carbonate

The changing source of terrestrial carbonate, as outlined in Section 2.2.2, leads into consideration of the behaviour of the terrestrial carbonate reservoir at large. In GECCO, the magnitude of carbonate weathering is dependent on both the temperature and available areal extent of carbonate to be weathered. There is no reason to imagine changes in the sink of carbonate should be reflected by an equal change in the source of carbonate, but changes in the source of carbonate should be reflected in the sink of carbonate (by manipulating the size of the terrestrial carbonate reservoir). To elaborate, when changes in temperature, availability or weatherability of terrestrially exposed carbonate cause a change in the weathering flux, the standard picture of the carbon cycle would suggest that the ocean accommodates the changing weathering flux through changes in the CCD. As mentioned above, some studies have suggested that the shallow ocean carbonate burial flux is saturation state dependent, but even if this is accurate there is no guarantee that an additional mole of carbonate weathering on land will equate to an additional mole of carbonate burial in the uplifting zone of the ocean floor. Changes in carbonate weathering are therefore able to change the size of the terrestrial carbonate reservoir. Assuming that the carbon cycle is a closed system, changes in the size of the terrestrial carbonate reservoir must be accommodated by equal and opposite changes in other carbon cycle reservoirs. The assumption of a

closed system is evident when considering the Earth at large, but is also often assumed for surficial reservoirs only because the role of the mantle in the carbon cycle is not well known. Proceeding with the assumption that the mantle is at steady state with respect to carbon, then a change in the size of the terrestrial carbonate reservoir must be accommodated in the atmosphere, the ocean, the sedimentary reservoir, or the supraslab environment.

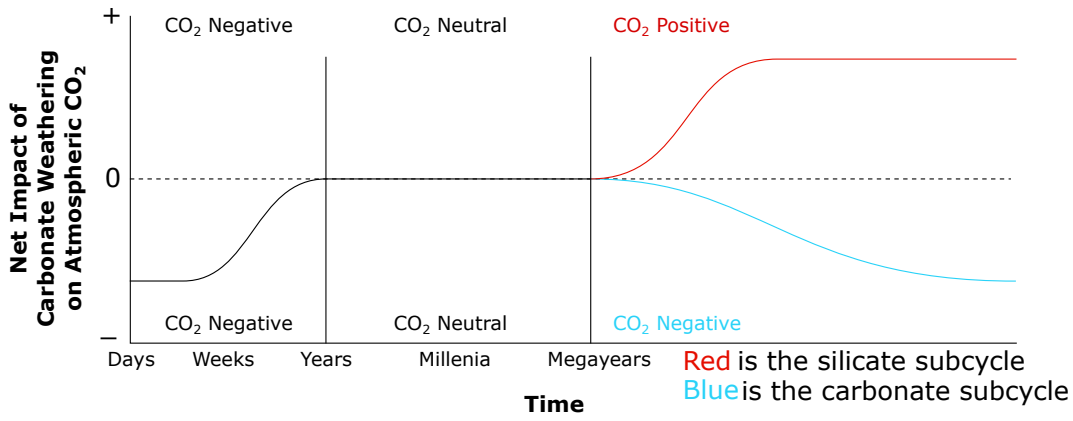

Figure 2.18: ***The net impact of a carbonate weathering event on atmospheric CO_2 evolves through time. Initially, on timescales of days to weeks, the impact is negative as the weathering reactions absorb one mole of CO_2 from the atmosphere. On timescales of years to millions of years, carbonate weathering is carbon neutral, because the mole of CO_2 that was initially consumed from the atmosphere is rereleased when carbonate is reformed in the ocean. The impact of carbonate weathering is then bifurcated depending on the pathway the carbon travels along. If carbon returns to being terrestrial (the carbonate subcycle - blue), then the same process begins again, meaning the impact is CO_2 negative. In contrast, if the carbon travels through a subduction zone (the silicate subcycle - red), it will be released volcanically into the atmosphere, becoming CO_2 positive on long timescales.***

This interpretation of the carbon cycle contrasts to conventional wisdom that carbonate weathering is carbon neutral on geological timescales. Carbon cycle models have therefore not often considered carbonate weathering, as on timescales of thousands to hundreds of thousands of years, the assumption may be made that the size of the terrestrial reservoir is constant (though this is often tacit), and therefore carbonate weathering is carbon neutral.

2.2.6 Ice Feedback

Having determined that variations in the size of the terrestrial carbonate reservoir can potentially be an important carbon cycle flux, it can be posited that this mechanism has the potential to provide a strong asymmetrical climate feedback. As stated above, when sea level falls by a large enough magnitude, the flux of sedimentary carbon being buried in the uplifting zone should approach zero. This means that the burial of ocean carbon must occur in the subsiding regions. This essentially means that all carbon burial will be processed

through the silicate subcycle, rather than the carbonate subcycle. Under the assumption of mantle steady state, this could provide a backstop to atmospheric CO_2 concentration, as any weathering which consumes CO_2 will return that CO_2 to the atmosphere after being processed through the silicate subcycle. In fact this feedback goes further, as focussing the burial of the products of carbonate weathering into the subsiding zone will ensure that the terrestrial carbonate reservoir is being mined of carbon, increasing the amount of carbon stored in other carbon cycle reservoirs, including the atmosphere.

2.2.7 Constraint on the Fate of Oceanic Carbon

The primary source of carbon into the oceanic carbonate system is riverine delivery of bicarbonate as a result of silicate weathering (Equation 1.1) and carbonate weathering (Equation 1.2). The primary oceanic carbon sink is consumption of CO_3^{2-} by calcareous plankton which is subsequently buried as $CaCO_3$. In fact, this is a simplification, as the source of carbon for calcification is not well known, but regardless of which form of carbon is taken up from the ocean, it must be converted to carbonate ion before its incorporation into calcite. In addition to the inorganic sink of carbon is the organic sink. Proceeding on the assumption that this picture is correct and complete, meaning there are no other major fluxes in addition to the carbonate system as depicted in Figure 2.19, a mass and charge balance can be performed for the carbonate system in isolation. The carbonate system as shown in Figure 2.19 has no influx of electrons or protons from other oceanic compounds at steady state. This assumption is warranted because, although as it is known that other oceanic species may also act as proton acceptors and donors, carbon is the most important of these (i.e. it has the largest contribution to alkalinity). At steady state especially, there is no reason to posit that there is an persistent flux of protons into or out of the carbonate system.

Mass balance:

$$R = G + B \tag{2.57}$$

Charge balance:

$$-1R = 0G - 2B \tag{2.58}$$

Rearrange charge balance:

$$B = \frac{1}{2}R \tag{2.59}$$

Substitute Equation 2.58 into Equation 2.57:

$$-(G + B) = -2B \tag{2.60}$$

Rearrange Equation 2.60:

$$G = B \tag{2.61}$$

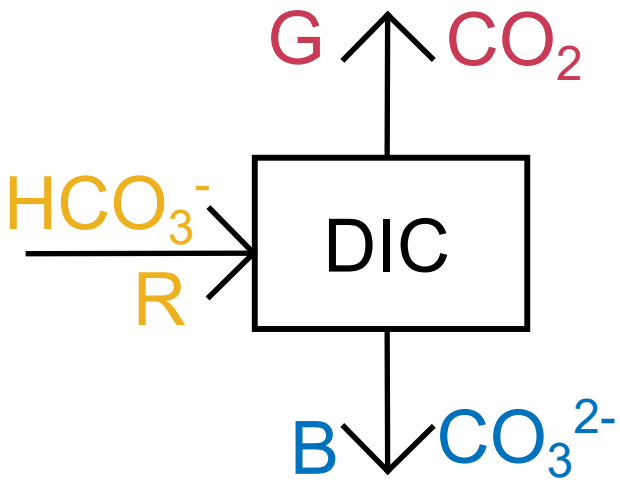

Figure 2.19: ***Input and output fluxes of carbon to and from the carbonate system are shown. Each flux is labelled with a carbon species and a letter to represent the magnitude of the flux (R for Riverine input in yellow, G for Gas exchange in red, and B for Burial in blue) used in Equation 2.57 through Equation 2.61.***

The source of oceanic carbon has a charge of -1 (primarily bicarbonate ions - flux R in Figure 2.19), and the sink has a charge of -2 (carbonate ions - flux B in Figure 2.19), therefore there must be an equal and opposite sink with neutral charge (see Equation 2.57 through Equation 2.61). This neutral sink is the release of CO_2 (flux G in Figure 2.19). This represents an important constraint on the fate of carbon delivered to the ocean, without any consideration of the details of carbonate chemistry, however can only be applied to steady state systems.

Applying charge balance to the oceanic inorganic carbon system (Equation 2.57 through Equation 2.61) therefore shows that about half of the carbon delivered to the ocean is buriable (termed the burial fraction), while the other half is released to the atmosphere (as seen in Figure 1.3). The organic carbon cycle is charge neutral, so is able to increase the buriable fraction.

2.2.8 Deep Earth Alkalinity

The subduction of carbonate, but release of CO_2 from the subterreanean reservoirs, is a sink of charged ions from the carbonate system. These are balanced by the cations which carbon species are bonded with (typically calcium or magnesium). However, the release of CO_2 from the subterranean reservoir does not have to be accompanied by the release of cations, so there is a persistent flux of calcium and magnesium oxides into subduction zone environments that may not be returned to the surficial environment. Calcium and magnesium oxides are extremely common rock forming compounds, so this flux can easily be accommodated, but may have important implications for long term carbon cycle and climate behaviour.

2.2.9 CO_2 Echoes

The nature of a closed carbon cycle is that when carbon is moved out of one reservoir, it must be moved into another. In the case of the long term carbon cycle, there is a progression from reservoirs at the Earth surface, to deep ocean reservoirs and then to lithological reservoirs, before return of carbon to the atmosphere. The nature of this behaviour means that when a pulse of carbon is released to the atmosphere, it will be moved into the ocean and then into sediment. This package of carbon is able to travel around the carbon cycle, revisiting the same reservoirs several times before dispersal. For example, if 1000GtC is released to the atmosphere as CO_2, additional weathering will occur to mitigate this carbon release, spreading that 1000GtC over the seafloor as calcium carbonate. On long timescales this 1000GtC will be subducted, and subsequently released back to the atmosphere as CO_2. This reappearance of the same CO_2 molecules in the atmosphere after a calculable timescale results in 'echoes' of CO_2 pulses. There are naturally diffusive processes that act to spread this carbon throughout the system. For instance, when calcium carbon is formed and buried, it will be preserved over a range of depths. This results in echoes that gradually fade over time, as carbon is repartitioned between the available reservoirs.

This echo behaviour causes oscillations in atmospheric CO_2 that are observed in many of the results presented in this thesis. The periodicity of these oscillations is determined by the cumulative time it takes for carbon to travel through the atmosphere, ocean and lithological reservoirs. By far the longest of these timescales is the time spent as sediment on the seafloor, and the next longest is the amount of time spent as sediment on a subducting slab underneath an overriding plate. As such, the time it takes for a package of carbon to travel

around the carbon cycle once is here referred to as the 'tectonic timescale'. The tectonic timescale was initially established as approximately 12Myr based on literature evidence for the time carbon spends between subduction zones and volcanic release (*Turner et al.*, 2000) and back of the envelope calculations using the distance between areas of 3km depth in the ocean and subducting margins, and an approximate horizontal plate velocity. The model was tuned to move carbon through the sedimentary reservoir over this timescale, and as such many of the results in this thesis display a strong 10Myr periodicity. This value has since been found to be a low in comparison to literature estimates, the importance of which is discussed in Section 2.3.1.

2.2.10 Summary

Overall several new carbon cycle behaviours have been established during the design of the GECCO model. These primarily concern the behaviour of sedimentary carbonate, both terrestrially and in shelf environments, which have previously been overlooked due to the assumed unimportance of carbonate on geological timescales. Silicate weathering, the canonical climate stabilising feedback, must be supported by a feedback which regulates the amount of subaerially exposed silicate, as if silicate weathering was controlled only by temperature then there may be a long term imbalance in the source and sink of terrestrial silicate. Finally, model development also suggests that ice has a key role to play in controlling the depocentre of sedimentation, which may feed into long term climate evolution due to recycling of subducting sediment. Having integrated these components into GECCO, it is now possible to begin to design the experiments which will inform Chapter 3 and Chapter 4.

2.3. GECCO Use

2.3.1 Establishing Steady States

The results presented in the following chapters all start from the same steady state situation. This is done to minimise the temporary flux imbalances caused by the method of model initialisation. By starting at steady state, any changes made during the model run can be easily and clearly causally linked to the ensuing results. Steady states are created by running the GECCO model for hundreds of millions of years with one or more conditions clamped to a specified value. Here, the initial steady state is formed by clamping the atmospheric CO_2 concentration then allowing the model to run until the fluxes are balanced, meaning the model has reached steady state. Due to the length of time the model must be run for this to occur, this is a computationally expensive procedure and therefore all model runs

presented here are initialised to the same steady state here. Unfortunately, there is large uncertainty in the CO_2 concentration that the model should be initialised to in order to be represent the climate at 70Ma. An initial CO_2 concentration of 600ppm was chosen based on the available data (Figure 1.15). Temperature and radiative forcing initial conditions were updated to reflect the new CO_2 concentration. Additional changes made to Preindustrial model parameters are detailed in Table 2.9.

Once created, a steady state is checked by releasing the clamps, then performing a 70Myr simulation without any driven forcings. This is referred to as the control run, and allows calculation of the amount of drift in model parameters caused by latent imbalances. The steady state that is created will never be perfect, so it is simply necessary to establish an acceptable drift threshold. The 600ppm atmospheric CO_2 steady state used here drifts by +50ppm over 70Myr, an average gradient of less than one millionth of a ppm per year, which is deemed well within acceptable limits. There is no reason to believe that a climate at steady state ever truly existed, especially on the long timescales considered here, so why initialise the model in this way? By starting from a steady state, it is possible to perform a simple control experiment which ensures that any deflection of the model output parameters is due to the forcings that are applied. In the case where a transient initial climate state is used to initialise the model, it is difficult to disentangle how much of the change in model output is due to the imposed drivers and how much is due to the initialisation procedure.

As previously stated (Section 2.1.6) the pH solver can fail at particularly challenging conditions - especially when DIC is low and atmospheric CO_2 concentration is high. The crash is therefore partially dependent on the choice of initial conditions. The initial carbonate system state displays a CCD which is consistent with available data, however the CCD is not well quantified so a broad range of carbonate system states are permissible. In addition the CCD is not exclusively a carbonate system parameter, as it depends on other factors such as productivity and production ratio, so there is some flexibility in determining additional carbonate system parameters. The methodology described here to reconstruct the Precenozoic carbonate system state results in a low DIC and alkalinity, which are particularly challenging conditions for the pH solver. This can result in the model crashing when pH falls rapidly, even if the fall is not particularly large.

The following chapters highlight the potential influence of changes in oceanic calcium and magnesium concentration, and changes in tectonic behaviour on the carbon cycle on Cenozoic timescales, rather than replicating the exact forcing that occurred. When performing analyses like this, it is necessary to change the feedback strength and then apply the same set of forcings in order to isolate the impact of a specific feedback. Changing the strength of a feedback has the potential to affect the initial state of the model, causing spurious rapid change driven by the imposed alteration. For example, the silicate weathering feedback strength could be adjusted by simply doubling the amount of silicate weathering that occurs at all temperatures. This would have the unintended side effect of doubling the silicate weathering flux at the initial condition, meaning it would therefore no longer be at steady state, and there would be a rapid drawdown of atmospheric CO_2 early in the model run forced entirely by the change that was made rather than reflecting any true behaviour of the system. In order to avoid cases like this, care has been taken when adjusting feedback strengths (as described in Section 2.4) to keep the initial condition as close as possible to steady state.

Parameter	Units	Estimated Value at 70Ma
Silicate Weatherability	fraction	0.5
Uplifting Carbon Speed	/yr	2.4×10^{-6}
Subsiding Carbon Speed	/yr	8×10^{-5}
Albedo	fraction	0.28
Initial ice mass	mol	0
Initial sea level	m	+140

Table 2.9: ***Parameters at 70Ma, where different to the standard initialised parameters outlined in Sections 2.1.3–2.1.11.***

The resulting carbon cycle steady state formed by the changes as described in Table 2.9 is outlined in Figure 2.20. Most of the reservoirs and fluxes are within the uncertainty of values as presented in Figure 1.17, though in many cases this is hard to establish as the values are known only in the present day and the value in the earliest Cenozoic is unclear. Many of the fluxes can also be constrained by dynamical consideration. For example, at steady state the burial flux of carbon in the deep sea must be equal to the subducting flux of carbonate, the return flux of carbon to the atmosphere and the silicate weathering flux. In many cases this is possible within the uncertainty of the values presented in Figure 1.17, however in some cases there is disagreement. These disagreements may be reconciled by relaxing the assumption of steady state (i.e. the specified fluxes do not have to be equal if the system is not at steady state), or by invoking inaccuracy in some of the observed fluxes, many of which are difficult to estimate.

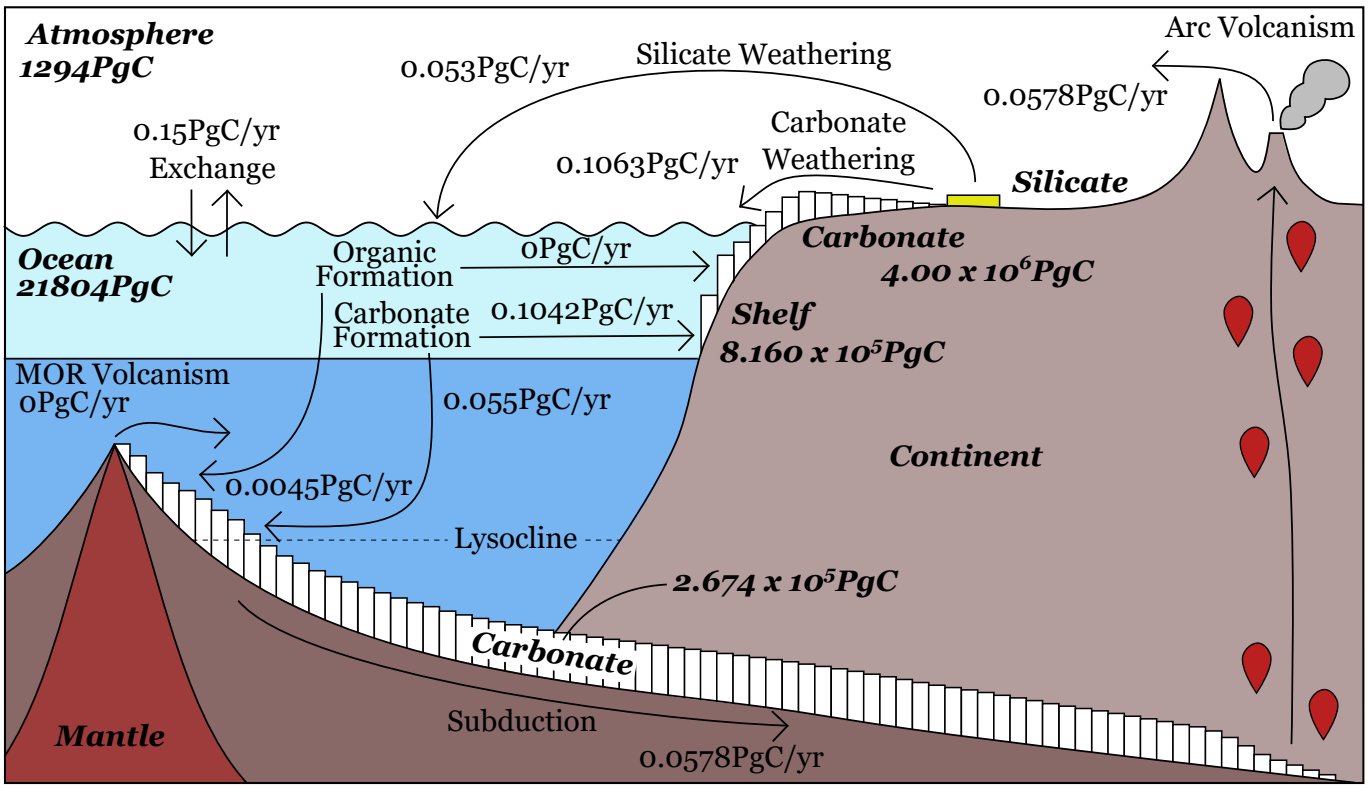

Figure 2.20: ***As in Figure 1.17, the magnitude of major carbon cycle fluxes and sizes of carbon cycle reservoirs is shown - here for the 600ppm atmospheric CO_2 steady state discussed in Section 2.3.1.***

By far the largest disparity between the modelled carbon cycle (as shown in Figure 2.20) and the estimated fluxes and reservoir sizes at 70Ma (as depicted in Figure 1.17), is the difference in sedimentary carbonate mass (in shelves, terrestrial settings and on the seafloor). The disparity in shelf carbonate mass is a result of the change in shelf area that occurred over the Cenozoic (see *Caves et al.* (2016)). GECCO does not resolve spatial variations in the shelf sea, so this change would need to be parameterised in some way. Despite the known increase in shelf sea areal extent at 70Ma relative to the present day, this does not necessarily correlate linearly with an increase in shallow carbonate burial - so there is still considerable uncertainty in the behaviour of shallow carbonate during the early Cenozoic. The deep sea carbonate reservoir is also substantially smaller than existing estimates of the inventory. There are two main reasons which underpin this difference. The first is that GECCO represents only basins in which active subduction is occurring. This naturally decreases the potential storage of carbonate sediment - and resolution of this issue is a potential future route for improvement of the model (as described in Section 2.5). The second reason for this low reconstructed seafloor carbonate mass is the tuning of the timescale over which sediment moves from deposition to subduction to 10Myr (as discussed in Section 2.2.9). This is known to be a low estimate, as the average age of subducting crust

is understood to be approximately 100Ma (*Stern*, 2002), though *Stern* (2002) also highlight that there is notable subduction of crustal material of a young age. Additionally, the sediment atop the subducting plate is younger than the underlying crustal material. Nonetheless, the existing timescale of 10Myr should be increased substantially to better approximate the carbon cycle at 70Ma. The influence of this change is comparatively minor, because sediment is inactive after deposition. Overall, the change in sedimentary mass is unlikely to cause any important change to the results as presented in this thesis other than allowing a more appropriate timescale of tectonic recycling, which would act to increase the repeat timescale of CO_2 echoes observed in many of the results presented here.

2.3.2 Model Verification and Validation

One of the most important, and yet perhaps least interesting, parts of building GECCO was the verification (ensuring everything was programmed as intended - e.g. there were no typographical errors which altered the model functionality) and validation (establishing that the intended functionality of the program accurately reflects the system in question - here ensuring that the coded behaviours appropriately represent the carbon cycle). Verification of the model code was achieved through a variety of means. In some circumstances, when using methods established in other publications or resources, check values were provided to enable rapid verification of the coded function - one particularly good example of this is *Zeebe* and *Wolf-Gladrow* (2001). In most instances however, the coded behaviour was developed from scratch, bespoke for the GECCO model. Verification of these components was primarily achieved by comparison to calculations performed by hand, checking and rechecking of code components, and inevitably the observation of unexpected behaviour which indicated that something had gone awry. Fortunately, most of the mathematics that governs GECCO functionality is relatively straight forward, and the component which had the largest potential risk in terms of transcription errors (the *Carbonate Chemistry Component* - Section 2.1.6) was associated with several check values and could be compared to existing pieces of software which perform almost identical calculations.

In the palaeoclimate discipline, validation is often the more difficult component of ensuring the model is behaving as desired. While the behaviour of almost every aspect of the carbon cycle is deeply complex when considering every detail, it is often the case that a simplified representation will retain the most salient dynamics. Part of the motivation for development of GECCO was a more mechanistic representation of the carbon cycle, and hopefully Chap-

ter 1 and Chapter 2 have outlined both the real world situation and the associated model representation clearly enough to establish that the behaviour of GECCO should be representative of reality. In addition to this, there are several model behaviours which lend credence to its design. As discussed in Section 2.3.1, one of the most practical ways of initialising the model is to clamp a parameter at a desired value, then allow the rest of the system to evolve until the fluxes are balanced, meaning the system has reached steady state. This has been performed for several parameters, though all results presented here have been initialised by clamping CO_2. In all cases, so long as the model is run in the clamped state for a sufficiently long interval and the parameters values chosen are not so ridiculous as to be impossible, GECCO approaches a steady state that is maintained when the clamp is released. The fact that GECCO is able to exist at, or near to, a steady state is the expected and ideal behaviour. Another method of validating that the model is representing the system properly is to modulate those behaviours in which the directionality of the result is known a priori. For instance, silicate weathering provides a sink for atmospheric CO_2 on the timescale of interest (Section 2.1.10), so increasing the silicate weathering flux through some means should result in CO_2 fall. Experiments such as these have been performed on many individual components in a piecemeal fashion, ensuring that the code in question is both verified and satisfactorily characterising the understood behaviour.

Finally, one method of simultaneously verifying and validating the model is implementing a detailed mass balance calculation. At all times within the model, the change in the total mass of carbon in the model should equal the sum of all the carbon fluxes. There are some computational complexities with this method though, because, while in an ideal representation of the carbon cycle no carbon would be lost of gained, the computer must discretise the fluxes through time. Essentially, the size of every reservoir and the fluxes between them can not be tracked to infinite precision. A large component of the lack of precision comes from the fact the model must extrapolate forward in time, assuming that the gradients in reservoir size are linear over the size of timestep. In essence this allows the equality between total mass of carbon in the system and the sum of all fluxes to drift through time, but nonetheless a reasonable threshold may be chosen for this discrepancy, often expressed as a percentage or in parts per million. The mass balance calculation was performed at several times during GECCO model development, and helped to identify problems where they occurred. The completed GECCO model is a closed system with respect to carbon, so it is only necessary to track the size of every reservoir and ensure that this is not variable through time. As stated

previously, the total mass of carbon will not stay exactly the same through time due to the computational methodology introducing the potential for drift, however so long as this drift is small relative to the total mass of carbon in the system then it can be safely ignored. This calculation has been performed for the full GECCO model, and the total mass of carbon was found to vary on the order of a billionth of its total size on timescales of tens of millions of years, well within reasonable limits.

2.4. Principal GECCO Feedbacks

In addition to novel carbon cycle behaviours, the GECCO model contains both known and previously unknown climate feedbacks. Four of these feedbacks are detailed here alongside how their strength may be adjusted within the model. This forms the basis for many of the results presented in the following two chapters.

2.4.1 Carbonate Compensation Feedback

Feedback Overview

The carbonate compensation feedback stabilises the saturation state of the deep ocean (*Ridgwell* and *Zeebe*, 2005). The feedback is understood to operate by shoaling and deepening of the CCD in response to changes in ocean saturation state. Changes in the depth of the CCD are thought to cause changes in the carbonate export flux until it is balanced with the oceanic carbonate influx. The depth of the CCD influences carbonate burial by changing the fraction of deep sea PIC flux that is buried as sediment, meaning that other factors are also able to at least transiently influence the carbonate burial flux, such as changes in rain ratio.

The carbonate compensation feedback is one of the best established feedbacks, and is generally considered to be both conceptually and mathematically understood (*Zeebe* and *Westbroek*, 2003; *Ridgwell* and *Zeebe*, 2005; *Boudreau et al.*, 2019). There is physical evidence of changes in sediment carbonate content at times when ocean carbonate chemistry is known to have changed, linking the boundary in the water column between carbonate supersaturation and undersaturation (the CSH) with the depth below which no carbonate sediment is preserved (the CCD). New research (*Hülse et al.*, 2017) is casting doubt on the behaviour of this feedback though, and the intuitive mechanics may not hold true when all factors are considered. For instance, if the offset between the CSH and CCD is variable through time, it is possible to somewhat decouple the CCD from carbon burial (Figure 2.21). Given the offset between the CSH and CCD is typically on the order of several hundred me-

tres (*Ridgwell* and *Zeebe*, 2005), a deepening of the CSH without coeval deepening of the CCD could feasibly result in meaningful changes in carbonate burial (*Greene et al.*, 2019).

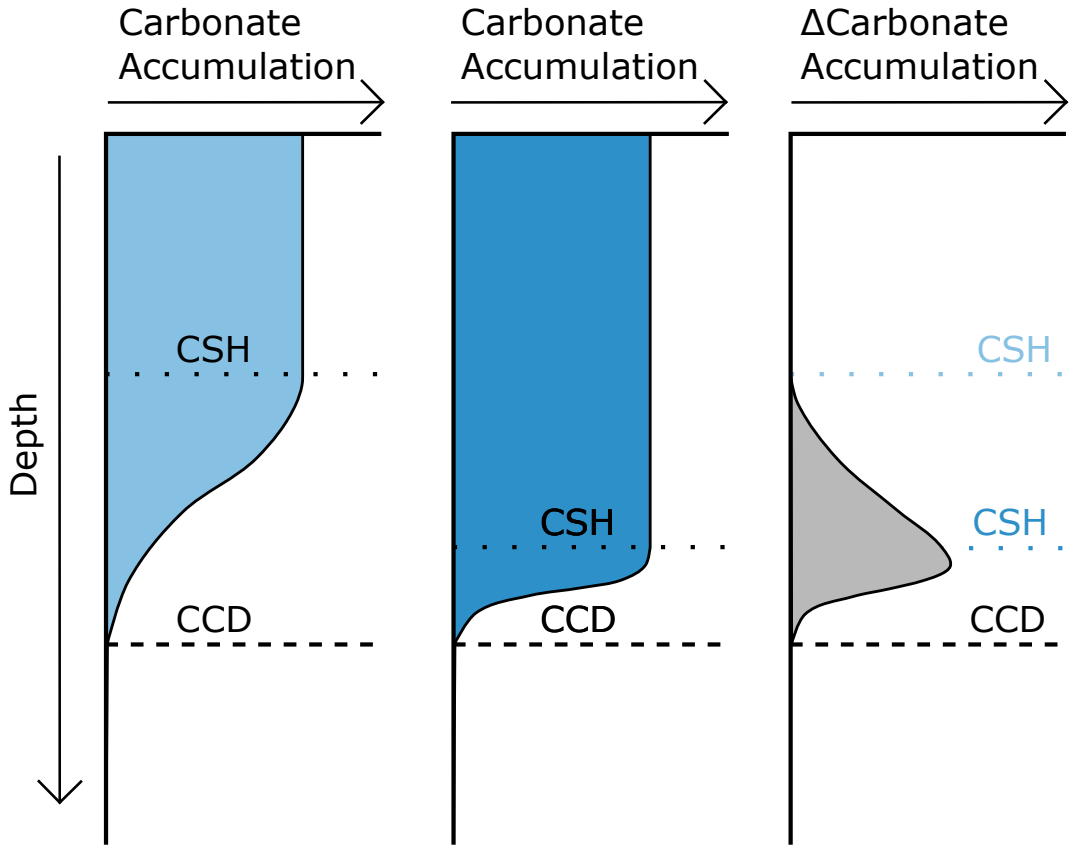

Figure 2.21: ***The first panel (light blue) shows a schematic of carbonate accumulation against depth when the CSH and CCD have a large separation. The second panel (dark blue) shows the same type of schematic but for the case where the CSH is deeper, but the CCD has not changed, meaning the CSH and CCD are closer together. The final panel shows the difference in carbonate accumulation between these two situations, where greater carbonate accumulation occurs when the CSH and CCD are closer together.***

In both deepwater and sediment porewater settings, decomposition of organic matter increases the acidity of the environment (by increasing DIC without affecting alkalinity). In the water column, this metabolic CO_2 is accounted for by changes in the CSH, but porewater CO_2 is able to reduce the burial flux of carbonate without changing the depth of the CSH, leading to a change in the CSH-CCD offset, potentially reversing the typical order of these horizons. This effect is not universal though, and appears to vary with factors such as organic rain rate and temperature (*Hülse et al.*, 2017). In the deep sea, the organic carbon burial flux is much less than the inorganic carbon burial flux, so is not the primary vehicle of carbon burial, but may still have a significant effect on the link between the CSH and carbonate burial flux.

An additional complication is the potential impact of abiotic carbonate precipitation. Hydrothermal circulation through ocean crust can result in the precipitation of carbonate. The magnitude of this flux has been estimated in the past (*Alt* and *Teagle*, 1999), but is not routinely incorporated into carbon cycle models of this kind. While the uncertainties surrounding the relationship between the CSH and CCD are particularly important for models, it does not change the fact that the ocean carbonate ion budget must be balanced at steady state, but the potential for abiotic carbonate to affect the ocean carbonate ion budget could change the magnitude of the role of the CCD in accommodating the necessary burial flux of oceanic carbonate ions. Anecdotally, this might help to explain the observation that the carbon cycle does not appear to undergo a massive perturbation in the wake of the evolution of pelagic calcifiers during the Triassic. This shift from a neritan to a cretan ocean mode would be expected to have major implications for ocean carbonate chemistry by changing the shallow ocean saturation state required to drive the right magnitude of oceanic carbonate ion output (*Zeebe* and *Westbroek*, 2003).

These complications fundamentally challenge our current understanding of the mechanisms relating water column chemistry to oceanic carbon burial. The feedback as employed within the model has no link between sedimentary organic carbon and sedimentary carbonate preservation. This situation is not ideal, but is in line with other models of the same complexity. Some models have a more detailed representation of the biogeochemical processes operating with the water column and sediments and are therefore able to perform more complex calculations to estimate the degree of porewater aerobic carbon respiration, and resulting carbonate dissolution, but this comes at significant computation cost. Overall, GECCO behaves in accordance with the traditional understanding of CCD mechanics, but may be updated in future once the relationship between organic and inorganic carbon burial, and the impact of abiotic carbonate precipitation are better understood. Despite the uncertainties in the exact mechanics underlying oceanic carbon burial, the carbonate compensation feedback is known to be important in balancing oceanic carbon input and output. It is therefore useful to be able to alter the strength of this feedback within the model in order to understand the potential importance of the carbonate compensation feedback, as it is currently understood, in determining climate stability.

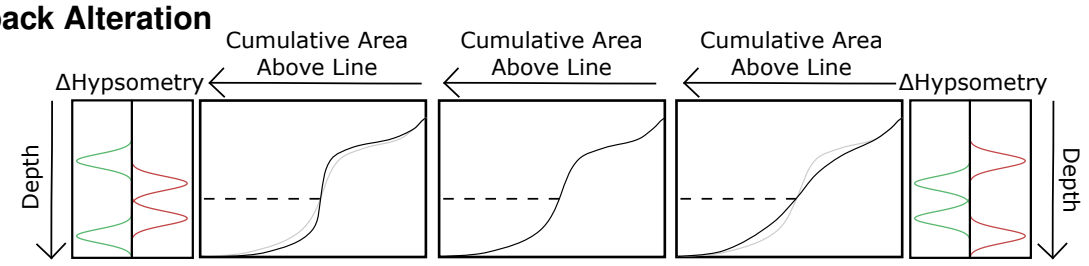

Figure 2.22: ***The central panel shows a reference condition hypsometry. From this state, the hypsometric gradient in the vicinity of the CCD (dashed black line) can be shallowed (left panel) or steepened (right panel). This is done by changing the hypsometry data using Gaussian distributions (lower panels), which add (green) and remove (red) seafloor area. The total seafloor area stays the same, however how this area is distributed with depth is altered based on the alignment of the Gaussian distributions. Seafloor area is added to depth ranges of the green Gaussian, and removed from depth ranges of the red Gaussian. Two pairs of Gaussians are used so that the initial CCD (grey in side panels) will result in the same initial carbonate burial fraction.***

The hypsometric curve can be steepened or flattened in order to change the relationship between the CCD and inorganic carbon preservation percentage (Figure 2.22 and Figure 2.23). The change in hypsometric gradient is achieved by using pairs of Gaussian distributions. One Gaussian distribution is used to remove a defined percentage of ocean crust from a controlled depth range, then a complementary Gaussian is used to replace this removed ocean crust at a different depth range. To keep the initial steady state as similar as possible, two pairs of Gaussians are used such that the net change in the hypsometry is negligible around the initial depth of the CCD (see Figure 2.22). Despite this, changes to the hypsometry do cause a change in the initial steady state by altering the proportion of land below sea level, which affects the fraction of ocean floor on which carbonate is buried. The change in hypsometry acts to change the strength of the carbonate compensation feedback as shown in Figure 2.23. The steeper the hypsometric gradient, the more change is required in the CCD to cause an equivalent change in carbonate burial. This means that ocean saturation state is more variable when the hypsometric gradient is steep, which is typically achieved through greater variation in the carbonate ion concentration.

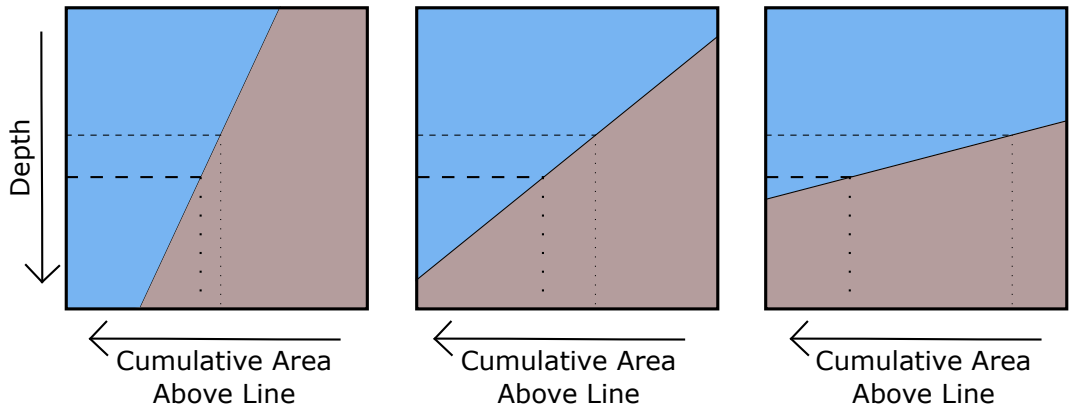

Figure 2.23: ***Changing the CCD (dashed black line) by the same vertical extent causes greater change in the area of seafloor when the hypsometry is more shallow. Shallow hypsometries therefore increase the sensitivity of carbonate burial to the CCD.***

2.4.2 Silicate Weathering Feedback

Feedback Overview

As described in Section 2.1.10, data suggest that there is a fairly well defined exponential relationship between atmospheric temperature and silicate weathering. Each mole of silicate weathering consumes two moles of CO_2 (Equation 1.1). When the products of weathering are used in the ocean to create calcium carbonate, one mole of the carbon is buried and the other returns to CO_2 (Equations 1.7–1.9). Assuming silicate weathering is entirely controlled by temperature, the net result of this process is stabilisation of temperature, and by extension atmospheric CO_2 concentration (where other radiative factors are not changing).

Feedback Alteration

In GECCO, the relationship between silicate weathering fraction and temperature is defined by an exponential relationship with three coefficients (Equation 2.47). The default values for those coefficients are established by assuming the final, additive coefficient is zero, and then fitting a curve to existing data (Figure 2.9). The relationship is manipulated by adjusting the third coefficient (somewhat analogous to the y intercept value of the silicate weathering-temperature curve), assuming the first coefficient remains the same, and then recalculating the second coefficient to ensure that the initial state of the model remains identical. This allows the silicate weathering feedback to be tuned in a predictable way (see Figure 2.24).

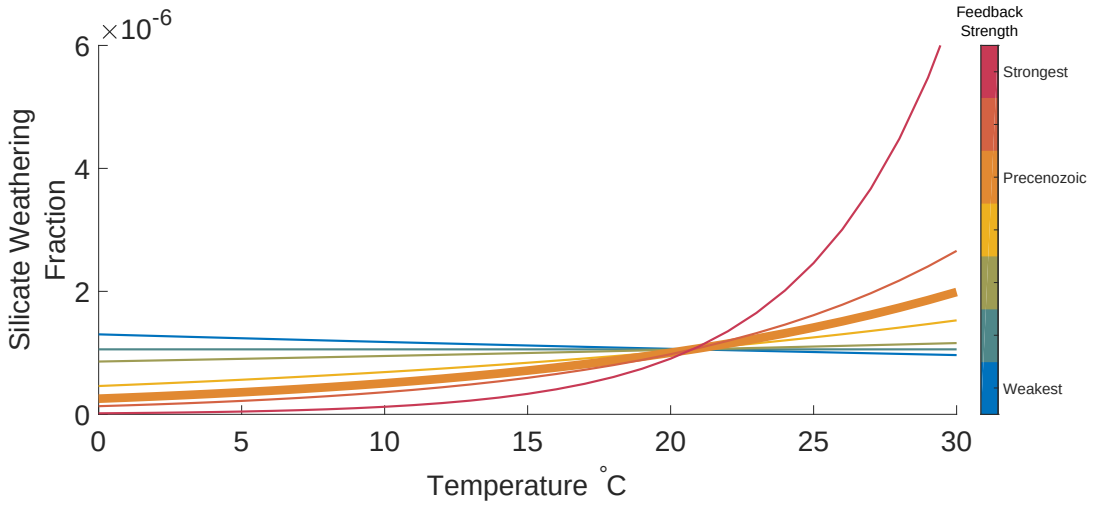

Figure 2.24: ***The relationship between the fraction of the exposed silicate area which is weathered, and the atmospheric temperature is tuned in order to strengthen or weaken the feedback. Stronger silicate weathering-temperature relationships are shown in hot colours, and weaker silicate weathering-temperature relationships are shown in cooler colours. The silicate weathering fraction at the initial temperature is the crossing point of curves.***

2.4.3 Carbonate Weathering Feedback

Feedback Overview

Carbonate weathering is traditionally thought to be carbon neutral on superannual timescales. This is because the carbonate weathering reaction that occurs terrestrially is reversed when carbonate is formed in the ocean, and the single mole of CO_2 that was removed from the atmosphere by weathering is reformed in the ocean. While this is accurate, it belies the effect of the transfer of carbon from the 'carbonate subcycle' to the 'silicate subcycle'. The terrestrial carbonate reservoir is large, and changes in carbonate weathering have the potential to change the terrestrial carbonate inventory over long timescales if the change in sink is not matched by a corresponding change in the terrestrial carbonate source. There is no a priori reason to expect that changes in terrestrial carbonate weathering will be exactly matched by changes in the source of terrestrial carbonate (here assumed to be primarily shallow ocean carbonate burial). It has been suggested that shelf carbonate burial is related to ocean saturation state (presumably driven by an assumption that calcifiers will struggle when the ocean acidifies), so there may be a link between the carbonate source and sink, but this is not obligated to be a one to one relationship. In other words, there is no known compelling reason to believe that the carbonate subsystem in isolation seeks balance. This allows changes in carbonate weathering to drive changes in the terrestrial carbonate reservoir size, which, in a closed system such as GECCO, means that at least one other reservoir much accommodate

that change. In GECCO, carbonate weathering is assumed to be controlled by temperature, by default showing the same relationship as between silicate weathering and temperature.

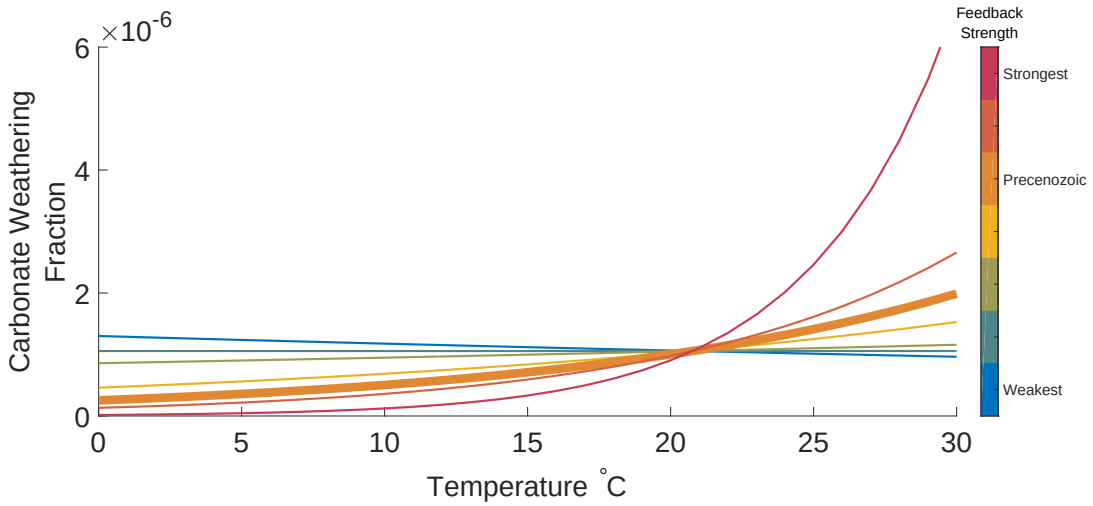

Figure 2.25: ***As in Figure 2.24, the relationship between the fraction of exposed carbonate that is weathered and temperature is controlled by an exponential curve defined by three unique coefficients that allow the curve to be steepened (hot colours) and shallowed (cool colours).***

Feedback Alteration

As with silicate weathering, the relationship between carbonate weathering fraction and temperature is defined by an exponential equation with three independent components (Equation 2.46). By specifying two coefficients, the third can be calculated to ensure that the initial model state remains the same, while the carbonate weathering response to temperature change is strengthened or weakened (Figure 2.25).

2.4.4 Phosphate Weathering Feedback

Feedback Overview

Changes in phosphate delivery to the ocean drive changes in productivity that affect the carbon cycle in two main ways. Firstly, changes in productivity directly affect the organic carbon production flux. In the GECCO model, the fraction of buried organic carbon is a fixed fraction of organic carbon production, so increases in productivity directly increase the organic carbon burial flux. Secondly, productivity change also has a more indirect impact through the CCD. The CCD controls the fraction of PIC production that is buried in sediment, so in order to maintain the same burial flux when productivity changes, the CCD must shift. All else being equal, an increase in productivity will cause a shoaling of the CCD.

Feedback Alteration
In GECCO, the riverine phosphate flux to oceans is determined by summing a specified fraction of silicate weathering, a specified fraction of carbonate weathering and an additional constant component. By adjusting the constant component, then recalculating the coefficients which control the proportionality to carbonate and silicate weathering, the initial phosphate flux can be kept the same while adjusting the feedback strength.

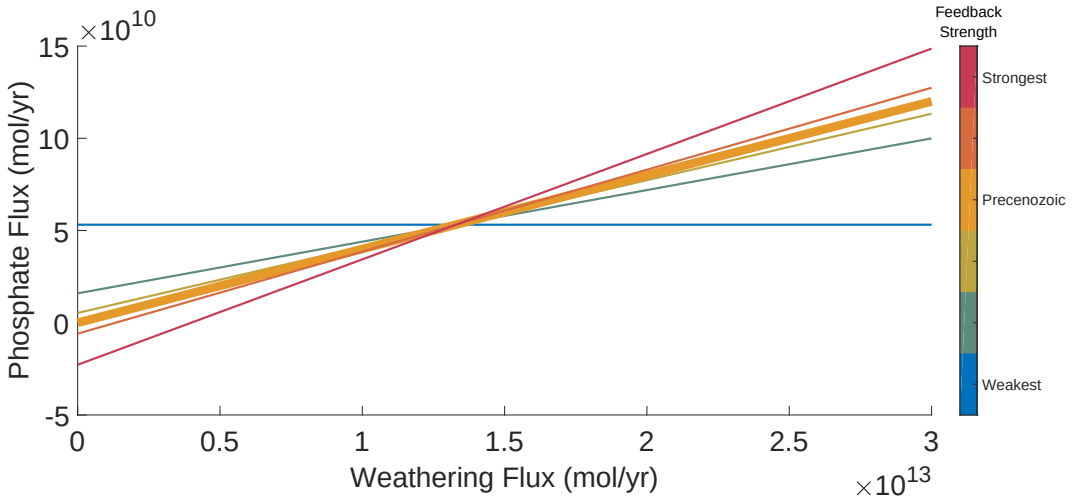

Figure 2.26: ***The phosphate weathering feedback is controlled by the relationship between phosphate weathering and other rock weathering. The feedback strengths go from a no feedback scenario (blue) to the strongest feedback scenario (red).***

2.4.5 Feedback Summary

In conclusion, there are four principal feedbacks that are identified for investigation of their role in determining long term carbon cycle trends. Two of these, the carbonate compensation and silicate weathering feedbacks, have been extensively studied and have known expected outcomes. In contrast, the expected impact of the carbonate weathering feedback and phosphate weathering feedback are less well defined.

2.5. Future Work

The model as presented above is a comprehensive representation of the long term carbon cycle, but as with any characterisation of a system, there are always improvements that can be made and advances in knowledge that should be incorporated into the model. Inevitably simplifications had to be made in order to produce a functioning model within a reasonable timeframe. Every effort has been made to ensure that these simplifications affect the conclusions of the studies presented here as little as possible, but nonetheless in certain circumstances it would be ideal to improve the representation of some carbon cycle components. Below a list of desired model refinements and improvements is presented alongside

the benefits such a change would likely bring.

- **Port GECCO to a lower level language**

  GECCO is written in Matlab, which is an ideal language for prototyping, and has a 'just in time' (JIT) compiler that means code runs comparatively quickly, but translating GECCO to a lower level language would enable greater control of the processing workflow and increased computational efficiency. In addition, Matlab requires an expensive license, and, while code can be distributed for free by having users install a Matlab runtime environment, in an ideal case GECCO would be open source software available for download without any external dependencies.

- **Incorporate oxygen and carbon isotopes**

  As outlined in Section 1.6.3, carbon and oxygen isotopes are extensively used in the interpretation of palaeoclimate. Incorporation of a calculation of the evolution of these isotope systems through time would enable direct comparison between model output and proxy reconstructions. Theoretically, the calculations for these isotopes could be performed after the model run completes, assuming that the fluxes are independent of the isotope system. While this is potentially beneficial in terms of modularity, it would likely be more computationally efficient to perform the calculations during the model run.

- **Allow specification of tectonic recycling efficiency**

  GECCO assumes that the total mass of carbon within the represented reservoirs of the system remains the same through time. This means that all carbon which is subducted must be put into another reservoir. As it currently stands, there is no representation of the mantle, which means carbon must be stored in the subterranean environment before volcanic release. There is no computational difficulty in implementing a parameter to control tectonic recycling efficiency, however one of the key advantages that GECCO provides over existing models is that there is no requirement to specify disconnected input and output fluxes of carbon, so allowing the tectonic recycling efficiency to be chosen necessitates the incorporation of a mantle reservoir. At present, both the amount of carbon stored in the mantle and how that carbon behaves are very uncertain, but in future it would be beneficial to examine the potential impact of incorporating the mantle as a carbon reservoir.

- **Add a terrestrial organic carbon reservoir**

The evolution of terrestrial inorganic carbon within GECCO informs many of the behaviours observed, indicating that terrestrial carbon cycling could be an important climate driver/feedback. Organic carbon deposited in very shallow ocean settings, and then uplifted, might form important deposits of terrestrial organic carbon, which could contribute meaningfully to the evolution of atmospheric CO_2. Addition of this reservoir would also solve one of the most undesirable simplifications made within GECCO - the assumption that no organic carbon burial happens at shallow ocean depths. This assumption is known to be inaccurate, however without a representation of terrestrial organic carbon, there is no reasonable pathway for uplifted organic carbon to take.

- **Change Calcium and Magnesium to state variables**

  Calcium and magnesium fluxes in the ocean are at least partially controlled by tectonic plate behaviour. Given these ions are known to be of importance in ocean carbon chemistry, and their concentrations are known to have varied over the Cenozoic, it would be beneficial to be able to drive their concentrations dynamically according to their mechanics. Currently there is a disconnect, in that the source/sink fluxes of calcium and magnesium are not affected by changes in tectonic behaviour, which may lead to erroneous conclusions. For example, if increasing plate speed results in a change to calcium and magnesium concentration that acts to draw down atmospheric CO_2 through changes to the oceanic carbonate system, but acts to increase atmospheric CO_2 through its effect on subterranean carbon storage, then there is a level of self mitigation to the system. If the converse is true, then the impact of changing plate speed may be twofold. Implementing the current understanding of the link between these parameters would further inform current understanding of the carbon cycle. Nonetheless, the investigation into the role of calcium and magnesium in driving carbon cycle trends is in itself novel, and implementing connections between drivers would only serve to further improve understanding.

While the changes listed above would be beneficial to GECCO, their omission is not cause for concern and should not have a major impact on the conclusions drawn from the studies presented in this thesis. Each chapter provides a section specifically to consider the potential limitations imposed by the model and the assumptions on which the conclusions are built. On many occasions said assumptions are made based on current understanding, though in some cases assumptions have been made due to the lack of available knowledge. No model can incorporate everything, and even if it could we do not yet know everything (which is a

prerequisite for incorporation into a model), but that does not prevent models from accurately representing the salient pieces of a system.

References

Alt, J. C., and Teagle, D. A. H., 1999, The uptake of carbon during alteration of ocean crust, *Geochimica et Cosmochimica Acta*, **63**(10), 1527–1535.

Anderson, L. a., and Sarmiento, J. L., 1994, Redfield ratios of remineralization determined by nutrient data analysis, *Global Biogeochemical Cycles*, **8**(1), 65–80.

Armstrong McKay, D. I., Tyrrell, T., and Wilson, P. A., 2016, Global carbon cycle pertubation across the Eocene-Oligocene climate transition, *Paleoceanography*, **31**, 311–329.

Banse, K., 1982, Marine Pelagial Cell volumes, maximal growth rates of unicellular algae and ciliates, and the role of ciliates in the marine pelagial, *Limnology*, **27**(6), 1059–1071.

Banse, K., 1992, Grazing, temporal changes of phytoplankton concentrations and the microbial loop in the open sea In *Primary Productivity and Biogeochemical Cycles in the Sea*, Plenum Press, New York.

Barnes, R., and Hughes, R., 1988, *An Introduction to Marine Ecology*, Blackwell Science Ltd, Malden, MA, 3rd edition.

Berger, W., Fischer, K., Lau, C., and Wu, G., 1987, Ocean carbon flux: global maps of primary production and export production In *Biogeochemical Cycling and Fluxes Between the Deep Euphotic Zone and Other Realms*, NOAA.

Boudreau, B. P., Middelburg, J. J., Sluijs, A., and Ploeg, R., 2019, Secular Variations in the Carbonate Chemistry of the Oceans over the Cenozoic, *Earth and Planetary Science Letters*, **512**, 194–206.

Broecker, W., and Peng, T.-H., 1982, *Tracers In The Sea*, Columbia University, New York.

Calmels, D., Gaillardet, J., and François, L., 2014, Sensitivity of carbonate weathering to soil CO2 production by biological activity along a temperate climate transect, *Chemical Geology*, **390**, 74–86.

Caves, J. K., Jost, A. B., Lau, K. V., and Maher, K., 2016, Cenozoic carbon cycle imbalances and a variable weathering feedback, *Earth and Planetary Science Letters*, **450**, 152–163.

Chuck, A., Tyrrell, T., Totterdell, I., and Holligan, P., 2005, The oceanic response to carbon emissions over the next century: investigation using three ocean carbon cycle models, *Tellus B*, **57**(B), 70–86.

Dasgupta, R., and Hirschmann, M. M., 2006, Melting in the Earth's deep upper mantle caused by carbon dioxide, *Nature Letters*, **440**(March), 659–662.

Davies, A. G., and Sleep, J. A., 1989, The photosynthetic response of nutrient-depleted dilute cultures of Skeletonema costatum to pulses of ammonium and nitrate; the importance of phosphate, *Journal of Plankton Research*, **11**(1), 141–164.

DeConto, R. M., and David Pollard, 2003, Rapid Cenozoic glaciation of Antarctica induced by declining atmospheric CO2, *Nature*, **1317**(2001), 1313–1317.

Dickson, A., and Goyet, C., 1994, *DOE - Handbook of methods for the analysis of the various parameters of the carbon dioxide system in sea water*, 2nd edition.

Dunne, J. P., Sarmiento, J. L., and Gnanadesikan, A., 2007, A synthesis of global particle export from the surface ocean and cycling through the ocean interior and on the seafloor, *Global Biogeochemical Cycles*, **21**(4), 1–16.

Edmond, J. M., and Huh, Y., 2003, Non-steady state carbonate recycling and implications for the evolution of atmospheric PCO2, *Earth and Planetary Science Letters*, **216**, 125–139.

Edwards, K. F., Thomas, M. K., Klausmeier, C. A., and Litchman, E., 2012, Allometric scaling and taxonomic variation in nutrient utilization traits and maximum growth rate of phytoplankton, *Limnology and Oceanography*, **57**(2), 554–566.

England, M. H., 1995, The Age of Water and Ventillation Timescales in a Global Ocean Model, *Journal of Physical Oceanography*, **25**, 2756–2778.

Follows, M. J., Ito, T., and Dutkiewicz, S., 2006, On the solution of the carbonate chemistry system in ocean biogeochemistry models, *Ocean Modelling*, **12**(3-4), 290–301.

Furnas, M. J., 1990, In situ growth rates of marine phytoplankton: Approaches to measurement, community and species growth rates, *Journal of Plankton Research*, **12**(6), 1117–1151.

Gerecht, A. C., Šupraha, L., Edvardsen, B., Probert, I., and Henderiks, J., 2014, High temperature decreases the PIC/POC ratio and increases phosphorus requirements in Coccolithus pelagicus (Haptophyta), *Biogeosciences*, **11**(13), 3531–3545.

Goldman, J. C., 1979, On phytoplankton growth rates and particulate C: N: P ratios at low light, *Limnology and Oceanography*, **31**(6), 1358–1363.

Greene, S. E., Ridgwell, A., Turner, S. K., Schmidt, D. N., and Pälike, H., 2019, Early Cenozoic Decoupling of Climate and Carbonate Compensation Depth Trends, *Paleoceanography and Paleoclimatology*, **-**, –.

Haas, H. D., Weering, T. C. E. V., and Stigter, H. D., 2002, Organic carbon in shelf seas: sinks or sources, processes and products, *Continental Shelf Research*, **22**, 691–717.

Hain, M. P., Sigman, D. M., Higgins, J. A., and Haug, G. H., 2015, The effects of secular calcium and magnesium concentration changes on the thermodynamics of seawater acid/base chemistry: Implications for Eocene and Cretaceous ocean carbon chemistry and buffering, *Global Biogeochemical Cycles*, 517–533.

Haq, B. U., Hardenbol, J., and Vail, P. R., 1988, Mesozoic and Cenozoic Chronostratigraphy

and Cycles of Sea-Level Change, *Sea-Level Changes*, **1**, 71–108.

Honisch, B., Ridgwell, A., Schmidt, D. N., Thomas, E., Gibbs, S. J., Sluijs, A., Zeebe, R., Kump, L., Martindale, R. C., Greene, S. E., Kiessling, W., Ries, J., Zachos, J. C., Royer, D. L., Barker, S., Marchitto, T. M., Moyer, R., Pelejero, C., Ziveri, P., Foster, G. L., and Williams, B., 2012, The Geological Record of Ocean Acidification, *Science*, **335**(6072), 1058–1063.

Hülse, D., Arndt, S., Wilson, J. D., and Munhoven, G., 2017, Understanding the causes and consequences of past marine carbon cycling variability through models, *Earth-Science Reviews*, **171**(March), 349–382.

Iglesias-Rodriguez, M. D., Buitenhuis, E. T., Raven, J. A., Schofield, O., Poulton, A. J., Gibbs, S., Halloran, P. R., and Baar, H. J. W., 2008, Response to Comment on "Phytoplankton Calcification in a High-CO2 World", *Science*, **322**(5907), 1466c–1466c.

IOC, IHO, and BODC, 2003, *Centenary Edition of the GEBCO Digital Atlas*,.

IPCC, 2001, *Climate Change 2001: The Scientific Basis. Contribution of Working Group I to the Third Assessment Report of the Intergovernmental Panel on Climate Change*, Cambridge University Press, Cambridge.

Jahnke, R., 1992, The phosphorus cycle In *Global Biogeochemical Cycles*, Academic Press, London.

Johnson, K. A., and Goody, R. S., 2011, The original Michaelis constant: Translation of the 1913 Michaelis-Menten Paper, *Biochemistry*, **50**(39), 8264–8269.

Kelemen, P. B., and Manning, C. E., 2015, Reevaluating carbon fluxes in subduction zones, what goes down, mostly comes up, *Proceedings of the National Academy of Sciences*, **112**(30), E3997–E4006.

Kump, L. R., 2018, Prolonged Late Permian-Early Triassic hyperthermal: failure of climate regulation? *Philosophical Transactions of the Royal Society A*, **376**, 1–9.

Lemarchand, D., Gaillardet, J., Lewin, A., and Allègre, C. J., 2002, Boron isotope systematics in large rivers: Implications for the marine boron budget and paleo-pH reconstruction over the Cenozoic, *Chemical Geology*, **190**(1-4), 123–140.

Lenton, T. M., and Watson, A. J., 2000, Redfield Revisited: Regulaition of nitrate, phosphate, and oxygen in the ocean, *Global Biogeochemical Cycles*, **14**(1), 225–248.

Li, G., Hartmann, J., Derry, L. A., West, A. J., You, C. F., Long, X., Zhan, T., Li, L., Li, G., Qiu, W., Li, T., Liu, L., Chen, Y., Ji, J., Zhao, L., and Chen, J., 2016, Temperature dependence of basalt weathering, *Earth and Planetary Science Letters*, **443**, 59–69.

Mackenzie, F., Ver, L., Sabine, C., Lane, M., and Lerman, A., 1993, C, N, P and S global

biogeochemical cycles and modeling of global change In *Interactions of C, N, P and S Biogeochemical Cycles and Global Change*, Springer-Verlag, Berlin.

Martin, J. H., Knauer, G. A., Karl, D. M., and Broenkow, W. W., 1987, VERTEX: carbon cycling in the northeast Pacific, *Deep Sea Research Part A, Oceanographic Research Papers*, **34**(2), 267–285.

Martiny, A. C., Pham, C. T. A., Primeau, F. W., Vrugt, J. A., Moore, J. K., Levin, S. A., and Lomas, M. W., 2013, Strong latitudinal patterns in the elemental ratios of marine plankton and organic matter, *Nature Geoscience*, **6**(4), 279–283.

Mason, E., Edmonds, M., and Turchyn, A. V., 2017, Remobilization of crustal carbon may dominate volcanic arc emissions, *Geochemistry*, **294**(July), 290–294.

McAllister, C., Shah, N., and Strichland, J., 1964, Marine phytoplankton photosynthesis as a function of light intensity: a comparison of methods, *J. Fish. Res. Board Can.*, **21**, 159–181.

Peucker-Ehrenbrink, B., 2009, Land2Sea database of river drainage basin sizes, annual water discharges, and suspended sediment fluxes, *Geochemistry, Geophysics, Geosystems*, **10**(6), 1–10.

Redfield, A. C., 1934, *On the Proportions of Organic Derivatives in Sea Water and Their Relation to the Composition of Plankton*, Univ Press Liverpool, Liverpool.

Ridgwell, A., and Zeebe, R., 2005, The role of the global carbonate cycle in the regulation and evolution of the Earth system, *Earth and Planetary Science Letters*, **234**(3-4), 299–315.

Romero-Mujalli, G., Hartmann, J., and Börker, J., 2018, Temperature and CO2 dependency of global carbonate weathering fluxes - Implications for future carbonate weathering research, *Chemical Geology*, 1–18.

Schlesinger, W., 1997, *Biogeochemistry: an Analysis of Global Change*, Academic Press, Waltham, MA, 3rd edition.

Stern, R. J., 2002, Subduction zones, *Reviews of Geophysics*, **40**(4), –.

Teng, Y. C., Primeau, F. W., Moore, J. K., Lomas, M. W., and Martiny, A. C., 2014, Global-scale variations of the ratios of carbon to phosphorus in exported marine organic matter, *Nature Geoscience*, **7**(12), 895–898.

Turner, S. P., George, R. M., Evans, P. J., Hawkesworth, C. J., and Zellmer, G. F., 2000, Time-scales of magma formation, ascent and storage beneath subduction-zone volcanoes, *Philosophical Transactions of the Royal Society A: Mathematical, Physical and Engineering Sciences*, **358**(1770), 1443–1464.

Tyrrell, T., 1999, The relative influences of nitrogen and phosohorus on oceanic primary production, *Nature*, **400**(6744), 525–531.

West, A. J., Galy, A., and Bickle, M., 2005, Tectonic and climatic controls on silicate weathering, *Earth and Planetary Science Letters*, **235**(1-2), 211–228.

Zeebe, R. E., and Westbroek, P., 2003, A simple model for the $CaCO_3$ saturation state of the ocean: The Strangelove, the Neritan, and the Cretan Ocean, *Geochemistry, Geophysics, Geosystems*, **4**(12), 1–26.

Zeebe, R. E., and Wolf-Gladrow, D., 2001, *CO2 in Seawater: Equilibrium, Kinetics, Isotopes*, Elsevier Ltd., Amsterdam, 3rd edition.

Zondervan, I., and Riebesell, U., 2002, Effect of CO2 concentration on the PIC/POC ratio in the coccolithophore Emiliania huxleyi grown under light-limiting conditions and different daylengths, *Journal of Experimental Marine Biology and Ecology*, **272**, 55–70.

Chapter 3 - The Impact of Changing Oceanic Calcium and Magnesium Concentration on the Carbon Cycle Over the Cenozoic

What could be smarter,
Than a grand attempt to barter,
With an information station,
And not expect frustration?

Abstract

Changes in ocean calcium and magnesium concentrations are related to changing hydrothermal circulation through seafloor crust as a result of variations in plate tectonics - an external driver. Oceanic calcium and magnesium concentrations have changed from 70Ma to present, and variation in the concentrations of these ions is known to affect the carbonate system, therefore may drive climate change over the Cenozoic. Previous work has established a method of quantifying the impact of ocean composition on acid base chemistry. By incorporating this method into the GECCO model (described in Chapter 2), it is possible to estimate the magnitude of carbon cycle change driven by changes in oceanic calcium and magnesium concentration. In line with available data, calcium concentration is driven to halve, and magnesium concentration to double over 60Myr. This is initially found to drive a $\sim$250ppm fall in atmospheric CO_2 but no long term trend in the CCD. The sensitivity of these results to four climate feedbacks is established by further ensemble runs with the same forcing but different feedback strengths. I find that the magnitude of CO_2 response is highly dependent on all the strength of each of the four principal feedbacks.

3.1. Introduction

3.1.1 Carbonate Chemistry

In order to understand the premise of this study, a detailed knowledge of ocean carbonate chemistry is required. An introduction to ocean carbonate chemistry is provided in Section 1.2.1, and a full discussion is included in Appendix B, however the most salient points are restated here:

- Oceanic calcium and magnesium ion concentration affect the partitioning of ocean proton donors and acceptors i.e. equilibrium 'constants', here referred to as Carbonate Chemistry K (CCK) values.
- Carbon in the ocean is present in three primary forms, each of which has a different valency, and is therefore affected by changes in oceanic ion composition.
- Calcium concentration has a direct impact on ocean saturation state:

$$\psi_C = \frac{[Ca^{2+}][CO_3^{2-}]}{k_{spC}} \tag{3.1}$$

- Calcium concentration has roughly halved over the Cenozoic (Figure 3.2).
- Magnesium concentration has roughly doubled over the Cenozoic (Figure 3.2).

Given the above statements - it is natural to pose the question, have changes in ocean ion composition, specifically the concentrations of calcium and magnesium, had an impact on the carbon cycle over the Cenozoic? Traditionally, oceanic calcium and magnesium concentrations might be assumed to affect the CCD, due to the change they drive in ocean carbonate chemistry, while their impact on atmospheric CO_2 could be assumed to be minimised by climate stabilising feedbacks. Understanding the true impact of changing oceanic composition on the carbon cycle requires a model which has a highly detailed carbonate chemistry component that is able to calculate the effect of changing oceanic calcium and magnesium concentration on the carbonate system, in concert with the dynamic behaviour of climate feedbacks. In addition to this, the feasible magnitude of calcium and magnesium concentration change must be established.

Evidence for the changes in oceanic calcium and magnesium concentration is primarily derived from halite fluid inclusions, which are able to provide absolute concentrations of oceanic ions, albeit with some caveats, assumptions and uncertainties (*Horita et al.*, 2002;

Brennan et al., 2013). There is also independent evidence that Mg/Ca ratio has roughly tripled from 70Myr to present, with most of the change occurring after 30Ma (Figure 3.2). The available data is summarised in Figure 3.2. Variations in oceanic calcium and magnesium ion concentrations are driven by a combination of changes in weathering fluxes, mid ocean ridge hydrothermal exchange and diagenetic formation of dolomite. Weathering of calcium-magnesium silicates and of carbonate lithologies provides a flux of calcium and magnesium into the ocean. Biotic and abiotic precipitation of calcium carbonate (and its preservation in lithological form) is a sink of calcium from the ocean. Magnesium is removed from the ocean by alteration of basaltic crust during hydrothermal exchange as well as by formation of dolomite.

The exact relationship between ocean composition and values which determine steady state partitioning of oceanic proton donors and acceptors is complex. The values that determine this partitioning are often referred to as 'equilibrium constants', despite the fact that they vary with temperature, pressure, salinity and ocean composition. Here these values are referred to as CCK's.

Experiments which seek to determine CCK's empirically use ocean water, fresh water, some form of imitation seawater that contains the major ocean constituents, or some type of brine that is not intended to represent the ocean. Despite previous efforts, CCK's remain poorly quantified at most solvent compositions, due to the large number of possible combinations of solutes for palaeo ocean compositions. The greatest focus is on the effect of calcium and magnesium ions, which have known strong interactions with the carbonate system (*Zeebe* and *Wolf-Gladrow*, 2001). Of the two, magnesium is thought to have the strongest ionic interaction with carbon species, and therefore to have the largest impact on CCK's (*Zeebe* and *Wolf-Gladrow*, 2001). On the other hand, calcuim has both an ionic interaction with the carbon species and is directly involved in the determination of saturation state (Equation 2.15) and therefore the formation and preservation of $CaCO_3$.

The canonical source of equations for CCK's (without the inclusion of ocean composition effects) is *Zeebe* and *Wolf-Gladrow* (2001), which gives a detailed description of many CCK's, and the calculations required to compute their value. To incorporate the effect of ocean composition, *Tyrrell* and *Zeebe* (2004) combined the equations in *Zeebe* and *Wolf-Gladrow* (2001) with sensitivity parameters estimated by *Ben-Yaakov* and *Goldhaber* (1973) to calculate the impact of calcium and magnesium on the CCK's. *Hain et al.* (2015) developed

a more detailed methodology, by using the ion pairing model MYAMI to estimate the CCK's at a range of calcium and magnesium concentrations before comparing MYAMI output to empirical data. The CCK's produced by *Hain et al.* (2015) using the MYAMI model are generally consistent with empirical data, however there are ongoing questions about the validity of specific behaviours (*Zeebe* and *Tyrrell*, 2018; *Hain et al.*, 2018) (see Section 3.4 for further discussion).

3.1.2 Effect of Calcium and Magnesium on the Carbonate System

As discussed above, calcium and magnesium concentrations affect the partitioning of carbon species in the ocean. Broadly speaking, modelling approaches neglect this aspect of carbonate chemistry, though some actively developed models do take this into account.

The assumption that the impact of changes in calcium and magnesium ion concentrations are negligible can sometimes be justified, such as on short timescales ($<$1Myr), in the comparatively recent past where changes in calcium and magnesium concentration relative to the present day are insignificant, or when the focus of the study is understanding trends in the simulated parameters, not their absolute value. Unfortunately these concepts are often elided, leading to deep time simulations which do not take account of differences in ocean composition.

Under the assumption that climate feedbacks would act to mitigate a forced change in atmospheric CO_2, it might be assumed that the impact of calcium and magnesium ion change can be ignored, particularly when the rate of change in calcium and magnesium concentration is slow. Conversely, where the change in ion composition is rapid, or an instantaneous perturbation is applied, the impact of the change would be expected to be maximised.

The error resulting from ignoring the required magnesium and calcium component of carbonate chemistry when calculating initial conditions is equivalent to an instantaneous shift in the parameters. By using an incomplete representation of the carbonate system models introduce compensating errors. For instance, by initialising a model with the correct CO_2 value, but with an incorrect carbonate system representation, DIC and alkalinity will be calculated incorrectly, potentially resulting in a carbon cycle which responds differently to perturbations. Similarly, if both degrees of freedom of the carbonate system are constrained but the effect of ocean composition is not considered, then alternative parameters in the model must be incorrect to allow the erroneous climate state to exist. Despite these problematic shortcom-

ings, some existing carbon cycle box models do not take ocean composition into account in the context of the carbonate system, or calculate the effect of changes in ocean composition on the initial conditions, but assume ocean composition is invariant through time Appendix A. This is due to a number of factors:

- This is a continuously evolving field, and novel methodologies continue to be published.
- The calculations required increase the computational expense of the model.
- A lot of time is required to recode existing programs.
- There is presently a focus on shorter time intervals, which is conflated with an irrelevance of calcium and magnesium ion concentration due to their invariance on timescales shorter than their residence times ($\sim$1Myr and $\sim$13Myr respectively (*Broecker* and *Peng*, 1982)). This neglects their impact on initial conditions of the model.

Calculations which require carbonate system parameters (such as the boron isotopic proxy), must also take account of differences in ocean composition. It could be assumed that feedbacks will act to minimise the impact of the imposed calcium and magnesium forcing, so modelling approaches may, under certain conditions and with caveats, neglect the forcing caused by slow changes in variables. Whereas with modelling approaches, it might be expected that feedbacks will stabilise the carbon cycle against an imposed forcing, changes to parameters used in data approaches cause an instantaneous, no feedback response, maximising the impact of the parameter change. In other words, each proxy reconstruction represents a single point in time, so feedbacks can not be invoked to mitigate the impact of input parameter changes. For this reason it is particularly important for applications involving reconstructions of a single point in time to have accurate representations of the carbonate system, and they have, in general, kept up to date with the current state of the art methods of quantifying the carbonate system.

3.1.3 Existing Cenozoic Carbonate System Quantifications

Only two carbonate system parameters are required to quantify all others (ignoring the comparatively minor influence of temperature, pressure, salinity and ocean composition), so there are many potential combinations of parameters that may be used to produce a full quantification of the carbonate system. For example, *Tyrrell* and *Zeebe* (2004) used changes in calcium ion concentration to constrain changes in deepwater carbonate ion concentration, based on the evidence that the carbonate compensation depth has been relatively invariant over the Cenozoic. By combining the carbonate ion concentration with atmospheric CO_2 data from the GEOCARB model, the remaining carbonate system parameters were calculated. This approach suggested that pH has increased by $\sim$0.5units from 70Ma to present and that DIC and alkalinity concentrations had remained roughly constant through time, a finding which has since been replicated using more up to date data and improved analysis in *Zeebe* and *Tyrrell* (2019). Another approach is to use boron isotopes as a proxy for ocean pH (*Tyrrell* and *Zeebe*, 2004; *Boudreau et al.*, 2019). By combining this with an additional carbonate system parameter derived from alternate methods (such as atmospheric CO_2), the two degrees of freedom may be satisfied to calculate the remaining parameters.

Currently, the datasets required to perform the quantification of the carbonate system over the Cenozoic are sparse, and subject to significant uncertainties, so these approaches are presently limited to identifying long term trends in carbonate system behaviour. However, if the carbonate system can be fully quantified over the Cenozoic, then one might ask if the drivers are not known from the datasets themselves. In terms of establishing the impact of changing calcium and magnesium concentrations, this can not be calculated from the data alone because the concentrations of these ions must also be known (in addition to many other factors) in order to properly quantify the carbonate system. Furthermore, approaches based on data analysis do not separate the impacts of drivers and feedbacks, whereas a model approach provides a causative link between driver and climate response, which is crucial in understanding the potential magnitude of response driven by calcium and magnesium ion concentration changes and other potential climate drivers.

3.1.4 GECCO Model

The Geologically Evolving Carbon Cycle and Ocean (GECCO) model is described in detail elsewhere (Chapter 2), but the most pertinent elements for this chapter are outlined here for clarity. GECCO allows the forcing of a time dependent oceanic calcium and magnesium concentration, which can be configured to replicate reasonable evolutions which could have occurred over the Cenozoic. The CSH is calculated by a specialised routine which takes into account changes in CCK's driven by changes in ocean composition, as well as the change in saturation state forced directly by the change in calcium concentration.

The GECCO model also contains a clear representation of multiple feedbacks, whose strengths may be manipulated as a sensitivity analysis (see Section 2.4). Overall, the GECCO model is ideally suited to testing the impact of carbonate system forcing on Cenozoic timescales.

3.2. Methods

3.2.1 Determining Cenozoic Calcium and Magnesium Evolution

The principal method used to estimate the calcium and magnesium concentrations of the palaeo ocean is analysis of fluid inclusions. For technical reasons, it is easier to calculate an estimate of magnesium:calcium ratio, and determining absolute concentrations of these ions is difficult. Unfortunately, the currently available calcium and magnesium concentration data points are very sparse, with fewer than 10 datapoints in each dataset over the Cenozoic, occurring primarily in a cluster at 35Ma and distributed between 10Ma and present (Figure 3.2). The residence time of magnesium in the ocean is $\sim$13Myr (*Broecker* and *Peng*, 1982), whereas the residence time of calcium is only $\sim$1Myr (*Broecker* and *Peng*, 1982). For both datasets the spacing of datapoints is greater than the residence time (Figure 3.2), so there is uncertainty in their evolution through time. That being said, the large disparity between the residence times of calcium and magnesium means it is reasonable to assume changes in the concentration of magnesium are slow relative to changes in calcium concentration. To constrain some of the uncertainty surrounding the evolution of these ions, it is possible to assume that the magnesium concentration follows a linear trend, and combine this with the Mg/Ca ratio, which is much better constrained, to calculate an independent estimate of the oceanic calcium evolution (see Figure 3.2).

To perform this calculation, I compiled the existing datapoints for Mg/Ca ratio over the Cenozoic. Regrettably, there were a number of problems with the original datasets, so several assumptions had to made to perform a fully probabilistic calculation, as listed below.

- Not every datapoint has associated age uncertainties. Where not stated, it is assumed that the age uncertainty on these datapoints is $\frac{1}{5}^{th}$ of the age itself.

- In most cases, the form of the probability distribution used to quantify uncertainties in the data is not specified. It is presumed that the uncertainties are specified based on a Gaussian distribution.

- The significance level of uncertainties is generally unspecified. Here 2σ uncertainties are required and it is assumed that any measurements for which the the sigma level is unclear are at 1σ, so these are correspondingly doubled.

- Any unspecified data value uncertainties are estimated by tripling the average uncertainty of other measurements within the same dataset to remain conservative.

These datapoints and their estimated/specified uncertainties are used to create a probability map for Mg/Ca ratio (using the method detailed in Appendix C). The path of optimal probability (shown in black in Figure 3.2) shows incongruous rapid change, which is known to be unlikely due to the relatively long residence times of both ions. As initial estimates of the evolution of both calcium and magnesium ion concentration, simple, linear fits are performed to the ion concentration data (Figure 3.2). Inferred uncertainties on these fits are a summation of two components. The first is the uncertainty in the datapoints themselves. The second is a time variable uncertainty, which scales with the distance between datapoints. It is assumed that the maximum gradient in magnesium concentration at any time is that which would produce a doubling of magnesium concentration over the residence time of 13Myr, and similarly the maximum gradient in calcium concentration at any time is that which would produce a doubling of calcium concentration over the residence time of 1Myr. For each ion, the addition of these two sources of uncertainty causes the total uncertainty to be of the same magnitude as the datapoints where those are available, and increases the uncertainty where no data is available.

There is now the possibility to somewhat independently estimate the evolution of Mg/Ca ratio, calcium concentration and magnesium concentration, and then further inform the calculation by using two parameters to estimate the other (because the system has two degrees of freedom and is overdetermined). This is done using a Bayesian methodology (discussed further in Appendix C) to combine the distributions estimated from the three datasets. The linear fits described above for each parameter are used as an estimate of the marginal

probability (for calcium this is shown by the light red shaded envelope in Figure 3.2). A prior is constructed for calcium ion concentration by combining the Mg/Ca ratio and magnesium ion concentration to calculate calcium ion concentration. The posteriour then shows the best estimate of calcium concentration evolution through time (red line in Figure 3.2), alongside associated uncertainties (dark red shaded region in Figure 3.2), which are a combination of the uncertainties in the calcium concentration, magnesium concentration and Mg/Ca ratio.

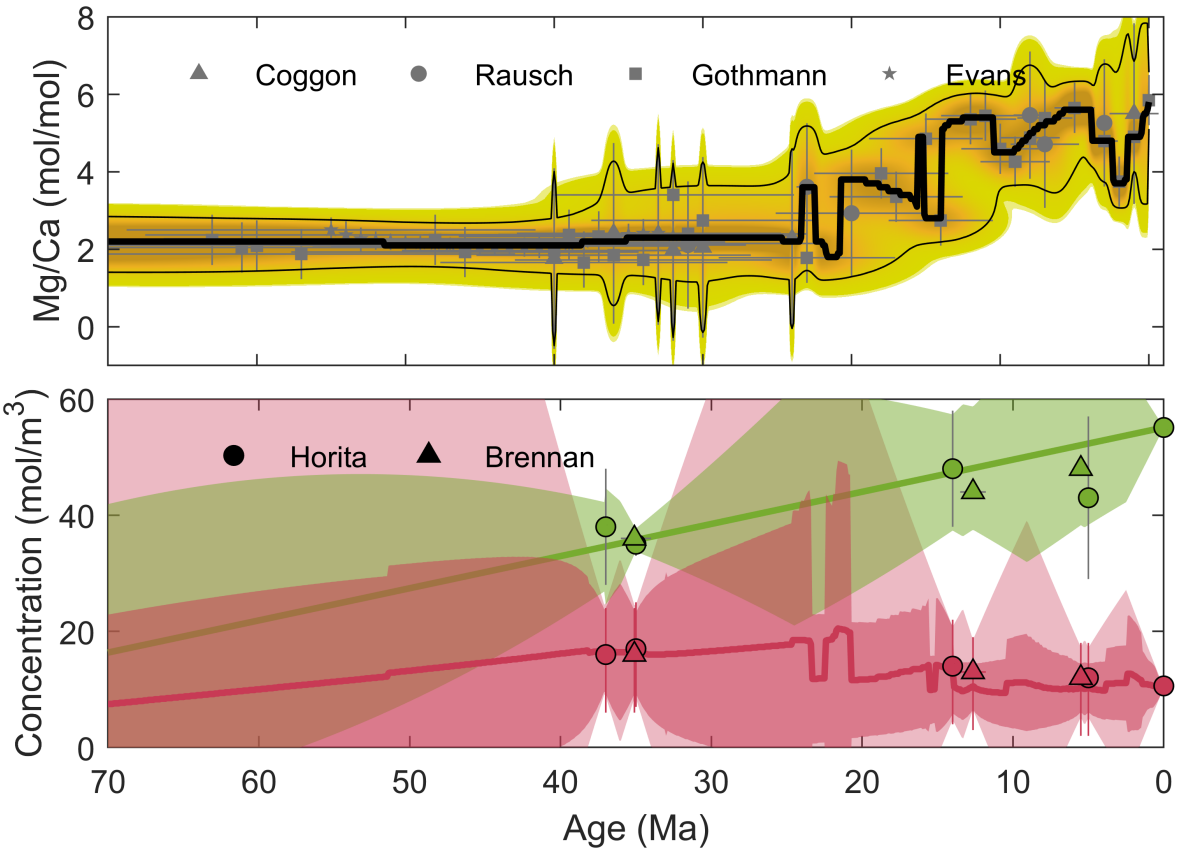

Figure 3.2: ***The upper panel shows the currently available Mg/Ca ratio datapoints in grey with associated uncertainties (*****Coggon et al.*****, *2010;* Rausch et al.*****, *2013;* Gothmann et al.*****, *2015). The probability map of Mg/Ca ratio is shown in yellow, with darker yellow indicating higher probability regions. The thick black line shows the path of optimal probability through the Mg/Ca space, and the outer black envelope delineates the 95% confidence interval. The thick blue line shows the average of the best ten randomly generated walks through the space.***
The lower panel shows the currently available palaeo magnesium concentration data (green markers) and calcium data (red markers) (**Horita et al.*****, *2002;* Brennan et al.*****, *2013). The linear trend through the magnesium datapoints is shown as a green line with uncertainties around this line are shown by the green envelope. The posteriour calcium evolution (red line - uncertainties in the dark red envelope) is calculated by combining the Ca marginal probability, with the Ca prior derived by combining the interpolated evolution of magnesium concentration and Mg/Ca.***

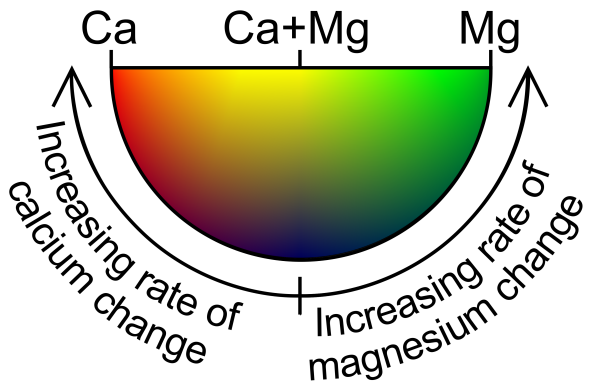

Figure 3.1: ***In this and all subsequent figures of this chapter, when the rate of change of both calcium and magnesium ions is slow, the data is plotted in a dark blue. Faster maximum rate of change in calcium concentration increases the redness of the line and faster maximum rate of change in magnesium concentration increases the greeness of the line. High maximum rates of change in both ions result in a yellow (green+red) colouration.***

The calculated evolution of calcium concentration shows a roughly linear trend. The predicted concentrations of both calcium and magnesium at 70Ma are consistent with existing estimations (*Hain et al.*, 2015). Uncertainties on these values are large, owing to both the lack of constraint on calcium and magnesium concentration in the early Cenozoic, and also to the large uncertainties on existing datapoints around 35Ma. Nonetheless, the combined evidence of a change in Mg/Ca ratio and changes in the absolute concentrations of calcium and magnesium (see Figure 3.2) demonstrate that significant changes in ocean ion composition could have taken place over the Cenozoic. The concentrations of calcium and magnesium used to initialise the model at 70Ma are chosen in line with previous studies (20mol/m^3 and 30mol/m^3 respectively) (*Tyrrell* and *Merico*, 2004; *Hain et al.*, 2015; *Zeebe* and *Tyrrell*, 2019), and are well within the uncertainties presented here. Having now established the estimated magnitude and rate of change of calcium and magnesium ion concentration over the Cenozoic, as well as their concentrations at 70Ma, it is possible to design an ensemble of model runs to simulate various possible evolutions of these drivers.

3.2.2 Driving Calcium and Magnesium Change

Time	Run	Ca		Mg		Ca	Mg
t (Myr)	Number	t_0	t_f	t_0	t_f	t	t
10	1	20	10	30	50	20	30
10	2	20	10	30	50	20	34
10	3	20	10	30	50	20	38
10	4	20	10	30	50	20	42
10	5	20	10	30	50	20	46
10	6	20	10	30	50	20	50
10	7	20	10	30	50	18	30
10	8	20	10	30	50	18	34
10	9	20	10	30	50	18	38
10	10	20	10	30	50	18	42
10	11	20	10	30	50	18	46
10	12	20	10	30	50	18	50
...	...	...	...	...	...	...	...
10	31	20	10	30	50	10	30
10	32	20	10	30	50	10	34
10	33	20	10	30	50	10	38
10	34	20	10	30	50	10	42
10	35	20	10	30	50	10	46
10	36	20	10	30	50	10	50
20	37	20	10	30	50	20	30
20	38	20	10	30	50	20	34
20	39	20	10	30	50	20	38
...	...	...	...	...	...	...	...
...	...	...	...	...	...	...	...
60	216	20	10	30	50	10	50

Table 3.1: ***Input values which control the calcium and magnesium evolution are shown. t_0 indicates the starting condition, t is the condition at the time in the first column, and t_f is the condition at the final timestep. Not all ensemble members are shown, ... is used to indicate skipped entries following the same pattern as above. The colour identifies the four key runs isolated for further analysis, with colour scheme in line with Figure 3.1.***

To begin, the model was initialised to a steady state (as discussed in Section 2.3.1) with 600ppm atmospheric CO_2 to reflect the estimated Precenozoic condition. From that steady state an ensemble of runs was created, each with a unique temporal evolution of calcium and magnesium concentrations. Every member of the ensemble has an initial calcium concentration of 20mol/m^3, a final calcium concentration of 10mol/m^3, an initial magnesium concentration of 30mol/m^3 and a final magnesium concentration of 50mol/m^3 (in agreement with the data shown in Figure 3.2, and *Hain et al.* (2015)). In order to produce a variety of oceanic calcium and magnesium concentration evolutions, an additional tie point for each ion was established between the end member concentrations. Each tie point consists of a time (between 10Myr and 60Myr at spacing of 10Myr), a calcium concentration at that time (between 10 and 20mol/m^3 with spacing of 2mol/m^3) and a magnesium concentration at that time (between 30 and 50mol/m^3 with spacing of 4mol/m^3).

Both calcium and magnesium are then linearly interpolated between the initial condition and the value at the tie point, and between the tie point and the final value. This design generates a grid based ensemble with six members in each dimension (a total of 216 runs) with values as shown in Table 3.1, and forcing as shown in Figure 3.3. Each run in this ensemble starts with initial conditions as described in Section 2.3.1 and constant conditions as prescribed in Section 2.1, intended to represent a 'Precenozoic' climate state. This means that all feedbacks are at their estimated Precenozoic strength, though the strength of most feedbacks at ∼70Ma is poorly constrained.

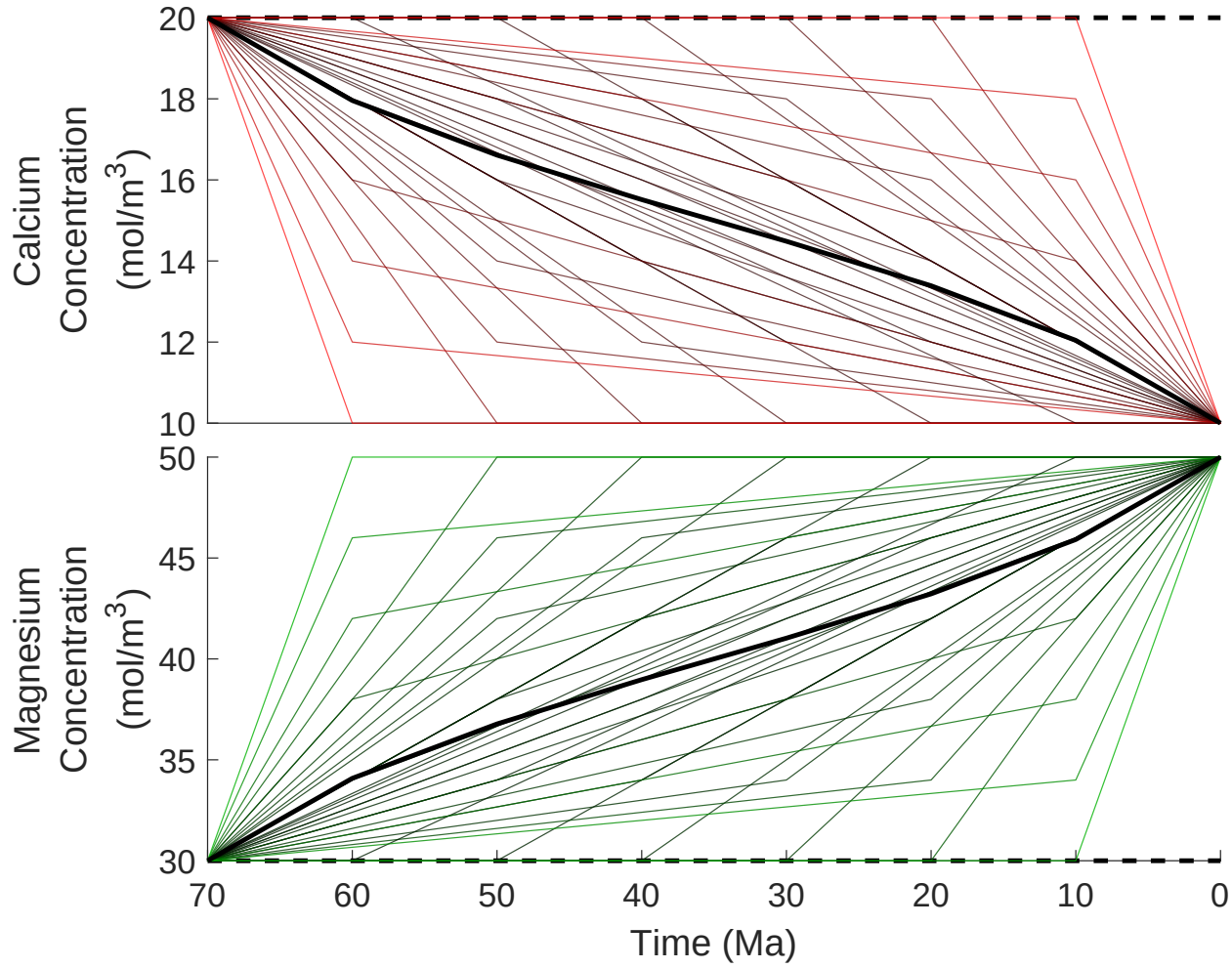

Figure 3.3: ***The forcing used in the ensemble of model runs detailed in Section 3.2.2 and Table 3.1 is shown. The upper subplot (red) shows the variety of calcium evolutions explored, while the lower subplot (green) shows the variety of magnesium evolutions explored. Stronger colouration is associated with a greater maximum rate of change in line with the scheme laid out in Figure 3.1.***

In order to establish the potential of calcium and magnesium ion concentrations to cause climate change, four illustrative members of the ensemble are chosen to undergo further testing, during which the strength of four feedbacks is altered before beginning the run. The four runs are chosen at the extremes of the ensemble, to represent: rapid change in both ions, rapid change in calcium concentration only, rapid change in magnesium concentration only, and slow change in both ions. These runs are highlighted in the coloured rows of Table 3.1, which correspond to the colour scheme as detailed in Figure 3.1, and are shown in bold in Figure 3.4.

The nature of the four feedbacks, and the methodology or their alteration is described in detail in Section 2.4, but a brief summary is provided here for clarity:

1. Alteration of the carbonate compensation feedback controls how responsive carbonate burial fraction is to the CCD, and is controlled by shallowing or steepening the hypsometric curve in the region of the CCD.

2. Changes to the silicate weathering feedback control the relationship between temperature and silicate weathering flux.

3. Changes to the carbonate weathering feedback control the relationship between temperature and carbonate weathering flux.

4. Manipulation of the phosphate weathering feedback controls how closely related the riverine phosphate flux is to the weathering of other lithologies.

As stated, the four key scenarios are run with the variation in the four specified feedbacks (carbonate compensation, silicate weathering, carbonate weathering and phosphate weathering), and results are analysed in terms of their long term climatic stability. For the moment, the driving mechanism behind the behaviours caused by changes in feedback strength is not discussed at length, as it can be difficult to disentangle the interactions between the effects of the forcing and the feedbacks. For example, if the effect of time variable silicate weatherability as a climate driver was the parameter of interest, then this would naturally be closely related to changes in the silicate weathering feedback. Therefore, in order to establish the effect of changing feedback strength, it is necessary to assess at least two climate drivers with variations in feedback strength.

In addition to the potential for changes in calcium and magnesium concentration to directly

cause climate change, it is also possible the changes in calcium and magnesium concentration to change the climate sensitivity to a carbon cycle perturbation. To investigate this potential, the four key forcing scenarios are run with an additional release of 20000GtC to the atmosphere 11Myr into the run (at 59Ma). This perturbation is not instantaneous, but is added according to a Gaussian distribution with a standard deviation of 0.3Myr.

In summary, these model experiments attempt to quantify the magnitude of carbon cycle and climate change driven directly by trends in oceanic calcium and magnesium ion concentration, and then to estimate the dependence of that climate change on feedback strength. In addition to the direct change, the potential for calcium and magnesium to change the climate sensitivity to a carbon cycle perturbation is examined.

3.3. Results

3.3.1 Precenozoic Ensemble

Results from the ensemble (Figure 3.4) reveal that driving calcium concentration to approximately halve and magnesium concentration to approximately double results in a $\sim$250ppm fall in steady state atmospheric CO_2, regardless of the timescale over which the calcium and magnesium concentration change. The spread in atmospheric CO_2 produced in the ensemble is related to the rate of change of calcium and magnesium ion concentration (Figure 3.4), such that the maximum transient change in CO_2 is observed when both calcium and magnesium undergo the largest and most rapid change (yellow ensemble members in Figure 3.4). The maximum temporal gradient of atmospheric CO_2 is reduced when only a single ion undergoes large and rapid change (Figure 3.4:calcium in red and magnesium in green). When both calcium and magnesium exhibit slower maximum rates of change then the resulting in CO_2 fall is also gradual. When the average of all ensemble members is taken (thick black line in Figure 3.4), the calcium and magnesium evolutions are roughly linear - in line with the inferred evolution from the analysis in Section 3.2.1. The ensemble may therefore be loosely interpreted as a probabilistic representation of the likely evolution of modelled variables, as calcium and magnesium ion concentration are more likely to travel through the central range of concentrations that be at either extreme.

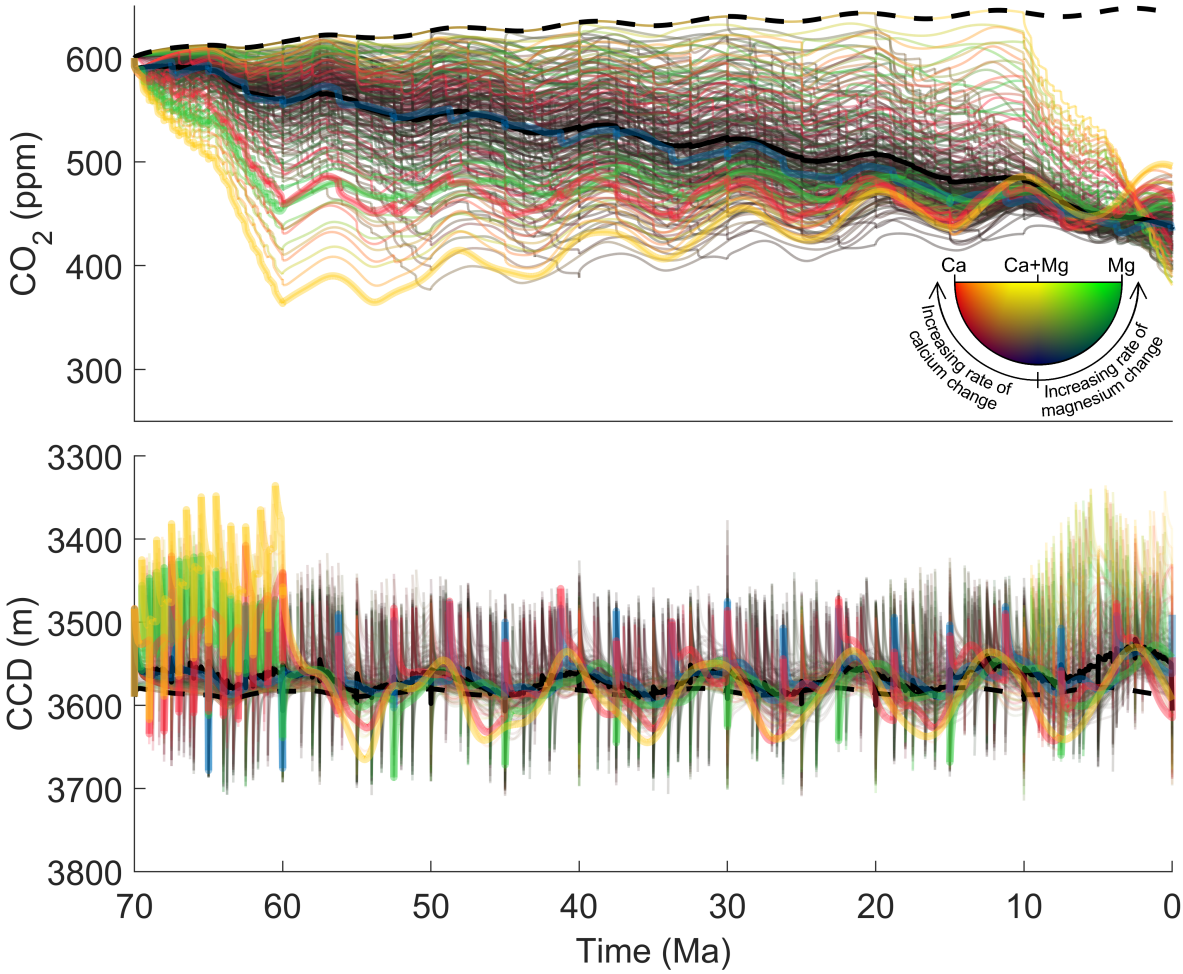

Figure 3.4: ***Atmospheric CO_2 and CCD evolutions from the ensemble during which calcium and magnesium ion concentrations were forced to change are shown. Each coloured line represents a single ensemble member. The lines are coloured by their maximum gradient, where red lines have a high maximum calcium gradient, green lines have a high maximum magnesium gradient, and where both of these gradients are high the colours are additive, i.e. yellow. The thick, dashed, black line shows the control run, where neither magnesium nor calcium concentration change from the initial condition. The thick, solid, black line shows the average of all ensemble members.***

The CCD is perturbed by the changes in CCK's driven by calcium and magnesium concentration evolution (see Section 3.4 for explanation of this effect), however these perturbations are always short lived relative to the timescales of interest and the CCD returns to the initial condition over timescales of hundreds of thousands of years. The ensemble mean CCD deviates from the control run only during the first and last 10Myr of the ensemble. This is an artefact of the ensemble design, which causes the most rapid changes in calcium or magnesium in the ensemble to occur between 70-60Ma and 10-0Ma, resulting in a sufficiently strong forcing to temporarily drive the CCD to differ from the control run.

The direction of change of additional carbonate system parameters is often inferred by using two primary carbonate system parameters. The observation that the CCD has remained at a constant depth, while atmospheric CO_2 has fallen, would imply that whole ocean pH, DIC and alkalinity should all rise. The ensemble shows an average rise in deep ocean pH from $\sim$7.7 to $\sim$8 units, an average rise in DIC of $\sim$0.5mol/m^3, and an average rise in alkalinity of $\sim$0.55mol/m^3 (see Figures 3.5–3.6). Caution must be taken when interpretting the results in this way, however, as while the carbonate system is generally said to have two degrees of freedom, this does not include the variation in CCK's driven by changes in temperature, pressure, salinity and ocean composition. For instance, at the same atmospheric CO_2 concentration and CCD, changes to calcium and magnesium ion concentration alter other carbonate system parameters through their effect on CCK's (so one would calculate a different DIC, for example). As such, driving significant changes in temperature, or ocean composition can result in an unexpected change to the carbonate system.

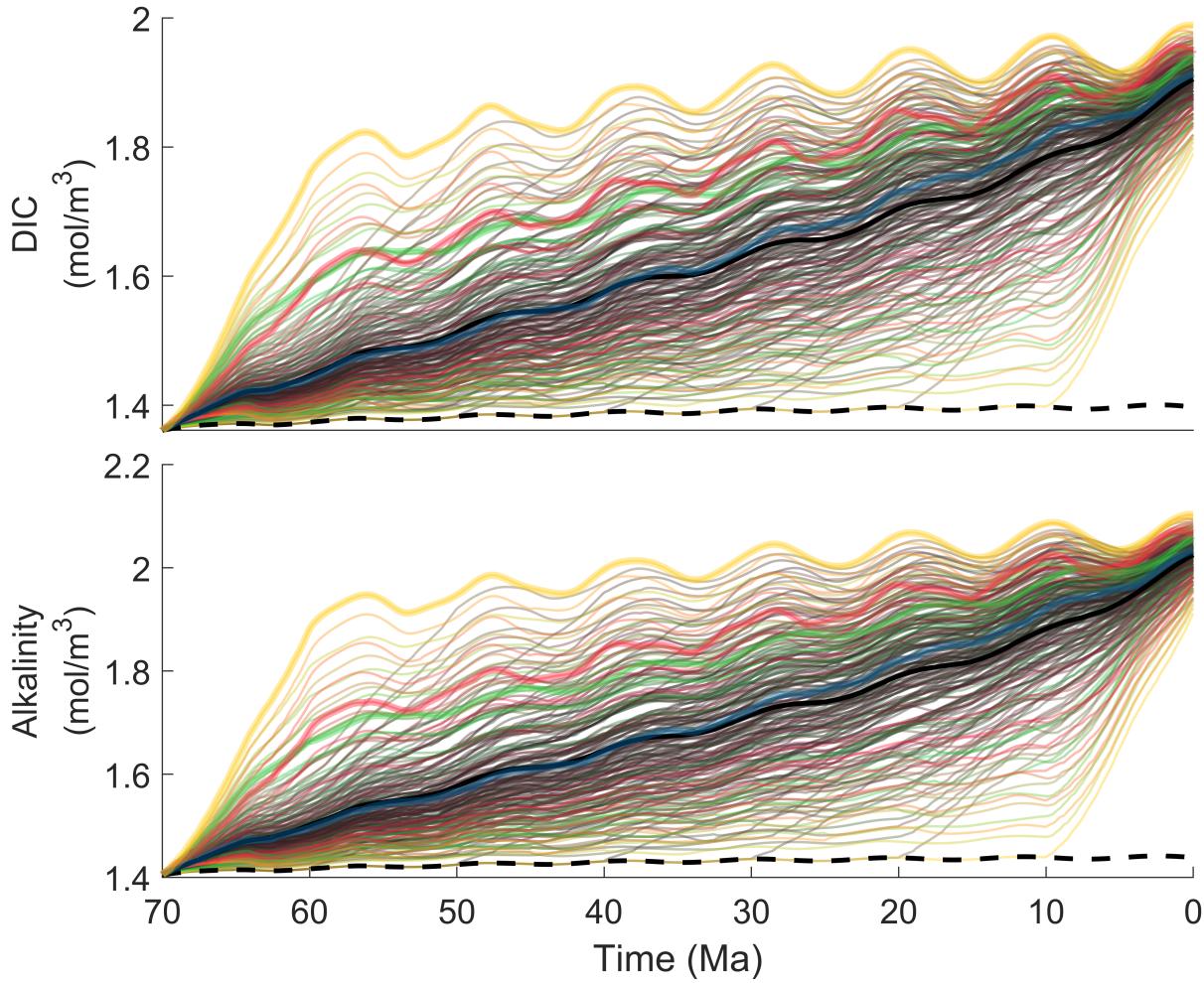

Figure 3.5: ***As in Figure 3.4, each line represents and individual ensemble member as is coloured by combinative maximum gradient in calcium (red) and magnesium (green) as described in Figure 3.1. The thick, black, dashed line shows the control run (without any forced calcium or magnesium change) and the thick, black, solid line represents an average of all ensemble members.***

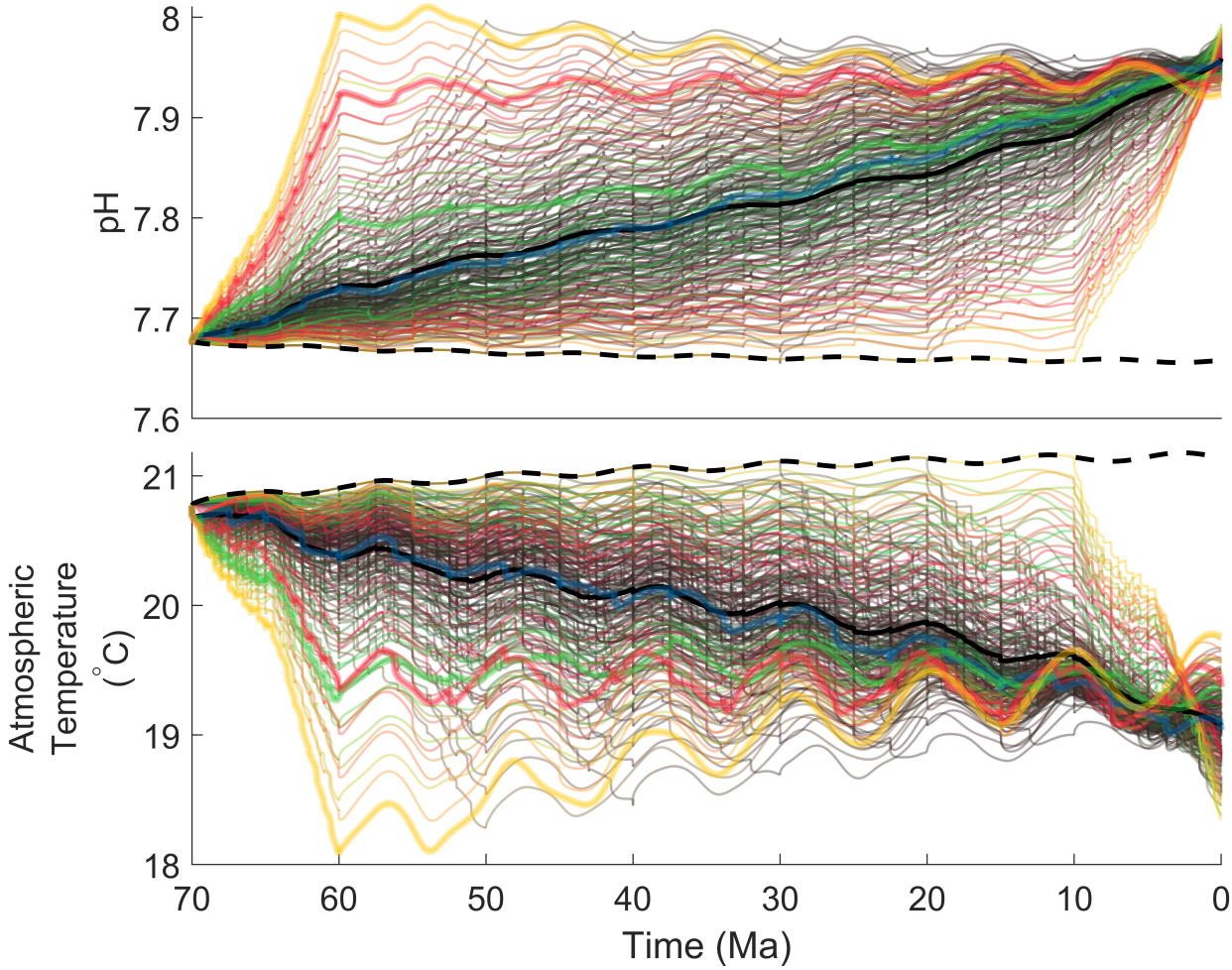

Figure 3.6: ***As in Figure 3.4, each line represents and individual ensemble member as is coloured by combinative maximum gradient in calcium (red) and magnesium (green) as described in Figure 3.1. The thick, black, dashed line shows the control run (without any forced calcium or magnesium change) and the thick, black, solid line represents an average of all ensemble members.***

Temperature falls from the initial condition of ∼20.5°C to ∼19°C due to the fall in atmospheric CO_2, which is roughly in line with the specified climate sensitivity (here 3.5°C/doubling of CO_2). This is also a contributing factor to the changes in the carbonate system observed within these model runs through its effect on the CCK's.

In summary, the imposed calcium and magnesium ion change drives approximately 250ppm of atmospheric CO_2 fall when feedbacks are at their estimated Precenozoic strength. The timescale of the change in ion concentrations does not exert a strong influence on the steady state condition that the model runs reach, but does strongly influence the temporal evolution of model parameters. As stated above in Section 3.2.2, four of these runs are isolated for further analysis. These analyses include an estimation of how the change in ion concentration could affect the climate response to a perturbation in Section 3.2.2, and how altering the feedback strength affects the trajectory of climate change driven by calcium and magnesium

concentration change.

3.3.2 Precenozoic Perturbation

Here, the four key runs specified in Section 3.2.2 are subjected to a large atmospheric CO_2 perturbation, the results of which are shown in Figure 3.7.

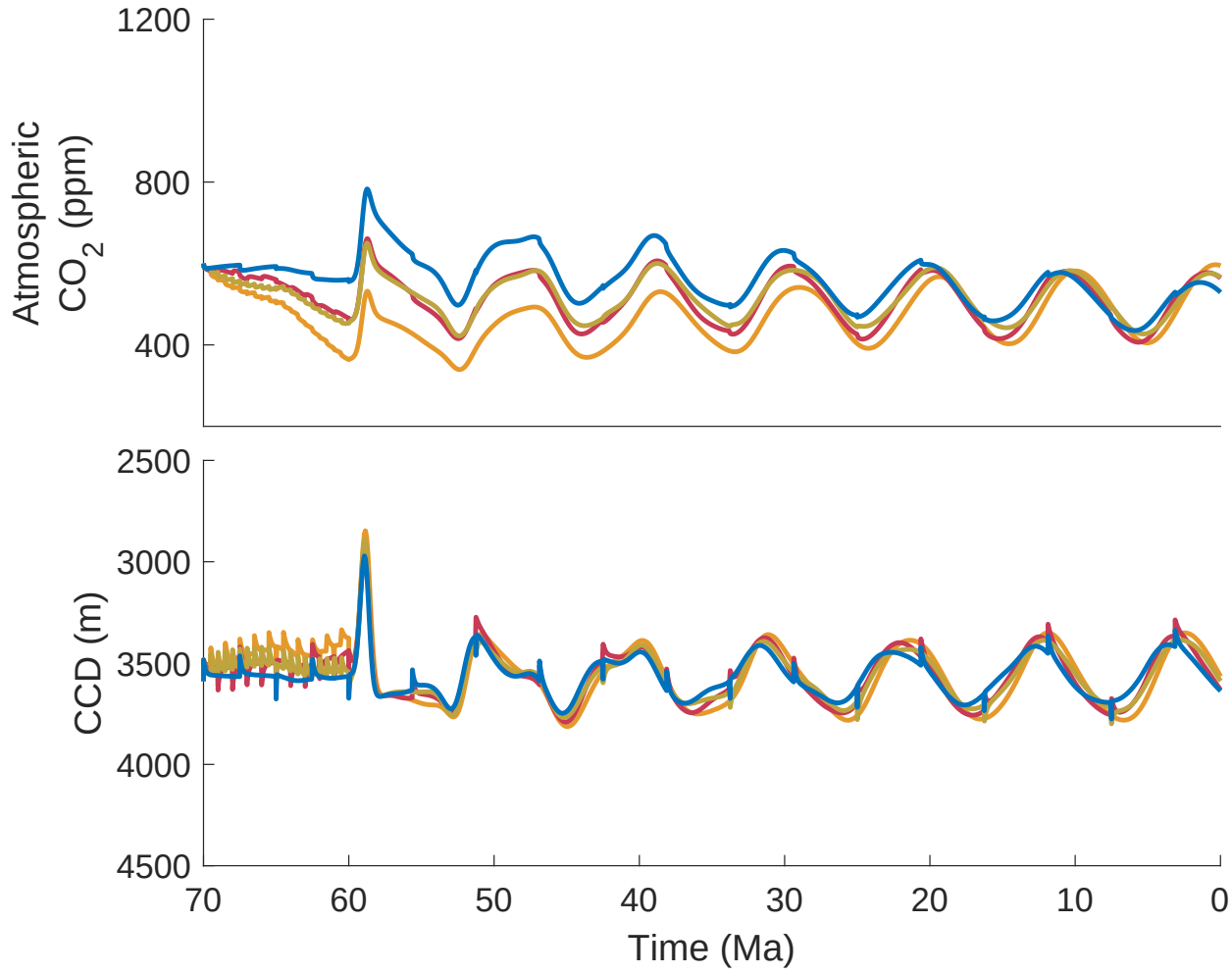

Figure 3.7: ***The climate sensitivity to a large carbon cycle perturbation is established by adding 20000GtC into the atmosphere according to a Gaussian with a mean at 59Ma and a standard deviation of 0.3Myr. This uses the four key runs identified in Section 3.2.2, coloured as in Figure 3.1.***

In the run where calcium and magnesium ion changes are slowest (blue in Figure 3.7), atmospheric CO_2 concentration rises by $\sim$200ppm due to the perturbation, then experiences ongoing oscillations with a period of about 10Myr and a scale of roughly 100ppm. Whereas in the run in which both calcium and magnesium are fastest (yellow in Figure 3.7), atmospheric CO_2 concentration rises by $\sim$150ppm, with subsequent oscillations of the same magnitude and spacing as in other runs. The evolution of the CCD in all runs appears almost identical,

though the run in which calcium and magnesium change the most quickly shows slightly greater shoaling of the CCD during the CO_2 perturbation. This shows the the climate has different sensitivity depending on the forcing scenario, likely due to the different amount of calcium and magnesium change that has occurred by 59Ma, when the perturbation occurs.

3.3.3 Carbonate Compensation Feedback

The carbonate compensation feedback acts to stabilise the climate by changing the magnitude of carbonate burial flux in the ocean (described in Section 2.4.1). The strength of this feedback is altered (as outlined in Section 2.4.1) to establish its importance in maintaining climate stability.

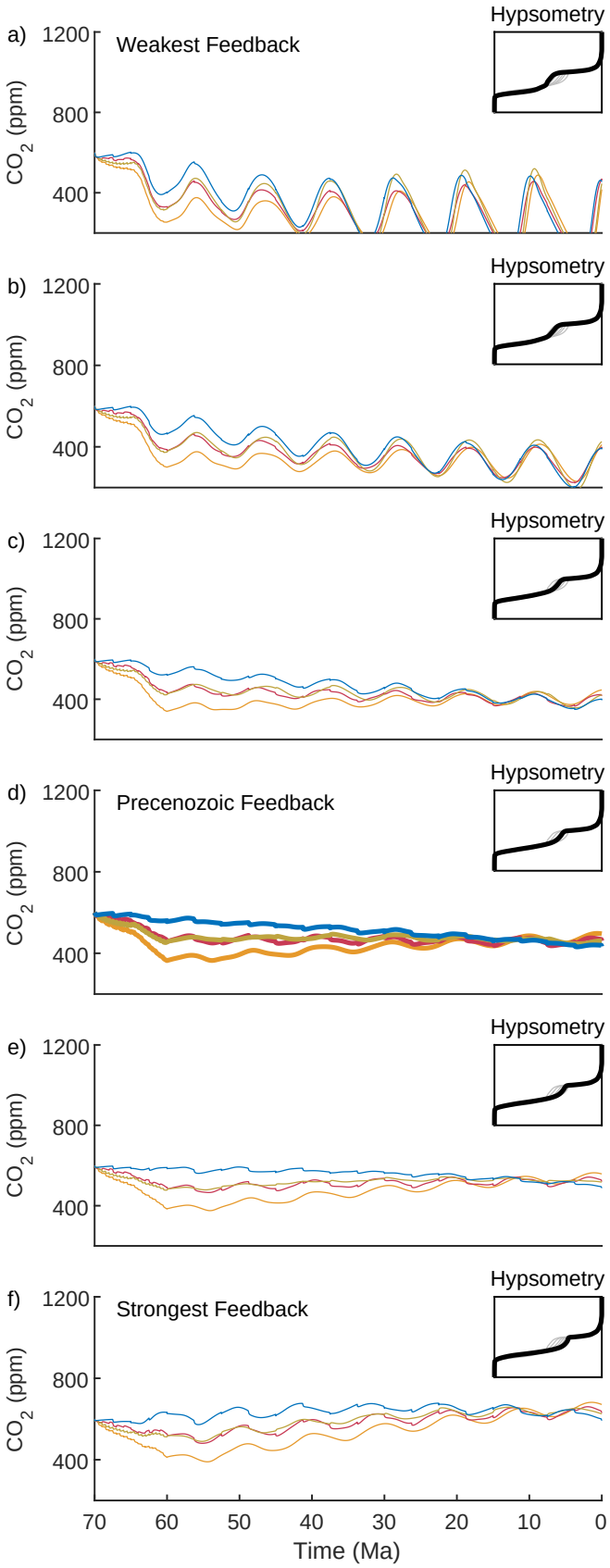

Figure 3.8: ***The CO_2 response to calcium and magnesium forcing using a variety of hypsometric profiles used to control the strength of the carbonate compensation feedback.***

Climate Response

Across the range of feedback strengths explored, all runs initially show different CO_2 and CCD evolutions (with transient differences of up to 200ppm and 200m respectively between different forcing scenarios), but these evolutions are convergent so by the end of the run these differences are minimal, regardless of the feedback strength. For both CO_2 and the CCD, the runs where both calcium and magnesium are forced to change rapidly (yellow in Figure 3.8) show the largest transient response at all feedback strengths.

Across all feedback strengths, the runs in which calcium changes quickly while magnesium changes slowly (red in Figure 3.8), and in which magnesium changes quickly while calcium changes slowly (green in Figure 3.8) show very similar evolutions.

The weakest feedback (Figure 3.8a) allows the calcium and magnesium forcing to drive the largest change in atmospheric CO_2, whilst stronger feedbacks progressively decrease the impact - this is especially noticeable when comparing the runs in which

calcium and magnesium ion concentration both change slowly (blue in Figure 3.8). The two weakest feedback scenarios (Figure 3.8a-b) result in growing oscillations in atmospheric CO_2 and the CCD, whereas stronger feedbacks (including the Precenozoic strength Figure 3.8d) show a stabilising trend.

In contrast to the ideal behaviour, changes in the hypsometric gradient result in a change in the initial steady state (described in Section 2.4.1), resulting in a long term negative CO_2 trend in runs with feedbacks weaker than the Precenozoic strength, and a long term positive atmospheric CO_2 trend in runs with particularly strong carbonate compensation feedback strength. This change to the initial steady state makes it impossible to tell whether changes in carbonate compensation feedback strength affect the steady state CO_2 achieved near the end of the model runs. Similarly, the prompting force that drives oscillations in atmospheric CO_2 and the CCD may also be a result of the change in the initial steady state. Nonetheless, the long term behaviour is clearly different as a result of the change in feedback strength.

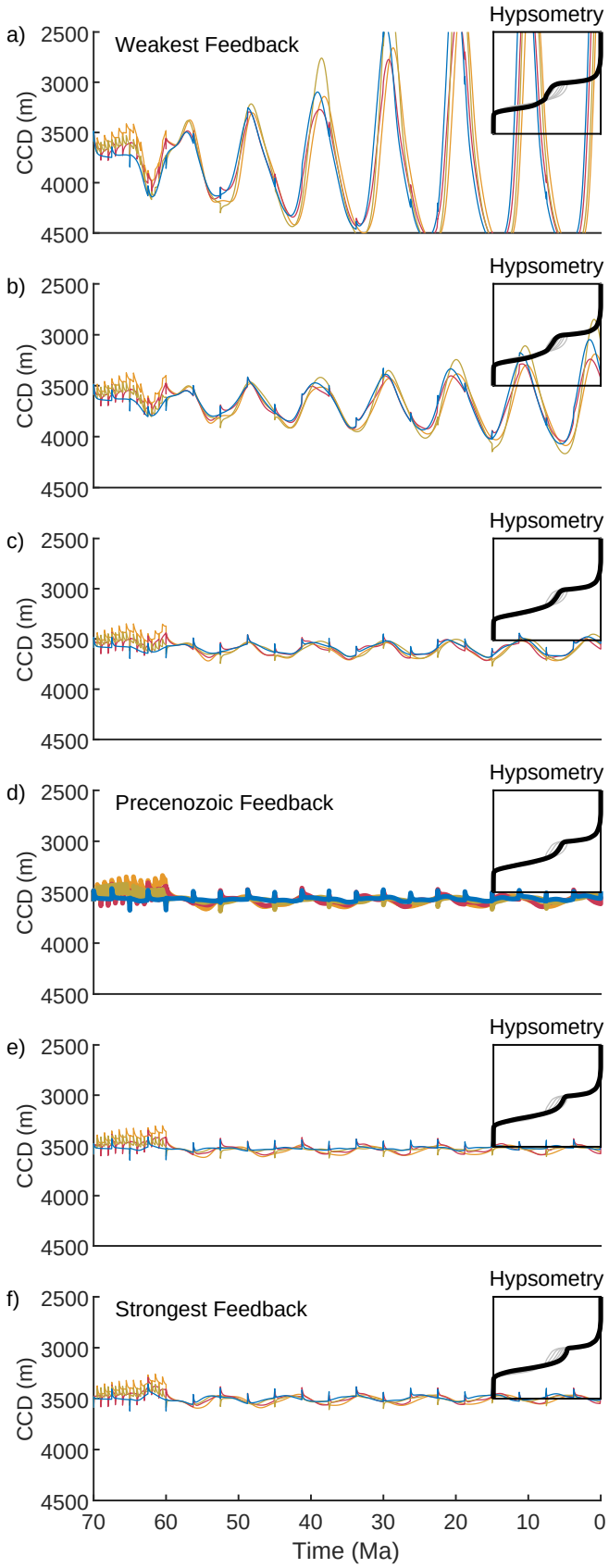

Figure 3.9: ***The CCD response to calcium and magnesium forcing using a variety of hypsometric profiles used to control the strength of the carbonate compensation feedback.***

Climate Response Summary
Strong carbonate compensation feedback strength results in the most stable climate evolutions. This aligns well with the expected model behaviour, as when the carbonate compensation feedback is strong, a small change in the CCD causes a large change in the carbonate burial flux, meaning the system is able to quickly return to steady state after a perturbation. Weakening the carbonate compensation feedback allows the development of oscillations in atmospheric CO_2 and the CCD, driven by the difficulty in affecting change in ocean carbon burial. Interestingly, all runs show a convergent evolution. Given all runs have identical forcing, this is perhaps to be expected, however indicates that feedbacks are dominating the long term evolution of climate in this ensemble.

3.3.4 Silicate Weathering Feedback

Silicate weathering has the potential to stabilise climate by changing the sink of atmospheric CO_2 in response to some combination of climate factors, as discussed in Section 1.2. If higher atmospheric CO_2 concentrations act to increase the CO_2 sink, as is believed to be the case, then this is a stabilising feedback. The four key scenarios are run with changing silicate weathering feedback strength by manipulating the silicate weathering-temperature relationship, as explained in Section 2.4.2. This allows examination of the sensitivity of the climate to changes in the response of the atmospheric CO_2 sink.

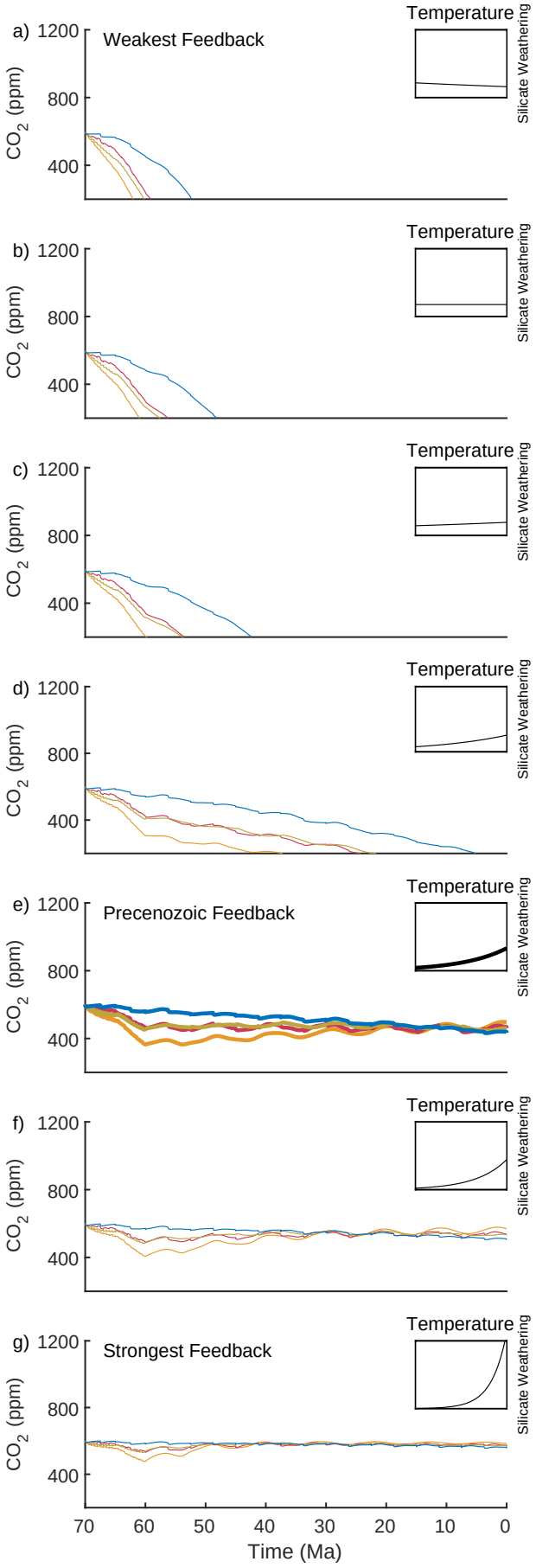

Figure 3.10: ***The CO_2 response to calcium and magnesium forcing using a variety of silicate weathering feedback strengths.***

Climate Response

In the ensemble of runs shown in Figure 3.10, when the silicate weathering feedback is weaker than the Precenozoic strength (Figure 3.10a-d) there is a pronounced difference between the run in which both calcium and magnesium ion change slowly (in blue) and other runs. The trend in atmospheric CO_2 and CCD appears the same, but the timescale over which the same decrease in atmospheric CO_2 is much longer when the change in ion concentrations is slowest. With increasing silicate weathering feedback strength, the transient differences in climate evolution between forcing scenarios are minimised, as is the difference in climate steady state achieved.

Model runs in which the silicate weathering response is reversed (higher temperature causes less silicate weathering - Figure 3.10a), or in which there is no relationship between silicate weathering and temperature (Figure 3.10b) show rapid climate destabilisation. Driving this runaway CO_2 loss requires only a modest reduction in silicate weathering feedback strength from the default Precenozoic condition (Figure 3.10c-d). A strengthening of the silicate weathering feedback (Figure 3.10f-g) causes a more constrained CO_2 evolution, and results in a final model state that is closer to the initial state.

The strong decrease in atmospheric CO_2 observed in runs with weaker silicate weathering feedbacks than the Precenozoic strength (Figure 3.10a-d) is associated with a long term shoaling of the CCD (Figure 3.11a-d). Interestingly, when the strength of the feedback is only slightly weaker than the Precenozoic condition (Figure 3.11d) the CCD appears to remain quite stable throughout the run despite the ongoing fall in atmospheric CO_2, until the model crashes.

There are transient perturbations to the CCD (the reason for which is detailed in Section 3.4), which are quickly removed before the CCD returns to the long term trajectory. Longer term oscillations can also be observed in some ensemble members (such as the run in which both calcium and magnesium ion concentration change rapidly with feedbacks at the Precenozoic strength - yellow in Figure 3.10e). These are the result of tectonic carbon recycling, but are of negligible magnitude.

In runs where destabilisation occurs, the CCD shoals by several hundred metres before the model crashes. The model crash is inferred to represent climatic destabilisation, because the ongoing decline in CO_2 shows no sign of slowing, however alternate feedbacks may kick in at low atmospheric CO_2 values which prevent

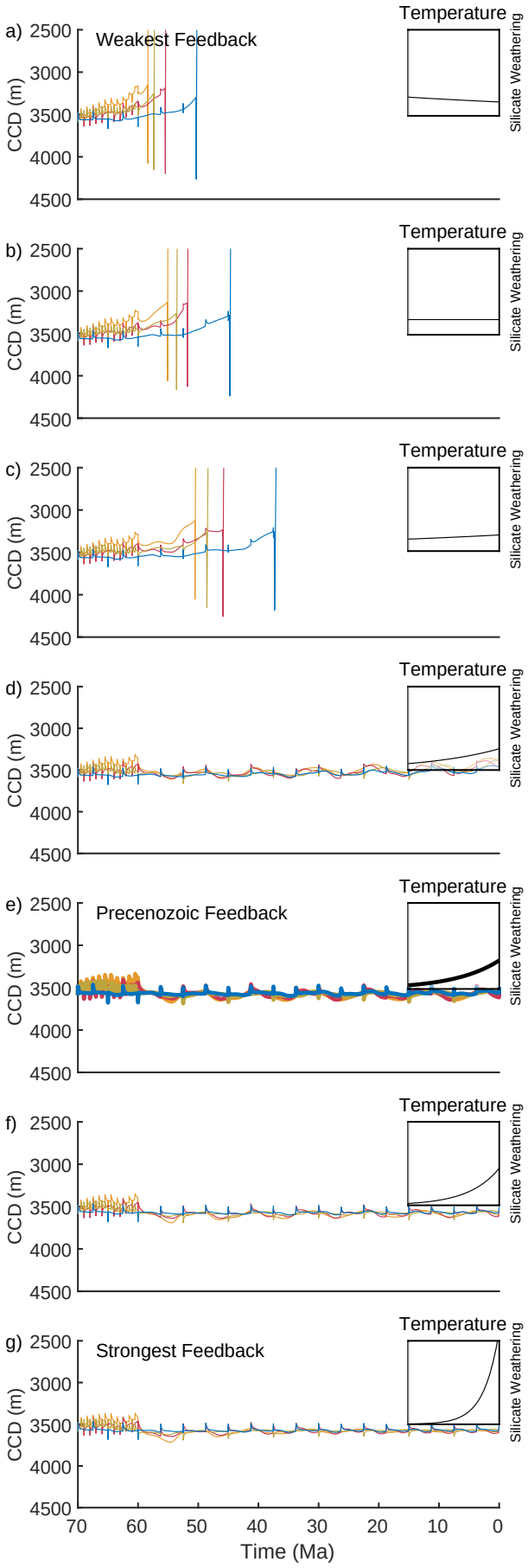

Figure 3.11: ***The CCD response to calcium and magnesium forcing using a variety of silicate weathering feedback strengths.***

atmospheric CO_2 exhaustion. The potential low CO_2 feedbacks are not observed either because the model does not incorporate them, or CO_2 does not reach low enough values before the carbonate chemistry routine is unable to function. Nonetheless, this ensemble shows that decreased silicate weathering feedback strength allows CO_2 to vary more greatly in response to a given driver.

Feedback Summary
A strong silicate weathering feedback constrains atmospheric CO_2 evolution, and stabilises climate against the oceanic calcium and magnesium forcing. When the silicate weathering feedback is even slightly weaker than the Precenozoic condition, atmospheric CO_2 exhibits a runaway decrease (Figure 3.10a-d). In spite of this destabilising CO_2, the CCD remains comparatively stable except where CO_2 reaches extreme values (Figure 3.11a-c). There is quite a sharp jump between climate destabilisation and ongoing climate stability, which may indicate that at a certain point this feedback becomes weaker than the climate driver, or weaker than other climate feedbacks, allowing model destabilisation.

3.3.5 Carbonate Weathering Feedback

Carbonate weathering, in contrast to the previous two feedbacks, may be viewed as a destabilising feedback. Conventional wisdom states that carbonate weathering is carbon neutral, as any carbonate formed in the ocean undoes the weathering reaction. This interpretation, though correct, is incomplete, as it only considers the fate of one of the two moles of carbon involved in the carbonate weathering reaction (Equation 1.2). For a closed system, migration of carbon into or out of the terrestrial environment requires accommodation by other reservoirs. The terrestrial reservoir must change in size if changes in carbonate weathering are not offset by an equal change in shallow carbonate burial, potentially driving important carbon cycle trends. There is large scope for this feedback to interact with other climate feedbacks. For example, any feedback which balances the source of terrestrial carbon with its sink will mitigate the impact of changes in carbonate weathering on the carbon cycle. As with the silicate weathering feedback, the carbonate weathering feedback strength can be tuned by manipulating the carbonate weathering-temperature relationship (as described in Section 2.4.3), which is, by default, the same as the silicate weathering-temperature relationship. These values control the fraction of the available reservoir that is weathered, and so changes in reservoir size may also affect the weathering flux. The carbonate weathering-temperature feedback is strengthened or weakened to establish the impact of this feedback on long term climate evolution.

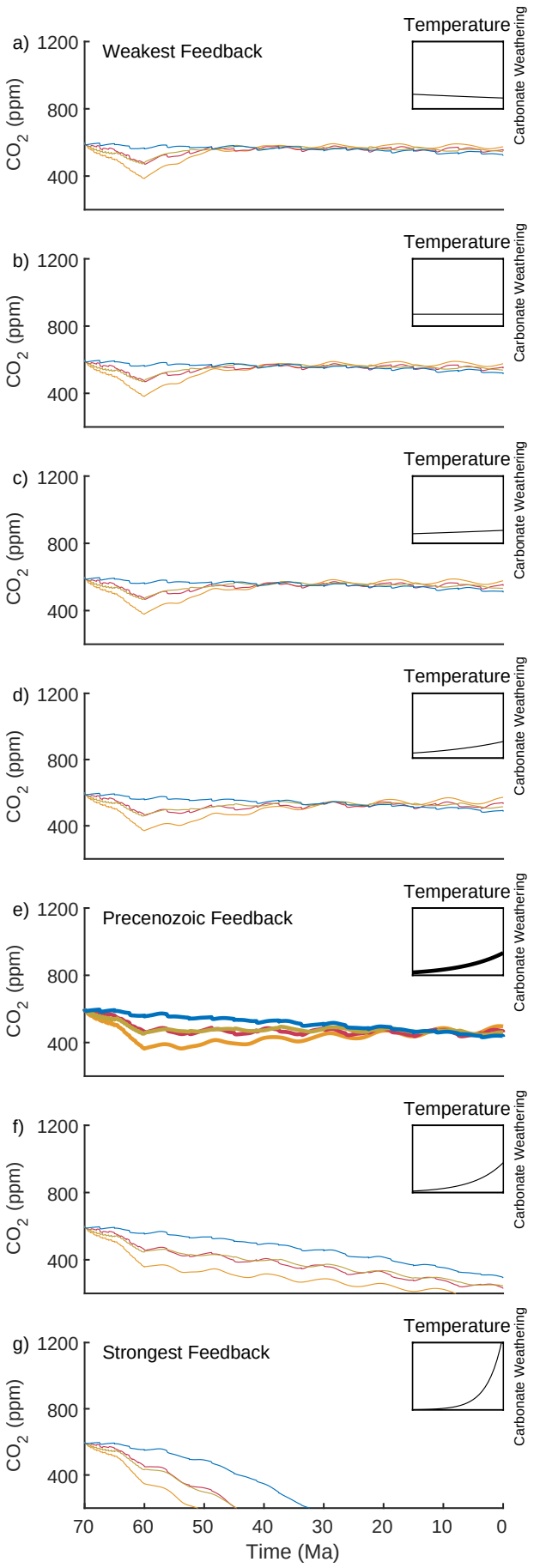

Figure 3.12: ***The CO_2 response to calcium and magnesium forcing using a variety of carbonate weathering feedback strengths.***

Climate Response

As with the silicate weathering feedback ensemble show in Figure 3.10, individual forcing scenarios all show a transient difference in atmospheric CO_2 from 70-50Ma. The transient difference in atmospheric CO_2 is $\sim$200ppm in all but the runs where carbonate weathering is particularly strong (Figure 3.10g). When the carbonate weathering feedback is weak or at the Precenozoic strength (Figure 3.12a-e) these transient differences are minimised by the end of the run, or in other words, the runs show a convergent atmospheric CO_2 evolution. When the carbonate weathering feedback is particularly strong (Figure 3.12f-g) it is unclear whether the runs are convergent or divergent, but all show the same decreasing trend in atmospheric CO_2 concentration.

The CCD appears especially stable when the carbonate weathering feedback is comparatively weak (Figure 3.13a-e), and is also stable when the carbonate weathering feedback is only slightly stronger than the Precenozoic strength (Figure 3.13f) though does display larger long term oscillations than when the carbonate weathering feedback is weaker. These oscillations are at maximum on

the order of tens of metres. By far the most CCD variability is observed when the carbonate weathering feedback is strongest (Figure 3.12g), which shows approximately 1km of CCD shoaling in all scenarios before the model crashes.

In terms of stability, when the carbonate weathering feedback is weak (Figure 3.12b-d), or even reversed (with increased temperature caused decreased weathering - as in Figure 3.12a), atmospheric CO_2 concentration remains stable, whereas when the carbonate weathering feedback is strong (Figure 3.12f-g), then atmospheric CO_2 exhibits a runaway negative trend. These results appear as the exact inverse of the silicate weathering feedback results (Section 3.3.4), not only directionally but also in that plots with a stable trend in Figure 3.10 show unstable trends in Figure 3.12, and vice versa. From the perspective of stability, the CCD shows the same pattern as atmospheric CO_2, stable when the carbonate weathering feedback is comparatively weak (Figure 3.13a-e), and unstable when the carbonate weathering feedback is comparatively strong (Figure 3.13g).

Of particular interest here is the second strongest carbonate weathering feedback (Figure 3.12f), which appears to show a midpoint between climate stability and

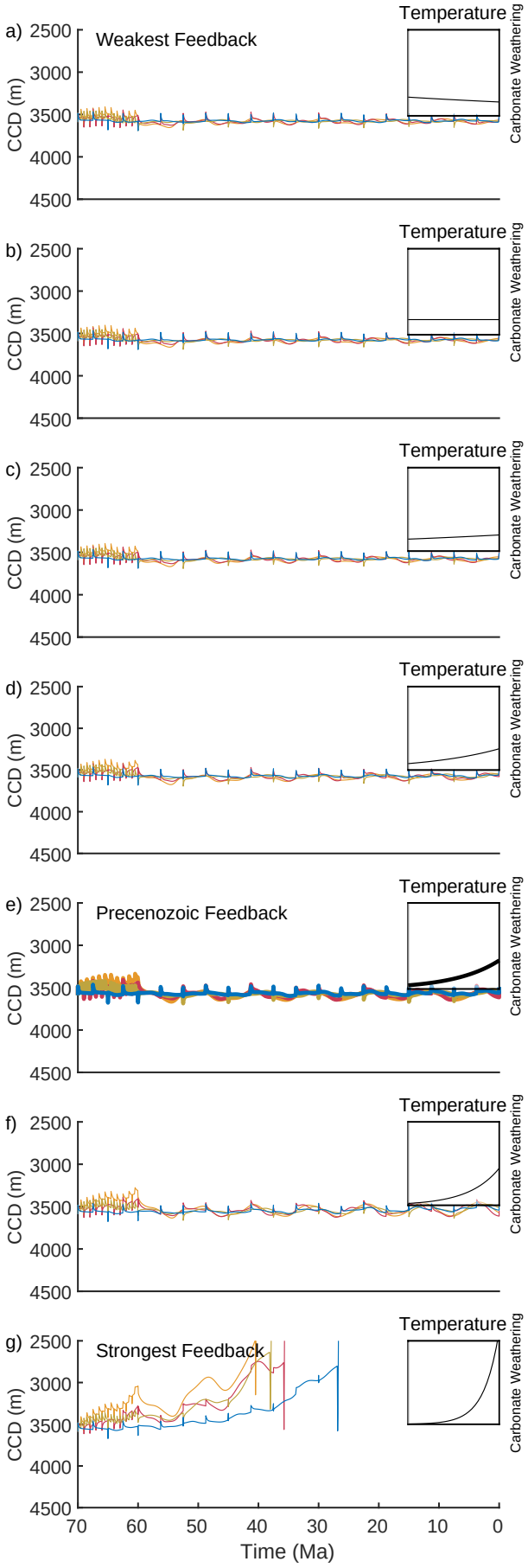

Figure 3.13: ***The CCD response to calcium and magnesium forcing using a variety of carbonate weathering feedback strengths.***

instability. It is unclear whether the decrease in CO_2 in these ensemble members would continue to decrease until atmospheric CO_2 exhaustion, or whether a low CO_2 steady state would be established.

Feedback Summary
When the carbonate weathering feedback is weak, atmospheric CO_2 and the CCD are particularly stable, and increasing carbonate weathering strength promotes a progressive increase in the variability of atmospheric CO_2. When the carbonate weathering feedback is particularly strong, atmospheric CO_2 exhibits a runaway decrease in response to all four driver scenarios. It appears there may be a sharp jump between seemingly stable climate evolutions and unstable climate evolutions, which could suggest that there is a threshold carbonate weathering feedback strength above which climatic instability is likely. Further inference of this behaviour is limited as the ensemble presented above only shows how the alteration of feedback strength affects the evolution in response to a single driver - if the same behaviour is seen as a result of changing carbonate weathering when a different driver is causing the initial climate response then it would be possible to be clearer on the mechanism which causes the observed behaviour.

3.3.6 Phosphate Weathering Feedback

The phosphate weathering feedback has the potential to drive carbon cycle change by changing oceanic primary productivity. This directly affects both organic carbon export and inorganic carbon export, as well as more indirectly causing changes in the CCD, as explained in Section 2.4.4. Due to the complex carbon cycle response to changing productivity, it is difficult to know what to expect when changing the phosphate weathering feedback strength. The simplest outcome would be that when temperature rises, a strong phosphate weathering feedback causes a permanent increase in organic carbon burial, and a transient increase in inorganic carbon burial, reducing atmospheric CO_2 and stabilising the climate, but this ignores the potential interactions with other carbon cycle feedbacks. To understand how the relationship between atmospheric CO_2 and changing oceanic primary productivity might affect long term climate stability, the four key scenarios are rerun with changing phosphate weathering-temperature relationships, controlled by manipulating the relationship between phosphate weathering and silicate/carbonate weathering, as described in Section 2.4.4.

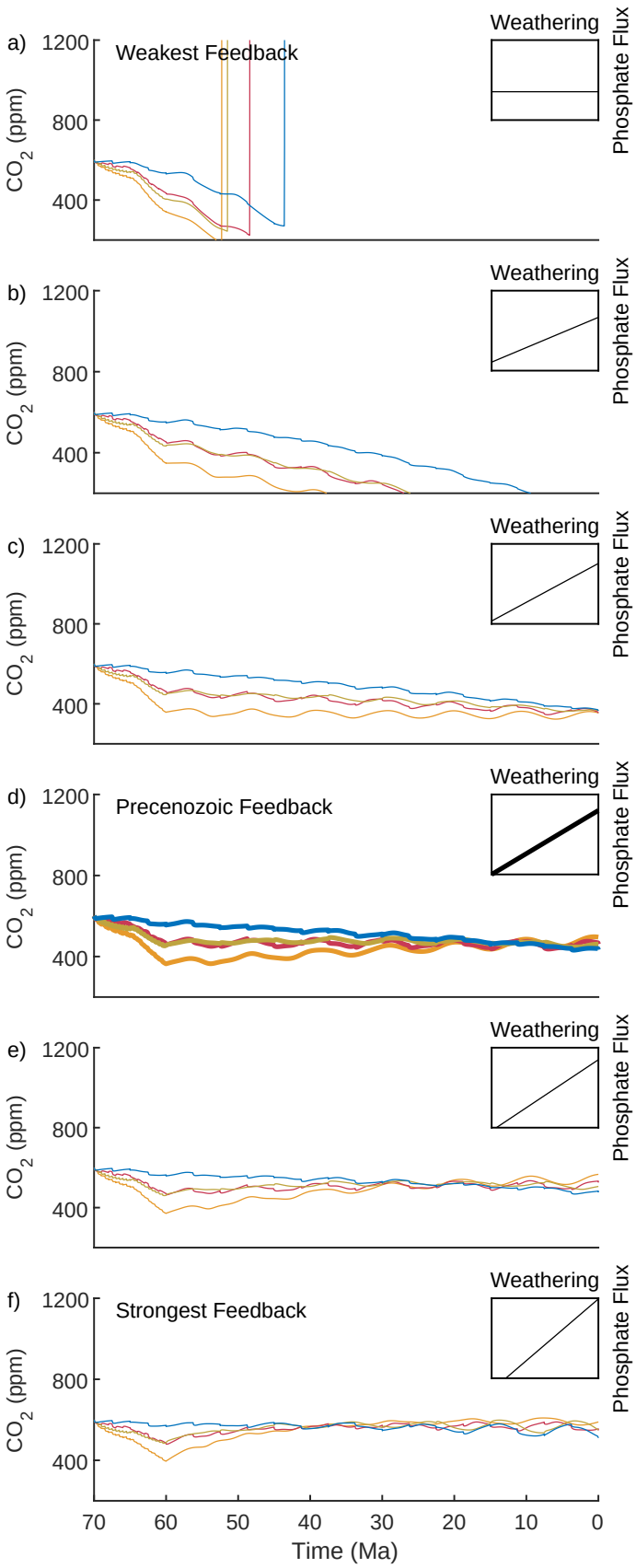

Figure 3.14: ***The CO_2 response to calcium and magnesium forcing using a variety of phosphate weathering feedback strengths.***

Climate Response

As with the other examinations of the impact of feedback strength, here atmospheric CO_2 shows a transient difference between forcing scenarios, which is sometimes removed by the end of the run but sometimes not. When there is no feedback (Figure 3.14a), the transient difference in atmospheric CO_2 between 70Ma and 50Ma appears to be largest, and the difference is noticeably smaller in runs where the feedback is at its strongest (Figure 3.14f). When looking at the CCD, the transient difference in simulations is more obvious, as the change in feedback strength results in a reversal in the sign of CCD change. When the feedback is weak (Figure 3.14a-c), the CCD initially shoals, whereas when the feedback is strong (Figure 3.14e-f), the CCD initially undergoes an transient deepening.

When there is no relationship between phosphate weathering and other weathering (Figure 3.14a), or this relationship is particularly weak (Figure 3.14b), atmospheric CO_2 undergoes a runaway decrease. In the no feedback scenarios, all four runs reach the point at which the model pH solver fails (see Section 2.3.1),

resulting in an unrealistic instantaneous rise in atmospheric CO_2. This is taken to indicate that the climate is trending towards instability, due to the rapidity of long term CO_2 fall. In contrast, when the phosphate weathering feedback is at the Precenozoic strength (Figure 3.14d), CO_2 exhibits a long term decline in all runs, but the concentration appears to be stabilising at a value that is not too dissimilar to the initial condition. When the phosphate weathering feedback is stronger than the Precenozoic condition (Figure 3.14e-f), the runs initially appear to be convergent, but in the final 20Myr seem to display oscillatory behaviour which is growing in magnitude.

Changing the strength of this feedback also affects the steady state CO_2 achieved near the end of the runs, with a stronger phosphate weathering feedback resulting in the final CO_2 concentration more closely matching the initial CO_2 concentration (Figure 3.14). Strengthening this feedback, however, does not necessarily result in climate stability. While a strong phosphate weathering feedback results in resilience to the imposed oceanic calcium and magnesium ion concentration change, it also appears to drive growing oscillations

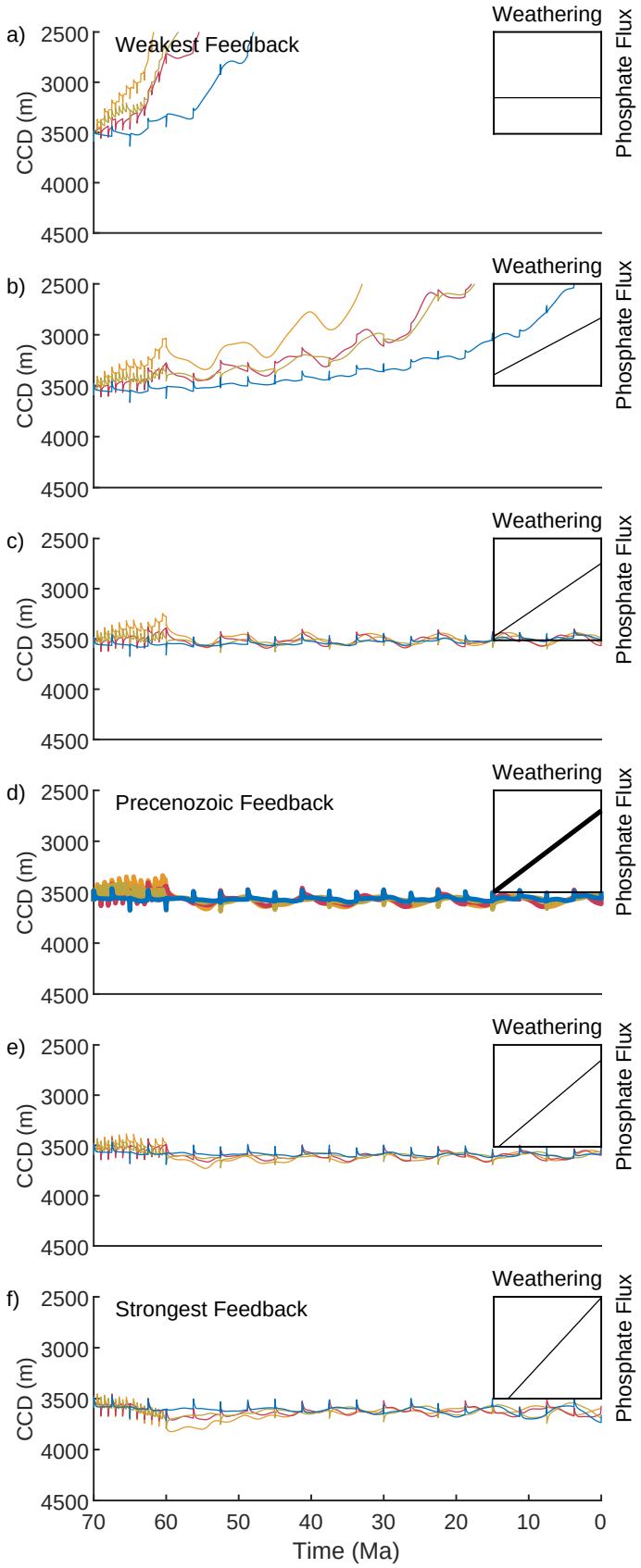

Figure 3.15: ***The CCD response to calcium and magnesium forcing using a variety of phosphate weathering feedback strengths.***

in CO_2, which may eventually become destabilising.

Feedback Summary
Both strong and weak phosphate weathering feedback strengths are associated with climate instability. In cases where the feedback is weak (Figure 3.14a-c), the initial negative CO_2 forcing is amplified by the lack of productivity response. In some situations, this appears to be a runaway response, but it may be that longer runs would show continued CCD adaptation until the carbon cycle is rebalanced. Ensemble members with a strength similar to the Precenozoic condition (Figure 3.14d) show stable CO_2 and CCD evolution. A strong phosphate weathering feedback (Figure 3.14e-f) is associated with growing oscillations in both CO_2 and the CCD. These appear small in these runs, but assuming the behaviour as observed would continue in longer runs, would prove destabilising.

3.3.7 Feedback Synthesis

Overall the GECCO model shows a high sensitivity to the strengths of all the feedbacks which are examined. Both the carbonate compensation and silicate weathering feedbacks have the expected result in terms of causing climate stabilisation, whereas carbonate weathering and phosphate weathering response was more difficult to predict in advance.

The close relationship between feedback strength and long term climate evolution is partly due to the intimate links between feedbacks, and changes in any one feedback affect the entire system. Of the feedbacks explored, three appear to show unidirectional trends (i.e. increasing feedback strength causes the opposite effect of decreasing the feedback strength), and one shows a bidirectional trend (increasing feedback strength initially causes one effect, but this is reverse once the feedback increases beyond a given strength).

3.4. Known Limitations

3.4.1 CCK's

CCK's have been measured in a variety of media, however remain relatively poorly sampled for realistic seawater compositions. This means that all calculations that provide CCK's for a spectrum of seawater compositions rely on interpolation and/or extrapolation of existing empirical data, possibly incorporating some dynamical knowledge of the system. In essence, all CCK's are only an estimation of the true value, due to the vast number of factors which can affect them. There is ongoing debate as to the best method of performing the estimation

of CCK's across a range of ocean compositions (*Zeebe* and *Tyrrell*, 2018; *Hain et al.*, 2018). The GECCO model currently uses the methodology and data described in *Hain et al.* (2015) by default, however will incorporate new formulations of the impact of ocean ion composition on the carbon cycle as these data become available. Some of the carbonate system behaviour observed by *Hain et al.* (2015) is not intuitive (*Zeebe* and *Tyrrell*, 2018), however this is currently the best available approach to the problem. Even though this estimation of CCK's is likely to be imperfect, they are nonetheless functional for the purpose of this study.

Hain et al. (2015) provide values for the CCK's over a range of 0 to 60mol/m^3 for both calcium and magnesium at a resolution of 1mol/m^3. Analysis of this dataset reveals that the relationship between ion concentration and CCK's is, in many cases, non linear, therefore the decision was taken to avoid interpolation of the values of *Hain et al.* (2015) and instead use a lookup table as a nearest neighbour approach. This approach leads to discontinuities in the value of a CCK in these simulations as the concentration of calcium or magnesium crosses over an integer value (e.g. there is a step change in the CCK value when calcium or magnesium changes from 1.99 to 2 mol/m^3). Discontinuities in these values factor into the carbon system calculations and result in sharp perturbations to carbonate system parameters, as can be observed in Figure 3.4. In reality the gradual evolution of CCK's would produce a smoother record than those presented here, but crucially, would have the same magnitude of impact on the timescales of interest. Furthermore, this approach has the serendipitous property of disentangling the long term, direct impact of calcium on saturation state and the perturbing, indirect impact of calcium on the CCK's. Any instantaneous perturbations observed in model results can be attributed to the crossing over of threshold values of calcium and magnesium concentration causing an instantaneous change in the CCK's. In contrast, the long term trend incorporates the combined forcing of changes in CCK's and direct changes in the saturation state.

3.4.2 Ca and Mg Concentration

In Section 3.2.1 a detailed calculation was presented which estimated the evolution of calcium concentration, magnesium concentration, and magnesium:calcium ratio through time. This calculation inherently relies on the available data, and is entirely independent of any consideration of how the sources or sinks of calcium and magnesium may have changed through time. These data are, however, difficult to acquire, especially when seeking the absolute ion concentration, which has led to a sparse sampling density for both calcium and

magnesium ion concentration over the Cenozoic. Compounding these difficulties was the lack of clear and consistent uncertainty reporting alongside original data, which hampered the statistical techniques applied in Section 3.2.1. Overall, the magnesium:calcium ratio is comparatively well constrained across the Cenozoic. Due to the long residence time of magnesium, the assumption that it is likely to have followed a roughly linear trend is reasonable. Calcium is particularly poorly constrained using only direct estimates, so the congruency of the calcium data and the estimated calcium concentration from the combination of magnesium:calcium ratio and magnesium concentration is promising. Nonetheless, it would be ideal to have a greater density of datapoints within the Cenozoic and further into the past.

3.4.3 Model Limitations

The GECCO model is not a perfect representation of reality, and includes simplifications and parameterisations (discussed at length in Chapter 2). Despite the need for simplification, carbonate chemistry and the CSH depth solver used used by GECCO are specifically designed to represent the impact of calcium and magnesium on the carbonate system, representing an improvement over past efforts, and so are unlikely to impact this study negatively. Uncertainty in the initial conditions that the model is tuned to may lead to differences in the absolute values of state variables reported here, however the direction of forcing will remain the same. To understand how the initial state of the model would affect Cenozoic carbon cycle and climate evolution, additional ensembles should be performed which experience the same forcing and have the same feedback strength but are initialised to a different steady state atmospheric CO_2 concentration. Unfortunately, developing a steady state requires the model to be run for hundreds of millions of years, which is highly computationally expensive, so was not feasible during this project due to the time constraints. The initialisation of the model at steady state has several advantages, even though it likely does not represent a climate state that truly existed (as discussed in Section 2.3.1), so it should be reiterated that the results of this study should be seen as an estimation of the potential magnitude of changes in oceanic calcium and magnesium concentration to drive carbon cycle and climate change on Cenozoic timescales.

3.4.4 Feedback Strength

The initial values prescribed in GECCO which control the various feedback strengths are, generally speaking, difficult to estimate. For some of the values the present day value is very poorly constrained (or there is no constraint), so estimating these values at 70Ma is particularly challenging. In most cases this is overcome by making assumptions of reasonable parameters which match similar known processes - for example, the carbonate weathering-temperature relationship is assumed to be equal to the silicate weathering-temperature relationship due to the lack of evidence to the contrary, and the known silicate weathering behaviour. The purpose of this study is also primarily an exploration of the potential for the ocean major ion forcing to cause meaningful climate change under a variety of climate feedback scenarios, so most of the problematic nature of the uncertainty in the initial strength of the feedback is mitigated by performing ensembles of runs in which the feedback strength is variable. There is still potential for problems resulting from the lack of knowledge about the feedback strength at 70Ma, as this would be expected to affect the steady state of the carbon cycle. This possibility is noted, but the only foreseeable solution is to improve the current understanding of feedback strength at 70Ma, which can then be fed into GECCO to refine the results presented here. The default estimate of feedback strength is likely to be at least reasonable, as it allows the simulation of a Preindustrial carbon cycle, and is not in contrast to any known records. Such a reasonable initial climate state is all that is required from the perspective of potential feedback strength in order to ensure that the results of this study remain robust. In addition to this, the parallel study presented in Chapter 4, which has an alternate forcing but the same variety of feedback strengths, serves to further increase confidence that the results are appropriately representing the influence of changing feedback efficacy.

3.5. Discussion

3.5.1 Comparison to Existing Data

The ensemble presented here and existing data describing the Cenozoic carbonate system should not be expected to quantitatively agree. Data driven approaches are only able to observe the climate as it was, whereas the ensemble results shown here identify how each parameter would have changed given only calcium and magnesium ion concentration as a driver. Nonetheless, it is informative to observe whether the trends driven by changes in

ocean composition are aligned with the current understanding of the carbonate system over the Cenozoic and, if so, what component of the observed change could feasibly be ascribed to the change in calcium and magnesium ion concentrations.

Based on the data presented in Figure 1.15, CO_2 fell from the peak Cenozoic value of $\sim$1000ppm to the Preindustrial value of $\sim$300ppm over about 50Myr. The CO_2 fall exhibited within the ensemble with feedbacks at the default Precenozoic strength is roughly 35% of that total CO_2 fall, which suggests that changes in ocean composition can be an important factor in Earth's long term CO_2 evolution, but how important this driver is depends strongly on feedback strength.

In the Precenozoic ensemble, steady state ocean pH rises by $\sim$0.3 units, which is directionally in agreement with existing data (*Tyrrell* and *Zeebe*, 2004; *Caves et al.*, 2016; *Anagnostou et al.*, 2016; *Sosdian et al.*, 2018). *Tyrrell* and *Zeebe* (2004) calculated that DIC and alkalinity remained roughly constant through the Cenozoic. In contrast to this, *Caves et al.* (2016) found that alkalinity was low in the early Cenozoic (roughly 1.4mol/m^3), rose to a peak value of $\sim$3mol/m^3 during the Eocene, fell again into the Miocene then rose to present day values. *Sosdian et al.* (2018) compiled the available estimates of DIC evolution from 25Ma to present, all of which show a flat, or increasing value through time. This compilation shows a DIC range of $\sim$1.5mol/m^3 to 2mol/m^3 at 25Ma, consistent with the range in DIC evolutions shown in Figure 3.5. The ensemble of runs presented here suggests that ocean composition favoured a carbonate system with lower DIC and alkalinity at 70Ma. If Precenozoic DIC and alkalinity concentrations were approximately the same as the present day, then an opposing factor must have acted to offset the impact of changing oceanic calcium and magnesium concentrations. There are three potential remedies that reconcile disparities between other datasets and the DIC reconstruction presented here:

1. A carbonate system parameter must change, for example *Tyrrell* and *Zeebe* (2004) use a CO_2 concentration of $\sim$1100ppm at 70Ma, much higher than the concentration of 600ppm used as the initial steady state here.

2. Parameters which are influenced by the carbonate system, such as the CCD, are changing for reasons not related to changes in carbonate chemistry. This allows a decoupling between apparent carbonate system parameters and oceanic carbonate chemistry (Section 2.4.1).

3. There are different approaches to quantify the impact of calcium and magnesium on CCK's, which can introduce important differences in the carbonate system reconstruction (see Section 3.4).

Clamping atmospheric CO_2 concentration at 600ppm, then allowing the system to evolve to steady state with parameters as specified in Section 2.1 except where altered as described in Table 2.9, results in a lower than Preindustrial concentration of DIC and alkalinity. Alternative combinations of parameters might yield different steady state, so by understanding both degrees of freedom in the carbonate system additional climatic information may be able to be extracted.

3.5.2 Synthesis of Results

For both atmospheric CO_2 concentration and CCD, all ensemble members that are stable converge and there is no evidence of the crossing of climate thresholds which could have caused the simulations to diverge. While this stabilised property of the ensemble is interesting, in all cases the forcing factor over the 70Myr simulation is the same, meaning that consistent final CO_2 may be an expected outcome. In all ensemble members with the Precenozoic feedback strength, the final atmospheric CO_2 concentration is $\sim$250ppm lower than the initial condition, while the CCD is at the same depth. Typically, changes in oceanic calcium and magnesium ion concentration might be thought to affect the CCD more than CO_2, as they are directly influencing ocean conditions and feedbacks such as the silicate weathering feedback are invoked as stabilisers of atmospheric CO_2. In fact, when oceanic calcium and magnesium concentrations are forced to change, this has an effect on both saturation state and aqueous CO_2. The carbonate compensation feedback attempts to restore the balance to the ocean carbon budget, but while the carbonate ion concentration changes, the CCD must remain at the same depth if the influx of carbon does not change. In the ensemble members with the default feedback strength, the weathering flux does decrease in response to falling CO_2, but the impact of this decrease on the CCD is mitigated by a decrease in productivity. The balance of feedbacks results in CO_2 decrease with a stabilised CCD.

It is often assumed that calcium is the strongest ionic driver of the carbonate system. While magnesium is known to have the strongest impact on CCK's due to the ion pairs that it forms (*Zeebe* and *Wolf-Gladrow*, 2001), calcium impacts both CCK's and the saturation state directly. To distinguish between the impact of calcium and magnesium ions, two runs were extracted from the ensemble, one with only calcium concentration changing, and the

other with only magnesium changing (Figure 3.16). The comparison of these results is detailed in Table 3.2.

Calcium	**Magnesium**
When calcium concentration is varied from 20 to 10mol/m^3 over 60Myr while magnesium concentration is held constant, there is $\sim$50ppm of atmospheric CO_2 fall.	When magnesium concentration is varied from 30 to 50mol/m^3 over 60Myr while calcium concentration is held constant, there is $\sim$50ppm of atmospheric CO_2 fall.
Until 60Myr into the run, calcium has a lesser impact.	Until 60Myr into the run, magnesium has a greater impact.
Calcium affects both CCK's and saturation state.	Magnesium affects only the CCK's.
Decreasing calcium concentration increases the activity of carbonate ions (CCD deepening perturbations in Figure 3.16).	Increasing magnesium concentration inhibits the activity of carbonate ions (CCD shoaling perturbations in Figure 3.16).
Decreasing calcium concentration decreases the saturation state (CCD shoaling).	Increasing magnesium concentration does not affect the saturation state.
Conflicting impacts	No conflicting impacts

Table 3.2: ***Each column describes by row the impact of the relevant ion on the carbonate system, broken down into individual effects in order to clarify the differences between these ions as drivers of carbon cycle change.***

The opposing effects of changing calcium concentration (outlined in Table 3.2) act to impede the impact of calcium ion concentration on the carbonate system. As can be seen in Figure 3.16, calcium and magnesium have approximately the same magnitude of impact on atmospheric CO_2, but magnesium concentration changes twice as much as calcium concentration. This shows that calcium is the strongest driver of carbonate system change on a mole for mole basis, however magnesium has had almost equivalent impact over the last 70Ma. The effects of calcium and magnesium are combinative rather than additive meaning that while calcium and magnesium are able to drive $\sim$50ppm of CO_2 change each, their combined effect has an impact of $\sim$250ppm at the Precenozoic feedback strength.

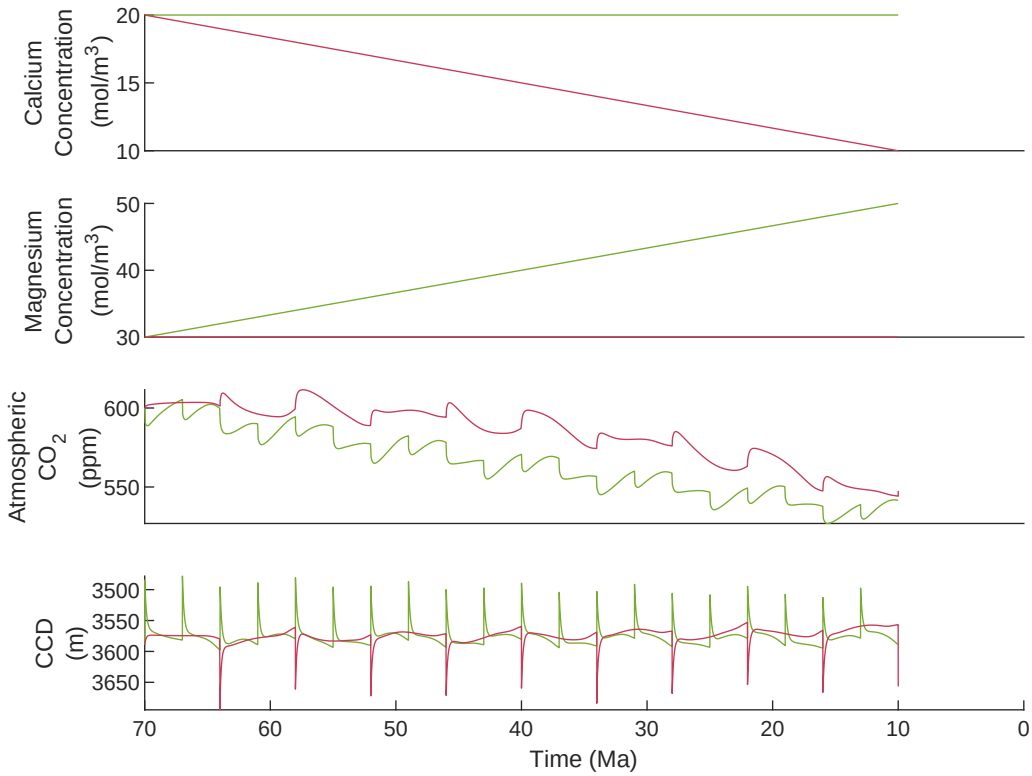

Figure 3.16: ***Two ensemble members are isolated to highlight the separate contributions of calcium ion concentration and magnesium ion concentration to atmospheric CO_2 and the CCD. The red line displays the scenario where magnesium concentration remains constant as oceanic calcium concentration evolves from 20 to 10mol/m^3. The green line shows the scenario where calcium concentration remains constants while oceanic magnesium ion concentration evolves from 30 to 50mol/m^3. Jumps in the CCD are caused by the decimated nature of data which informs the calculation for the impact of calcium and magnesium concentration on CCK's, detailed further in Section 3.4.***

By examining the temporal gradients in ion concentrations, it is possible to estimate the role of feedbacks (Figure 3.17) in restraining or amplifying the driven change. When the temporal gradient of an ion is steep, atmospheric CO_2 shows the greatest change (the ΔCO_2 relative to steady state is highest), whereas when the same change in ion concentration is forced over a greater time interval, the ΔCO_2 is reduced, indicating that climate feedbacks are mitigating some of the driven change (Figure 3.17). Interestingly, when the magnesium concentration is instantaneously changed (upper right panel in Figure 3.17) the impact on atmospheric CO_2 is much larger than the impact of an instantaneous change in oceanic calcium concentration (upper left panel in Figure 3.17). This difference is attributed to contrast in the timing of impacts driven by ions on CCK's and the timing of impacts driven by changed in calcium concentration on the saturation state. The effect of calcium and magnesium on

the oceanic carbonate system is essentially instantaneous, but, while the change to saturation state driven by changes in calcium concentration is immediate, the ocean takes time to adapt to the new saturation state by movement of the CCD.

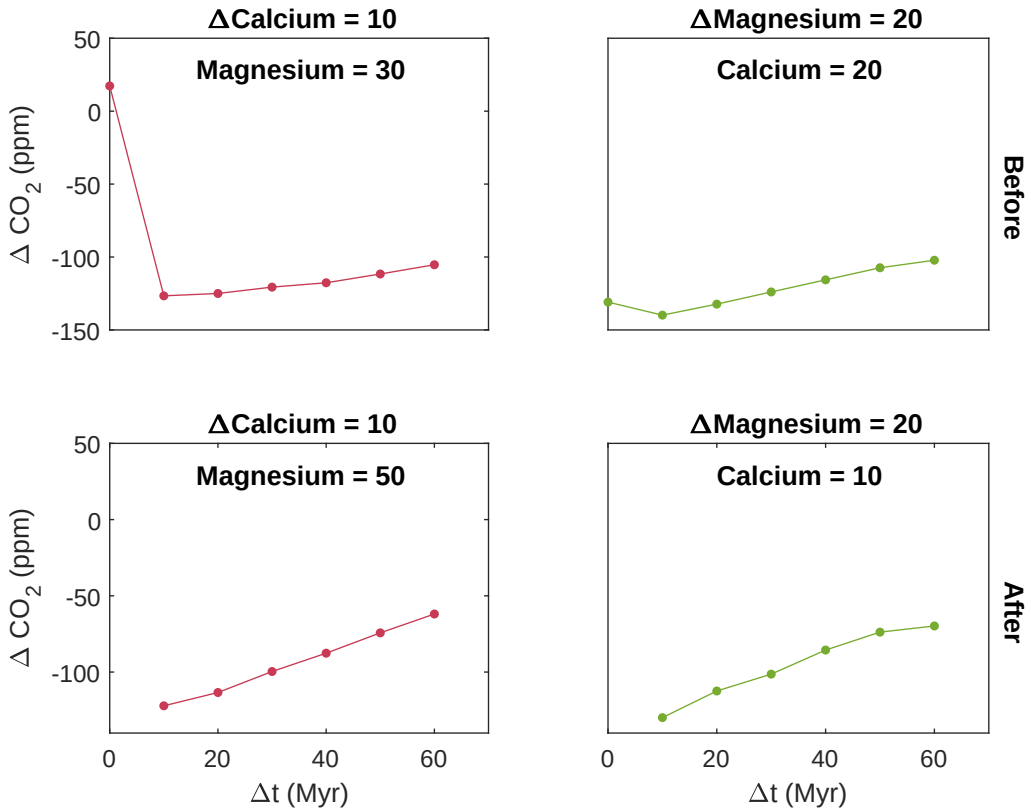

Figure 3.17: ***Lines in red show scenarios where calcium concentration evolves as magnesium concentration remains constant, while green lines show ensemble members where magnesium concentration evolves while calcium concentration remains static. For all ensemble members shown here the feedbacks are at the Precenozoic strength. Upper panels show the results where the static ion remains at the initial condition ('before'), whereas the lower panels show the static concentration remains at the final condition ('after'). In general, larger $\triangle t$ values result in decreased $\triangle CO_2$, indicating that feedbacks are reducing the impact of the imposed forcing.***

3.6. Conclusions

1. **Changes in ocean composition have the potential to play an important role in carbon cycle trends during the Cenozoic.**

   The changes in calcium and magnesium ion concentrations thought to have occurred over the Cenozoic are sufficient to drive an important component of carbon cycle change, particularly when feedbacks are conducive to atmospheric CO_2 change. Using the Precenozoic feedback strength, atmospheric CO_2 falls by about 250ppm from the initial condition.

2. **The imposed change in oceanic calcium and magnesium ion concentration does not appear to affect the response of the climate to a perturbation.**

   Though there is some variation in the $\triangle CO_2$ driven by the large atmospheric perturbation shown in Figure 3.7, this is likely due to the different amount of calcium and magnesium ion change that has occurred before the perturbation, rather than an indication that changing ion concentration is affecting climate stability. Changing ion concentrations are known to alter the ocean buffering capability (*Hain et al.*, 2015), but on long timescales, the perturbation appears to drive roughly the same atmospheric CO_2 change.

3. **Magnesium and calcium drive greater carbon cycle change when their concentrations vary inversely, rather than individually or in tandem.**

   The impacts of calcium and magnesium on CCK's are such that their covariance should cause the greatest change in the carbonate system, however due to the conflicting impacts of calcium on the carbonate system (as outlined in Table 3.2) there is a synergistic change when calcium and magnesium change inversely.

4. **The magnitude of climate response to the change in oceanic calcium and magnesium ion concentration is strongly dependent on climate feedback strength.**

   Ensembles of runs show that the amount of change in both the atmospheric CO_2 concentration and CCD is heavily dependent on the feedback strength. Strong carbonate compensation and silicate weathering feedbacks promote climate stability, whereas a strong carbonate weathering feedback causes instability, and either strong or weak phosphate weathering feedback causes climate instability.

3.7. Future Work

Significant improvements could be made to current understanding of the impacts of changes in calcium and magnesium concentration by improving the datasets themselves. Additional data would be extremely useful to quantify the temporal evolution of both calcium and magnesium ions. Large advances could also be made by clarifying the nature of uncertainties on existing data, which, although invaluable, could be significantly refined to narrow the uncertainty window. This would serve to further constrain the forcing with which to drive the model. The impact of this forcing is also uncertain, as there is ongoing disagreement about the best method of quantifying the impact of changing ion concentration on the carbon cycle (*Hain et al.*, 2015; *Zeebe* and *Tyrrell*, 2019).

References

Anagnostou, E., John, E. H., Edgar, K. M., Foster, G. L., Ridgwell, A., Inglis, G. N., Pancost, R. D., Lunt, D. J., and Pearson, P. N., 2016, Changing atmospheric CO_2 concentration was the primary driver of early Cenozoic climate, *Nature*, **533**(7603), 380–384.

Ben-Yaakov, S., and Goldhaber, M. B., 1973, The influence of sea water composition on the apparent constants of the carbonate system, *Deep-Sea Research and Oceanographic Abstracts*, **20**(1), 87–99.

Boudreau, B. P., Middelburg, J. J., Sluijs, A., and Ploeg, R., 2019, Secular Variations in the Carbonate Chemistry of the Oceans over the Cenozoic, *Earth and Planetary Science Letters*, **512**, 194–206.

Brennan, S. T., Lowenstein, T. K., and Cendon, D. I., 2013, The major-ion composition of cenozoic seawater: the past 36 million years from fluid inclusions inmarine halite, *American Journal of Science*, **313**(8), 713–775.

Broecker, W., and Peng, T.-H., 1982, *Tracers In The Sea*, Columbia University, New York.

Caves, J. K., Jost, A. B., Lau, K. V., and Maher, K., 2016, Cenozoic carbon cycle imbalances and a variable weathering feedback, *Earth and Planetary Science Letters*, **450**, 152–163.

Coggon, R. M., Teagle, D. A. H., Smith-Duque, C. E., Alt, J. C., and Cooper, M. J., 2010, Reconstructing Past Seawater Mg/Ca, *Science*, **327**(February), 1114–1117.

Gothmann, A. M., Stolarski, J., Adkins, J. F., Schoene, B., Dennis, K. J., Schrag, D. P., Mazur, M., and Bender, M. L., 2015, Fossil corals as an archive of secular variations in seawater chemistry since the Mesozoic, *Geochimica et Cosmochimica Acta*, **160**, 188–208.

Hain, M., Sigman, D., Higgins, J. A., and Haug, G. H., 2018, Response to Comment by Zeebe and Tyrrell on The Effects of Secular Calcium and Magnesium Concentration Changes on the Thermodynamics of Seawater Acid/Base Chemistry: Implications for the Eocene and Cretaceous Ocean Carbon Chemistry and Buffering Mathis, *Global Biogeochemical Cycles*, **32**(5), 898–901.

Hain, M. P., Sigman, D. M., Higgins, J. A., and Haug, G. H., 2015, The effects of secular calcium and magnesium concentration changes on the thermodynamics of seawater acid/base chemistry: Implications for Eocene and Cretaceous ocean carbon chemistry and buffering, *Global Biogeochemical Cycles*, 517–533.

Horita, J., Zimmermann, H., and Holland, H. D., 2002, Chemical evolution of seawater during the Phanerozoic, *Geochimica et Cosmochimica Acta*, **66**(21), 3733–3756.

Rausch, S., Böhm, F., Bach, W., Klügel, A., and Eisenhauer, A., 2013, Calcium carbonate

veins in ocean crust record a threefold increase of seawater Mg/Ca in the past 30 million years, *Earth and Planetary Science Letters*, **362**, 215–224.

Sosdian, S., Greenop, R., Hain, M., Foster, G., Pearson, P., and Lear, C., 2018, Constraining the evolution of Neogene ocean carbonate chemistry using the boron isotope pH proxy, *Earth and Planetary Science Letters*, **498**, 362–376.

Tyrrell, T., and Merico, A., 2004, Emiliania huxleyi: bloom observation and the conditions that induce them, *Coccolithophores: From Molecular Processes to Global Impact*, 585–604.

Tyrrell, T., and Zeebe, R. E., 2004, History of carbonate ion concentration over the last 100 million years, *Geochimica et Cosmochimica Acta*, **68**(17), 3521–3530.

Zeebe, R. E., and Tyrrell, T., 2018, Comment on The Effects of Secular Calcium and Magnesium Concentration Changes on the Thermodynamics of Seawater Acid/Base Chemistry: Implications for Eocene and Cretaceous Ocean Carbon Chemistry and Buffering by Hain et al. (2015), *Global Biogeochemical Cycles*, **32**(5), 895–897.

Zeebe, R. E., and Tyrrell, T., 2019, History of carbonate ion concentration over the last 100 million years II : Revised calculations and new data, *Geochimica et Cosmochimica Acta*, 1–20.

Zeebe, R. E., and Wolf-Gladrow, D., 2001, *CO2 in Seawater: Equilibrium, Kinetics, Isotopes*, Elsevier Ltd., Amsterdam, 3rd edition.

Chapter 4 - The Influence of Changes in Outgassing Lag on the Carbon Cycle Over Cenozoic timescales

What could be more grand,
Than to look across the land,
And wonder at all we see,
Then say how it came to be?

Abstract

Plate tectonics moves carbonaceous sediment from the deep sea into subduction zones, and some of the carbon in this sediment is understood to be returned to the surficial reservoir through volcanic outgassing of CO_2. Given this potential link between sediment on the descending slab and future volcanic outgassing, changes to the processes which govern the behaviour of slab sediments and the supraslab (sediment between the slab and Earth surface) carbon reservoir might be expected to drive climate change. One of the primary factors governing the link between sediment and climate is the timescale over which the sediment is moved from the seafloor to a subduction zone, and then the time taken for the carbon within sediments to move from the subduction zone to volcanic release (here termed the outgassing lag). Here, the GECCO model is used to simulate a gradual change in the outgassing lag to assess the impact this has on the carbon cycle and climate. As expected, when the outgassing lag is decreased, atmospheric CO_2 rises, and when the outgassing lag is increased, atmospheric CO_2 falls. The magnitude of transient carbon cycle response is dependent on both the strength of the driver and the strength of the feedback response, whereas the steady state climate is primarily dependent on the feedback strength. This is shown by further model runs in which the same forcing is applied but key parameters have been changed to tune the strength of each of four specific feedbacks. The sensitivity of the climate to each feedback examined is greater than previously appreciated. Collectively, it is shown that a 'chance' driver such as tectonics is able to cause long term climate change, but the magnitude of the climate response is strongly modulated by the strength of climate and carbon cycle feedbacks.

4.1. Introduction

Plate tectonics is currently understood to be predominantly or wholly an external or 'chance' driver. There have been suggestions that, in some instances, deep carbon behaviour could be related to climate, for example through variations in ice volume and associated change in lithospheric pressure (*Jull* and *Mckenzie*, 1996; *Kelemen et al.*, 1997; *Jellinek et al.*, 2004; *Huybers* and *Langmuir*, 2009), however these links do not establish climate as a major control on plate tectonic behaviour. Proceeding on the assumption that tectonics is an external climate driver, there is a fundamental asymmetry in their interaction because tectonics is feasibly able affect the climate whilst the climate is mostly unable to affect plate tectonics. Given Earth has remained habitable for an extremely long period of time, indicating at least moderate climate stability, and external drivers (including plate tectonics) could feasibly have undergone extremely large changes during that time, there are two potential end member hypotheses to explain ongoing climate stability:

The net forcing of external drivers has been so weak as to be incapable of causing the planet to become inhospitable.

Climate feedbacks have mitigated the potential for external drivers to cause climate destabilisation.

Alternatively some kind of hybrid of both hypotheses is correct, for instance perhaps external drivers have not been strong enough to overwhelm climate feedbacks and cause climate instability. This hypothesis is more nuanced that it first appears, as the strength of feedbacks may have changed through time, as may have the forcing required to drive climate inhospitability (i.e. there may be steady state climates which allow the planet to exist on the edge of the habitable zone, meaning even small perturbations may be sufficient to tip the climate over the edge). Looking to plate tectonics specifically, there is reason to believe that there have been significant changes which have influenced the carbon cycle, both during the Cenozoic and in the more distant past (*Van Der Meer et al.*, 2014). Changes in ocean basin arrangement, changes in sea level driven by change in plate buoyancy and changes in continental configuration have all been driven by plate tectonics during the Cenozoic (*Haq et al.*, 1988; *Scotese et al.*, 1988). In conclusion, global scale changes in tectonics appear to have been dramatic enough to have potential impacts on the carbon cycle, and merit further quantitative investigation.

The sedimentary carbon reservoir, though extremely large, is often omitted from consideration of the carbon cycle due to its extremely long response time. Sedimentary rock may be crudely segregated into several primary subdivisions, terrestrial (subaerially exposed on the Earth's surface), submarine (at the seafloor), subterranean (buried within the Earth) and mantle (typically on a downgoing slab). The reservoir of sediment that is presently terrestrial is thought to be the largest of these components, however the submarine reservoir is also large in comparison to other surficial reservoirs. The carbon content of both the mantle and subterranean reservoirs are particularly poorly constrained, so may also be important carbon cycle reservoirs - possibly larger even than the terrestrial reservoir. Submarine sediment is often subdivided into shallow, shelf sediment and deep sea sediment, but can also be subdivided by its behaviour, moving topographically upwards (towards terrestrial exposure), moving topographically downwards (towards a subduction zone), or topographically static (such as in a passive basin), as outlined in Section 2.2.2. Sediment is moved topographically downwards through the action of seafloor spreading. Hot, buoyant crust is formed at a Mid-Ocean Ridge (MOR), then sinks and moves laterally as it cools. This has the effect of moving sediment from the location of its deposition towards a deeper water site. This process is especially typical for carbonate sediments, due to their propensity to be preserved at topographic highs as a result of the corrosivity of the deepest ocean water to carbonate. Sediment is moved topographically upwards through the actions of plate tectonics or mantle dynamics driving uplift. This may be regional uplift, for example as driven by an approaching mantle plume, or may be more localised to specific pieces of tectonic plate which are being obducted by collisional tectonics. The controls on which regions are moving in which direction are complex three dimensional processes, related to the driving forces of slab pull, ridge push and mantle convection and plate buoyancy. In addition to the direct control of plate tectonics, additional processes such as changes in mantle buoyancy and formation of accretionary prisms may change the topographic motion of sediment. Nonetheless, it is reasonable to make the assumption that, to first order, sediment will follow one pathway if moving topographically downward and another if moving topographically upward.

Sediment that moves topographically downwards is destined to be subducted. Subduction occurs when two plates collide and the plate of greater density moves underneath the overriding plate. The oceanic plate is of greater density than the surrounding mantle (*Davies*, 1992), so once angled downwards it continues to sink (*Zhao*, 2004). The subducting slab is subject to increasing pressure and temperature as it descends and sediments are particu-

larly exposed to these changing conditions, as they sit at the upper edge of the slab, whereas the slab core remains thermally insulated. At depth, the carbon is liberated, either due to metamorphic decarbonation or partial melting then transported towards the surface, facilitated either through incorporation into melt or the action of fluids (*Dasgupta* and *Hirschmann*, 2010; *Kelemen* and *Manning*, 2015; *Mason et al.*, 2017). There are three possible carbon pathways after subduction:

- Remain with the slab deep into the mantle
- Release from the slab followed by migration and reprecipitation in the crust
- Release from the slab followed by migration to the surface before volcanic release as CO_2

For a system at steady state, the fluxes into and out of the Earth's interior must balance. If carbon were to be buried permanently in the mantle after going through a subduction zone, it might be expected that the surficial reservoir of carbon would be quickly depleted of carbon. Therefore the continued presence, but not overabundance, of carbon in the atmosphere-ocean system indicates that there is some link between the sink of carbon from the surficial carbon cycle (subducting carbonate sediment) and the source of carbon to the atmosphere (the volcanic outgassing flux). Whether this link is predominantly through the wider mantle or arc volcanism is not yet clear (*Mason et al.*, 2017).

The fraction of carbon removed from the subducting slab and recycled to the Earth surface (here referred to as the tectonic recycling efficiency) is highly uncertain. Similarly, the mantle recycling efficiency for carbon (the fraction of carbon which returns to the surface after entering the mantle) is poorly constrained. It might be assumed that the combined efficiency of both processes is close to 100%, i.e. that the mantle is at steady state with respect to its carbon content, however this is far from certain. Based on mass balance estimates, *Kelemen* and *Manning* (2015) estimated that the mantle carbon reservoir is approximately at steady state, meaning that carbon release (both at Mid Ocean Ridge (MOR) environments and in arc settings) is approximately equal to to carbon transfer into the mantle. *Mason et al.* (2017) used carbon isotope analysis to gauge the fraction of volcanic outgassing that is being generated from subducting sediment, and determined that approximately 50% of slab carbon is being recycled to the surface. *Mason et al.* (2017) suggested that the source for some of the volcanic carbon is assimilation of country rock in the vicinity of rising magma, however the

exact nature of this relationship is unclear. What is clear, however, is that the flux of carbon into the Earth's interior appears to be related to future release of carbon, either volcanically or at MORs. This relationship is poorly quantified even in the present day, and may have changed through Earth history as the mantle has gradually cooled (*Davies*, 1992). A strong link between carbon subduction and deep carbon release would be expected to promote climate stability, by maintaining a consistent total mass of carbon in non mantle reservoirs. Whereas if there are important external carbon sources or mantle carbon storage is able to vary through time then this could decrease climate stability.

Of key importance in understanding the impact of this feedback is determining the timescale over which subducted carbon is recycled. The time taken from plate subduction to potential surficial carbon release can be split into two components: the time taken for carbon to travel with the slab to a depth at which carbon is liberated, and the time taken for that liberated carbon to migrate to the surface. Assuming that the carbon is wholly recycled through arc volcanism, and none penetrates further into the mantle, then the factors controlling the time taken for carbon migration are:

Time on slab

- Plate angle
- Plate velocity
- Plate deformation
  (which may alter the velocity as the plate enters the plate travels through the subduction zone)
- Local mantle heat flow regime
  (which determines the relevant temperature conditions)
- Fluid concentration and composition

Time for migration

- Fluid composition/viscosity
- Fluid pathways
- Ascent velocity
- Country rock/country rock fabric
  (which might impede or facilitate fluid flow)

Assuming that the majority of carbon is removed from the slab before reaching the deep mantle, the two timescales may be summed to calculate the total amount of time between subduction and volcanic outgassing, which is here termed the 'outgassing lag'. There is variability in subduction zones (both within individual subduction zones and between different subduction zones), so the outgassing lag is best thought of as a distribution rather

than a single number. The form of this distribution is uncertain, but as with other complex phenomena dependent on a large number of independent factors, it is likely to be approximately Gaussian in shape. For example, plate angle has a limited range of feasible values and is likely to be clustered around a mean value and unlikely to occur at the extremes, as this would require an extreme deviation from the typical conditions. The combination of a series of independent Gaussian distributions is itself a Gaussian distribution. Even if the form of some of the subprocesses which contribute to the outgassing lag are not Gaussian, though the subprocesses are not independent there is enough randomness that it is not unreasonable to apply the central limit theorem and conclude that the form of the outgassing lag distribution is likely to be roughly Gaussian. There is no a priori reason to establish a particular value for the mean or spread of the outgassing lag distribution, so it is necessary to look to datasets that give some indication of these values.

4.1.1 Available Data

There are two broad categories of data that inform this study. The first are the datasets that give an indication of the model parameters, either the initial conditions or constant values. These datasets are discussed further in Chapter 2 within the context of model development. The second type of dataset are those that vary with time, either as forcings used in the model or as reconstructions of model predicted variables, which are discussed further here except where the results are relevant to all model output (such as the palaeo CO_2 and CCD datasets), which are presented in Chapter 1.

^{10}Be is created by cosmic ray interaction with oxygen and nitrogen in the atmosphere (*Tera et al.*, 1986). ^{10}Be migrates from the atmosphere to the ocean, and is incorporated into sediments through various pathways (*Tera et al.*, 1986). The final incorporation of ^{10}Be into sediment occurs near to subduction zones, when they are exposed to ocean water for the last time (*Brown et al.*, 1982). ^{10}Be was thought to have a half life of $\sim$2.5Myr (*Merrill et al.*, 1960), however has recently been found to have a much shorter half life of 1.388 $\pm$0.018Myr (*Middleton et al.*, 1993; *Chmeleff et al.*, 2010). ^{10}Be has been detected in arc volcanic emissions (*Brown et al.*, 1982; *Tera et al.*, 1986), proving that the outgassing lag must be less than 4-5 times the half life, depending on the detection limit. The outgassing lag must therefore be comparatively short, with a maximum time of $\sim$7.5Myr. Further information can be gained by observation of uranium series disequilibria. Fluid that has interacted with the downgoing slab will have a lead isotope signature at disequilibrium, which persists for $\sim$350kyr (*Turner*

et al., 2000). It is therefore possible to deconvolve the time spent as sediment on the slab (at maximum ∼7Myr), and the time spent in the fluid phase ascending towards the surface (a maximum of ∼350kyr). A summary of these results was collated by *Turner et al.* (2000), who estimated that fluid release occurs anywhere between one and several hundred kilo-years before eruption, and that sediments contribute to magma sources 0.35-4Myr before eruption.

While these methods allow some constraint on the mean outgassing lag, there is still a large amount of uncertainty as to the present day value, and the temporal evolution of the lag through time is even less clear. Due to fact that the majority of the outgassing lag is time spent on the slab, it is logical to infer that, to first order, changes in the mean outgassing lag follow changes in average global plate tectonic speed. Figure 4.1 shows how plate speed is estimated to have varied during the Cenozoic (*Zahirovic et al.*, 2015). Based on current understanding, changing the amount of time spent on the slab, or the amount of time spent in the supraslab environment should transiently alter the volcanic outgassing flux, leading to changes in atmospheric CO_2 and climate. During the Cenozoic, the rise then fall of plate speed foreshadows a broad scale rise then fall of atmospheric CO_2 (see Figure 4.1), so it is tempting to infer that changes in tectonics are driving a CO_2 response with a lag, which, based on these data, appears to be about 10Myr. Looking on a longer timescale, however, fails to show convincing evidence for a consistent relationship between plate tectonic speed and atmospheric CO_2 (Figure 4.1). On such long timescales there are a large number of factors that affect atmospheric CO_2, so the fact that there is no obvious relationship does not eliminate any possibility of a link between tectonics and atmospheric CO_2, but does show that plate tectonic speed is unlikely to be the dominant driver, although the relationship could be masked by the uncertainties in both datasets. Nonetheless, there is a logical reason to believe that changes in tectonics may cause changes in volcanic outgassing (and therefore atmospheric CO_2), and the currently available data do not discount this link, especially within the Cenozoic where plate speed and atmospheric CO_2 show a similar evolution. In summary, the available data do not definitely shown a relationship between atmospheric CO_2 and tectonics, nor do they definitively rule out a connection.

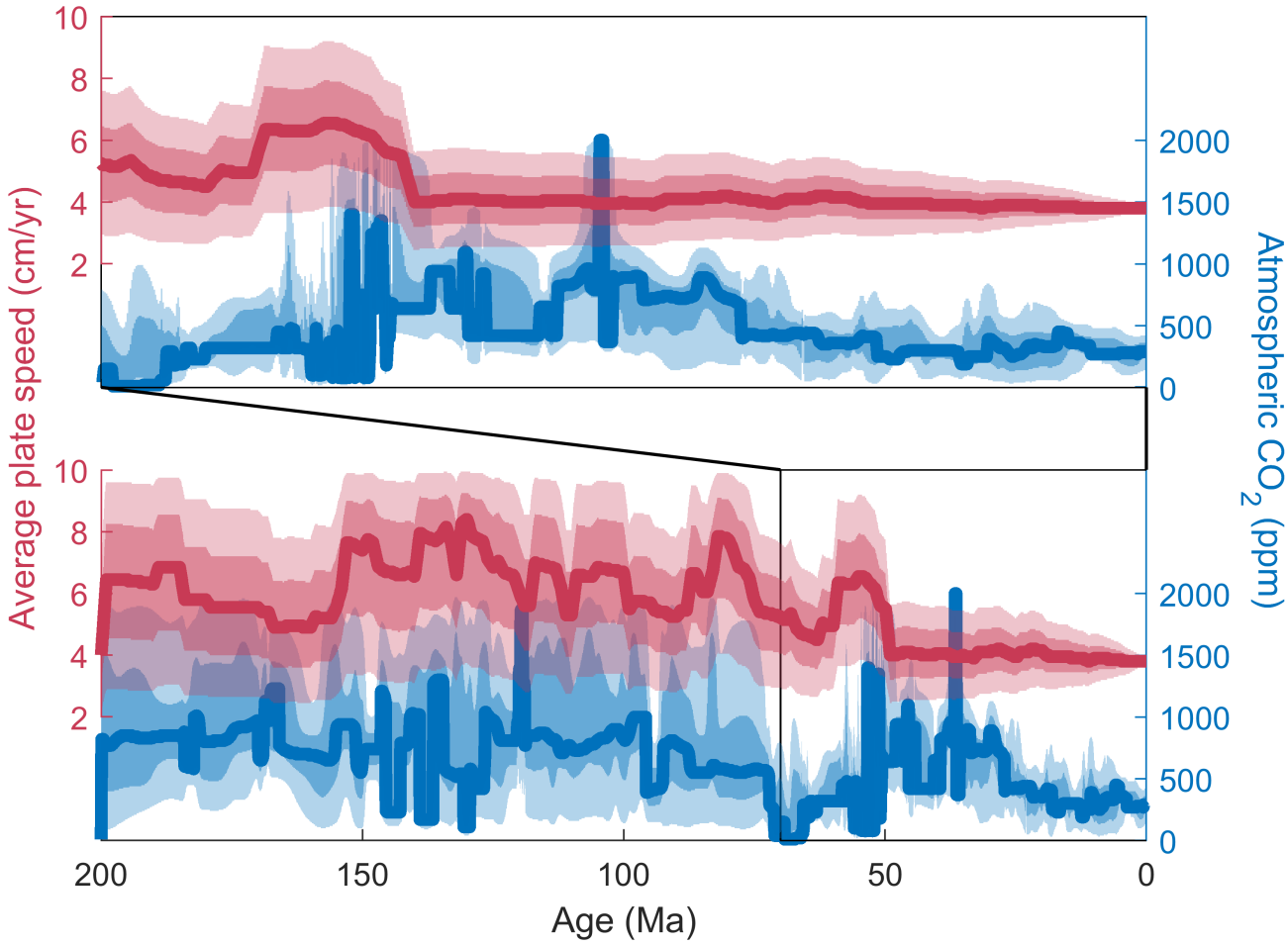

Figure 4.1: ***Average global tectonic plate speed from* Zahirovic et al. *(2015) is shown in red, with 1 and 2 sigma uncertainties in the strongly and weakly shaded bars respectively. The atmospheric CO_2 record from* Foster et al. *(2017) is plotted in blue, also with 1 and 2 sigma uncertainties shaded.***

4.2. Methods

As discussed in Section 2.3.1, the model is initialised to a steady state with atmospheric CO_2 concentration at 600ppm. From that established steady state, an ensemble of runs is performed where the mean outgassing lag is driven to change with a variety of magnitudes and over a variety of timescales, as described in Table 4.1 and shown in Figure 4.2. When the mean outgassing lag is small, oscillations in the carbon cycle would be expected to travel through the system more quickly, potentially causing the climate to respond more quickly. In contrast, when the mean outgassing lag is large, this would be expected to increase the memory of the system to past changes in carbon burial, causing greater temporal disconnect between the forcing and response.

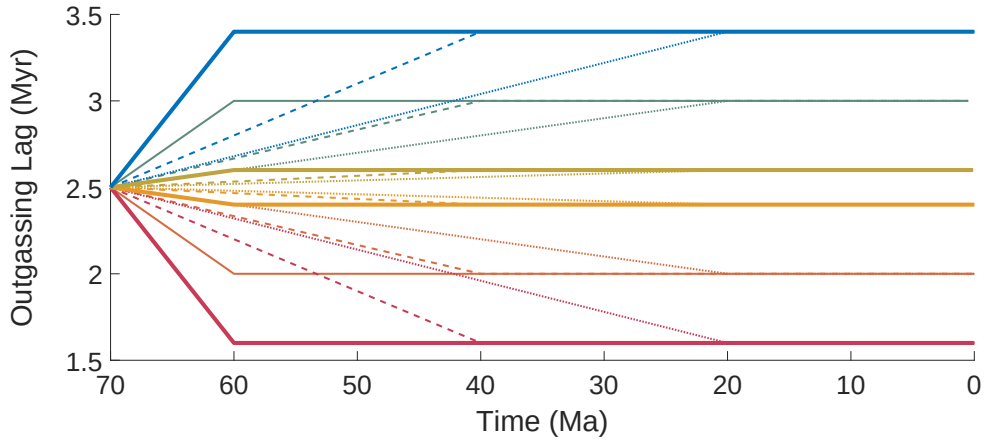

Figure 4.2: ***An ensemble of models are performed by initialising to the same model steady state then applying a variety of tectonic forcing factors, changing outgassing lag as shown. The timescale of outgassing lag change is shown by the line style: soild = 10Myr, dashed = 30Myr, dotted = 50Myr. Hot colours indicate that the mean outgassing lag has decreased from the initial condition, while cool colours indicate where the mean outgassing lag is forced to increase.***

In addition to the ensemble in which the mean outgassing lag is varied, an additional ensemble is performed within which the 'outgassing spread' (the standard deviation of the Gaussian distribution that represents the outgassing lag) is altered. When the spread in the outgassing lag is decreased, this would be expected to cause oscillations in volcanic CO_2 to last longer, maintaining their peaks and troughs through a greater number of tectonic cycles, due to the fact that the carbon is less spread out through time each time it passes through a subduction zone.

Four example tectonic scenarios are chosen (x's in Table 4.1, and bold in Figure 4.2), and the sensitivity of the results to feedback strength is analysed by performing ensembles wherein parameters which control the strength of the four identified climate feedbacks are altered (as discussed in Section 2.4). The results of these ensembles are shown in Section 4.3. The results of these sensitivity runs are not designed to represent the potential tectonic forcing that has occurred over the Cenozoic, but are instead intended to quantify the sensitivity of climate to tectonic forcing, and the dependence of this sensitivity on climate feedback strength.

Change Timescale (Myr) \ Final Outgassing Lag (Myr)	1.6	2.0	2.4	2.6	3.0	3.4
10	x	•	x	x	•	x
30	•	•	•	•	•	•
50	•	•	•	•	•	•

Table 4.1: ***The forcing factors that define the tectonic ensemble are shown, with bullets indicating standard ensemble members and crosses indicating key tectonic scenarios. Key tectonic scenarios are coloured as in Figure 4.3.***

4.3. Results

4.3.1 Precenozoic Ensemble

A decrease in the outgassing lag drives a persistent rise in atmospheric CO_2 (red in Figure 4.3) when parameters are at the default values for the Precenozoic steady state (as specified in Section 2.1 and Table 2.9). Conversely, increasing the outgassing lag results in a persistent fall in atmospheric CO_2 (blue in Figure 4.3). The greater the change in outgassing lag, the greater the corresponding change in atmospheric CO_2. The timescale of change in outgassing lag does not have a significant impact on the steady state atmospheric CO_2 value reached, but does change the time taken to shift towards the new steady state atmospheric CO_2. In all ensemble members with the Precenozoic feedback strength, the climate remains stable over the modelled interval and there is no evidence of behaviour which might eventually result in climate instability. The peak ΔCO_2 relative to the initial condition is $\sim$200ppm, and occurs where the outgassing lag is forced to decrease by 0.9Myr over 10Myr. An equivalent increase in the outgassing lag drives a smaller CO_2 fall of $\sim$100ppm, due to the nonlinear climate response, most notably in silicate and carbonate weathering. In contrast to atmospheric CO_2, the CCD, though transiently perturbed by up to 100m, does not exhibit a long term trend. The CCD is most variable in end member runs where the change in outgassing lag is largest (blue and red in Figure 4.3).

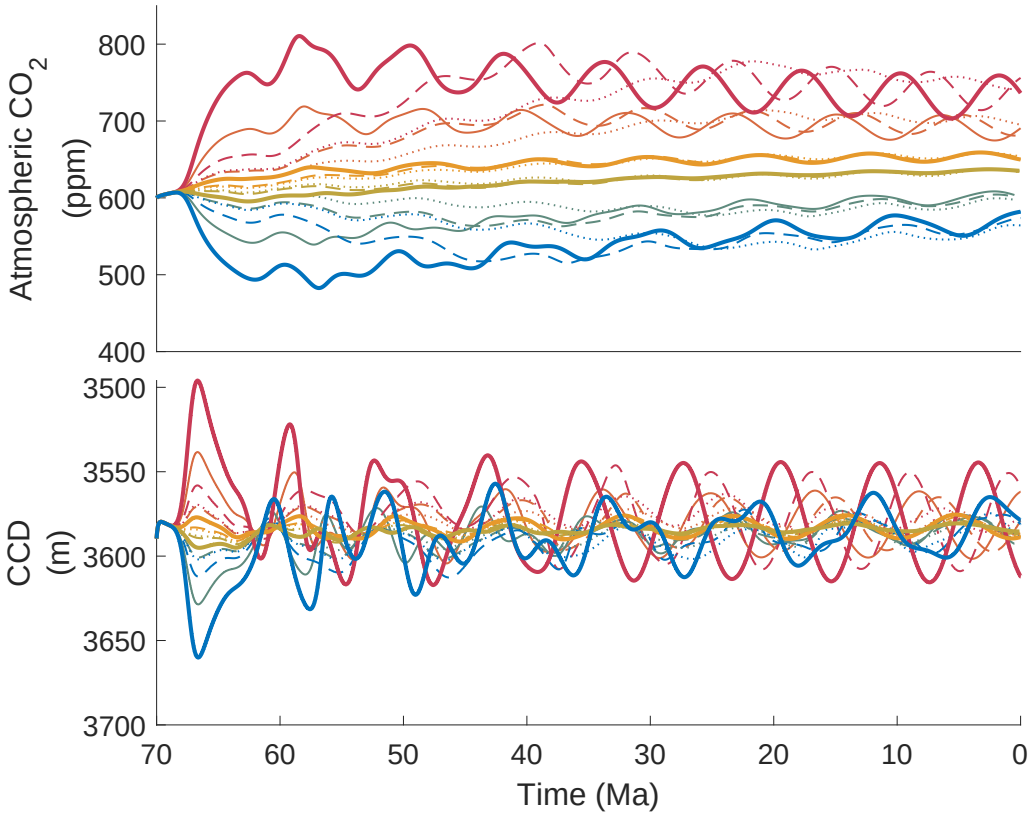

Figure 4.3: ***Results from the full ensemble of runs depicted in Figure 4.2 are shown for atmospheric CO_2 and the CCD. Decreases in the outgassing lag (hot colours) cause a rise in CO_2, while increases in the outgassing lag (cool colours) cause a fall in atmospheric CO_2. Different timescales are shown by line style as in Figure 4.2. Four scenarios are shown in bold (as prescribed in Table 4.1), these are the reference scenarios used to test the impact of changes in feedback strength below.***

These runs reveal the presence of oscillations in both atmospheric CO_2 and the CCD on timescales of approximately 10Myr. Their phase appears to be related to the outgassing lag, with decreases in the mean outgassing lag resulting in oscillations with a shorter, and seemingly more consolidated, wavelength. When the mean outgassing lag is forced to increase, oscillations are still observed but their pattern is less sinusoidal and appears to be a combination of frequencies. In fact, focussing on the first 20Myr of the run with the largest decrease in mean outgassing lag (red in Figure 4.3), the pattern of oscillations in the CCD does not appear to be sinusoidal, but from 50Ma onwards the pattern is well established. In contrast, the largest increase in mean outgassing lag (blue in Figure 4.3) results in oscillations which do not show clear sinusoidal behaviour within the 70Myr interval, though there does appear to be a simplification of the waveform towards the end of the run. This may be related to a resonance, or a characteristic timescale, in the system.

A sufficiently large perturbation to the outgassing lag could conceivably drive climate destabilisation, however the magnitude of perturbation required is so large as to be infeasible, at least within the Cenozoic. The model is prevented from exploring the effect of greater decreases in the mean outgassing lag as a result of the way in which the calculation is performed. Greater increases in the mean outgassing lag could be simulated, and would be expected to result in a longer term (though still transient) suppression of volcanic outgassing, which would drive a fall in atmospheric CO_2. Such a fall could be a sufficiently strong driver to cause dramatic climate change, depending on the efficacy of stabilising climate feedbacks.

In addition to the direct impact of changes to the outgassing lag on carbon cycle stability, there is potential for an indirect impact by changing the response of the system to a perturbation. To examine this potential, a series of runs have been performed in which the outgassing lag is varied using the same six tectonic temporal evolutions as shown in Figure 4.2, followed by a perturbation to volcanic outgassing as described in Section 4.2. In two of the six ensemble members, this causes the model to crash as a result of the pH solver returning a complex value (see Section 2.3.1 for discussion of this phenomenon). This does not indicate that the climate state became unstable at this time, but does show that the state of the carbonate system is far from the present day state and is changing rapidly.

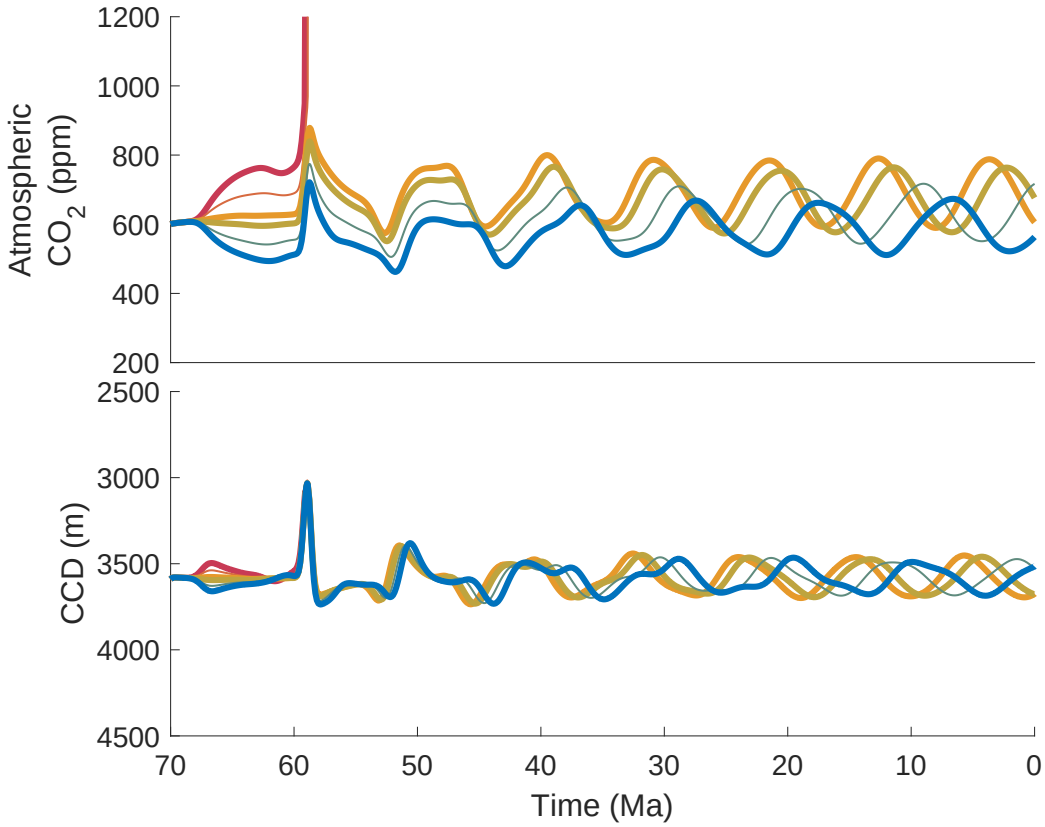

Figure 4.4: ***Outgassing lag follows the same temporal evolution as shown in Figure 4.2 for runs in which the change in outgassing lag occurs over 10Myr (from 70-60Ma). A perturbation to atmospheric CO_2 is driven by adding a Gaussian distribution to the outgassing time series, which adds 20000GtC centred at 11Myr into the run (59Ma), with a spread of 0.3Myr.***

All ensemble members that do not crash have approximately the same magnitude of CO_2 and CCD response. The CO_2 response propagates through the system, with oscillating atmospheric carbon content as a result of tectonic recycling of carbon. The echoes of the initial pulse can be clearly observed in all tectonic scenarios, with a period of approximately 10Myr. While the phase of the initial pulse is the same in all scenarios, there is progressive dephasing through the modelled interval due to the nature of changing the outgassing lag (which changes the timescale of tectonic carbon recycling). The oscillations do not appear to be growing in magnitude, and there is no evidence of behaviour that would cause climate destabilisation. Model runs that do crash do not do so because of runaway climate feedbacks, but instead crash due to the failure of the pH solver under certain conditions, as outlined in Section 2.3.1. In summary, changes to the outgassing lag do affect the long term behaviour of the carbon cycle but do not show evidence of changing the climate response to a perturbation from the perspective of stability.

4.3.2 Feedback Strength

To address the potential for changes in the outgassing lag to directly drive climate instability, the four key tectonic scenarios outlined in Table 4.1 are simulated with a variety of feedback strengths, as discussed in Section 4.2. The CO_2 and CCD model output are displayed in a consistent format below, coloured as in Figure 4.3. Each plot is composed of a series of subplots, representing the variety of feedback strengths. For each subplot, the feedback strength is shown in the inset panel, and the subplots are organised from weakest feedback at the top to strongest feedback at the bottom. The subplot with results displayed using thick lines shows the default Precenozoic feedback strength.

4.3.3 Carbonate Compensation Feedback

The carbonate compensation feedback acts to stabilise the saturation state of the deep ocean by changing the carbonate burial flux, which alters the ocean carbonate system (described more fully in Appendix B). In order to establish how contingent the results presented in Section 4.3.1 are on the chosen carbonate compensation feedback strength, the four key tectonic scenarios (specified in Table 4.1 and bold in Figure 4.2) are run with different bathymetric profiles. The hypsometric gradient is shallowed or steepened in the region of the CCD to control the feedback strength, as discussed in Section 2.4.1.

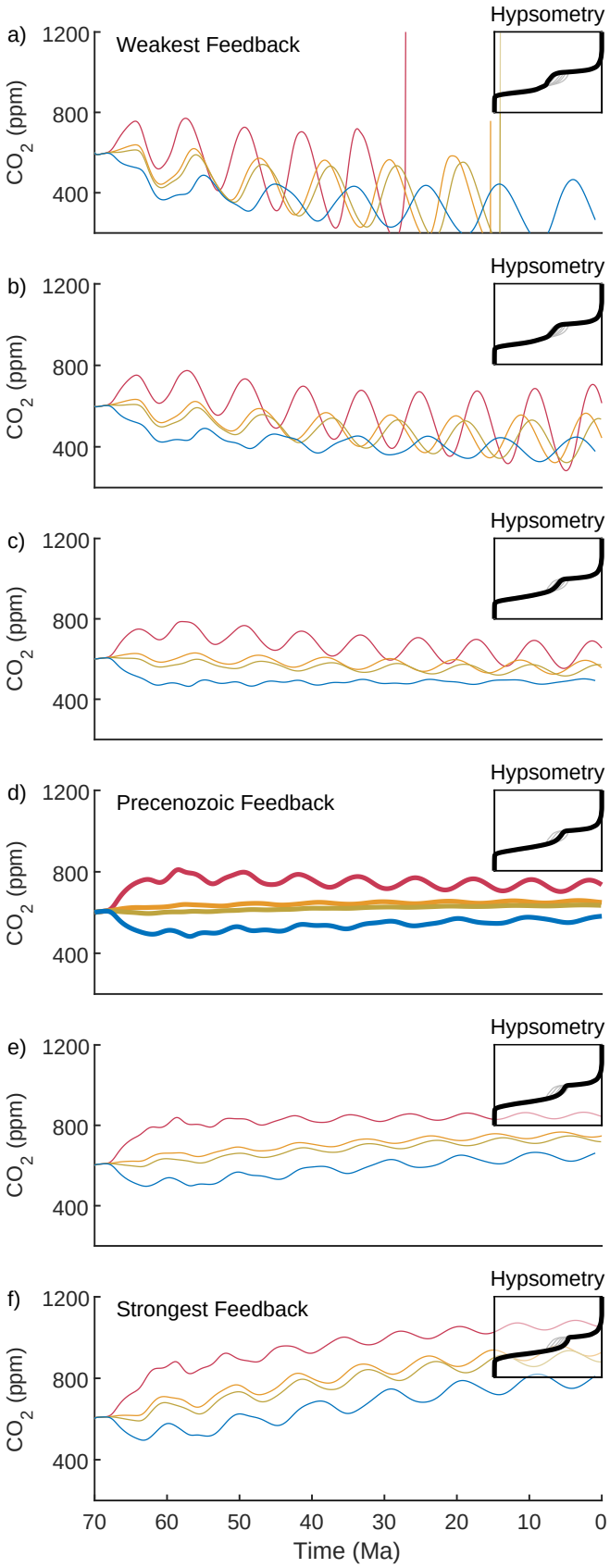

Figure 4.5: ***The CO_2 response to tectonic forcing using a variety of hypsometric profiles used to control the strength of the carbonate compensation feedback. Inset panels show the hypsometry with fractional cumulative area (from 100 to 0%) on the x axis and height (from -10000m to 10000m) on the y axis.***

Climate Response

At all carbonate compensation feedback strengths explored in this ensemble, atmospheric CO_2 concentration initially shows the same pattern between scenarios. Driving a decrease in outgassing lag (red and yellow in Figure 4.5) results in CO_2 rise, whereas driving an increase in outgassing lag (green and blue in Figure 4.5) causes CO_2 fall.

When the carbonate compensation is weak (Figure 4.5a-b), atmospheric CO_2 concentration and the CCD exhibit growing oscillations, which results in some scenarios in which the model crashes. When the carbonate compensation feedback is weakest (Figure 4.5a), the three strongest forcing scenarios cause the model to crash, and even the weakest forcing scenario (blue in Figure 4.5a) would be expected to crash given more run time, due to the observed growing oscillations in both atmospheric CO_2 and the CCD. In runs with a stronger carbonate compensation feedback (Figure 4.5c-d), the climate evolution appears stable. Oscillations in atmospheric CO_2 and the CCD are still observable, particularly in the atmospheric CO_2 concentration, but these are either damped or

stable. The CCD is especially invariant when the carbonate compensation feedback is strong (Figure 4.5 e-f), whereas atmospheric CO_2 displays a long term rise in these runs.

Overall, there is a progressive shift from long term CO_2 fall to long term CO_2 rise with increasing carbonate compensation feedback strength, regardless of driver strength. The reason for this is a slight change in the total submarine area as a result of the feedback alteration (as described in Section 2.4.1). The effect is comparatively minor, but drives long term model drift. This potentially contributes to the instability observed when carbonate compensation feedback is weakest (Figure 4.5a), but only accelerates the destabilisation that would result from growing CO_2 oscillations.

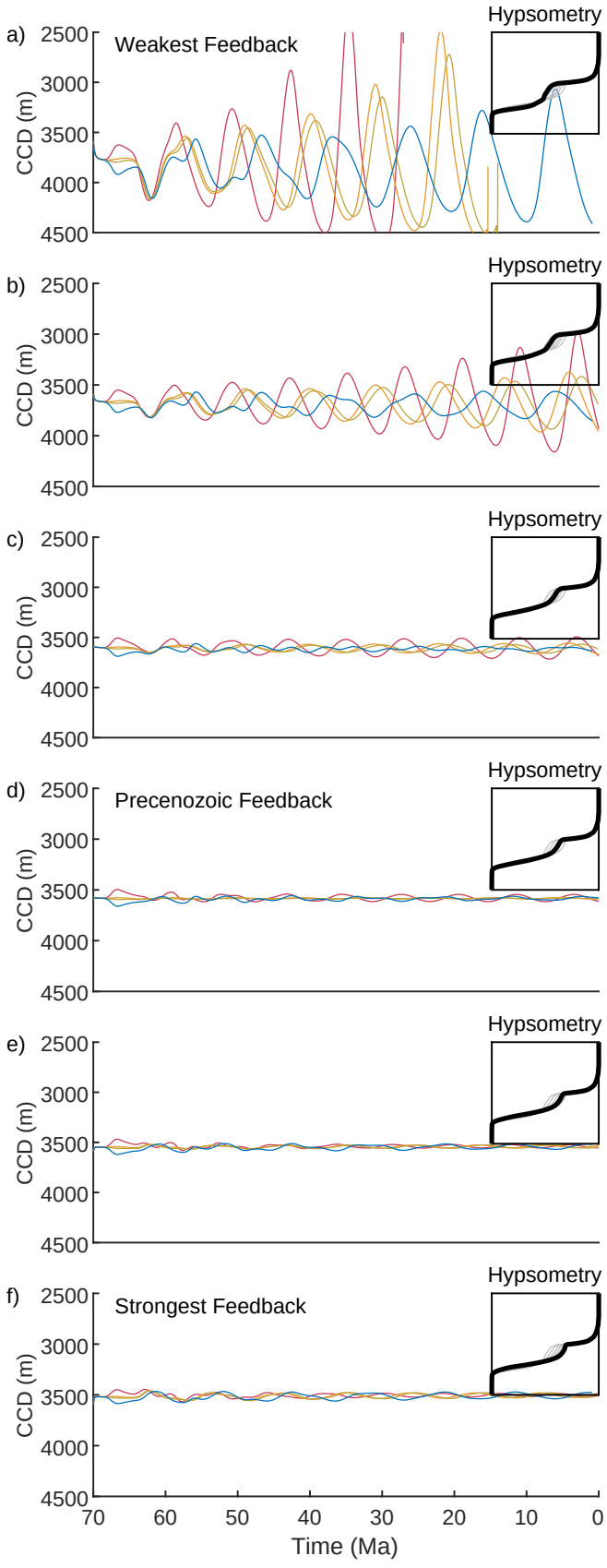

Figure 4.6: ***The CCD response to tectonic forcing using a variety of hypsometric profiles used to control the strength of the carbonate compensation feedback. Inset panels show the hypsometry with fractional cumulative area (from 100 to 0%) on the x axis and height (from -10000m to 10000m) on the y axis.***

Climate Response Summary
Steep hypsometric gradients mean that the CCD has to shift more dramatically to cause an equivalent change in carbon burial fraction. This results in unstable climatic oscillations when the hypsometric gradient in the vicinity of the CCD is meaningfully steeper than the present day. Conversely, shallow hypsometric gradients stabilise the CCD, and by extension the rest of the climate system.

4.3.4 Silicate Weathering Feedback

The silicate weathering feedback is a stabilising feedback that is caused by the relationship between climate factors and silicate weathering, as described in Chapter 1. In GECCO, the link between silicate weathering and climate is controlled by a temperature dependence (Section 2.1.10), therefore to adjust the strength of this feedback the silicate weathering-temperature relationship is either strengthened or weakened, as described in Section 2.4.2.

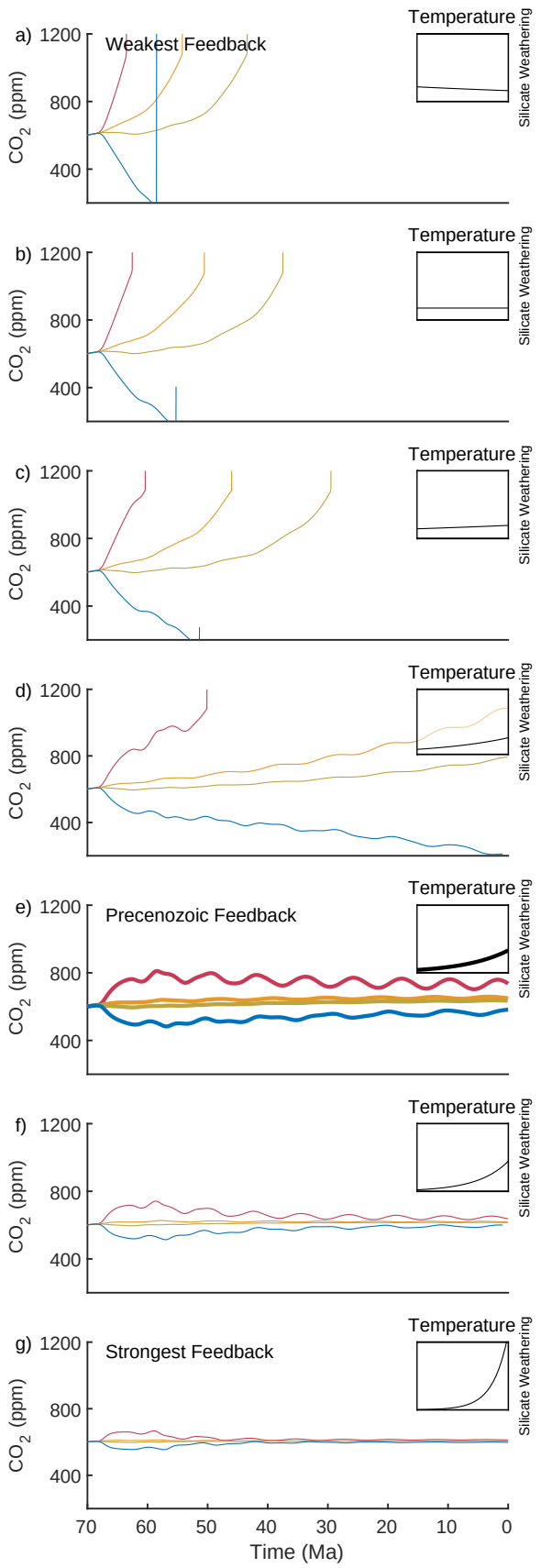

Figure 4.7: ***The CO_2 response to tectonic forcing using a variety of silicate weathering feedback strengths controlled by the silicate weathering-temperature relationship.***

Climate Response

The driver scenarios explored in this ensemble are equal but opposite, meaning that runs shown in red in Figure 4.7 experience the same forcing as those shown in blue in Figure 4.7, but in the opposite direction (as described in Section 4.2). Interestingly, the results do not appear to be symmetrical, as might be expected from such a forcing, because the forcing scenario shown in green in Figure 4.7 shows a positive trend at times when the feedback permits a long term atmospheric CO_2 trend (Figure 4.7a-d). The reason for this behaviour is long term drift in the model steady state used to initialise the runs. As discussed in Section 2.3.1, there is a +50ppm drift in the control run over 70Myr. This drift is able to overpower the relatively weak forcing scenario shown in green in Figure 4.7, resulting in a net long term positive CO_2 trend at this driver strength across all feedback strengths.

The CCD shows very little variation in every member of the silicate weathering feedback ensemble (Figure 4.8). Large spikes in the CCD are observed just prior to model crash (Figure 4.8), but these are not realistic and are a result of the failure of the pH solver used (see Section 2.3.1). When the silicate weathering feedback is weak (Figure 4.8a-c) the CCD shows the most change, but this is only on the order of 200m before

the model crashes. Runs in which the strength of the silicate weathering feedback is similar to the Precenozoic condition (Figure 4.8d-f) tend to show stable climate evolutions. The run with the strongest silicate weathering feedback (Figure 4.7g) shows a very constrained evolution of the CCD, though in the first 15Myr the change driven by the tectonic forcing appears to last longer than when the feedback is slightly weaker (Figure 4.7f).

All forcing scenarios with a weaker silicate weathering feedback than the initial condition result in climate destabilising behaviour (Figure 4.7a-d). The Precenozoic condition already has a weaker silicate weathering feedback than the present day due to the implemented decrease in silicate weatherability (Table 2.9). Stronger silicate weathering-temperature relationships than the Precenozoic condition result in less CO_2 variability, and a more consistent steady state atmospheric CO_2 concentration at the end of the run (Figure 4.7f-g).

Apparently coincidentally, the Precenozoic parameters (bold in Figure 4.7) result in a climate on the edge of stability. Strong tectonic forcing results in long term CO_2 oscillations, and a change in the CO_2 concentration at steady state. The oscillations do, however, appear to be slowly drawing atmospheric CO_2 back towards the initial condition, though when the silicate

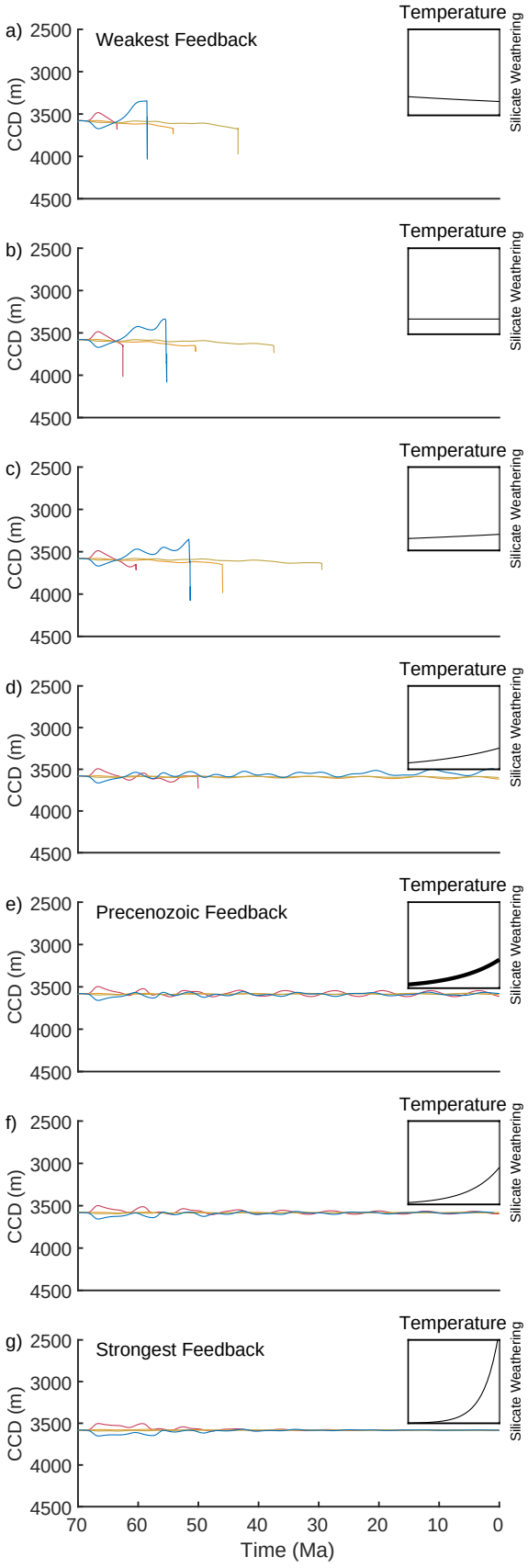

Figure 4.8: ***The CCD response to tectonic forcing using a variety of silicate weathering feedback strengths controlled by the silicate weathering-temperature relationship.***

weathering feedback is stronger, atmospheric CO_2 returns towards the initial condition much more quickly. When the silicate weathering feedback is at the Precenozoic strength (Figure 4.7e), there is a change in the long term CO_2 concentration, whereas in runs with a stronger silicate weathering feedback (Figure 4.7f-g) CO_2 is drawn back to the initial condition.

Climate Response Summary
A strong silicate weathering feedback promotes climate stability, in line with prior expectations. A modest reduction in the feedback strength from the estimated Precenozoic condition results in rapid climate destabilisation.

4.3.5 Carbonate Weathering Feedback

The carbonate weathering feedback controls the relationship between temperature and carbonate weathering flux. In many ways this is similar to the silicate weathering feedback, but crucially the sink of atmospheric CO_2 is different. For this reason carbonate weathering may be viewed as a destabilising feedback, as carbonate weathering can mobilise the large reservoir of terrestrial carbonate (Section 2.4.3).

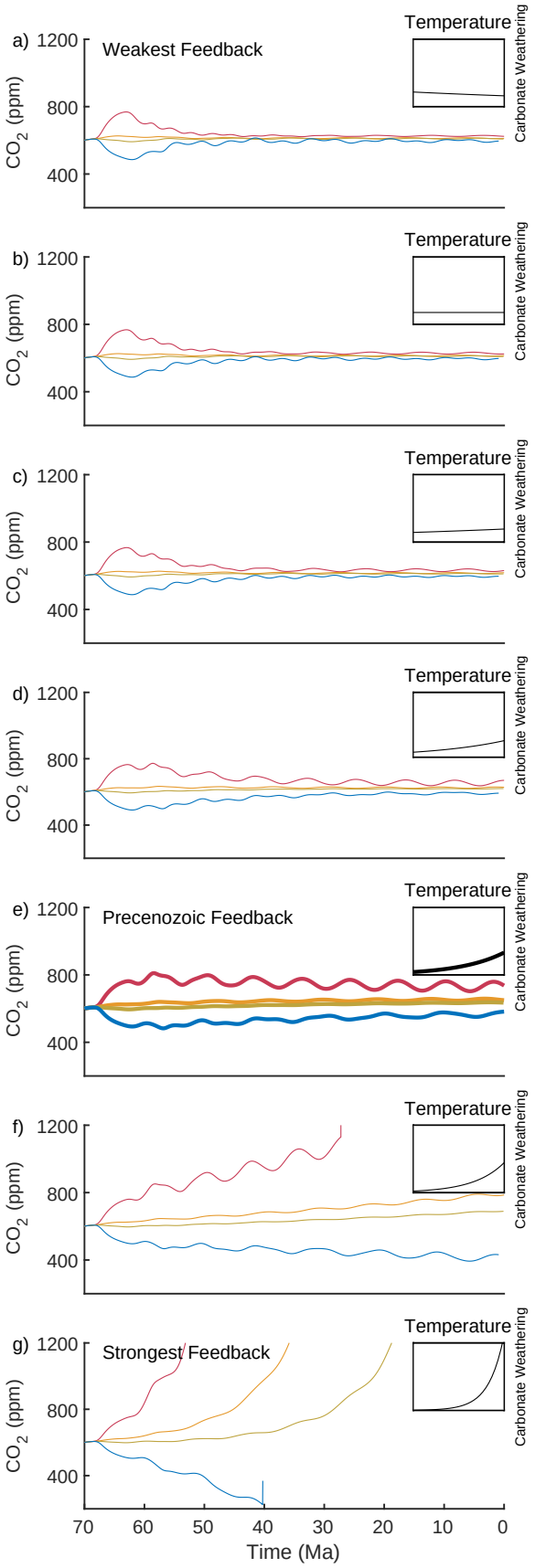

Figure 4.9: ***The CO_2 response to tectonic forcing using a variety of carbonate weathering feedback strengths controlled by the carbonate weathering-temperature relationship.***

Climate Response

In all members of this ensemble there is a transient difference in atmospheric CO_2 concentration between forcing scenarios in the first 10Myr (Figure 4.9). This transient difference appears to be of roughly the same magnitude regardless of feedback strength, approximately 200ppm in the positive direction and 150ppm in the negative direction. In some runs the atmospheric CO_2 evolution is divergent (Figure 4.9f-g), whereas in others it is highly convergent (Figure 4.9a-d).

The largest decrease in outgassing lag in this ensemble, at the Precenozoic carbonate weathering feedback strength (at which point the relationships between carbonate weathering and temperature, and silicate weathering and temperature are the same, as described in Section 2.1.10), causes atmospheric CO_2 concentration to rise transiently by $\sim$200ppm, before falling slowly and perhaps approaching a new long term steady state (red in Figure 4.9e). Similarly, the largest increase in outgassing lag explored here causes atmospheric CO_2 to fall by $\sim$150ppm before trending towards the initial condition and perhaps reaching a new steady state (blue in Figure 4.9e). In both of these runs there are clear oscillations in atmospheric CO_2 which have a magnitude of up to 100ppm and a period of $\sim$10Myr. In all tectonic scenarios at

the Precenozoic carbonate weathering feedback strength (Figure 4.10e), the CCD remains stable and does not vary much from the initial condition, with a maximum of ∼100m of change. Oscillations are also observed in the CCD, particularly when the decrease in outgassing lag is largest (red in Figure 4.10e), though these are of small magnitude (on the order of tens of metres), they have the same period as the oscillations in atmospheric CO_2.

When the carbonate weathering feedback is weaker than the Precenozoic condition (Figure 4.9a-d), atmospheric CO_2 concentration experiences only a transient perturbation before returning to the initial condition. Similarly, the evolution of the CCD in runs where the carbonate weathering feedback is weak (Figure 4.9a-d) is highly constrained, varying no more than ∼100m from the initial condition. In contrast, when the carbonate weathering feedback is stronger than the Precenozoic condition (Figure 4.9f-g) atmospheric CO_2 shows a progressive divergence from the initial condition, and when the carbonate weathering feedback is strongest (Figure 4.9g) all tectonic scenarios crash. The CCD varies by up to 500m in runs with the strongest carbonate weathering feedback (Figure 4.10g), whereas when the feedback is only moderately stronger than the Precenozoic condition (Figure 4.10f)

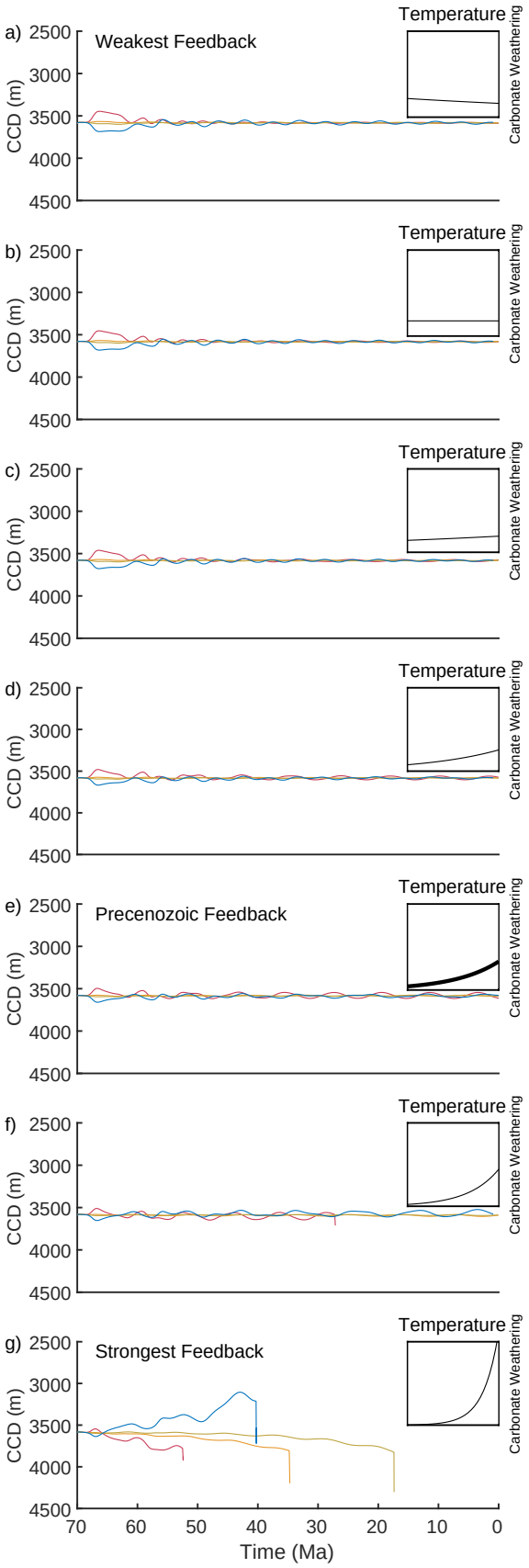

Figure 4.10: ***The CCD response to tectonic forcing using a variety of carbonate weathering feedback strengths controlled by the carbonate weathering-temperature relationship.***

then the CCD evolution is constrained, varying only slightly more than in runs with a weaker carbonate weathering feedback (Figure 4.10a-e).

Climate Response Summary
A strong relationship between carbonate weathering and temperature facilitates climate instability, whereas a weak relationship promotes climate stability. The turning point between stability and instability is the Precenozoic carbonate weathering feedback strength.

4.3.6 Phosphate Weathering Feedback

The phosphate weathering feedback controls the relationship between riverine phosphate flux and the weathering of other lithologies (carbonate and silicate), as described in Section 2.4.4. This affects both organic carbon burial, and inorganic carbon burial through changes to the CCD.

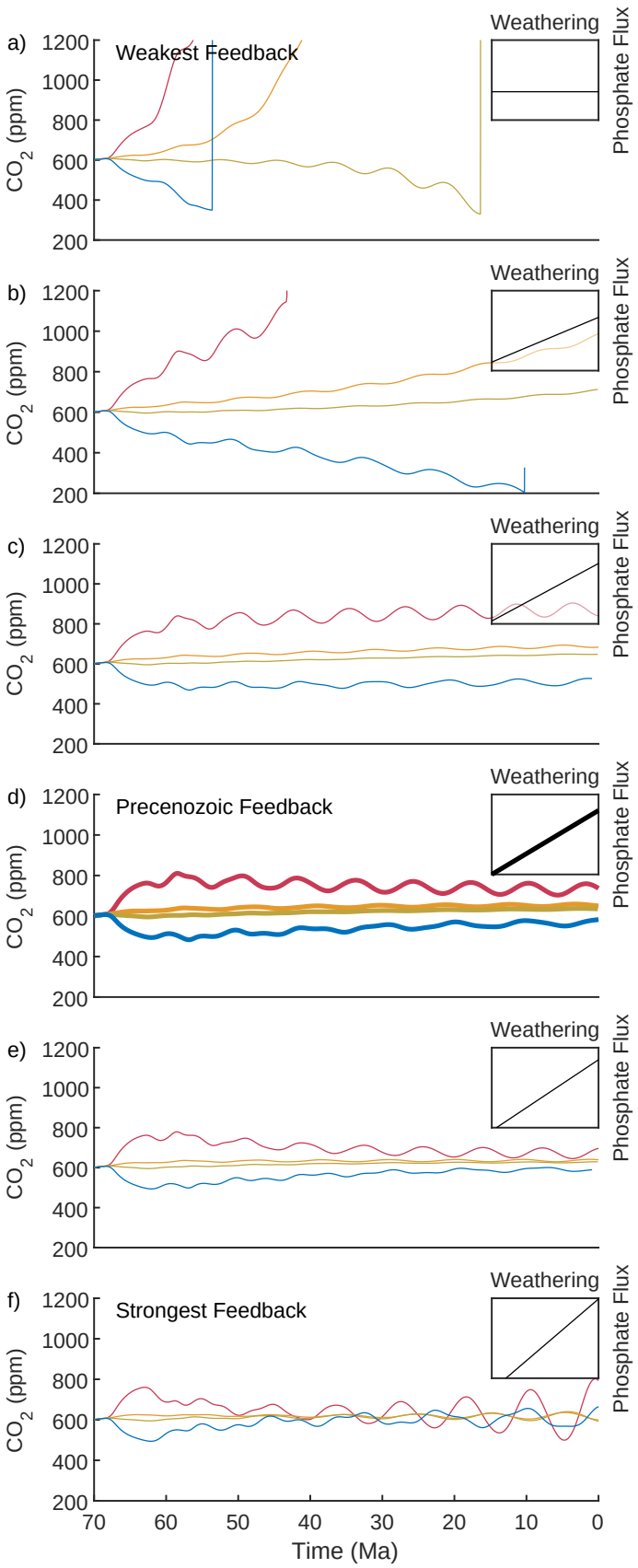

Figure 4.11: ***The CO_2 response to tectonic forcing using a variety of phosphate weathering feedback strengths controlled by the relationship between phosphate flux and weathering.***

Climate Response

The first 10Myr of each simulation in the phosphate weathering ensemble shows approximately the same evolution regardless of the phosphate weathering feedback strength (Figure 4.11). The largest decrease in outgassing lag (red in Figure 4.11) causes atmospheric CO_2 to rise by about 200ppm, and the largest increase in outgassing lag (blue in Figure 4.11) causes atmospheric CO_2 to fall by about 150ppm. The CCD evolution, however, is different depending on the phosphate weathering feedback strength (Figure 4.12). When the phosphate weathering feedback is non existent and the outgassing lag decreases (red in Figure 4.12a), the CCD shows a strong deepening trend from the outset, whereas when the phosphate weathering feedback is strongest and the outgassing lag decreases (red in Figure 4.12f) the CCD initially shoals. These trends are reversed for the opposite tectonic forcing (blue in Figure 4.12a and Figure 4.11f respectively).

In terms of stability, runs with a no phosphate weathering feedback (Figure 4.11a) or a weak phosphate weathering feedback (Figure 4.11b)

show unstable, divergent evolutions of CO_2. This is especially notable when the tectonic forcing is strong (red and blue in Figure 4.11a-b), but the strong forcing only accelerates the destabilisation as this is also seen in runs with weaker tectonic forcing (yellow and green in Figure 4.11a-b). When the phosphate weathering feedback is particularly strong (Figure 4.11f) the atmospheric CO_2 perturbation is initially drawn back towards the initial condition, however by the end of each run the atmospheric CO_2 concentration is beginning to oscillate. These oscillations appear to be growing through time, meaning the climate is unstable. The atmospheric CO_2 concentration is therefore unstable when the phosphate weathering feedback is particularly strong or weak.

The most stable atmospheric CO_2 evolutions occur when the phosphate weathering feedback is close in strength to the Precenozoic condition (Figure 4.11c-e). Interestingly, the steady state atmospheric CO_2 achieved at the end of the run appears to be strongly controlled by the strength of the phosphate weathering feedback. When the phosphate weathering feedback is slightly

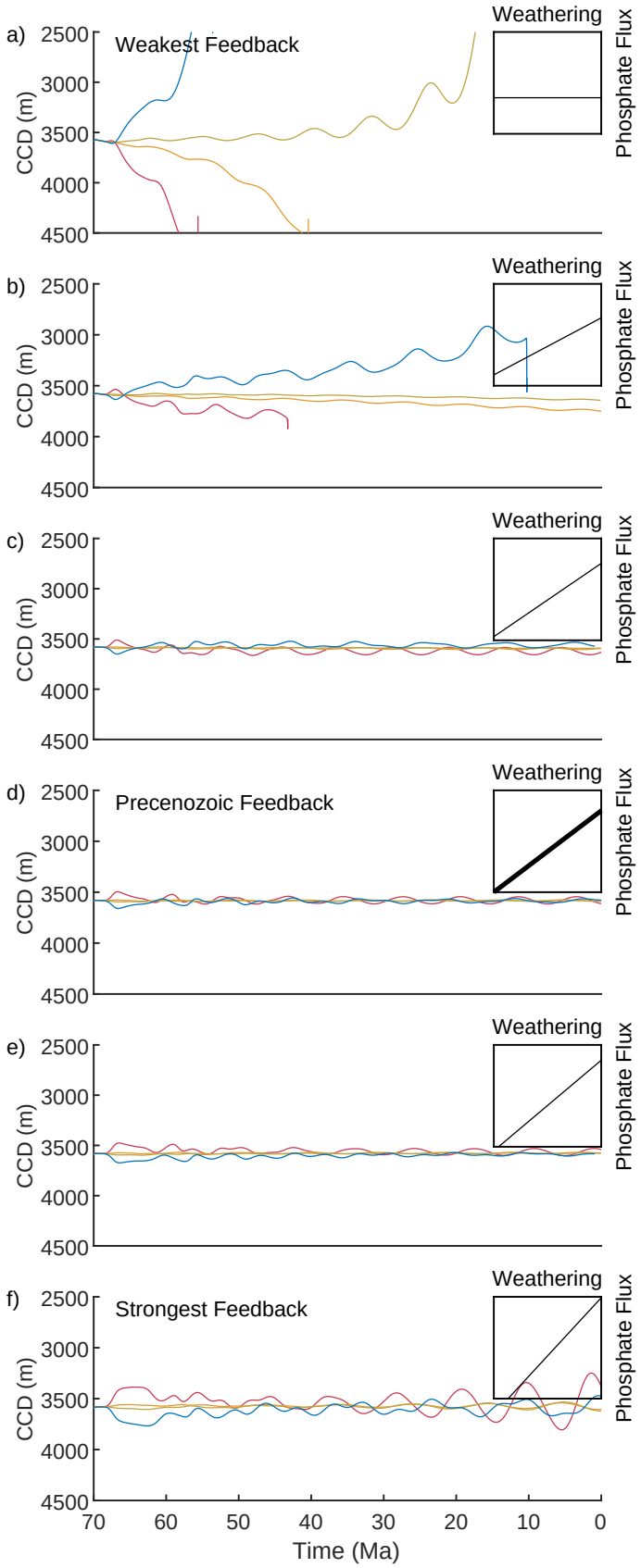

Figure 4.12: ***The CCD response to tectonic forcing using a variety of phosphate weathering feedback strengths controlled by the relationship between phosphate flux and weathering.***

weaker than the Precenozoic strength (Figure 4.11c) the steady state atmospheric CO_2 reached is further from the initial condition than when the phosphate weathering feedback is slightly stronger than the Precenozoic strength (Figure 4.11e).

Climate Response Summary
Both the weak and strong productivity feedback result in climate instability, indicating that a moderate feedback strength is the most ideal in terms of climate stability. This feedback also appears to have a strong influence on the steady state atmospheric CO_2 achieved at the end of the run.

4.4. Known Limitations

4.4.1 Uncertainty in Tectonic Recycling

As has previously been described in Section 1.2.4, the fraction of carbon which is recycled back to surficial reservoirs is not yet clear. There are indications that the mantle is approximately at steady state with regard to its carbon concentration (*Dasgupta* and *Hirschmann*, 2010; *Kelemen* and *Manning*, 2015; *Mason et al.*, 2017), but whether this is a long term steady state, or only applicable to the relatively recent geological past is as yet uncertain. Not only is the fraction of recycled carbon uncertain, but the pathway through which this recycling takes places is also unclear. Some the flux is likely to come through arc volcanism, though the amount of carbon in arc volcanic emissions that is from the deep mantle, and the amount that is from assimilation of country rock is not yet clear (*Mason et al.*, 2017). These uncertainties are important in determining the timescale over which carbon is recycled, which has implications for the potential for carbon cycle drivers and feedbacks to cause climate instability.

4.5. Discussion

4.5.1 Comparison to Existing Data

The ensemble of tectonic forcings and feedback strengths presented here is not designed to be representative of the Cenozoic. Nonetheless, it is informative to analyse the climate variability in model output relative to proxy datasets to learn which, if any, forcings and feedback strengths produce a climate evolution that agrees with available data. Over the course of the Cenozoic, atmospheric CO_2 rose by $\sim$500ppm to a peak at $\sim$52Ma, then fell by about 700ppm over the next 50Ma or so, as shown in Figure 1.15. Tectonic forcings which initially cause a decrease in atmospheric CO_2 can immediately be discounted, as can any runs which cause a runaway change in CO_2. None of the stable model runs presented here

exhibit a long term trend in the CCD, in contrast to the deepening shown by most records (Figure 1.16). This means that at least one degree of freedom in the carbonate system does not conform to the Cenozoic trend. Runs which best match with the other constraint (atmospheric CO_2), are those in which the outgassing lag decreases by the largest amount examined in this ensemble, and those in which carbonate weathering is particularly weak, or silicate weathering is particularly strong, with the carbonate compensation and phosphate weathering feedbacks left at their default strength. This combination of feedbacks would be expected to minimise the variation in carbon delivery to the ocean, so if the CCD is to deepen in accordance with current understanding, an additional factor such as productivity or PIC:POC production ratio must have changed significantly over the Cenozoic. Even in the scenarios with characteristics resulting in the best agreement between model output and proxy datasets, the model CO_2 response is smaller and less variable than data suggest atmospheric CO_2 has been during the Cenozoic. This is unsurprising, and reinforces the hypothesis that there have likely been multiple important carbon cycle and climate drivers over the Cenozoic. Nonetheless, it is reasonable to suggest that changes in tectonics could have been a contributory factor to Cenozoic atmospheric CO_2 evolution.

4.6. Conclusions

There are three main conclusions from the work presented in this chapter:

1. **Tectonics, an external forcing, is able to drive important carbon cycle perturbations.**

   Using the established Precenozoic parameters, a decrease in outgassing lag of 0.9Myr causes a $\sim$150ppm rise in steady state atmospheric CO_2, whereas an increase in outgassing lag of 0.9Myr causes a fall of $\sim$80ppm in steady state atmospheric CO_2. In both scenarios the long term CCD remains at the initial condition of $\sim$3600m. The maximum imposed change in the mean outgassing lag is 36% of its initial value, much less than the maximum possible magnitude of change, so large changes in the mean outgassing lag therefore have the potential to drive important changes in atmospheric CO_2.

2. **The change in outgassing lag does not alter the sensitivity of the climate to a perturbation.**

   By making the changes to the mean outgassing lag, then forcing a carbon cycle perturbation by adding a large mass of CO_2 to the atmosphere, I show that the response of the system is unchanged between various tectonic scenarios. Though two of the six model runs in this ensemble crash, this is due to a problematic high CO_2, low DIC climate system which causes a failure of the pH solver used in the model, rather than any indication of climate instability.

3. **The magnitude of climate response to a tectonic forcing is dependent on the strength of stabilising and destabilising feedbacks.**

   A few key tectonic scenarios were tested across a wide range of feedback strengths. These experiments show that the climate is highly sensitive to all tested feedbacks, but is stable at feedback strengths close to those of the Precenozoic initial condition.

References

Brown, L., Klein, J., Middleton, R., Sacks, I. S., and Tera, F., 1982, ^{10}Be in island-arc volcanoes and implications for subduction, *Nature*, **299**, 718–720.

Chmeleff, J., Blanckenburg, F. V., Kossert, K., and Jakob, D., 2010, Nuclear Instruments and Methods in Physics Research B Determination of the ^{10}Be half-life by multicollector ICP-MS and liquid scintillation counting, *Nuclear Inst. and Methods in Physics Research, B*, **268**(2), 192–199.

Dasgupta, R., and Hirschmann, M. M., 2010, The deep carbon cycle and melting in Earth's interior, *Earth and Planetary Science Letters*, **298**(1-2), 1–13.

Davies, G. F., 1992, On the emergence of plate tectonics, *Geology*, **4**, 963–966.

Foster, G. L., Royer, D. L., and Lunt, D. J., 2017, Future climate forcing potentially without precedent in the last 420 million years, *Nature Communications*, **8**, 1–8.

Haq, B. U., Hardenbol, J., and Vail, P. R., 1988, Mesozoic and Cenozoic Chronostratigraphy and Cycles of Sea-Level Change, *Sea-Level Changes*, **1**, 71–108.

Huybers, P., and Langmuir, C., 2009, Feedback between deglaciation, volcanism, and atmospheric CO_2, *Earth and Planetary Science Letters*, **286**(3-4), 479–491.

Jellinek, A. M., Manga, M., and Saar, M. O., 2004, Did melting glaciers cause volcanic eruptions in eastern California? Probing the mechanics of dike formation, *Journal of Geophysical Research*, **109**, 1–10.

Jull, M., and Mckenzie, D., 1996, The effect of deglaciation on mantle melting, *Journal of Geophysical Research*, **101**, 21815–21828.

Kelemen, P. B., and Manning, C. E., 2015, Reevaluating carbon fluxes in subduction zones, what goes down, mostly comes up, *Proceedings of the National Academy of Sciences*, **112**(30), E3997–E4006.

Kelemen, P. B., Hirth, G., Shimizu, N., Spiegelman, M., and Dick, H. J. B., 1997, A review of melt migration processes in the adiabatically upwelling mantle, *Philosophical Transactions of the Royal Society of London. Series A: Mathematical, Physical and Engineering Sciences*, 283–318.

Mason, E., Edmonds, M., and Turchyn, A. V., 2017, Remobilization of crustal carbon may dominate volcanic arc emissions, *Geochemistry*, **294**(July), 290–294.

Merrill, J., Lyden, E., Honda, M., and Arnold, J., 1960, The sedimentary geochemistry of the beryllium isotopes, *Geochimica et Cosmochimica Acta*, **18**(1-2), 108–129.

Middleton, R., Brown, L., Dezfouly-Arjomandy, B., and Klein, J., 1993, On ^{10}Be standards

and the half-life of ^{10}Be, *Nuclear Inst. and Methods in Physics Research, B*, **82**(3), 399–403.

Scotese, C. R., Gahagan, L. M., and Larson, R. L., 1988, Plate tectonic reconstructions of the Cretaceous and Cenozoic ocean basins, *Tectonophysics*, **155**, 27–48.

Tera, F., Brown, L., Morris, J., Sacks, I. S., and Middleton, R. O. Y., 1986, Sediment incorporation in island-arc magmas : Inferences from ^{10}Be, *Geochimica et Cosmochimica Acta*, **5**, 535–550.

Turner, S. P., George, R. M., Evans, P. J., Hawkesworth, C. J., and Zellmer, G. F., 2000, Time-scales of magma formation, ascent and storage beneath subduction-zone volcanoes, *Philosophical Transactions of the Royal Society A: Mathematical, Physical and Engineering Sciences*, **358**(1770), 1443–1464.

Van Der Meer, D. G., Zeebe, R. E., Van hinsbergen, D. J. J., Sluijs, A., Spakman, W., and Torsvik, T. H., 2014, Plate tectonic controls on atmospheric CO_2 levels since the Triassic, *Proceedings of the National Academy of Sciences*, **111**(12), 4380–4385.

Zahirovic, S., Müller, R. D., Seton, M., and Flament, N., 2015, Tectonic speed limits from plate kinematic reconstructions, *Earth and Planetary Science Letters*, **418**, 40–52.

Zhao, D., 2004, Global tomographic images of mantle plumes and subducting slabs: Insight into deep Earth dynamics, *Physics of the Earth and Planetary Interiors*, **146**(1-2), 3–34.

Chapter 5 - Conclusions

What more could be asked,
Than to look into the past,
And determine our planet's evolution,
In hope of a climate revolution.

This chapter begins by synthesising the results presented throughout this thesis. The presentation of results in previous chapters has been a little atypical, as, while many projects follow comparatively linear trajectories where each set of results build upon the last, this project was structured slightly differently. The building of the GECCO model required a surprising amount of innovation because most previous models were not focussed on the same niche, and I therefore came up against problems which had not previously been encountered. In Chapter 3 and Chapter 4 GECCO was applied in such a way that results from each study were not only informative in their own right, but combine to give even more information. The investigation of the same driver at a variety of feedback strengths and the same feedback strengths with different climate drivers allows a much better understanding of the factors controlling climate on Cenozoic timescales. Following that synthesis, the findings are summarised into a few pivotal points from each chapter. These summary findings are then reviewed in the context of the key questions outlined in Section 1.8 and reiterated below, and their relevance to the field of palaeoclimate at large is discussed. Finally, I provide some recommendations for future work which would improve either the model itself or the outcomes of the model.

5.1. Synthesis of Thesis Results

Chapter 3 and Chapter 4 focussed on establishing the impact of a specific driver to cause long term carbon cycle trends, including establishing the sensitivity of those carbon cycle trends to climate feedback strength. These chapters had a driver-centric focus however, and the conclusions only sought to establish the potential effect of each carbon cycle driver. By viewing the results of both chapters in concert, the mechanism and potential efficacy of each feedback can be examined, and therefore understood in its ability to mitigate the impact of carbon cycle forcings in general.

Carbonate Compensation Feedback

In both Chapter 3 and Chapter 4, changes in the hypsometric gradient designed to control the strength of the carbonate compensation feedback (Section 2.4.1), showed that when the carbonate compensation feedback was strong, both the CCD and atmospheric CO_2 were invariant, whereas when the carbonate compensation feedback was weak, both the CCD and atmospheric CO_2 displayed growing oscillations inferred to cause climate instability. There is also an unintended side effect, which resulted in all runs with a weak carbonate compensation feedback exhibiting a long term decline in atmospheric CO_2 concentration, whereas runs with a strong carbonate compensation feedback display along term gradual rise in atmospheric CO_2 concentration. As described in Section 2.4.1 this is due to a change in the total seafloor area (though the area above the CCD was kept constant).

The mechanism of driving the growing oscillations is inferred to be an increase in the response time of the CCD, which drives an increase in the offset between steady state carbon burial at a given CO_2 level, and the occurring carbon burial flux. This is outlined in Figure 5.1.

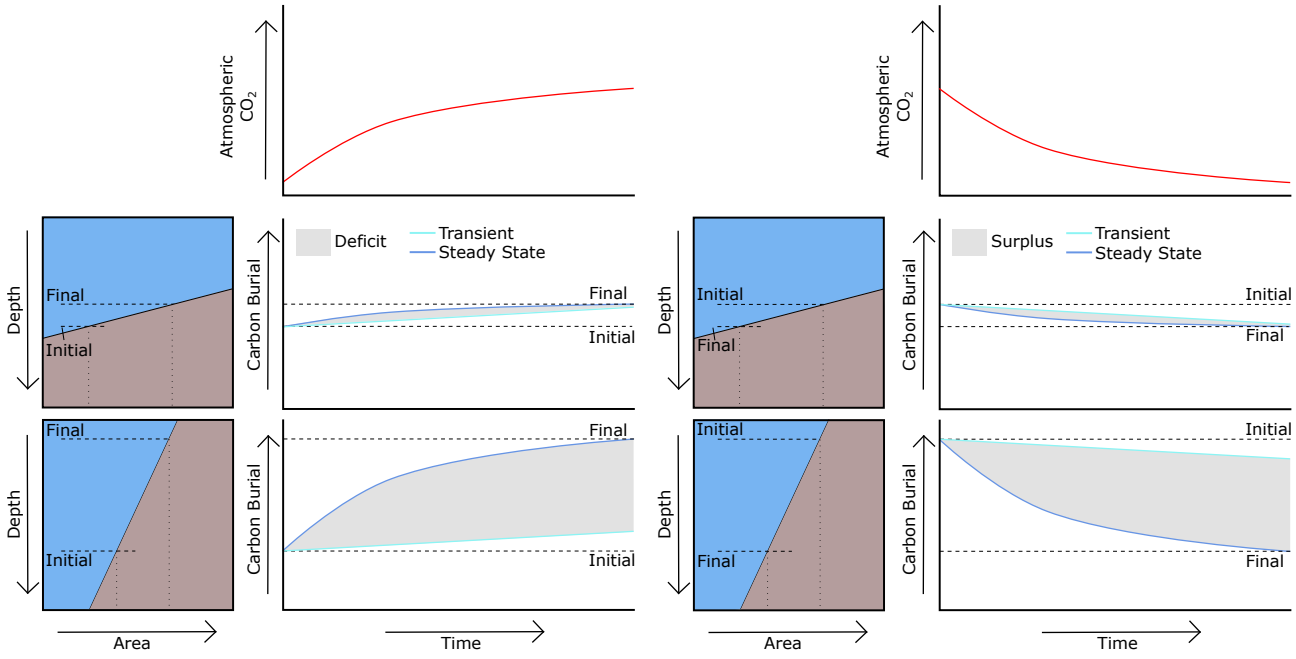

Figure 5.1: ***As atmospheric CO_2 rises (left side), carbon burial must increase in order to accommodate that greater influx of carbon to the ocean from increased weathering. When the hypsometric gradient is shallow in the vicinity of the CCD (upper panel), the carbonate burial flux can rapidly approach the steady state carbonate burial flux (i.e. the ocean approaches steady state quickly). In contrast, where the hypsometric gradient is shallow (lower panel), the carbonate burial flux rises slowly, leading to a deficit in carbonate burial relative to steady state. The same effect occurs in reverse when CO_2 falls (right side).***

When the hypsometric gradient in the region of the CCD is steep, and therefore a large

vertical movement of the CCD is required to adapt carbonate burial by the same amount, it is feasible that oscillations could be developed when the CCD is never able to reach the steady state value. In this case, there will be continual, periodic, surpluses and deficits in carbon burial, which propagate through subduction zones, resulting in a periodicity in volcanic outgassing. The oscillations in volcanic outgassing can be directly observed in model results, as shown in Figure 5.2.

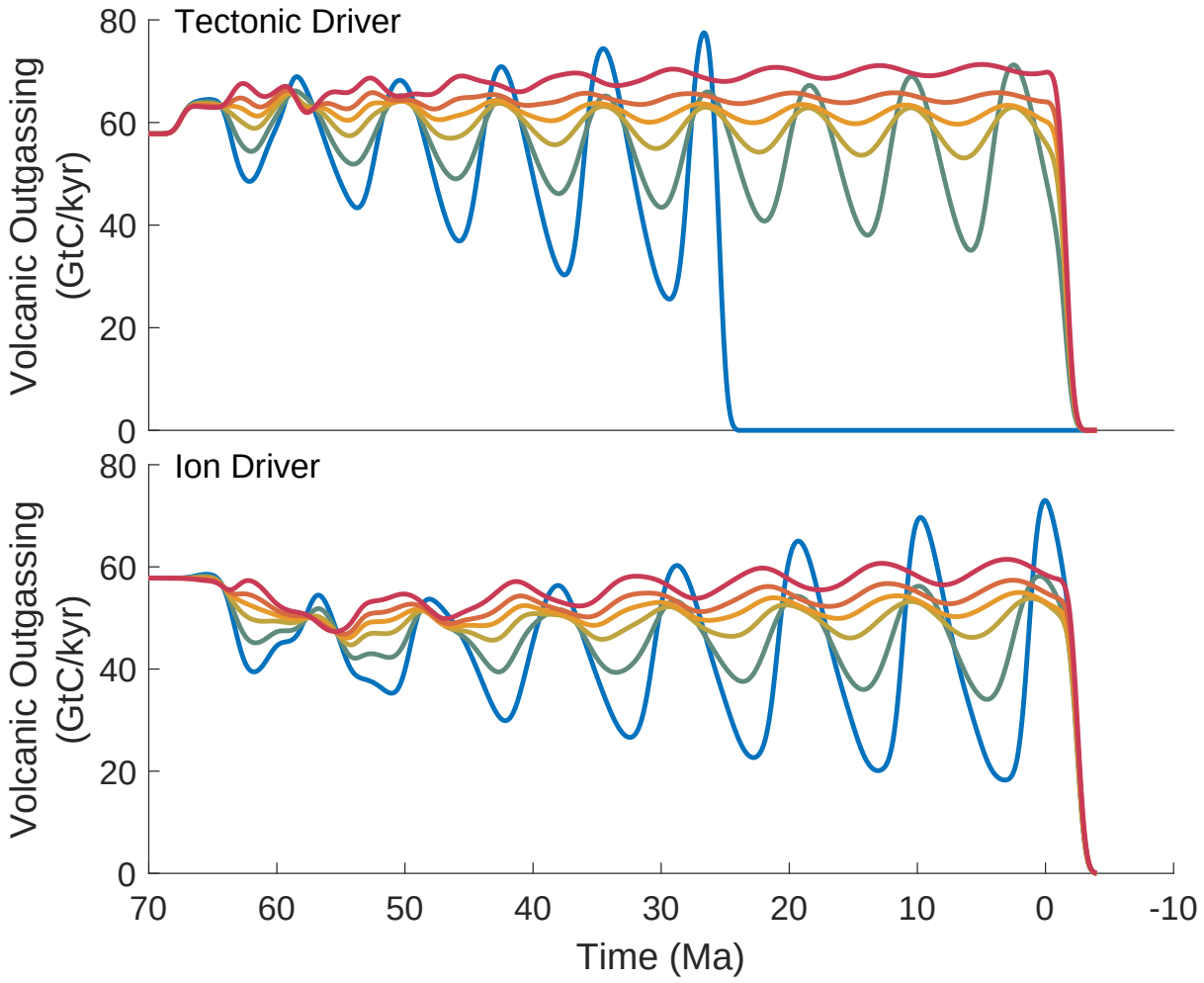

Figure 5.2: ***Two forcing scenarios are shown with variable carbonate compensation strength. When the hypsometric gradient in the vicinity of the CCD is shoaled (warmer colours), the temporal evolution of volcanic outgassing is mostly invariant. In contrast, progressive steepening of the hypsometric gradient (cooler colours) results in progressively larger oscillations in the volcanic outgassing flux.***

Given this impact of changes in hypsometric gradient on the carbon cycle, one might question whether there is a reason why the distribution of bathymetric depths should be such that the acclimatisation of the CCD does not take so long as to result in climate instability. In GECCO, though the sedimentary carbon mass is dynamic, the bathymetry is static. It

could be the case that changes in the depocentre of carbonate act to stabilise the hypsometric profile. This might actually be an expected outcome, as when estimating an idealised distribution of land area against topographic height, it would be reasonable to suggest this should be somewhat Gaussian (where most land is neither at the extremely high heights, or the extremely low depths). This idealised Gaussian would be perturbed by the presence of the ocean, which provides a discontinuity at which height significant deposition should occur, and the presence of the shelf seas, which can be built up by biological growth. These processes may act to maintain the depocentre of sediment such that the hypsometric profile is roughly stable through time, which provides a reason why the carbonate compensation is the strength that is currently observed.

Weathering Feedbacks

Chapter 3 and Chapter 4 both evaluated the sensitivity of the driven climate response to variation in the silicate and carbonate weathering feedbacks. Runs in which the silicate weathering feedback was stronger than the Precenozoic feedback showed stable and constrained climate evolutions, whereas runs in which the silicate weathering feedback was weaker than the Precenozoic feedback showed destabilising trends. Runs in which the silicate weathering feedback was roughly equivalent to the estimated Preceonzoic feedback strength displayed a middle ground, whereby the steady state atmospheric CO_2 concentration changed, but a steady state was nonetheless achieved. Similarly, but in the opposite sense, runs in which the carbonate weathering feedback was weaker than the Precenozoic strength showed stable trends, and runs in which the carbonate weathering feedback was stronger then the Precenozoic strength showed destabilising trends. Again, runs with approximately the same carbonate weathering feedback strength as the estimated Precenozoic strength allow the steady state atmospheric CO_2 concentration to vary without resulting in what appears to be runaway change.

While the weathering parameters appear to result in a climate on the edge of stability, it may be more reasonable to conclude that the relative strength of weathering feedbacks is crucial in determining stability, rather than the strength of either weathering feedback in isolation. Results could then be interpretted to show that when the silicate weathering feedback is stronger than the carbonate weathering feedback, then the climate evolution is stable, whereas when carbonate weathering feedback is stronger then the climate is unstable. This could go some way to explaining the reason why the Precenozoic parameters appear to be on the border line of stability, as the weathering coefficients for both silicate and carbonate

are set to the same values. Such a mechanism could also provide a clear path to climate stability, as it could be that for reasons of planetary composition and thermodynamics, the response of silicate weathering is likely to be stronger than the response of carbonate weathering.

In this case, the mechanism for climate destabilisation is the increased mobility of terrestrial carbonate. In GECCO, accommodation of additional carbon flux to the ocean occurs by shoaling and deepending of the CCD, in line with current understanding of the carbonate compensation feedback. If the response of carbonate weathering to changes in temperature is strong, then this is able to move a large mass of carbonate from the terrestrial environment into deep sea sediment. This deep sea sediment is lithified and eventually subducted, and some fraction of the slab carbon is recycled back to the atmosphere through volcanism. This mechanism allows carbonate weathering to contribute to the atmospheric CO_2 reservoir on long timescales. The variations in the mass of exposed carbonate are directly observed in model results, as shown in Figure 5.3.

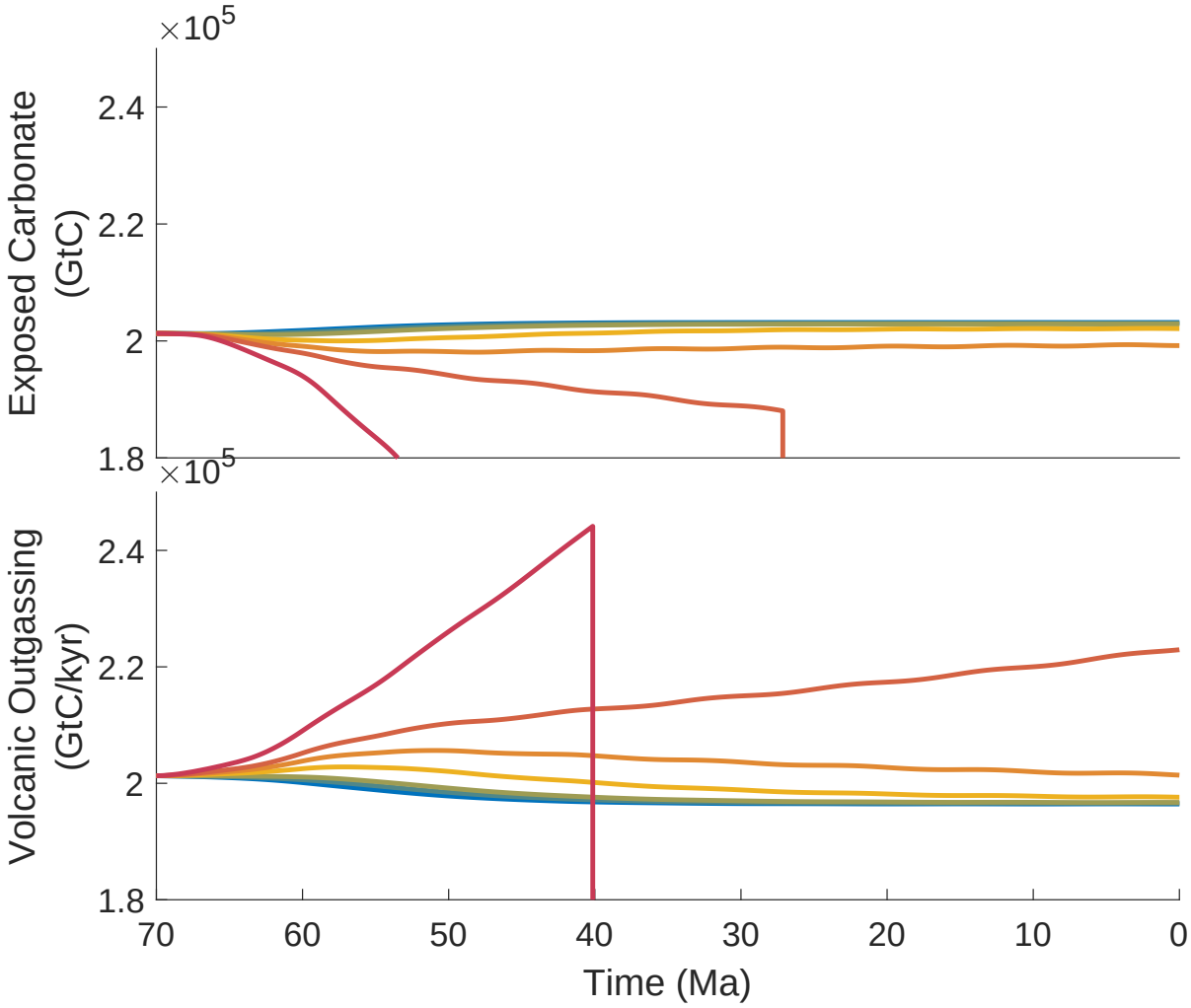

Figure 5.3: ***The two different styles of driver are plotted with variable carbonate weathering feedback strength. Though the drivers cause the system to trend in opposite directions, the feedback strength is clearly controlling the level of variability. When the carbonate weathering feedback is strong (warmer colours), then there is progressive mining of the terrestrial carbonate reservoir, resulting in a decrease in the mass of exposed carbonate through time. Progressive weakening of the carbonate weathering feedback (cooler colours) results in increasing stability in the mass of exposed carbonate through time.***

For the phosphate weathering feedback, climate destabilisation occurs when the feedback is too weak or too strong. Again, the standard Precenozoic values result in a stable system. This is somewhat inevitable, as the initialisation process converges towards a stable system, but the phosphate weathering strength has not been specifically tuned outside of assembling literature estimates of the modern day phosphate flux. As the phosphate flux is also tied to the weathering flux, it may also be that the relative strength of phosphate response compared to the silicate/carbonate weathering response is an important factor in determining long term climate stability, rather than simply the phosphate feedback strength. In the Precenozoic condition, both silicate and carbonate weathering have the same response to temperature. As phosphate weathering is, using the Precenozoic values, entirely dependent on a combination of the silicate and carbonate weathering flux, phosphate weathering also has the same response to temperature in the Precenozoic runs. There is therefore some level of equivalence, in that a doubling of rock weathering products results in a doubling of phosphate weathering products, fuelling a doubling in productivity and necessitating a doubling in ocean carbon burial. This may explain why in many of the model runs shown here the CCD is invariant. Altering the strength of the phosphate weathering feedback relative to the silicate and carbonate weathering strength can decouple this equivalence. For example, by reducing the response of phosphate weathering to rock weathering, any changes in carbon burial must be wholly accommodated by changes in the CCD, rather than combined coeval changes in the CCD and productivity. This may also help to explain why the feedback drives climate instability at both low and high strengths. At low phosphate weathering strengths, there is no change in organic carbon burial, and the dynamic range of the CCD is static. Crucially this prohibits changes in the shallow PIC burial flux, which results in changes in the source of terrestrial carbonate, and increases the variability in the terrestrial carbon reservoir (as shown in Figure 5.4).

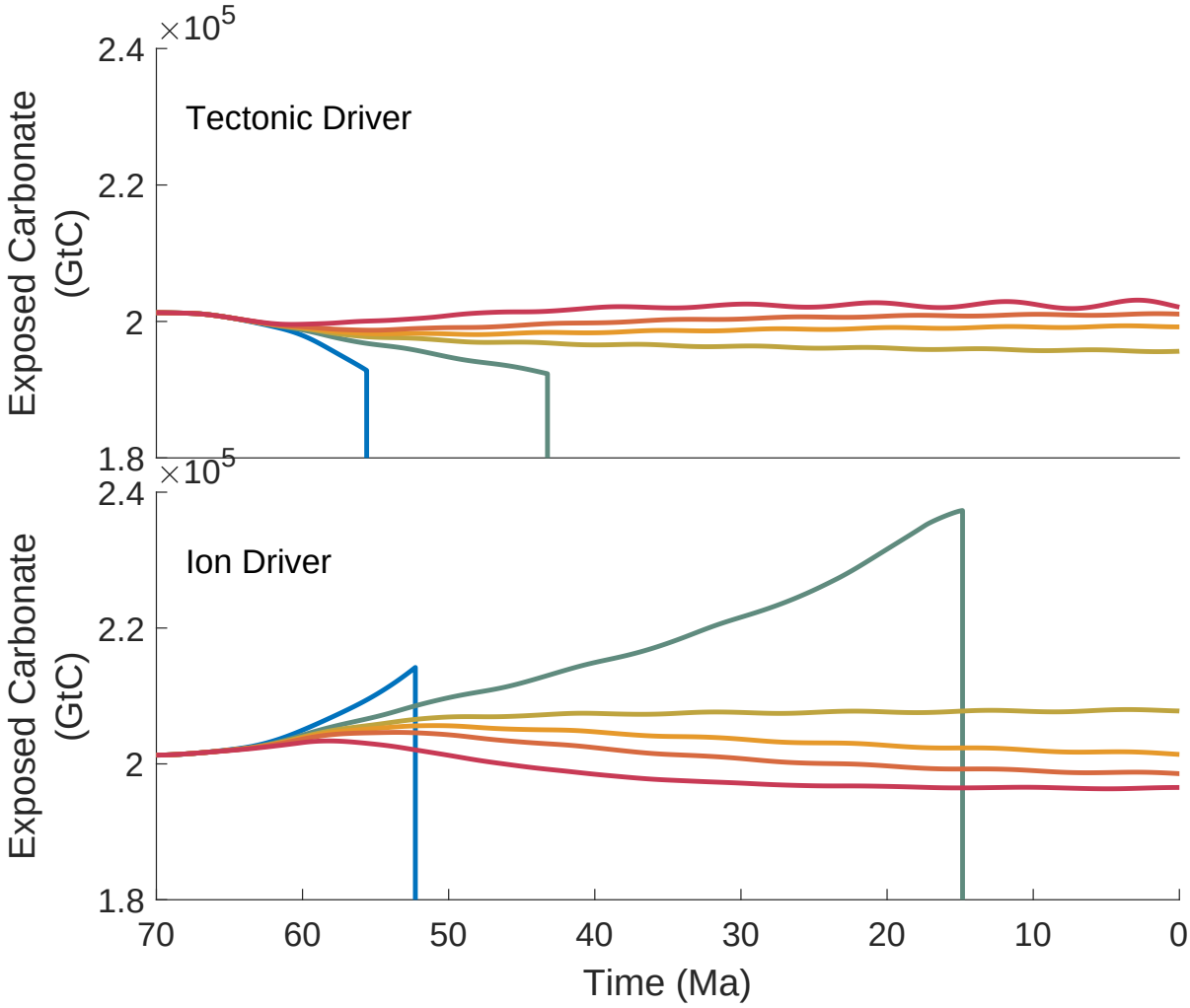

Figure 5.4: ***Two forcing scenarios with variable phosphate weathering strength are shown. When the phosphate feedback is weak (cooler colours), the mass of exposed carbonate varies rapidly through time, because the source of terrestrial carbonate does not fluctuate much and the weathering response to the driven change is large. When the phosphate weathering feedback is much stronger, the flux of PIC burial in shallow environments is much more variable, allowing the mass of exposed terrestrial carbonate mass to stay stable through time.***

In the contrasting case, where the phosphate weathering feedback is particularly strong, changes in phosphate weathering drive large changes in productivity (as shown in Figure 5.5), which in turn drive large changes in shallow ocean PIC burial, and large changes in the steady state CCD depth. This causes oscillations in both volcanic outgassing and the terrestrial carbonate inventory, which result in climate destabilisation.

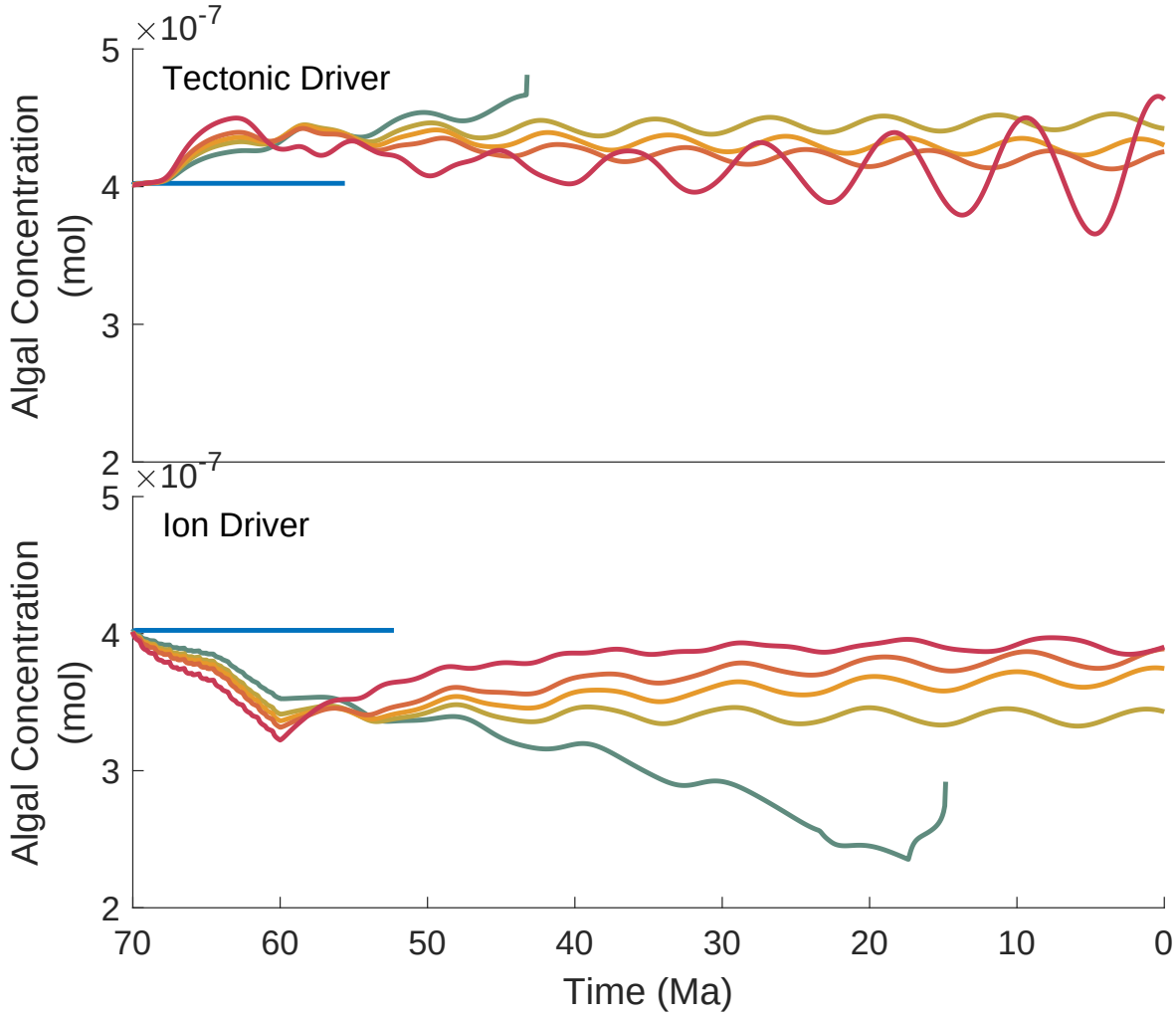

Figure 5.5: ***Two drivers with variable phosphate weathering feedback strength are shown. When the phosphate weathering feedback is weak or non existent (cooler colours), the algal concentration undergoes less long term variation. When the phosphate weathering feedback is particularly strong (warmer colours), growing oscillations in algal concentration are developed.***

5.1.1 Synthesis Summary

The model shows a high sensitivity to all of the feedbacks shown here. Many of these feedbacks are caused by an interplay of CCD dynamics and weathering of terrestrial carbonates - which has previously been overlooked as it is often assumed to be carbon neutral. Though this is appropriate on timescales up to millions of years, when approaching the timescale over which carbon is recycled back to the atmosphere through subduction zones, the carbon neutrality of carbonate weathering is no longer a valid assumption.

All ensemble runs presented here assume that all tectonic recycling of carbon occurs through arc volcanism, whereas if a non-negligible fraction of carbon enters the mantle then this might decrease the potential for developing destabilising oscillations in volcanic outgassing.

This does not affect many of the conclusions drawn here, as, while it changes the absolute magnitude of perturbation required to persist through tectonic recycling and the feedback strengths required to drive oscillatory behaviour, it does not change the nature of the mechanics of processes presented here. In essence, the direction of the trends described here is expected to remain the same, even if the absolute or relative magnitude of feedbacks required to maintain climate stability is different.

5.2. Summary of Thesis Findings

Chapter 1 contains a description of the existing knowledge relevant to the questions above, including compilations of datasets seeking to clarify and elucidate Cenozoic carbon cycle trends. The carbon cycle is widely studied, however the focus of previous studies is often on shorter timescales than those of interest here. There remain several components of carbon cycle behaviour that are not well understood, such as controls on shelf carbonate burial, CCD mechanics and the mantle carbon reservoir. Despite these poorly understood components, the primary fluxes of carbon on million year timescales are known. By applying a rigorous, mathematical approach to the long term carbon cycle, the areas requiring further research are highlighted, and the potential uncertainty resulting from those areas can be estimated. Proxy CO_2 data remain relatively sparse over the Cenozoic, and different approaches yield inconsistent results. Compilations, such as those by *Beerling* and *Royer* (2011) and *Foster et al.* (2017) suggest that the long term Cenozoic CO_2 trend is clear, however, especially in the early Cenozoic, this trend is liable to change in future as more data become available. Additional datasets and their relevance to the carbon cycle are discussed in Chapter 1.

Chapter 2 is an explanation of methods used to develop the GECCO model, an algorithm capable of testing carbon cycle hypotheses. Chapter 2 describes each component of the model in turn, specifying the equations used, the parameters required, the values chosen, and the uncertainty in those values where possible. By combining each of these components, a complex carbon cycle box model is developed, which is able to perform multimillion year simulations on a standard desktop PC. The features of this model which are specifically useful for work on Cenozoic timescales, or which represent an improvement over previous research, are highlighted.

Chapter 3 details how changes in ocean composition, specifically changes in calcium and magnesium ion concentration, affect the carbon cycle on million year timescales. Using the

best estimate of parameters for the early Cenozoic, it is shown that changes in calcium and magnesium could have driven ∼-250ppm of atmospheric CO_2 change. The magnitude of CO_2 change, however, is highly dependent on the strength of climate feedbacks.

Chapter 4 is an investigation into the potential impact of changes in the lag between subduction of sediment and outgassing of carbon (the 'outgassing lag'). The effect of changes in the spread value associated with that mean lag is also simulated. A change in the mean outgassing lag results in a change in subterranean carbon storage, which is repartitioned into other reservoirs, including the atmosphere. Increasing mean outgassing lag results in a fall in atmospheric CO_2, while decreasing mean outgassing lag causes an increase in atmospheric CO_2. The response to this forcing is highly dependent on the strength of climate feedbacks, all of which show the same patterns as shown for oceanic calcium and magnesium concentration change.

5.3. Review of Key Questions

1. **How resistant is the climate to 'chance' forcings?**

   This question was investigated using two case study examples of chance forcings which have known interactions with the carbon cycle.

   (a) Calcium and Magnesium Concentration as a Chance Climate Driver

   Using the *Hain et al.* (2015) method of calculating the impact of calcium and magnesium on the carbonate system, and a detailed statistical process to estimate the temporal evolution of calcium and magnesium concentration, the initial estimate of the impact of calcium and magnesium concentration on atmospheric CO_2 on atmospheric timescales was +250ppm. Further ensemble runs showed this to be highly dependent on feedback strength, indicating that the changes in oceanic calcium and magnesium concentration could have been an important Cenozoic CO_2 driver if feedbacks stabilising atmospheric CO_2 were not strong, or feedbacks destabilising CO_2 were strong.

   (b) Tectonic Behaviour as a Chance Climate Driver

   A change to the timescale over which carbon is returned to the atmosphere after recycling in subduction zones was found to drive CO_2 change commensurate with the magnitude of change driven in tectonics. The maximum driven change was on the order of 200ppm at the Precenozoic feedback strengths, but would likely

be greater if the outgassing lag had been driven to experience greater change. Nonetheless, this provides evidence that this driver could have caused important changes in atmospheric CO_2 on Cenozoic timescales. Further ensemble members in which the strength of feedbacks was varied showed that all feedbacks exert a strong influence on the long term atmospheric CO_2 evolution.

Combining these two studies allows greater insight into the relative role of the forcing and feedback response, because the two studies have completely different mechanisms of carbon cycle forcing but the same variety in feedback strengths. As stated above, both studies find that all four of the key feedbacks here exhibit a strong control on the evolution of atmospheric CO_2. The directionality of these feedbacks does not depend on the forcing, meaning that the influence of these feedbacks is a robust finding in the results. Overall, climate stability is associated with runs where the carbonate compensation feedback and silicate weathering feedback are strong, the carbonate weathering feedback is weak, and the phosphate weathering feedback is neither strong nor weak.

2. **Can any potential carbon cycle drivers be deemed unimportant on Cenozoic timescales?**

Of the two drivers examined, both were found to drive meaningful changes in atmospheric CO_2 when feedbacks were at certain strengths. Typically, calcium and magnesium concentration would be expected to influence the CSH and CCD rather than atmospheric CO_2, but this is not found to be the case here. Instead, the reservoir in which the change in carbon content is observed is dependent on the relative strength of climate feedbacks. If the carbonate compensation feedback is particularly strong, then the CSH and CCD will be stabilised against the forced carbonate system change, and carbon must move into or out of another reservoir (for example, the atmosphere). If both the carbonate compensation feedback and silicate weathering feedback are strong, then carbon may be moved into sediments, the subterranean reservoir or terrestrial carbonate.

Similar conclusions can be drawn from Chapter 4, which sometimes displays a long term change in atmospheric CO_2 driven by the change in subterranean reservoir size, and at other times stabilises atmospheric CO_2 despite the change in subterranean

reservoir size. This appears to be related to the relative strength of climate feedbacks. If feedbacks which regulate atmospheric CO_2 are strong, then this will push any change in carbon into another reservoir. Stabilising feedbacks could therefore be viewed as a type of competition, where each feedback is attempting to stabilise the component of the system over which it has dominion. When feedbacks are of roughly equal strength, then there will be some amount of change in all the appropriate reservoirs, whereas when one stabilising feedback dominates in strength, any changes in the carbon cycle will be forced out of the stabilised component. Destabilising feedbacks may be viewed as mitigating the ability of the stabilising feedbacks to maintain their reservoir state.

In summary, no carbon cycle drivers can be determined to be irrelevant to the long term carbon cycle, because the apportioning of carbon in the wake of a perturbation is dependent on the strength of climate feedbacks. This means that even relatively weak drivers may cause important changes in atmospheric CO_2 when climate feedbacks which regulate the atmosphere are particularly weak relative to feedbacks which stabilise other reservoirs.

3. **Could realistic external forcing lead to climates inimical to life?**

   As should be unsurprising, given the already established interpretations above, the answer to this question is entirely dependent on the strength of climate feedbacks. Both forcings examined here drive on the order of 200ppm of CO_2 change when feedbacks are kept at their Precenozoic strength, from the initial steady state of 600ppm. While large enough to be an important constituent of the Cenozoic trend, this amount of atmospheric CO_2 change is nowhere near sufficient to drive climate inhospitability. The change in CO_2 over the Cenozoic is much greater when stabilising feedbacks such as silicate weathering are weakened. So the question may be reframed as: Could stabilising climate feedbacks be sufficiently weak (or destabilising feedbacks sufficiently strong) at any point in Earth's history that a reasonable strength driver could have resulting in a runaway climate state? This is a much more difficult question to answer, as it is difficult even in the modern day to estimate the strength of long term climate feedbacks, and even more difficult in the past. If the climate were in a state with particularly high sensitivity to perturbations, then there may be a driver strong enough to temporarily drive the planet outside of the habitable zone. Alternatively, if the driver in question can in some way affect the climate feedbacks (for example by reducing the

areal extent of weatherable silicate, or maximising the mobility of the terrestrial carbonate reservoir), then it may be possible to drive permanent inhospitability by increasing the efficacy of stabilising or destabilising feedbacks, causing the system to undergo runaway change (such as is observed in the unstable oscillations shown in several model runs).

The results presented here give reason to believe that, rather than the absolute strength of climate feedbacks, it is their relative strength that determines climate stability. The behaviour of the model suggests that when the response of carbonate weathering is stronger than the response of silicate weathering, the climate will be unstable. Similarly, when the phosphate weathering feedback is particularly weak or strong, relative to the silicate and carbonate weathering feedbacks, then the climate is unstable. Interestingly, the minimum atmospheric CO_2 variability occurs when the silicate weathering feedback is at its strongest. When the feedbacks are of approximately equal strength then long term shifts in the steady state climate are observed. This potentially leads to a neat reason for planetary stability, which is that the silicate weathering feedback is relatively strong, for reasons of planetary composition or thermodynamics. If this hypothesis is true, it would suggest that planets with similar chemistry and dynamics would be likely to be climatically stable, simply due to the nature of the relative behaviour of silicates and carbonates.

5.4. Relevance to the Field

The understanding of planetary stability is integral to our understanding of the Universe. So far as we know, Earth is unique in that it supports complex life, and a prerequisite of that life is the long term habitability of the planet. Understanding how likely a given planet is to remain stable, and how common climatically habitable planets are throughout the Universe, is a key component of estimating how common life is throughout the Universe. Closer to home, the modelling of Earth's long term stability has important implications for our future. If the feedbacks stabilising Earth are particularly weak, then the release of large volumes of carbon into the atmosphere would be expected to drive a climate shift that would last indefinitely. It has already been shown that the actions of humanity will affect the climate for hundreds of thousands of years (*Tyrrell et al.*, 2007), this work shows that there is potential for the impact to last millions of years.

5.5. Future Work

The GECCO model has the potential be used in a myriad of further studies. Some of these would require, or be made easier by, improvements to the model, and intended future developments to GECCO are outlined in Section 2.5. Nonetheless, GECCO v1.0.0 provides a comprehensive new tool for exploration of long term carbon cycle and palaeoclimate connections. In future, GECCO could be applied to further explore many other potential carbon cycle drivers, such as: plate speed/other plate tectonic factors, silicate weatherability, changes in sedimentary carbon storage and changes in the average depth at which subduction occurs. As well as the exploration of novel climate drivers, there are additional feedbacks which could be investigated for their potential efficacy to stabilise the climate, such as change in ice volume.

In addition to the potential future development and applications of the GECCO model, there some potential refinements to the studies presented in Chapter 3 and Chapter 4. Starting with Chapter 3, one of the biggest uncertainties in that study was the calculation of how calcium and magnesium ion concentration varied across the Cenozoic. These uncertainties could be vastly reduced by collecting additional data, especially around the beginning of the Cenozoic. As is the nature of such things, the uncertainties in most parameters increase when going further back in time, which means that the uncertainty is greatest at the initial condition. The results of both Chapter 3 and Chapter 4 are contingent upon a single steady state with 600ppm atmospheric CO_2. An improvement to both studies would be to vary the initial state of the model, within the known uncertainties. Unfortunately the creation of steady state climates is a computationally intensive procedure, often requiring several days of computing to ensure the steady state is accurate enough to be used on Cenozoic timescales. Compounding this issue is that there is not only uncertainty in the state variables, but also in the other variables that govern model behaviour, such as the calcium and magnesium concentrations at 70Ma.

5.6. Final Word

Overall this thesis has attempted to integrate up to date knowledge of the long term behaviour of carbon into a new carbon cycle box model for use on multimillion year timescales. This has resolved some existing questions over the implications of particular carbon cycle behaviours, but has also opened up new questions, highlighting what is not yet known. Application of this new model to simulation of two potential Cenozoic climate drivers has

shown that the magnitude of long term climate change is highly dependent on the strength of climate feedbacks. The strength of the driver changes the magnitude of transient climate change, but feedbacks appear to control the long term steady state, or long term trend. Comparison of the consequences of same changes in feedback strength in the context of two different carbon cycle drivers allows an interpretation of the driving mechanism that underlies the behaviours observed in the wake of feedback changes. This highlights several previous underappreciated mechanisms as crucial in controlling long term climate response to carbon cycle drivers.

References

Beerling, D. J., and Royer, D. L., 2011, Convergent Cenozoic CO_2 history, *Nature Geoscience*, **4**(7), 418–420.

Foster, G. L., Royer, D. L., and Lunt, D. J., 2017, Future climate forcing potentially without precedent in the last 420 million years, *Nature Communications*, **8**, 1–8.

Hain, M. P., Sigman, D. M., Higgins, J. A., and Haug, G. H., 2015, The effects of secular calcium and magnesium concentration changes on the thermodynamics of seawater acid/base chemistry: Implications for Eocene and Cretaceous ocean carbon chemistry and buffering, *Global Biogeochemical Cycles*, 517–533.

Tyrrell, T., Shepherd, J. G., and Castle, S., 2007, The long-term legacy of fossil fuels, *Tellus, Series B: Chemical and Physical Meteorology*, **59**(4), 664–672.

What could be better,
Than to type in every letter,
Of equations big and small,
Am I done yet? Not at all!

Appendix A - Extant Carbon Cycle Models

Below, a number of existing carbon cycle models still used within the palaeoclimate community are discussed, roughly in order of increasing complexity. The focus is on the limitations of each model which make it unsuitable for use in this study.

A.1. BLAG

One of the earliest carbon cycle model was the BLAG (named for the creators Berner, LAsaga and Garrels (*Berner et al.*, 1983)) model. The BLAG model was designed to operate on timescales of millions of years, so had to simulate geological processes, meaning factors such as weathering, biogenic calcite formation, and volcanic CO_2 degassing were considered. The primary basis of the model is the control of weathering fluxes by atmospheric CO_2 and temperature. This link forms a negative feedback which stabilises long term climate. The most salient criticisms of the model were twofold:

- The BLAG model did not have an oceanic organic carbon reservoir.
- The BLAG model assumed that weathering fluxes are primarily controlled by temperature and CO_2, as opposed to changes in terrestrial relief or weatherability.

To resolve the problems created by the omission of the organic carbon subcycle, a new carbon cycle model (GEOCARB) was created (detailed further in Section A.2). The response to the potential importance of changing weatherability through time was more contentious, and the debate on the relative influence of these factors is ongoing to this day.

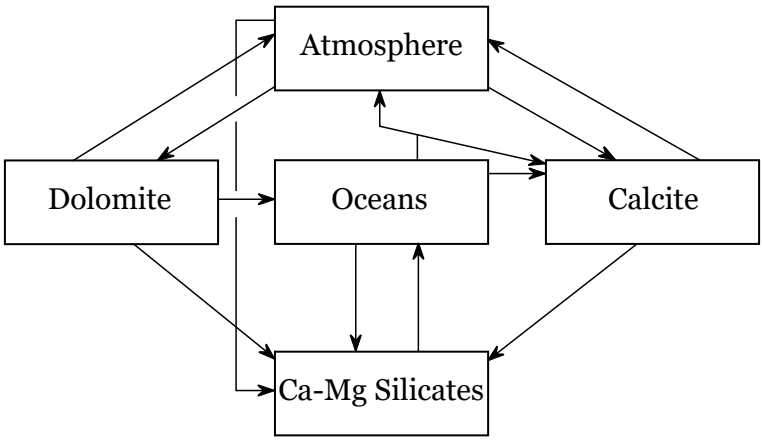

Figure A.1: ***Schematic of the BLAG Model from*** **Berner et al.** ***(1983).***

The fluxes in the BLAG model are calculated by simplistic parameterisations of physical processes which seek to retain at least some of the dynamic behaviour, however are not intended to represent carbon cycle processes mechanistically. There is no representation of the CCD, the spatial distribution of sedimentary carbon, or the mechanics of plate tectonics which move sedimentary carbon into towards subduction. Generally speaking, the BLAG model represents processes using correlative connections rather than causative connections.The initial conditions were carefully chosen, alongside several time evolving parameters and the assumption that the system was at steady state at 100Ma, so that the calculated present day fluxes were in line with literature estimates of the time.

Results from the BLAG model suggested that seafloor spreading rate and changes in land area are important drivers of the long term carbon cycle. These factors are both related to plate tectonics, and *Berner et al.* (1983) suggested that tectonics is a previously unexplored major climatic control.

While the BLAG model contains many ideal components to answer the questions posed in Section 1.8, the lack of realistic link between components limits the usefulness of the model. Despite the computational efficiency of the BLAG model, the time required to set up legacy code and understand the details of its functionality would outweigh the benefits of using an existing model.

A.2. GEOCARB

The GEOCARB model (*Berner*, 1991) can, in some ways, be considered a successor to the BLAG model. GEOCARB incorporates only three primary carbon reservoirs: carbonate sediment, organic carbon and a combined ocean and atmosphere box. The fluxes between these reservoirs represent weathering, metamorphic decarbonation, and burial. The simplicity of GEOCARB allowed it to be run for hundreds of millions of years without excessive run time and the improvement

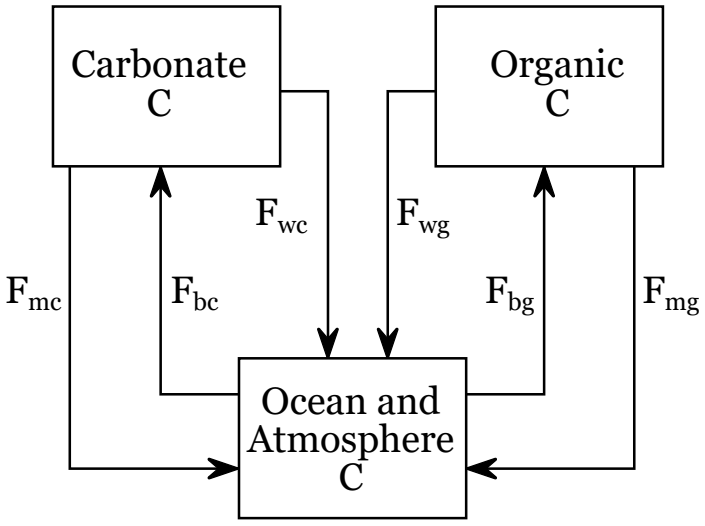

Figure A.2: ***Schematic of the GEOCARB model from* Berner *(1991).***

of computer processors in the intervening thirty years since GEOCARB's development means that it is now possible to run the model very quickly. Part of the reason for the development of GEOCARB was to address the shortcomings of the earlier BLAG model, which did not include an organic carbon reservoir. Results from the initial experiments with GEOCARB did not identify a single driving factor for atmospheric CO_2 trends from 570Ma to present, and instead *Berner* (1991) suggested a combination of factors were acting as carbon cycle drivers.

A revision of the parameters used by GEOCARB was made by *Berner* (1994) (GEOCARB II), who updated the data used for seafloor subudction/spreading rate and temperature, as well as making updates which incorporated the impact of uplift and allowed variation in the total crustal carbon reservoir size. Using the second iteration of GEOCARB, *Berner* (1994) found that uplift was an important driver of Cenozoic climate, but that changes in atmospheric CO_2 as a result of changes in seafloor spreading rate were not. *Berner* (1994) also found that the fall in the solar constant has had an impact on the carbon cycle, resulting in decreasing atmospheric CO_2 concentration on very long timescales. Finally, *Berner* (1994) highlighted the importance of shelf-deep sea partitioning of carbon burial in determining long term atmospheric CO_2 trends.

A second revision (GEOCARB III) was a comparatively minor, iterative update to parameters used in GEOCARB II (*Berner* and *Kothavala*, 2001). The major findings from GEOCARB III matched those of GEOCARB I and II, however exhibited a higher Mesozoic atmospheric CO_2 concentration. *Berner* and *Kothavala* (2001) attribute this to the effect of plants on weathering processes, and changes to the link between temperature and CO_2 concentration.

While GEOCARB was an excellent tool for exploring long term carbon cycle trends, it had to be heavily simplified in order to be computationally efficient enough to run for hundreds of millions of years on the machines available at the time. In order to achieve this, expressions were derived for a series of rate laws. These parameterisations do not mechanistically represent many key carbon cycle processes. The ocean and atmosphere are presumed to be a series of steady states, and the temporal resolution of the data produced is one point per million years. In order to reproduce the Phanerozoic CO_2 trend, initial parameters are tuned, and a series of complex, time varying input factors are used. *Berner* (1991) reproduce the Phanerozoic CO_2 trend to first order, which is then refined in subsequent publications by slight alterations to the model itself or the input parameters. Despite the positive aspects

of the GEOCARB series of models, the lack of mechanistic link between reservoirs makes this model better suited to understanding the direction of change in atmospheric CO_2 as a result of the input drivers, but the magnitude and timing of reservoir response is not well characterised.

A.3. JModel

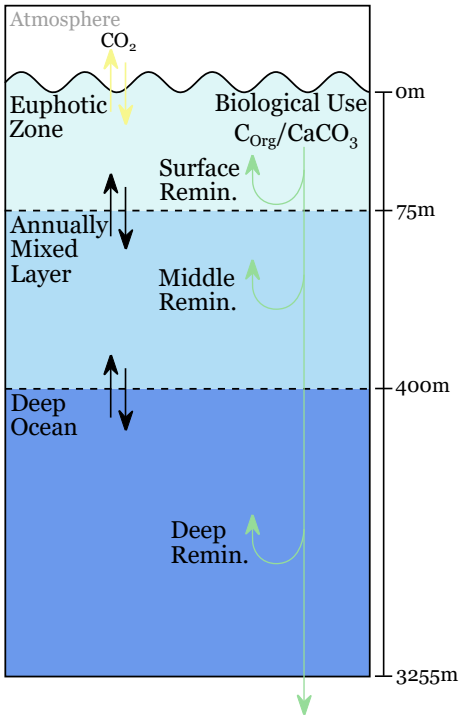

Figure A.3: ***Schematic of the JModel.***

The JModels (*Chuck et al.*, 2005) are a series of models primarily focussed on nutrient cycling, one of which incorporates carbon fluxes. The carbon JModel is intended to run on comparatively short timescales, and as such does not have a representation of sediments, or geological carbon cycle fluxes. It is included here primarily as the representation of the ocean in the GECCO model is based on the same type of box structure as the JModel. Usage of the JModel has been primarily focussed on anthropogenic CO_2 emission and its effect over the next 1 million years. The JModel is able to run several thousands years of simulation within a few seconds, however runs approaching millions of years take hours to complete. It is clear that the JModels are not suitable for investigating the impact of geological factors on the carbon cycle, as it does not include the required reservoirs. In addition to this, the lack of volcanic outgassing flux (dynamic or static) and weathering algorithm means that the Preindustrial steady state to which the model is tuned is unusual. The Preindustrial ocean was a source of CO_2, however in the JModel the Preindustrial tuning results in an ocean with no net air-sea gas exchange.

An adaptation of the JModel, referred to as MWT08, does incorporate the volcanic CO_2 source and weathering sink, however does not incorporate any additional factors (such as sedimentary carbon or plate tectonics). MWT08 has been used for more palaeo work than the original JModel, for example a study focussing on the Eocene-Oligocene transition (*Armstrong McKay et al.*, 2016).

A.4. LOSCAR

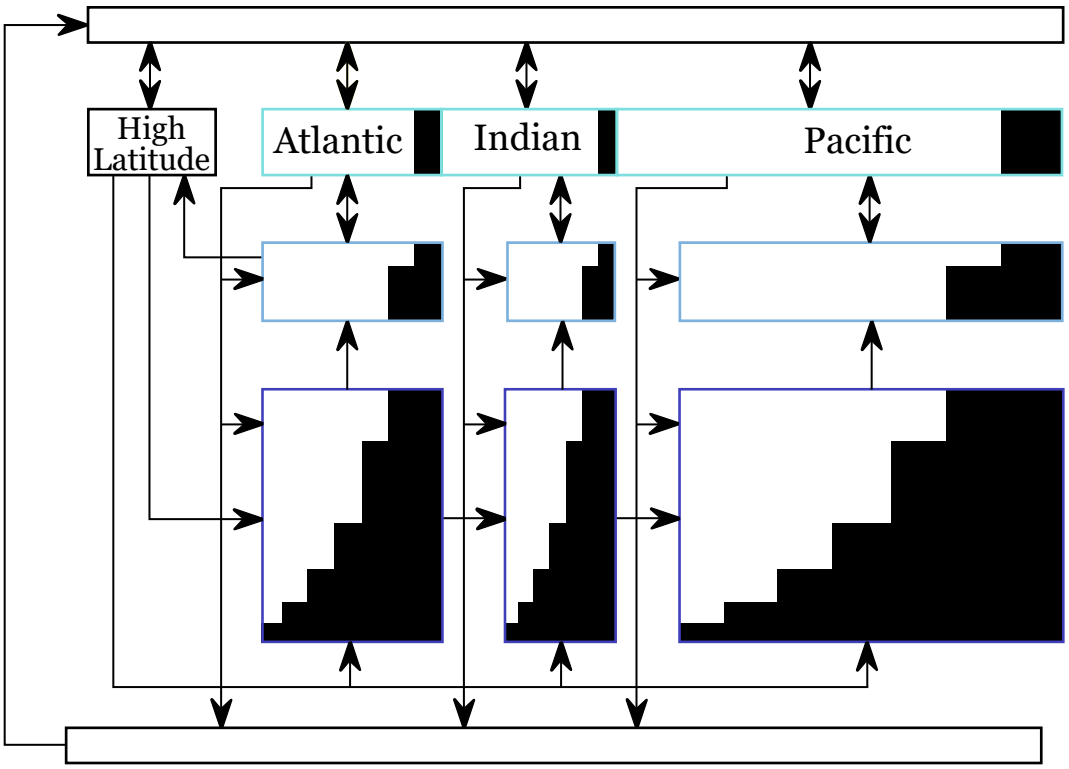

Figure A.4: ***Schematic of the LOSCAR model from*** **Zeebe** ***(2012).***

The Long-term Ocean-atmosphere-Sediment CArbon cycle Reservoir model (LOSCAR) seeks to model the carbon cycle on time scales from hundreds to millions of years. The focus of LOSCAR is on the representation of sediment, which is coupled to a detailed oceanic carbonate system. This has the benefit of being able to represent not only deposition of sediment, but also its dissolution, however these sediments are not subject to plate tectonic motion - in other words the sedimentary carbon sink is not related to the volcanic carbon source. Long term balance is achieved by choosing an initial condition for CO_2, which feedbacks then drive the system towards.

LOSCAR is comparatively well documented, which fuels its continued use in the palaeoclimate community. LOSCAR is quoted as being able run several thousand years of simulation in a few seconds, however scaling this up to performing Cenozoic runs would mean 70Myr of simulation would be expected to take on the order of 20 hours. The major omission from LOSCAR which prohibits it use within this study is the lack of link between buried sediment, subduction, and volcanic outgassing. Having said this, the diagram (Figure A.4) from *Zeebe* (2012) does appear to show some link between sediment and volcanic outgassing, but, if

this flux does exist, it is thought to be a static value rather than evolving through time.

A.5. CYCLOPS

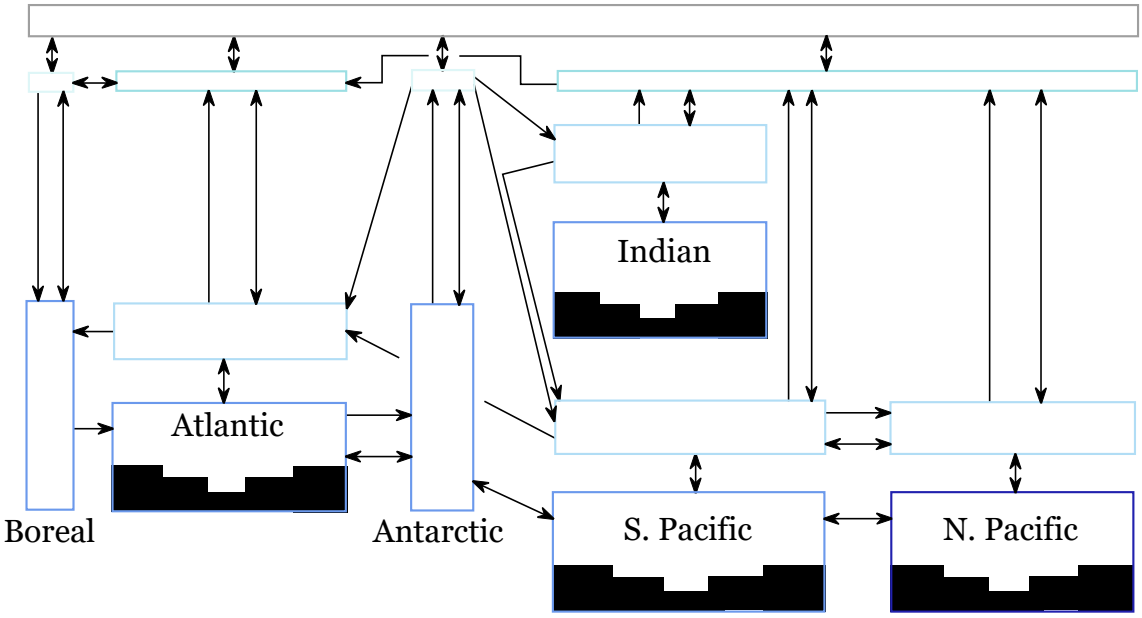

Figure A.5: ***Schematic of the CYCLOPS model from*** **Keir** ***(1988).***

The Carbon cYCLe and Ocean Productivity Simulation (CYCLOPS) model was original presented in *Keir* (1988), and has since been significantly improved (*Hain*, 2013). CYCLOPS is able to perform multi-million, and even multi-billion year runs due to its high computational efficiency, however is focused on the atmospheric and oceanic parts of the carbon cycle. So far, the applications of CYCLOPS have focussed on reconstructing glacial-interglacial CO_2 variation (*Hain*, 2013).

CYCLOPS neglects the lithological components of the carbon cycle, which must be specified as boundary conditions. This includes the specification of weathering fluxes, the volcanic outgassing flux, and the riverine carbon flux. The original publication associated with the CYCLOPS model (*Keir*, 1988) is now quite old, and the model has since been heavily modified, but no publication specifically detailing the current state of the CYCLOPS model is currently available. In summary, while CYCLOPS is more than efficient enough to perform the required simulations, it is lacking crucial features which prevent usage for this study, and the lack of documentation makes it difficult to assess whether this model is feasible for any given study.

A.6. cGENIE

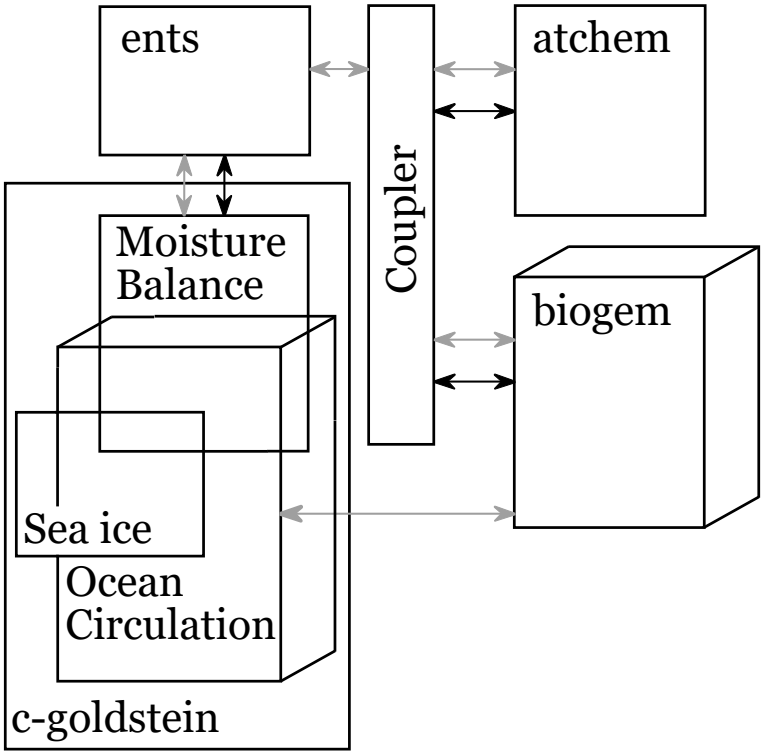

Figure A.6: ***Schematic of the cGENIE model after*** **Ridgwell** ***and*** **Hargreaves** ***(2007).***

cGENIE (Gridded ENabled Integrated Earth system model) is the only EMIC (Earth system Model of Intermediate Complexity) detailed here. cGENIE has a much greater spatial resolution than the box models described above, and has a much more complex and detailed representation of the biogeochemical cycle than existing carbon cycle box models. The advantage of this complexity is the excellent representation of the carbon cycle, with highly detailed components which can suit most applications.

There are two primary downsides to such complex models. The first is the model efficiency, which is comparatively low. The time taken by the model depends on the options chosen, however, generally speaking cGENIE produces a few thousand years of results per day. Assuming a speed of 5000 years per day, it would taken nearly 33 years to perform a single continuous simulation covering the Cenozoic. The second downside is that with software so complex is becomes impossible to truly understand each and every piece of the model, meaning some level of trust in the curator of the codebase is required. Not only this, but where there are thousands of parameters to be set, it is easy to overlook an important parameter. Due to the feasible length of runs, there are no geological factors incorporated into cGENIE, so it entirely unsuitable for the answering the questions posed here, however provides an interesting counterpoint in terms of available carbon cycle models.

Appendix B - Carbonate Chemistry

The concept of carbonate chemistry is explained with some detail in Section 1.2.1, but the behaviour of carbon species in the ocean is highly complex, so a more detailed 'ground up' explanation is provided here for reference.

It is typically said that the carbonate system, that is, the way in which inorganic carbon species behave in the ocean, has two degrees of freedom. Accepting this premise for the moment, what does 'two degrees of freedom' mean? An example that is somewhat less complex that carbonate chemistry may be given in the form of a rectangle. A rectangle can be defined by two numbers, for example the width and height. Once the width and height are known, then the area may be calculated, as may the perimeter, the length of the diagonal, the aspect ratio, or any other conceivable property concerning the size of the rectangle (see Figure B.1). Crucially, taking any two of these measurements, the rest may be calculated (for example, from the area and perimeter, it is possible to calculate the width and height). A rectangle is therefore an archetypal example of a system with two degrees of freedom, and it is hopefully intuitive to imagine that this limits the feasible behaviour that can be observed (for instance, if the height of a rectangle goes down while the width stays the same, the area must also decrease).

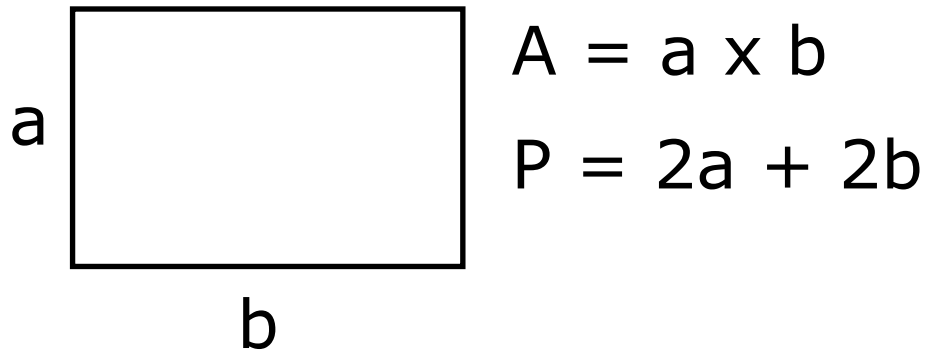

Figure B.1: ***A rectangle is an example of a system with two degrees of freedom. The sides, a and b, can be used to calculate the area (A) and the perimeter (P) as shown.***

Above, the premise of a system of two degrees of freedom was accepted, but does the carbonate system really have only two degrees of freedom? Mostly, yes. Just as with the rectangle, it is possible to calculate all carbonate system parameters from just two known values. Where this comes undone however, is that some variability can also be driven by temperature, pressure, salinity and ocean composition. The impact of these parameters is minor in comparison to the effect of the two main carbonate system parameters (typically

DIC and alkalinity), but they are needed to perform the calculation. To once again draw analogy to the rectangle, this might be represented by including the width of the border lines of the rectangle in the calculation. Typically the border is so thin as to be considered negligible, nonetheless, when the border thickness is changed then the size of the rectangle also changes, though normally to a much more minor extent than direct changes in the length of the sides. Around the standard ocean conditions, the changes driven by ancillary factors are small, but they can have important consequences in several situations (detailed below).

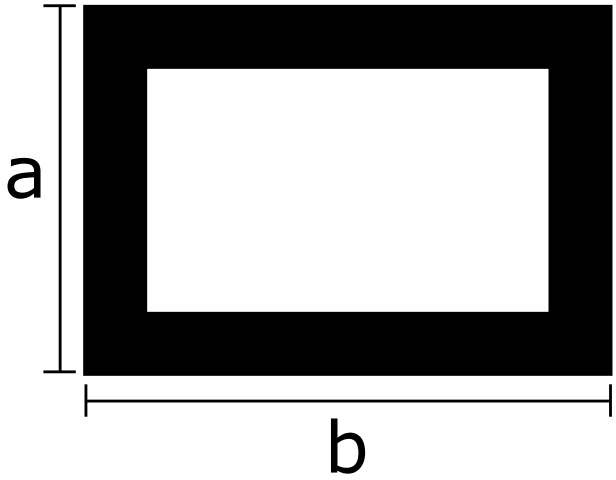

Figure B.2: ***In typically situations, the thickness of the sides of the rectangle are negligible (as in Figure B.1, but when the thickness of the sides becomes an appreciable fraction of the total size then it can affect calculations of other parameters noticeably.***

Again accepting, for the moment, that the carbonate system has two degrees of freedom, one might ask what carbonate system parameters can be defined. The first are simply the concentrations of individual inorganic carbon species in the ocean: [CO_2] (aqueous CO_2), [H_2CO_3] (carbonic acid), [HCO_3^-] (bicarbonate) and [CO_3^{2-}] (carbonate ion). These species exist in dynamic equilibrium. Of the four species, carbonic acid is particularly unstable, such that the concentration in the ocean at any one time is negligible and it is therefore typically ignored. Having established the three primary forms of carbon for consideration, it is possible to write stoichiometric equations which express the ratio of products to reactants as a single value, which is dependent on temperature, pressure, salinity and ocean composition. These values are often referred to as 'equilibrium constants' despite not being constants, but here are referred to as CCK's (Carbonate Chemistry K values). This may seem strange, as it would be expected that in order to properly represent the system, the activities of each ion should be taken into account. This is indeed the case, but in the form of the equations shown here, the activities of ions have been parameterised into the CCK value.

Out of the three forms of carbon several other parameters can be defined. The first is Dissolved Inorganic Carbon (DIC) which simply represents the total concentration of all three carbon species (Equation 1.3). Another is alkalinity which is a form of oceanic change balance in which carbon species are heavily involved (Equation 1.4). The equation shown in Chapter 1 is a simplification of the full calculation, which incorporates additional ions which are able to be proton donors or acceptors. There are many ions which can be considered, but there are diminishing returns from incorporating additional ions. The most important ions are the carbonate system, the boron system, the silica system and the phosphate system (*Zeebe* and *Wolf-Gladrow*, 2001). The final parameter considered here is saturation state, which is the ratio of calcium and carbonate ion concentrations to their expected solubility at a given temperature, pressure, salinity and ocean composition (Equation 1.6). This value essentially gives a ratio of the amount of calcium carbonate the water is holding to the amount it would be expected to hold. Perversely, most surface water is 'supersaturated' with respect to calcium carbonate, meaning it is holding more than would be expected. How is this possible? The answer comes down to dynamics. Spontaneous precipitation of calcium carbonate does not occur in meaningful quantities until the saturation state reaches values of 10 or more, below which the precipitation is extremely slow. This allows the ocean to maintain a high level of supersaturation.

Returning to the analogy of the carbonate system and the rectangle, it was mentioned above that in some situations the effects of typically minor influences may become relevant. One immediately apparent example is the increase in pressure that is experienced when descending in the ocean. Changes in surface ocean pressure are minor in comparison to the change in pressure that occurs when travelling from the surface ocean to several kilometres depth. Large changes in pressure are able to drive important variations in the carbonate system through their effect on saturation state, predominantly through changes to the solubility product. In this case then, the width of the line used to draw the rectangle is able to make important changes to the overall area. In fact, this mechanic is crucial in forming a solubility horizon in the ocean, above which the ocean is supersaturated with respect to calcium carbonate and below which it is undersaturated. This horizon is called the CSH. Carbon is exported to the CSH by falling carbonate tests created by surface dwelling calcifying organisms. In an idealised scenario, these tests would only make it so far as the CSH before being instantaneously dissolved, though of course this is not the case. Dissolution of tests begins as they pass below the CSH, but is dynamically slow, meaning that the

tests may be preserved below the CSH. Another horizon can therefore be defined, below which no carbonate is preserved, based on observation of the sediments. This is called the Carbonate Compensation Depth (CCD). Intuitively the CCD should sit somewhere below the CSH, however organic carbon remineralisation in sediments may acidify the porewater microenvironment, prohibiting the preservation of carbonate without affecting the CSH.

The carbonate system is highly complex, and the picture as presented above is a simplified picture of the components relevant to this project (primarily the influence of changes in CCK's driven by various factors, and the ensuing impact on the CCD). For further details, please refer to *Zeebe* and *Wolf-Gladrow* (2001).

Appendix C - Statistical Techniques

For the purpose of data analysis, several statistical techniques have been developed and applied to different datasets in this thesis. Rather than cluttering each chapter with a lengthy description of the mathematical methodology, these techniques are collected here and referred to as appropriated. This also beneficial in that it keeps the methodology separate from the specific application in each chapter.

C.1. Probability Map

In recent years, there has been a concerted effort to improve the calculation of uncertainties in palaeoclimate datasets. This means that many datasets now have quantified uncertainties in both value itself and the age of that sample. This can lead to difficulties when plotting particularly dense datasets though, as the uncertainties begin to overlap and inhibit any sensible interpretation. To solve this, I have developed a new data processing technique which calculates so called probability maps from datasets made up of many datapoints each of which has quantified uncertainties on the values of interest.

The method works by taking a range of interest for both dimensions and forming a grid. For each datapoint, the probability of the value being in each grid cell is calculated. This creates a three dimensional matrix, where each slice is a probability map for each datapoint. These individual probability maps are summed to collapse all datapoints into a single probability map. A normalisation factor must then be applied to each column to account for the different density of measurements through time. For instance, imagine that there were two measurements whose most likely value was in the same column, this might lead to a total probability in that column exceeding unity. Each column is therefore normalised so that the sum of that column is equal to 1, which makes the assumption that the value has an equal chance of being somewhere within the specified range through time.

From the probability map a line of 'optimal probability' can be drawn by simple connecting the maximum of each column. This line shows where the data show the value to be most likely, but does not consider any temporal effects.

C.2. Bayesian Inference

In Chapter 3, there was a need to combine two somewhat independent estimates of calcium concentration. One was the marginal probability, the probability of calcium being at a given concentration based only on the calcium concentration data presented inFigure 3.2. The other was the prior, which was constructed by combining estimates of magnesium:calcium ratio an magnesium concentration. The marginal probability and prior probability are combined to form the posteriour distribution (as shown in Figure C.1), which refines the most likely value of calcium concentration with associated uncertainties.

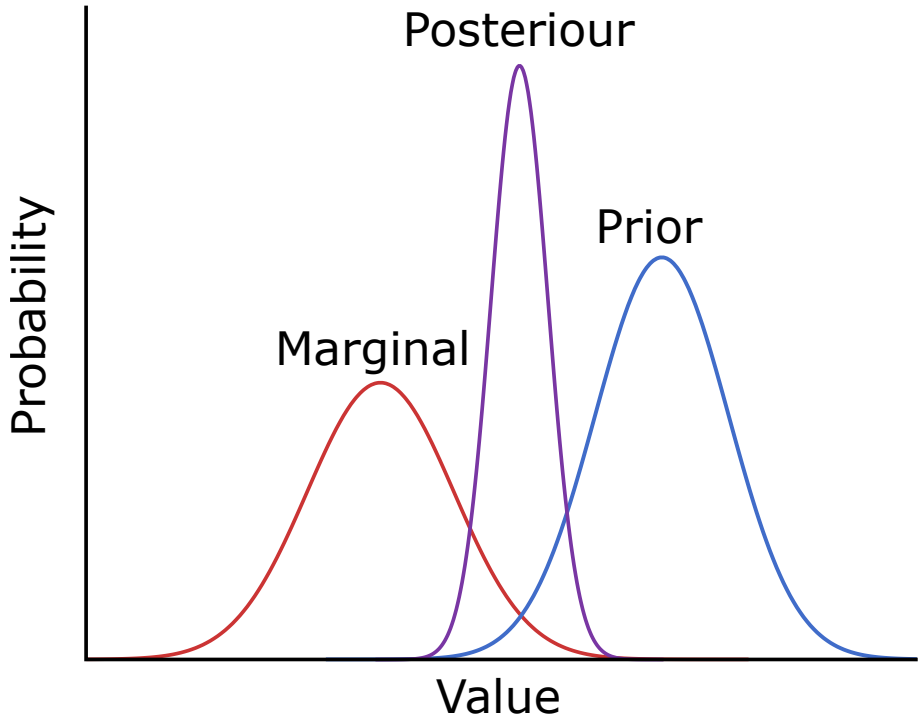

Figure C.1: ***Schematic of a simple Bayesian methodology to combine the marginal probability (red) and prior distribution (blue) to form the posteriour (purple). The posteriour has the highest probability where the marginal and prior overlap.***

References

Armstrong McKay, D. I., Tyrrell, T., and Wilson, P. A., 2016, Global carbon cycle pertubation across the Eocene-Oligocene climate transition, *Paleoceanography*, **31**, 311–329.

Berner, R. A., 1991, A model for atmospheric CO_2 over Phanerozoic time, *American Journal of Science*, **291**(4), 339–376.

Berner, R. A., 1994, GEOCARB II: a revised model of atmospheric CO2 over Phanerozoic time, *American Journal of Science*, **294**(1), 56–91.

Berner, R. A., and Kothavala, Z., 2001, GEOCARB III: A revised model of atmospheric CO2 over Phanerozoic time, *American Journal of Science*, **301**(2), 182–204.

Berner, R. A., Lasaga, A. C., and Garrels, R. M., 1983, Carbonate-silicate geochemical cycle and its effect on atmospheric carbon dioxide over the past 100 million years, *American Journal of Science*, **283**(7), 641–683.

Chuck, A., Tyrrell, T., Totterdell, I., and Holligan, P., 2005, The oceanic response to carbon emissions over the next century: investigation using three ocean carbon cycle models, *Tellus B*, **57**(B), 70–86.

Hain, M. P., *Glacial/Interglacial and Deglacial Changes in Ocean Circulation and Their Consequnces for the Global Carbon Cycle : a Model Study Presented To the Faculty of Princeton University in Candidacy for the Degree of Doctor of Philosophy Recommended for Accept* PhD thesis, 2013,.

Keir, R. S., 1988, On the Late Pleistocene ocean geochemistry and circulation, *Paleoceanography*, **3**(4), 413.

Ridgwell, A., and Hargreaves, J. C., 2007, Regulation of atmospheric CO2 by deep-sea sediments in an Earth system model, *Global Biogeochemical Cycles*, **21**(2), 1–14.

Zeebe, R. E., 2012, LOSCAR: Long-term Ocean-atmosphere-Sediment CArbon cycle Reservoir model v2.0.4, *Geoscientific Model Development*, **5**(1), 149–166.

Zeebe, R. E., and Wolf-Gladrow, D., 2001, *CO2 in Seawater: Equilibrium, Kinetics, Isotopes*, Elsevier Ltd., Amsterdam, 3rd edition.